

**INVESTIGATING THE BIOLOGY OF INNATE LYMPHOID CELLS
AT BARRIER SITES AND THEIR DRAINING LYMPHOID TISSUE**

By

EMMA ELIZABETH DUTTON

A thesis submitted to the University of Birmingham

For the Degree of DOCTOR OF PHILOSOPHY

Institute of Immunity and Immunotherapy

College of Medical and Dental Science

University of Birmingham

September 2018

UNIVERSITY OF
BIRMINGHAM

University of Birmingham Research Archive

e-theses repository

This unpublished thesis/dissertation is copyright of the author and/or third parties. The intellectual property rights of the author or third parties in respect of this work are as defined by The Copyright Designs and Patents Act 1988 or as modified by any successor legislation.

Any use made of information contained in this thesis/dissertation must be in accordance with that legislation and must be properly acknowledged. Further distribution or reproduction in any format is prohibited without the permission of the copyright holder.

ABSTRACT

Within this investigation a robust ILC identification method was used to identify ILCs and their subsets, comparing them across non-lymphoid and lymphoid tissues. ILCs were distributed differently across the analysed tissue and it was identified that surface marker expression, used to identify ILCs, was varied depending on location. The importance of digestion protocols was also highlighted, observing reduced expression of identification markers under harsher digestion protocols. Upon identifying ILCs, the role of the co-stimulatory molecule, inducible co-stimulator (ICOS), in their homeostasis was assessed. ILCs were not perturbed in the absence of ICOS:ICOSL interactions, suggesting a redundant role in ILC maintenance. This directed the aim of the investigation towards assessing ILC migration between non-lymphoid and lymphoid tissues. Photoconvertible Kaede mice were used to observe ILCs migration into peripheral LNs, with ILC1s likely entering in from the blood, in a CCR7-dependent manner. ILCs egressed from the LN in an S1P-dependent manner and recirculated through contralateral LNs. Minimal ILC migration through the lymphatics was detected from the ear to the draining LN, however, was modestly increased under skin inflammation. Combined these data reveal fundamental new insight into the biology of ILCs at barrier sites and LNs, identifying a migratory population of ILCs.

ACKNOWLEDGEMENTS

I would firstly like to thank Dr David Withers for being a fantastic supervisor during my PhD. I have thoroughly enjoyed my 4 years working in his lab and really appreciate all of his help and support. This project has been really interesting and I can't thank Dave enough for his patient input and encouragement throughout.

Thank you to my co-supervisor Dr Kai-Michael Toellner and everyone in the Withers and Lane labs for their supportiveness and providing me with useful advice during my studies. I would especially like to thank Dominika Gajdasik, Claire Willis and Rhys Jones alongside Emma Mackley, Clare Marriott, Emily Halford, for giving me so many fond memories.

I would also like to thank people within the IBR for supporting me through this PhD and making my time here really enjoyable. I would especially like to thank Claire Dempsey for making the last four years in Birmingham so much fun.

Working with MedImmune and being exposed to research within industry has been a fantastic opportunity in my PhD. I would like to thank everyone on at MedImmune, especially Ana Camelo for making me feel so welcome and part of the team.

Finally, I would like to thank my family and friends, especially my mum and dad for keeping me going when things got tough and constantly supplying me with chocolate biscuits and hummus.

TABLE OF CONTENTS

Chapter 1. INTRODUCTION	1
1.1 THE IMMUNE SYSTEM.....	1
1.2 THE INNATE IMMUNE SYSTEM.....	2
1.2.1 Recruitment of innate immune cells to the site of infection	2
1.2.2 Migratory properties of the innate immune system.....	3
1.3 THE ADAPTIVE IMMUNE SYSTEM.....	4
1.3.1 T cells.....	4
1.3.2 Activation of the adaptive immune system	5
1.3.3 CD4 ⁺ T cell Activation	6
1.3.4 Effector T helper cells.....	7
1.4 INNATE LYMPHOID CELLS.....	10
1.4.1 Group 1 ILCs	11
1.4.2 Group 2 ILCs	13
1.4.3 Group 3 ILCs	14
1.4.4 Regulatory ILCs	15
1.4.5 ILC Plasticity.....	15
1.5 ILC DEVELOPMENT	17
1.6 FUNCTIONS OF ILCS.....	19
1.6.1 Gastrointestinal tract	19
1.6.2 Lung.....	26
1.6.3 Skin.....	29
1.6.4 Secondary lymphoid tissue.....	30
1.7 MIGRATORY PROPERTIES OF ILCS	34
1.8 AIMS OF THIS INVESTIGATION	36
Chapter 2. MATERIALS AND METHODS	38
2.1 MICE STRAINS.....	38
2.2 MEDIUMS AND REAGENTS.....	39
2.2.1 Mediums	39
2.2.2 Gey's solution	39
2.3 PREPARING CELL SUSPENSIONS	40

2.3.1	Lymph nodes and spleen.....	40
2.3.2	Lung.....	41
2.3.3	Small intestine lamina propria	41
2.3.4	Ear skin	42
2.3.5	Blood	43
2.3.6	Lymph node stromal digestion.....	43
2.4	MAGNETIC-ACTIVATED CELL SORTING.....	43
2.4.1	CD45 ⁺ enrichment	43
2.4.2	ILC enrichment	44
2.5	FLOW CYTOMETRY	44
2.5.1	Extracellular staining	44
2.5.2	Intracellular staining.....	45
2.5.3	Intracellular staining in Kaede mice	46
2.5.4	Flow cytometry analysis	46
2.6	IMMUNOFLUORESCENCE MICROSCOPY	50
2.6.1	Preparation of frozen tissue slides	50
2.6.2	Immunofluorescence staining of tissue	51
2.6.3	Analysis of immunofluorescence stained tissue	52
2.7	PHOTOCONVERTIBLE KAEDE MICE.....	54
2.7.1	Photoconvertible Kaede mice	54
2.7.2	Violet light conversion of the brachial lymph node	55
2.7.3	Violet light conversion of the ear	55
2.7.4	Violet light conversion of the head	55
2.8	EAR INFLAMMATION MODELS	56
2.8.1	Calcipotriol topical application to the ear	56
2.8.2	Aldara topical application to the ear	56
2.9	FTY720 MOUSE MODELS.....	56
2.9.1	FTY720 administration	56
2.9.2	FTY720 in combination with previous models	57
2.10	ETHICAL APPROVAL.....	57
2.11	STATISTICAL ANALYSIS.....	57
Chapter 3. CHARACTERISATION OF ILCs		58

3.1	INTRODUCTION	58
3.1.1	Project Aims	61
3.2	RESULTS.....	61
3.2.1	ILC populations are identified within lymphoid and non-lymphoid tissues	61
3.2.2	ILC3 subsets are not evenly distributed between assessed tissues	62
3.2.3	ILC2s phenotype differs between assessed tissues.....	65
3.2.4	Lineage ⁻ IL-7R α ⁺ cells lacking classical ILC TF expression are a true ILC population 69	
3.2.5	ILC identification via TF is affected by digestion protocols	70
3.2.6	Various surface markers are downregulated under a harsh digestion protocol.	76
3.2.7	ILCs are located within secondary lymphoid tissues within mouse and human .	80
3.3	SUMMARY	85
Chapter 4. DETERMINING THE ROLE OF ICOS AND ICOSL INTERACTIONS IN ILC HOMEOSTASIS.....		91
4.1	INTRODUCTION	91
4.1.1	Project Aims	94
4.2	RESULTS.....	94
4.2.1	ILC populations are not perturbed in the absence of ICOSL expression	94
4.2.2	Minimal impact of ICOS:ICOSL on the phenotype of ILC2s	95
4.2.3	Minimal impact on ILC3 subgroups in the absence of ICOSL	102
4.2.4	Perturbations of ILC3 subgroups in the absence ICOS	107
4.3	SUMMARY	112
Chapter 5. DETERMINING THE MIGRATORY PROPERTIES OF ILCs WITHIN PERIPHERAL LNS		116
5.1	INTRODUCTION	116
5.1.1	Lymphocyte entry into the LNs via HEVs.....	116
5.1.2	Lymphocyte migration into the LV via the lymphatics system.....	118
5.1.3	Lymphocyte egress from LNs occurs in an S1P dependent manner	119
5.1.4	Retention of lymphocytes within the LN.....	121
5.1.5	Models used to track migration in vivo	121
5.1.6	Migratory properties of ILCs.....	123
5.1.7	Project Aims	123
5.2	RESULTS.....	124

5.2.1	ILCs consist of migratory and tissue-resident populations within the bLN	124
5.2.2	Migration into the bLN is dependent on CCR7	127
5.2.3	Photoconversion does not result in the accumulation of cells within the bLN .	131
5.2.4	ILCs egress from the bLN in an S1P dependent manner	131
5.2.5	ILC1s are the most migratory subset of ILCs within the bLN.....	139
5.3	SUMMARY	147
Chapter 6. ASSESSING THE MECHANISMS OF ILC MIGRATION BETWEEN SKIN AND DRAINING PERIPHERAL LN		158
6.1	INTRODUCTION	158
6.1.1	Project Aims	159
6.2	RESULTS.....	160
6.2.1	Minimal ILC migration to the auLN from the ear steady state	160
6.2.2	Atopic Dermatitis causes an increase in ear and auLN cellularity	163
6.2.3	ILC migration is induced under an atopic dermatitis inflammation model	172
6.2.4	ILCs migrate into the ear in atopic dermatitis inflamed skin.....	179
6.2.5	Cell migration into the ear from surrounding skin	183
6.2.6	ILC migration is dependent on inflammatory conditions	185
6.2.7	ILC homeostasis is perturbed in <i>Ccr6</i> ^{-/-} mice	191
6.2.8	ILCs migrate into the inflamed ear in a CCR6 dependent manner	199
6.3	SUMMARY	205
Chapter 7. DISCUSSION.....		214
7.1	ILCS ARE DISTRIBUTED THROUGHOUT LYMPHOID AND NON-LYMPHOID TISSUES 214	
7.1.1	TF are a useful tool in the efficient identification of ILC subsets	215
7.1.2	The digestion protocol affects the identification of ILC subsets	216
7.2	ICOS EXPRESSION IS NOT REQUIRED FOR ILC MAINTENANCE UNDER STEADY STATE CONDITIONS	218
7.2.1	Differences in mouse biology as a result of differing animal facilities	218
7.2.2	Publication of negative results is required within the scientific field.....	219
7.2.3	Co-stimulatory molecules are required for ILC function	220
7.3	ILCS MIGRATE UNDER STEADY STATE CONDITIONS IN PERIPHERAL LNS.....	221
7.3.1	ILC1s possess similarities in migratory properties to cNK cells	223
7.3.2	ILC2s and ILC3s are mainly tissue-resident under steady state.....	226

7.3.3	Do migratory and tissue-resident ILCs possess different functions?	229
7.4	ILC MIGRATION UNDER INFLAMMATION.....	231
7.4.1	ILCs are recruited into the inflamed ear skin	232
7.4.2	ILCs accumulate within challenged peripheral draining LNs	234
7.4.3	Accumulation of ILCs within the LN suggests a role in crosstalk with the adaptive immune system.....	236
7.5	CONCLUDING REMARKS.....	238
Papers arising from this thesis:		240
APPENDIX – LIST OF REFERENCES.....		241

LIST OF FIGURES

Figure 1.1. Th cell and ILC subsets and cytokine production	16
Figure 1.2. ILC Development	20
Figure 3.1. Characterisation of ILCs in lymphoid and non-lymphoid tissue	63
Figure 3.2. Quantification of ILCs in lymphoid and non-lymphoid tissue.....	64
Figure 3.3. Analysis of ILC3 subsets isolated from different tissues.....	66
Figure 3.4. Characterisation of ILC2s isolated from different tissues	68
Figure 3.5. Evidence that Lineage ⁻ IL-7Rα ⁺ GATA-3 ⁻ RORγt ⁻ T-bet ⁻ cells are ILCs.....	71
Figure 3.6. Identification of the ILC population is unaffected by the ear digestion protocol .	73
Figure 3.7. Expression of lineage markers used to identify ILCs was not decreased under the ear digestion protocol	74
Figure 3.8. ILC transcription factor expression is reduced under the EDP	75
Figure 3.9. Identification of various markers used to phenotype ILCs have decreased expression under the ear digestion protocol	77
Figure 3.10. Poor ILC isolation from ear skin using milder enzymatic digestion	79
Figure 3.11. Identification of ILC3s in murine lymphoid and non-lymphoid tissues	81
Figure 3.12. Identification of ILC2s and ILC3s in adult human mLN.	83
Figure 3.13. Phenotyping of ILC3s within human adult tonsil.....	84
Figure 4.1. Minimal impact on ILC populations in the SI LP of <i>Icosl</i> ^{-/-} mice.....	96
Figure 4.2. No impact on ILC populations within the mLN of <i>Icosl</i> ^{-/-} mice	97
Figure 4.3. Minimal impact on ILC populations in the lungs of mice lacking ICOSL expression	98
Figure 4.4. Minimal impact on ILC2 phenotype in the absence of ICOSL in the SI LP	100

Figure 4.5. No impact on ILC2 phenotype in the absence of ICOSL in the mLN	101
Figure 4.6. Minimal impact on ILC2 phenotype within the lung of <i>Icosl</i> ^{-/-} mice	103
Figure 4.7. ILC3 subsets are not perturbed in the absence of ICOSL in the SI LP	104
Figure 4.8. ILC3 subsets are not perturbed in the mLN of <i>Icosl</i> ^{-/-} mice	105
Figure 4.9. Minimal impact on ILC3 subsets in ICOSL deficient lungs	106
Figure 4.10. Normal ILC populations in the SI LP of <i>Icosl</i> ^{-/-} mice	108
Figure 4.11. ILC3 subsets are not perturbed in the SI LP of <i>Icosl</i> ^{-/-} mice	109
Figure 4.12. Reduced numbers of ILC3s in the mLN of <i>Icosl</i> ^{-/-} mice	110
Figure 4.13. Reduced numbers of all ILC3 populations in the mLN of <i>Icosl</i> ^{-/-} mice	111
Figure 5.1. Lymphocyte entry into the LN	120
Figure 5.2. Tracking dynamic changes in immune cell composition of a peripheral LN	126
Figure 5.3. Stromal populations within the bLN remain Kaede Red 72 hours after photoconversion	128
Figure 5.4. Migration of ILCs is CCR7 dependent	130
Figure 5.5. CCR7 dependent trafficking of $\gamma\delta$ T cell subsets	132
Figure 5.6. Photoconversion does not result in the accumulation of ILCs within the LN	133
Figure 5.7. ILCs have the ability to egress in an S1PR1 dependent manner	135
Figure 5.8. Inhibition of S1P mediated egress directly results in the accumulation of ILCs ..	137
Figure 5.9. ILCs recirculate into contralateral LNs	138
Figure 5.10. Kaede Green and Kaede Red ILCs express migratory and resident markers, respectively.	140
Figure 5.11. Identification of ILC subsets in the bLN using cell surface markers	142
Figure 5.12. The majority of ILC migration at 72 hours are ILC1s	144

Figure 5.13. cNK cells are able to recirculate through draining LNs.....	146
Figure 5.14. CCR7 ⁺ CD62L ⁺ ILC1s are located within the blood	148
Figure 5.15. Summary Diagram of ILC migration within bLN Kaede model	150
Figure 5.16. Summary Diagram of proposed model of ILC subset migration	151
Figure 6.1. Photoconversion does not elicit $\gamma\delta$ T cell IL-13 production.....	162
Figure 6.2. Tracking migration of immune cells in the ear and draining auLN.....	164
Figure 6.3. Establishment of the MC903 atopic dermatitis model.....	166
Figure 6.4. An increase in all ILC subsets is observed within the auLN of atopic dermatitis mice.....	168
Figure 6.5. Atopic dermatitis elicits an increase in ILC2s within the ear	169
Figure 6.6. Atopic dermatitis elicits an increase in $\gamma\delta$ T cells within the ear	171
Figure 6.7. Increase in LCs within the auLN and ear of atopic dermatitis mice	173
Figure 6.8. ILC migration into the draining auLN increases upon MC903 induced inflammation.....	175
Figure 6.9. Proliferation of ILCs within the auLN is a contributing factor to their expansion.....	176
Figure 6.10. Blocking ILC S1P dependent migration does not affect ILC expansion within the auLN	178
Figure 6.11. Atopic dermatitis drives enhanced ILC recruitment to skin	181
Figure 6.12. A true population of migratory ILCs enter the inflamed ear	182
Figure 6.13. Minimal migration of T cells occurs from the opposite ear into the inflamed ear	184
Figure 6.14. Migration from adjacent skin to inflamed ear is limited in atopic dermatitis model	186

Figure 6.15. Aldara induced psoriasis stimulates an inflammatory response within the auLN	188
Figure 6.16. Aldara induced psoriasis stimulates an inflammatory response within the ear	190
Figure 6.17. ILCs migrate into the inflamed skin of Aldara treated mice	192
Figure 6.18. CCR6 is expressed on all ILC subsets within the ear and auLN	194
Figure 6.19. ILC1s and ILC2s are deficient in auLN of <i>Ccr6</i> ^{-/-} mice	195
Figure 6.20. ILCs are unchanged within ears of <i>Ccr6</i> ^{-/-} mice	196
Figure 6.21. <i>Ccr6</i> ^{-/-} mice are unable to elicit a comparable inflammatory response in the ear compared to WT mice.....	198
Figure 6.22. <i>Ccr6</i> ^{-/-} The expansion of ILC2s within the auLN of MC903 treated mice is CCR6 dependent.....	200
Figure 6.23. The expansion of ILC2s within the ear of MC903 treated mice is CCR6 dependent	201
Figure 6.24. ILCs migrate from the inflamed skin into the draining LN independently of CCR6	202
Figure 6.25. The migration of ILCs into inflamed skin is dependent on CCR6.....	204
Figure 6.26. Summary Diagram of ILC migration between the skin and draining LN.....	213

LIST OF TABLES

Table 2.1. Mouse strains used within this investigation	38
Table 2.2. Staining buffer	39
Table 2.3. Culture media	39
Table 2.4. Staining solution for immunofluorescence microscopy	39
Table 2.5. Gey's solution	40
Table 2.6. Microbeads used in cell separation	44
Table 2.7. Fluorescent activated cell labelling reagents used for flow cytometry	47
Table 2.8. Minimal proportions of tissues stained	49
Table 2.9. Primary and biotinylated antibodies	50
Table 2.10. Fluorochrome-conjugated streptavidin.....	50
Table 2.11. Blocking serums used in flow cytometry	50
Table 2.12. Immunofluorescence primary antibodies	53
Table 2.13. Immunofluorescence secondary and streptavidin antibodies	54
Table 3.1. Summarising table of markers expression compared between the EDP and LDP..	78

LIST OF ABBREVIATIONS

-/-	knock out
α -LP	α -lymphoid precursors
μ L	microliter
μ m	micrometre
AD	atopic dermatitis
AHR	aryl hydrocarbon receptor
APC	antigen presenting cell
auLN	auricular lymph node
axLN	axillary lymph node
BEC	blood endothelial cell
bLN	brachial lymph node
BM	bone marrow
BMSU	biomedical serviced unit
BRDU	bromodeoxyuridine
BSA	bovine serum albumin
CCL	C-C motif chemokine ligand
CCR	chemokine receptor
CD	cluster of differentiation
CD62L	L-selectin
CHILP	common helper lymphoid progenitor
cLN	cervical LN
CLP	common lymphoid progenitor
cNK cell	conventional natural killer cell
CP	cryptopatches
CS	cell surface
CTLA-4	cytotoxic T lymphocyte-associated molecule 4
CXCL	C-X-C motif chemokine ligand
CXCR	C-X-C chemokine receptor
D0	day 0
D2	day 2
D4	day 4
D5	day 5
DAPI	4',6-diamidino-2-phenylindole
DC	dendritic cell
DETC	dendritic epidermal T cells
DMEM	Dulbecco's Modified Eagle Medium
DNA	deoxyribonucleic acid
DPBS	Dulbecco's phosphate-buffered saline
EDP	ear digestion protocol
EDTA	Ethylenediaminetetraacetic acid
EILP	early innate lymphoid progenitor
EOMES	eomesdermin
FACS	fluorescent activated cell sorting
FBS	foetal bovine serum

Foxp3	forkhead box P3
FRC	fibroblastic reticular cells
Fut2	fucosyltransferase 2
GATA-3	GATA binding protein 3
GFP	green fluorescent protein
HBSS	Hank's balanced salt solution
HDM	house dust mite
HEC	high endothelial cells
HEV	high endothelial venules
i.p.	intraperitoneal
IBD	Inflammatory bowel disease
ICAM-1	intercellular adhesion molecule 1
iCD3 ϵ	intracellular CD3 ϵ
ICOS	inducible co-stimulatory
ICOSL	inducible co-stimulatory ligand
Id2	DNA-binding protein inhibitor 2
Id3	DNA-binding protein inhibitor 3
IFN	interferon
Ig	immunoglobulin
iILC2	inflammatory innate lymphoid cell group 2
IL	interleukin
IL-7R α	interleukin 7 receptor alpha
ILC	innate lymphoid cell
ILC1	innate lymphoid cell group 1
ILC2	innate lymphoid cell group 2
ILC3	innate lymphoid cell group 3
ILCP	innate lymphoid cell precursor
ILCreg	regulatory innate lymphoid cell
ILF	isolated lymphoid follicles
iLN	inguinal LN
IQM	imiquimod
ISC	intestinal stem cell
KG	Kaede Green
KLH	keyhole limpet hemocyanin
KLRG1	killer-cell lectin like receptor G-1
KR	Kaede Red
LCMV	lymphocytic choriomeningitis virus
LDP	lung digestion protocol
LEC	lymphatic endothelial cell
LED	light emitting diode
LFA-1	lymphocyte function-associated antigen 1
LN	Lymph nodes
LP	lamina propria
LT	lymphotoxin
LTi - cells	Lymphoid Tissue inducer cells

MACS	magnetic-activated cell sorting
MADCAM1	mucosal addressin cell adhesion molecule 1
MAP	mitogen-activated protein
MC903	Calcipotriol (C ₂₇ H ₄₀ O ₃)
mg	milligram
MHC	major histocompatibility complex
MHCI	major histocompatibility complex class I
MHCII	major histocompatibility complex class II
mL	millilitres
mLN	mesenteric lymph node
mM	millimolar
NCR	natural cytotoxic receptor
NFIL3	nuclear factor interleukin-3 regulated
nILC2	natural innate lymphoid cell group 2
NK cells	natural killer cells
Nm	nanometres
OCT	optimal cutting temperature
OVA	ovalbumin
OX40	tumour necrosis factor receptor superfamily, member 4
OX40L	tumour necrosis factor receptor superfamily, member 4 ligand
PD-1	programmed cell death-1
PI3K	phosphatidylinositol 3-kinase
PLZF	promyelocytic leukaemia zinc finger
PP	Peyer's patches
PRR	pathogen recognition receptors
RANK	receptor activator of nuclear factor κ B
RANKL	receptor activator of nuclear factor κ B Ligand
RAG	recombination activation gene
Reg	regenerating gene family proteins
RNA	ribonucleic acid
ROI	region of interest
ROR α	retinoid-related orphan receptor alpha
ROR γ t	retinoid-related orphan receptor gamma-t
rpm	revolutions per minute
RPMI	Roswell park memorial institute
S1P	sphingosine-1-phosphate
S1PR	sphingosine-1-phosphate receptor
SA	streptavidin
SI	small intestine
SILT	solitary intestinal lymphoid tissues
SLT	secondary lymphoid tissue
ST2	interleukin-33 receptor
T-bet	T-box transcription factor
TCR	T-cell receptor
TF	transcription factor

Tfh	T follicular helper
TGFβ	transforming growth factor β
Th	T helper
TLR	toll like receptor
TM	Thermolysin medium concentration
TNF	tumour necrosis factor
TRAIL	tumour necrosis factor-related apoptosis-inducing ligand
Treg	T regulatory cell
TrN	triple negative
trNK	tissue-resident natural killer cell
TSLP	thymic stromal lymphopoietin
UC	ulcerative colitis
UV	ultraviolet
VC	vehicle control
VCAM-1	vascular cell adhesion molecule
WT	wild type

Chapter 1. INTRODUCTION

1.1 THE IMMUNE SYSTEM

The immune system is the body's mechanism for dealing with the invasion of harmful microorganisms, termed pathogens, preventing them from causing disease. Barrier sites such as the lung, gastrointestinal tract and skin provide the first line of defence against pathogen entry, with a physical and chemical barrier, involving the production of anti-microbial proteins and mucins (1-3). These barrier sites are constantly exposed to a variety of pathogens but are also colonised by commensal bacteria, which whilst helping protect against pathogens under certain conditions may themselves become pathogenic (4). The immune system evolved to discriminate between pathogenic and non-pathogenic microorganisms, achieved by the development of a two sided immune system, the innate and adaptive (5, 6). The innate immune system is the first response to pathogen invasion, detecting non-self/danger signals, with a plethora of cells being recruited to the point of entry to combat infection (6). Under certain circumstances this initial response alone, is insufficient in the eradication of pathogens, in which the adaptive response is then involved to effectively combat pathogen invasion in an antigen-specific manner (5, 7, 8). Adaptive immunity also possesses the ability to develop memory, which upon pathogen re-invasion activates a quick response and a faster clearance of infection (9).

A key factor in the development of an effective immune response is the regulation of the migration and/or retention of innate and adaptive immune cells. This enables the recruitment of innate immune cells to the site of infection followed by the induction of adaptive immunity.

1.2 THE INNATE IMMUNE SYSTEM

1.2.1 Recruitment of innate immune cells to the site of infection

Pathogen invasion, through penetration of the protective epithelial cell barrier, requires the initiation of a quick response to control and prevent pathogen dissemination. Leukocytes residing within the tissue at the area of infection are principal for an effective localised immune response, which is controlled by the cells of the innate immune system.

Barrier sites contain innate monocyte-derived macrophages and dendritic cells (DCs) which contribute to the initial line of defence, recognising microbial ligands via pathogen recognition receptors (PRRs) (1, 2, 10-12). These cells aid pathogen clearance via the process of phagocytosis alongside the production of cytokines and chemokines initiated by the activation of specific PRRs called toll like receptors (TLR) (10, 12-17). Cytokines and chemokines are both small soluble proteins which elicit their effects by binding to their specific receptors on other cells (10, 12, 17). Cytokines act in an autocrine or paracrine manner, affecting the behaviour of cells, either by suppressing or enhancing their activation level, whereas chemokines are important in driving the directional migration of cells towards highly concentrated chemokine areas (18, 19). TLR driven activation of innate immune cells results in their release of chemokines, such as C-C motif Chemokine Ligand (CCL) 2, driving the recruitment of innate immune cells such as neutrophils, natural killer (NK) cells, monocytes and DCs towards the site of infection, aiding pathogen clearance (20, 21). Production of the cytokines interleukin (IL)-1 β , tumour necrosis factor (TNF)- α and IL-12, also produced by epithelial cells, are important in the activation of the vascular endothelium, aiding cell recruitment and activating lymphocytes, such as NK cells (2, 22-24). Innate lymphoid cells (ILCs) are also described as an

innate population residing at barrier sites that contribute to the early innate cell cytokine production and therefore the regulation of pathogen clearance (25-28). Efficient pathogen clearance relies on macrophages and DCs to recruit innate cells to the site of infection, driving inflammation.

1.2.2 Migratory properties of the innate immune system

Innate cells are mainly located within barrier sites and it is now understood that some populations are completely tissue-resident, including tissue-resident macrophages that remain within the tissue throughout the immune response (29). These cells are important in the rapid recruitment of innate lymphocytes, such as neutrophils, from the blood into certain tissues (29). In addition to DCs function in driving the clearance of pathogens via phagocytosis within the inflamed tissue, they are able to uptake, process and present antigen via the major histocompatibility complex (MHC) (11, 30-32). Within the infected tissue, combined TNF- α and TLR stimulation drives DCs to develop into a mature phenotype, polarizing MHC-peptide expression to the plasma membrane and the upregulation of co-stimulatory molecules cluster of differentiation (CD) 80 and CD86 (31-33). The role of co-stimulatory molecules in the activation of the adaptive immune system will be discussed later. DC maturation is further accompanied by the downregulation of chemokine receptors associated with tissue-residency and upregulation of C-C chemokine receptor (CCR) 7, which enables mature DCs to become a migratory population (34, 35). This maturation process of tissue-resident DCs into mature migratory antigen presenting cells (APCs), enables them to leave the site of infection via the lymphatics and migrate into draining secondary lymphoid tissue (SLTs) with processed antigen from the site of infection. This maturation is key to the activation of the adaptive immune response.

1.3 THE ADAPTIVE IMMUNE SYSTEM

Activation of the adaptive immune system is required to mount a sufficient antigen-specific response to resolve infection, with a lack of adaptive immunity leading to a fatal outcome upon pathogen exposure (7, 8). The adaptive immune system comprises of T cells and B cells which, unlike innate immune cells, express the antigen specific receptors T cell receptor (TCR) and immunoglobulin (Ig) B cell receptor respectively (5, 36). This enables the development of a response specific to the invading pathogen. During cell development the receptor undergoes somatic gene recombination, which gives rise to a multitude of receptors on individual cells, specific to a range of pathogens (36, 37). This mechanism of specific receptor domain rearrangement is dependent on recombination activation genes (RAG) 1 and RAG2 (36-38). These genes have been targeted in murine models to study the immune system, creating RAG deficient mice which lack adaptive immunity (36-38). The antigen specificity of T and B cells enables a tailored immune response separating adaptive immunity from innate, which instead responds in a similar manner independent of the invading pathogen. Whilst B cell activation and development is required for the production of antigen specific Ig release and the resolution of inflammation, the pathway involved in the activation of T cells will be focused on throughout this report.

1.3.1 T cells

T cells are subdivided into multiple groups based on their phenotype and functional contribution to the immune response. The TCR is comprised of two glycoproteins chains, either α and β chains ($\alpha\beta$ TCR) or γ and δ chains ($\gamma\delta$ TCR) (39). The majority of T cells are $\alpha\beta$ T cells, which are abundant in SLTs (6). This is compared to $\gamma\delta$ T cells which are fewer and mainly

reside at epithelial and mucosal barrier sites, possessing innate abilities blurring the lines between the innate and adaptive responses (6, 40). Within both $\alpha\beta$ and $\gamma\delta$ T cells the TCR is associated with the CD3 module, termed the TCR-CD3 complex, which is paramount in the efficient transduction of TCR signalling and T cell activation (41). The TCR-CD3 complex only recognises cognate antigen when presented by MHC, in which there are two subsets, MHC class I (MHCI) and class II (MHCII) (39, 42-44). $\alpha\beta$ T cells can be further subdivided based on their expression of the accessory receptors CD4 and CD8 (42, 45). Both CD4⁺ and CD8⁺ T cells are activated by their TCR-CD3 complex initiating their development into effector T cells eliciting their functions immediately, or their development into memory T cells which upon pathogen re-encounter can rapidly produce an antigen specific response (45). CD8⁺ T cells are the cytotoxic branch of the $\alpha\beta$ T cell subset, able to recognise peptide presented by MHCI and function in the protection against intracellular bacteria, viruses and tumorigenic cells (44). Cytotoxic CD8⁺ T cells elicit their functions through the release of interferon- γ (IFN- γ), TNF- α , cytotoxic granules and are able to signal through the TNF family proteins, inducing cell death (42, 45, 46). CD4⁺ T cells, however, do not function as cytotoxic cells and are referred to as T helper (Th) cells, restricted to activation via MHCII (42). Upon recognition of the MHCII-antigen complex naïve CD4⁺ T cells develop into mature effector T cells and elicit their functions by producing effector cytokines, contributing to regulating the immune response (42, 47).

1.3.2 Activation of the adaptive immune system

Naïve T and B cells are highly migratory populations, recirculating through the blood and SLT (48). T cells migrate through SLT in search of processed antigen presented via MHC (44, 48). Processed antigen can be presented by MHCII on APCs such as DCs, which as discussed earlier,

mature within the site of infection developing the ability to migrate and leave via the lymphatics (31-33). Due to the low frequency of TCRs that are specific to the invading pathogen, and the small number of APCs expressing specific cognate antigen, the probability of TCR recognition of MHCII-antigen is low (9). To overcome this APCs are directed to SLT, such as the lymph node (LN) in which naïve T cells recirculate, increasing the chance of TCR:MHCII-antigen interactions between naïve T cells and APCs (9). This emphasises the importance of the migratory properties of innate immune cells to link these two sides of the immune system. LNs are vascularised structures with direct drainage from the lymphatic system providing a niche microenvironment in which circulating naïve T cells from the blood and innate APCs, from the draining peripheral tissues, become concentrated and their interactions facilitated (49). The blood and lymphatics provide a constant influx of lymphocytes to the LN, which are segregated upon entry into T cell zones and B cell follicles (49-51). This is tightly controlled by the stromal network producing key chemokines such as CCL19, CCL21 and C-X-C motif ligand (CXCL) 13, controlling lymphocyte entry and migration to specific zones (49-52). Naïve T and B cells are thought to spend up to 12 hours and 24 hours, respectively, scanning the LN for cognate antigen, in which they leave the LN and re-enter the circulation if none is found (53). Upon antigen encounter within the LN a series of steps occurs leading to the activation of the naïve T cells via the TCR.

1.3.3 CD4⁺ T cell Activation

Activation of naïve CD4⁺ T cells is a well-regulated multi-step process which requires the TCR on naïve CD4⁺ T cells to recognise and bind MHCII-antigen complex on APCs (54). This interaction alone stimulates the naïve T cell out of a quiescence phase, however, is insufficient for the effective generation of mature effector T cells, which requires further stimulation

through co-stimulatory molecules expressed on mature APCs (55-57). The receptor CD28 is constitutively expressed on naïve T cells and post TCR:MHCII-antigen interactions binds to its ligands CD80 and CD86 on mature APCs initiating T cell proliferation, IL-2 production and cell survival (55-57). As a regulatory mechanism, cytotoxic T lymphocyte-associated molecule-4 (CTLA-4) is upregulated on T cells post activation and competes with CD28 (58, 59). This controls and limits the proliferation process of T cells, stopping the immune response when appropriate (58, 59). CD28 co-stimulation is not the only, although is the most robust, manner in which T cell activation is assisted. Signalling through CD28 regulates the expression of other co-stimulatory molecules expressed on activated T cells including inducible co-stimulatory (ICOS), tumour necrosis factor receptor superfamily, member 4 (OX40) and CD40L (54, 55, 57). ICOS binds to ICOS ligand (ICOSL) which can be expressed on immune and stromal cells, promoting survival, proliferation and maturation of T cells (60-62). The expression of OX40 ligand (OX40L) is induced on APCs, with OX40:OX40L interactions, in conjunction with CD28:CD80/86 stimulations, elongating proliferation of activated T cells and promoting cytokine production (63, 64). CD40, the receptor for CD40L is expressed on B cells with these interactions promoting B cell survival and maturation alongside the formation of germinal centres, required for the effective development of B cells and their antibody response (65, 66).

1.3.4 Effector T helper cells

Efficient activation of naïve CD4⁺ T cells via TCR:MHCII-antigen and co-stimulatory interactions, leads to the differentiation into effector Th cells which are subdivided into different subsets based on their expression of transcription factors (TF) and cytokine production (47). Pioneering work profiling effector T cells, initially identified two subsets Th1

and Th2 cells, with Th1s expressing the T-box TF (T-bet) producing IFN- γ and TNF- α and Th2s being GATA binding protein 3 (GATA-3)⁺ and producing the cytokines IL-4, IL-5, IL-9 and IL-13 (47, 67). The differentiation of Th cells is determined by multiple factors including cytokine signalling and strength of TCR interactions, which are regulated by the type of pathogen invasion (47, 68, 69). Th1s are induced under IFN γ , IL-2 and IL-12 signalling and the effector cytokines produced are involved in immune responses against intracellular pathogens, including bacteria and viruses (69-71). Th2s cytokine production is important in the expulsion and protection against helminth infections, with their differentiation and function being driven by IL-4, IL-33, IL-25 and thymic stromal lymphopoietin (TSLP) (68, 69, 72-74). In addition to the protective roles of these Th cells, they have also been associated with disease development, including multiple sclerosis and rheumatoid arthritis by Th1s and allergic responses and atopic diseases by Th2s (47, 75, 76). Following the discoveries of Th1 and Th2 cells, the identification of additional subsets was discovered, including Th17 cells, T regulatory cells (Tregs), T follicular h (Tfh) cells and the more recently described Th9 cells (47, 68). The TF retinoic acid receptor-related orphan receptor- γ t (ROR- γ t) drives Th17 cell development and the production of IL-17A, IL-17F and IL-22, which are important in the clearance of extracellular pathogens (77-79). Tregs are involved in the suppression and control of the immune response through different mechanisms. For example, they use inhibitory receptors and produce anti-inflammatory cytokines including IL-10, and transforming growth factor β (TGF β), alongside IL-35, regulating the proliferation of antigen-stimulated T cells, including to self-antigen (80-82). The development and function of Tregs depends on the expression of the TF forkhead box P3 (Foxp3) and in addition to differentiating from naïve CD4⁺ T cells within the periphery, Tregs also develop within the thymus which are termed natural Tregs (82, 83).

Tfh cells are important in the development of the humoral B cell response. They are required for the maturation and function of germinal centres which are paramount for B cell affinity maturation and survival signals to developing B cells (84-86). As discussed, IL-9 is a cytokine related to Th2 cells and is involved in stimulating the production of mucus and activation of innate immune cells (87-89). However, recent publications have identified a separate source of IL-9 by Th9 cells which require TGF- β and IL-4 signalling for their development, either directly from naïve T cells or from Th2 cells (88, 90, 91).

Upon development and expansion of the effector CD4⁺ Th cell populations, which takes about 2 days, clearance of infection is dependent on the migration of particular Th cell subgroups to the inflamed tissue (9, 47). Th cells leave the LN via the lymphatics and enter the blood travelling to the site of infection (9). Post infection, the majority of effector Th cells die, however some develop into memory T cells which migrate within the blood and non-lymphoid tissue in a similar manner to Th cells (9). Memory T cells are crucial in the efficient induction of adaptive memory responses upon pathogen re-invasion (9). Furthermore, within recent years tissue-resident memory T cells have also been identified, contributing to the quick response against reinvading pathogens at the site of infection (92-94).

There is clear evidence that effector populations can switch function and fate indicating plasticity. Th17 cells can adopt the characteristics of Th1s, producing both IL-17 and IFN- γ (95, 96). In some situations, Th17s can fully convert from their original subset into Th1s, as demonstrated by Hirota et al., through the use of fate mapping cells (95). Under experimental autoimmune encephalomyelitis Th17 cells downregulated their expression of ROR γ t and

upregulated T-bet enabling their production of IFN- γ and their shut off of IL-17 production becoming ex-Th17 cells (95).

1.4 INNATE LYMPHOID CELLS

ILCs are a recently classified subgroup of innate immune cells which are distributed throughout the body in lymphoid and non-lymphoid tissues (97). ILCs share similarities with effector Th cells in their ability to produce effector Th cytokines upon activation and their developmental pathways, with both differentiating from common lymphoid progenitors (CLP) in an IL-2 dependent manner (98-102). However, ILCs are a distinct population of lymphocytes, separate to T cells and were originally identified based on their lack of lineage marker expression, differentiating them from common innate cells (25, 103). Furthermore, their effector Th cytokine production occurs within the early innate stages of pathogen infection, compared to the later adaptive Th cell response (25, 28, 97, 103, 104). Confirming that ILCs are not part of the adaptive immune response, the lineage negative population were still functionally present and able to produce effector cytokines upon stimulation in *Rag*^{-/-} mice (25, 103, 105-108). This also shows that ILCs are not dependent upon the RAG recombinase complex to generate antigen specific receptors. Instead it was discovered that ILCs typically rely on soluble factors produced by cells such as myeloid cells and epithelial cells, for their activation and function (97, 109).

ILCs ability to rapidly produce effector cytokines alongside their positioning at barrier sites makes them an important early source of Th cytokines, upon pathogen invasion (25, 103). ILCs are now an established population with their functions being defined in multiple tissues contributing to the clearance of pathogen invasion, regulation of commensal microorganisms,

repair of damaged tissue and maintenance of epithelial barriers (26, 28, 97, 104, 108, 110, 111). However, dysregulated ILC cytokine production has also been linked to the development of particular inflammatory diseases (104, 112).

Effector Th cytokine production by ILCs enables them to be divided into subgroups similar to Th1s, Th2s and Th17 cells. According to their cytokine profile and TF expression ILCs are classified into group 1 ILCs, group 2 ILCs and group 3 ILCs (101). Recently a fourth subset of ILCs has been proposed, named regulatory ILCs (ILCregs), however, these are only described in one publication and remain controversial within the literature (113).

1.4.1 Group 1 ILCs

Group 1 ILCs are identified according to their expression of the TF T-bet and their ability to produce the cytokines TNF- α and IFN- γ upon stimulation, similar to effector Th1 cells (108, 114). Group 1 ILCs are further subdivided into conventional natural killer (cNK) cells and innate lymphoid cell group 1 (ILC1) (28, 101). cNK cells were initially identified in 1975 as an innate lymphocyte population that were similar to cytotoxic T cells, with the ability to travel within the blood, surveying and killing tumour cells and viral or intracellular bacterial infected cells (115-117). However, cNK cells do not respond in an antigen specific manner and can be activated via cell surface receptors, such as the natural cytotoxic receptor (NCR) NKp46 (118). This is why upon recent ILC nomenclature, cNK cells have been classified within this group (101). cNK cells elicit their cytotoxic abilities through the release of perforin and granzymes alongside the expression of the TNF-related apoptosis-inducing ligand (TRAIL) (115, 118-125). Additionally, cNK cells release IFN- γ and TNF- α which have anti-viral, -tumour and -bacterial functions such as stimulating macrophage phagocytosis (23, 24, 126). Due to the cytotoxic

capability of cNK cells, they are classified separately from other ILCs as cytotoxic ILCs, with the remaining ILCs, across all other groups, being termed helper ILCs (28, 101). A distinct feature of cNK cells, compared to ILC1s, is the expression of eomesdermin (EOMES) which is required for their development and function and subsequently is used in the discrimination of cNK (EOMES⁺ T-bet⁺) cells from ILC1s (EOMES⁻ T-bet⁺) (27, 127, 128). In addition, ILC1 development is dependent on IL-7 signalling, with IL-7 being redundant in the development of cNK cells (27, 128). IL-7 dependency is a common factor amongst all helper ILCs, therefore expression of IL-7 receptor α (IL-7R α) is used as a hallmark in the identification of Lineage⁻ helper ILCs (27, 28, 101). Similar to cNK cells, stimulation of NKp46 on ILC1s upregulates TRAIL expression and the ability to induce cell apoptosis on cells expressing TRAIL receptors (124, 129). Further to NKp46, depending on their function and location, ILC1s can be activated by IL-12, IL-18 or IL-15 to produce their effector cytokines including IFN- γ and TNF- α (104, 129-132). The identification of cNK and ILC1 subsets is currently being developed in the group 1 ILC field, with different ILC1s being identified within the salivary glands and liver (133). cNKs functions are well described within the literature, partly due to their early discovery (134). The recent identification of ILC1s, as a distinct population from cNK with a similar cytokine profile and innate ability, raises the possibility that ILC1s may contribute to the previously described functions of cNK cells. With the current ability to identify cNK cells and ILC1s separately, through TF expression, further research is required into the specific functions of ILC1s and cNK cells to determine whether they elicit distinct or combined effects (135).

1.4.2 Group 2 ILCs

Innate lymphoid cell group 2 (ILC2s), before the establishment of a uniformed nomenclature, were initially identified as a variety of cells termed nuocytes, natural helper cells and innate helper 2 cells (25, 102, 103). Albeit having different names, all cell populations were identified within the same year on their basis of lacking lineage markers, producing an innate source of Th2 cytokines, being activated by IL-25 and IL-33 and providing protection against helminth infections (25, 102, 103). These publications were central in the establishment of ILCs as a separate population to Th cells, with ILC2s being able to produce IL-13 in the early innate phases of the immune response to helminths in the absence of an adaptive immune system (25, 103). Nuocytes, natural helper cells and innate helper 2 cells were later classified into one group with their development and maintenance being dependent on the TF GATA-3 and signalling through the IL-7R α (25, 102, 103, 136). More recently, alongside IL-25 and IL-33, TSLP, produced by epithelial cells, has also been identified as another cytokine important in the activation of ILC2s (25, 103, 112). ILC2s have further been subdivided into two groups based on their sensitivity to IL-25 and IL-33 (108). IL-25 sensitive ILC2s, which lack the IL-33 receptor (ST2), termed inflammatory ILC2s (iILC2s), express high levels of killer-cell lectin like receptor G-1 (KLRG1), and although barely detectable in the lung under steady state, their proliferation is increased upon IL-25 but not IL-33 stimulation (108). Comparatively, natural ILC2s (nILC2s) are found in the steady state lung and are responsive to IL-33 rather than IL-25 (108). Upon helminth infection, iILC2s expand within the lung prior to nILC2s, providing the main source of IL-13, upregulating ST2 expressing and developing into a nILC2 phenotype (108). In addition to the production of interleukins, ILC2s also elicit their functions through the

release of epidermal growth factor amphiregulin, which is important in the maintenance and repair of epithelial barriers (110).

1.4.3 Group 3 ILCs

Innate lymphoid cell group 3 (ILC3s) are similar to effector Th17 cells in that they express the TF ROR γ t and produce the cytokines IL-22 and/or IL-17A (108, 114). The first subgroup of ILC3s discovered were lymphoid tissue inducer cells (LTi cells), which are located within the embryo and are paramount in the organogenesis of LNs (111, 137, 138). Before the identification and classification of ILCs, ROR γ t⁺ NKp46⁺ innate immune cells were identified to produce IL-22 within the gut (26, 105). These cells were classified as a separate population to cNK cells and T cells on the basis of lacking cNK cell effector functions, CD3 expression and their successful development and identification in *Rag*^{-/-} mice (26, 105). The development and function of ROR γ t⁺ NKp46⁺ cells was dependent on the presence of intestinal commensal bacteria, with germ free mice lacking ROR γ t⁺ NKp46⁺ cells (26, 105). Such cells are now confirmed as ROR γ t expressing ILC3s that lack lineage markers associated with common innate immune cells and adaptive immune cells (130, 139).

ILC3s can be further grouped based on their expression of CCR6 and NKp46, including NKp46⁻ CCR6⁺ LTi-like cells, NKp46⁺ CCR6⁻ NCR⁺ ILC3s and NKp46⁻ CCR6⁻ NCR⁻ ILC3s (130, 139). Interestingly, ILC1s are not the only ILC subgroup that depend on T-bet for their function. NCR⁺ ILC3s also depend on T-bet and are absent in T-bet deficient mice (130). This joint expression of T-bet and ROR γ t enables them to also produce IFN- γ in response to IL-12 (127, 130). Although all group 3 ILCs can be stimulated by IL-23, LTi-like cells are able to produce IL-17 and IL-22, compared to NCR⁺ and NCR⁻ ILC3s which both produce IL-22 (139).

1.4.4 Regulatory ILCs

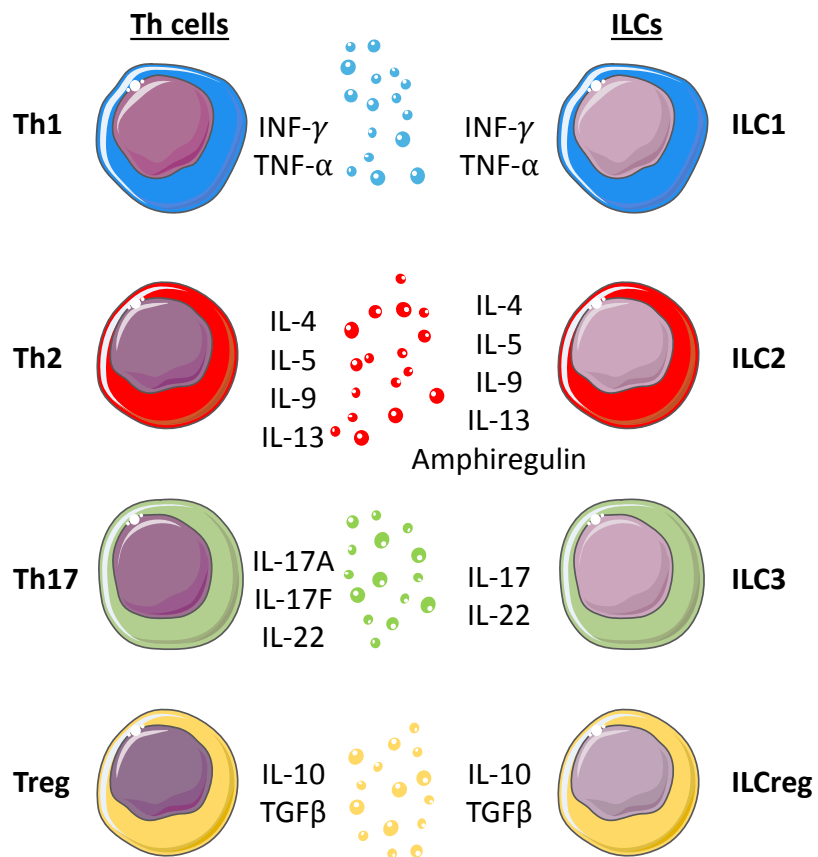
Since the definition of a universal nomenclature in 2013, the functional relevance of ILCs has been explored in multiple tissues under homeostatic and inflammatory conditions (101). More recently, in 2017, a fourth ILC subset was proposed, termed ILCregs (113). ILCregs were described as negative for lineage markers but express IL-7R α and deoxyribonucleic acid (DNA) binding protein inhibitor 2 (Id2), defining them as ILCs and are identified through the production of IL-10 (113). ILCregs were shown not to express any typical ILC TF such as T-bet, GATA-3 or ROR γ t and were therefore identified as a distinct subgroup from ILC1s, ILC2s and ILC3s (113). ILCregs share similarities with Tregs as upon stimulation they produce TGF β and IL-10, yet ILCregs lack Foxp3 expression (113). ILCregs respond to TGF β in an autocrine manner and are suggested to play a role in the regulation of inflammation, directly suppressing ILC1 and ILC3s (113). In the same year, IL-10 production was also linked to IL-33 responsive ILC2s within the lung, involved in reducing the chronic papain dependent recruitment of eosinophils (140). Currently the source of IL-10 production by ILCs is under debate within the literature and further research into this area is required. A summary of ILC and Th cell subgroups and their cytokine expression is shown in Figure 1.1.

1.4.5 ILC Plasticity

The establishment of a uniformed nomenclature facilitates the clear identification of ILC subsets based on their TF and cytokine profile. However, similar to Th cells, ILCs possess a level of plasticity and dependent on environmental stimuli, appear to be able to change their phenotype, including TF expression and cytokine profile and function, shifting from being identified in one subgroup to another (141-143). The shift in TF expression usually results in

Figure 1.1. Th cell and ILC subsets and cytokine production

Th cells, on the left hand side and ILCs, on the right hand side, are subdivided into different subgroups based on their expression of cytokines. Th1 and ILC1s both express IFN- γ and TNF- α , Th2 and ILC2s both produce the type 2 cytokines IL-4, IL-5, IL-9 and IL-13. ILC2s further possess the ability to release amphiregulin. Th17 and ILC3s are able to release IL-17 and IL-22 upon activation and Tregs alongside the newly suggested population of ILCregs produce IL-10 and TGF β .



the ILC changing their cytokine production to that driven by the TF, however, a change in TF expression doesn't always amount in a change of cytokine production, with ILC3s production of IL-17 and IL-22 being unaffected by inhibition of ROR γ t (144). NCR⁻ ILC3s can upregulate T-bet expression and co-express ROR γ t and T-bet, enabling the production of IFN- γ (130, 141). NCR⁺ ILC3s are further able to downregulate ROR γ t becoming ROR γ t⁻ T-bet⁺ NCR⁺ ILC1s (ex-ILC3s) shown by Vonarbourg et al., using genetically tagged ILC3s (141). This plasticity is dependent on the microbiota, which stabilises ROR γ t expression for the development of NCR⁺ ILC3s from NCR⁻ ILC3s, and the absence of IL-7 signalling enabling the downregulation of ROR γ t and therefore development into ex-ILC3s (130, 141).

Similar to ILC3s, ILC2s also possess the ability to acquire an ILC1 phenotype (142). During viral infections ILC2s are able differentiate into an ILC1 phenotype, with IL-12 and IL-18 driving the downregulation of GATA-3 and upregulation of T-bet, alongside the ability to produce IFN- γ (142). However, direct fate cell mapping specific to ILC2s has not been used to show direct evidence of cellular conversion. ILC1s are the dominant ILC subset involved in the clearance of viral infections, potentially explaining the conversion of ILC2→ILC1s (142). Under certain conditions dysregulated ILC2 differentiation into ILC1s is believed to play a role in the development of chronic obstructive pulmonary disease, with an increase in ILC1s correlating with disease severity (142).

1.5 ILC DEVELOPMENT

ILC development occurs within the foetal liver during embryonic development and within the bone marrow (BM) in adults (136, 145, 146). Similar to T and B cells they arise from the CLP, which differentiate from multipotential hematopoietic stem cells, then undergo several

developmental stages before complete maturation (97, 127). Nuclear factor IL-3 regulated (NFIL3) and inhibitor and Id2, which is regulated by NFIL3, are required alongside IL-7 to promote the differentiation of CLPs into $\alpha 4\beta 7^+$ α -lymphoid precursors (α -LP) (25, 97, 127, 147-150). Id2 is essential for the development of all ILCs via inhibiting the TFs E proteins that are required for the development of T and B cells (102, 136, 145, 149, 151-154). This drives the commitment of the α -LP to an ILC lineage (102, 136, 145, 149, 151-154). α -LP differentiate into early innate lymphoid progenitors (EILP) which under IL-15 signalling upregulate EOMES and commit to the EOMES⁺ pre-NK progenitor lineage, before their development into mature EOMES⁺ T-bet⁺ cNK cells (128, 131, 149, 155, 156). EILP that do not commit to the cNK lineage depend on GATA-3, which drives the upregulation of IL-7R α , for differentiation into the common helper innate lymphoid progenitor (CHILP) committing the lineage fate to all helper ILCs (127, 136, 151, 157). GATA-3, although associated with ILC2s, is required for the development of all helper ILC subsets, with conditional knock outs deficient in GATA-3 expression in hematopoietic stem cells, lacking the development of helper ILCs (136, 151, 157). The maturation of CHILP into innate lymphoid cell precursor (ILCP) via the upregulation of the TF promyelocytic leukaemia zinc finger (PLZF) commits the development of ILCPs into ILC1s, ILC2s and NCR⁻ ILC3s only (98, 127). Similar to cNK cells, the development of LT_i-like cells occurs from a higher developmental stage and differentiates from CHILP rather than ILCP. ILCP and CHILP both follow similar developmental pathways to give rise to LT_i-like cells and NCR⁻ ILC3s, respectively, with both pathways being dependent on IL-7R α signalling alongside expression of ROR γ t and the aryl hydrocarbon receptor (AHR) (127, 137, 141, 155, 158). As discussed, the upregulation of T-bet in NCR⁻ ILC3s results in their differentiation into NCR⁺ ILC3s (130, 141). Differentiation of ILCPs into ILC1s or ILC2s is driven by IL-15 or IL-7 signalling,

respectively (127, 136, 156, 159). ILC1 development depends on the upregulation of T-bet whereas ILC2s require the combined upregulation of GATA-3 and retinoid-related orphan receptor α (ROR α) alongside Notch signalling to develop into mature ILC2s (127, 136, 156, 159). ILCs developmental pathway is summarised in Figure 1.2.

1.6 FUNCTIONS OF ILCs

ILCs function through a range of mechanisms within lymphoid and non-lymphoid tissues. ILCs rapid production of cytokines was important in the identification and classification of ILCs, within earlier studies and elicits many of their functions in a similar manner to Th cells (25, 104, 105). More recent publications have additionally attributed their mechanism of action to their expression of cell surface proteins. LT α cells and LT α -like cells express lymphotoxin (LT) $\alpha_1\beta_2$, which interacts with cells expressing the LT β receptor (LT β) R (111, 160, 161). Furthermore, subsets of ILC2s and ILC3s express MHCII which augments their interactions with the antigen specific TCR:CD3 complex on T cells, providing a direct mechanism of regulating the adaptive immune system (162-164). Under healthy conditions ILCs in these areas are able to support the normal function of tissues, however, upon dysregulation ILCs have also been associated with inflammatory diseases (28). The role of ILCs in the regulation and protection of non-lymphoid and lymphoid tissue will be discussed below.

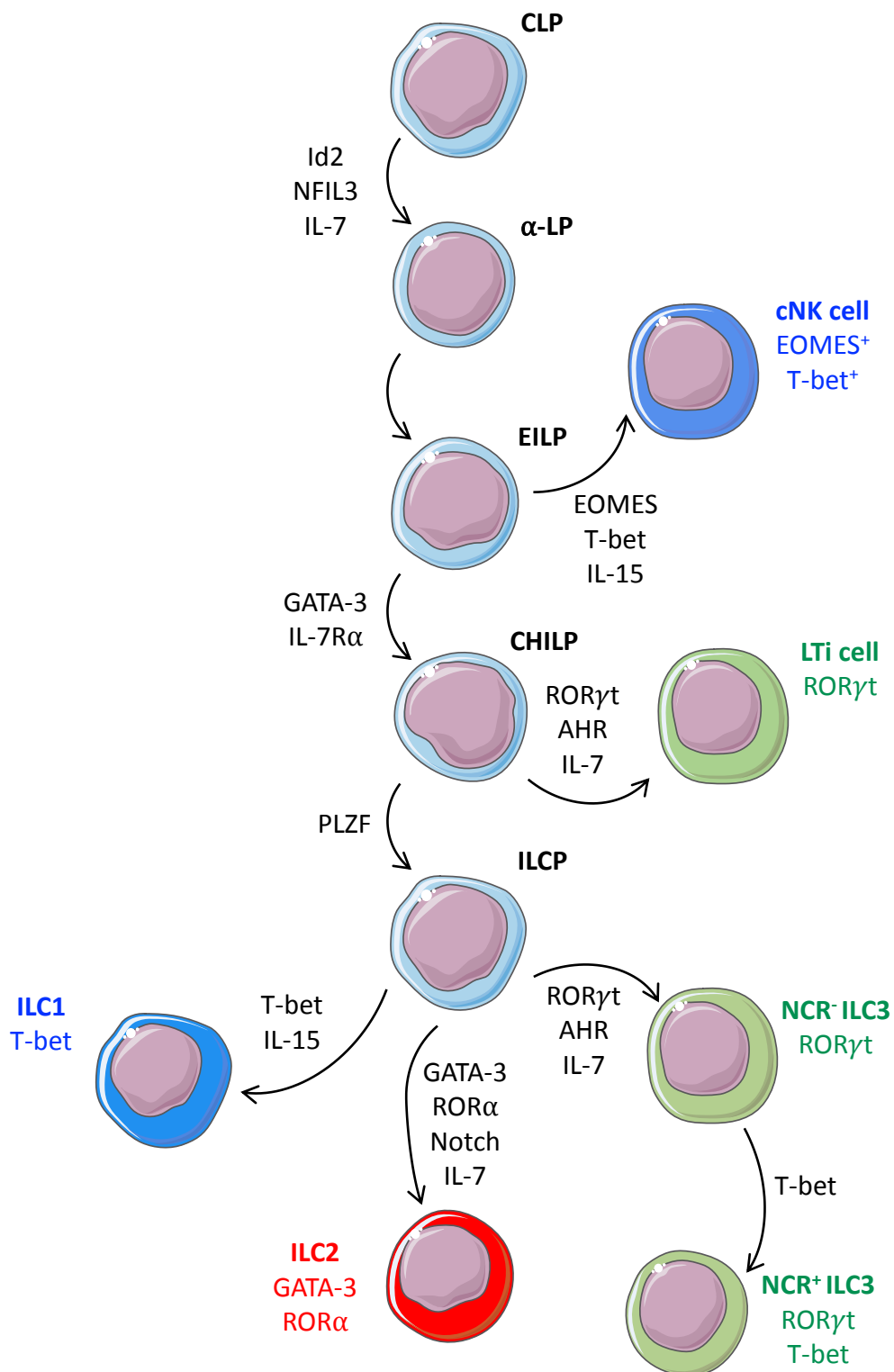
1.6.1 Gastrointestinal tract

The gastrointestinal tract is the largest mucosal barrier and has developed alongside commensal bacteria to allow the absorption of nutrients from the diet whilst preventing the unwanted invasion of pathogens (2). The gut is lined with a number of specific lymphoid structures including Peyer's patches (PP), which develop before birth, and solitary intestinal

Figure 1.2. ILC Development

ILC development occurs within the BM developing from the CLP. Upon IL-7 signalling and upregulation of NFIL3 and Id2 the CLP develops into the α LP and subsequently the EILP which is committed to the ILC lineage. EILP upregulate EOMES and T-bet in an IL-15 dependent manner to develop into cNK cells, whereas IL-7 signalling and GATA-3 expression drives the development of the CHILP. Upregulation of ROR γ t, AHR and IL-7 signalling drives the development of LT α i cells. This is similar for the development of NCR $^{-}$ ILCs, which initially requires CHILP to upregulate PLZF differentiating into an ILCP. NCR $^{-}$ ILC3s are able to upregulate T-bet expression driving the expression of NKp46 becoming an NCR $^{+}$ ILC3s. The ILCP finally gives rise to both ILC1s, which required IL-15 stimulation and T-bet expression and ILC2s which development requires GATA-3, ROR α , Notch and IL-7 signalling.

Diagram adapted from Serafini et al., (127).



lymphoid tissues (SILT) which develop after birth (165). SILTs consist of small cryptopatches (CP) and isolated lymphoid follicles (ILF) which largely comprise of LT α i-like cells (165). LT α i-like cells are also found outside SILTs within the lamina propria (LP), however NCR $^{+}$ ILC3s are more abundant within these areas (26, 105). All ILC3s are important producers of IL-22, which within SILTs, promotes the growth and proliferation of intestinal stem cell (ISC) niches which maintain a normal epithelial integrity post epithelial damage (166, 167). This was demonstrated by the absence of ILC3, in ROR γ t deficient mice, resulting in augmented damage within the intestine in response to i.p administration of methotrexate (167). Within the LP ILC3s production of IL-22 promotes a protective role against extracellular bacteria by promoting epithelial cell release of anti-microbial peptides (26, 168). Early production of IL-22 in *Citrobacter rodentium* infections, promotes the production of the anti-microbial regenerating gene family proteins, (Reg)III β and RegIII γ , aiding clearance of infected mice and repair after epithelium damage (169-172). IL-22 production by ILC3s is controlled by IL-23, with recognition of microbial ligands stimulating the release of IL-23 by macrophages and DCs, regulating ILC3 function (173-175). Alongside the clearance of pathogens, ILC3s production of IL-22 plays a role in the regulation of commensal bacteria (162, 176). The removal of ILCs in *Rag1* knock out ($^{-/-}$) mice resulted in the peripheral propagation of commensal bacteria, to areas such as the spleen and liver, resulting in systemic inflammation (176). Administration of IL-22 reduced bacterial load within these sites, suggesting that ILC3s production of IL-22 may prevent commensal bacteria dissemination (176). However, these experiments were conducted in *Rag1* $^{-/-}$ mice, suggesting that ILC3s may play a redundant role in the presence of a functioning adaptive immune system (176). ILC3 production of IL-22 and LT α β $_2$ expression have also been shown by Goto et al., to induce fucosyltransferase 2 (Fut2) expression in

intestinal epithelial cells (168). Fucosylation results in the production of fucose which is important in the survival and maintenance of commensal bacteria, aiding the protection against *Salmonella typhimurium* (168).

Additional functions of ILC3s within the gut are dependent on specific mechanisms unique to different subsets. Alongside IL-22, LT α -like cells are able to produce IL-17 which also regulates extracellular pathogens by stimulating epithelial cells to produce and release anti-microbial proteins (177-179). Furthermore, LT α -like cells provide LT $\alpha_1\beta_2$ signals to ISCs contributing to the recruitment of B cells and DCs into ILFs, promoting the release of IgA required in the protection against mucosal pathogens (160, 180).

Cytokine production by ILC3s has already been suggested to play a role in suppressing the dissemination of commensal bacteria (176). Hepworth et al., discovered an additional role of NCR $^+$ ILC3s in regulating commensal bacteria by direct interactions with CD4 $^+$ T cells. (162, 163). NCR $^+$ ILC3s express high levels of MHCII and exhibit antigen processing and presenting abilities (162). Despite this, NCR $^+$ MHCII $^+$ ILC3s lack the co-stimulatory molecules, CD80, CD86 and CD40 and are consequently unable to stimulate naïve T cells through TCR:MHCII-antigen interactions (162). This results in TCR:MHCII-antigen interactions between CD4 $^+$ T cells and ILC3s, limiting the proliferation and expansion of CD4 $^+$ T cells that are specific to commensal bacteria as well as inducing cell death of activated commensal bacteria-specific T cells (162, 163). This was shown through the selective deletion of MHCII expression on ILCs resulting in an increase in CD4 $^+$ T cell proliferation and production of commensal bacteria specific IgG (162). This indicates a homeostatic role of ILC3s in the direct suppression of the adaptive immune response by preventing a CD4 $^+$ T cell response against commensal bacteria.

Alongside ILC3s, ILC2s are also important in the homeostasis of the gut (181). The epithelium under steady state produces IL-25 via tuft cells, maintaining a constant level of IL-13 production by ILC2s (181). Upon infection with *Heligmosomoides polygyrus*, tuft cell hyperplasia resulted in an increased production of IL-25, further activating ILC2s production of IL-13, aiding pathogen clearance (181). IL-4 production by ILC2s is also important in the expulsion of enteric helminth infections, contributing to the clearance of *Heligmosomoides polygyrus* infection in a manner independent of IL-2 signalling (182). Within the gut type 2 cytokines have been associated with the 'weep and sweep' process. IL-4, IL-5, IL9 and IL-13 have been shown to increase helminth expulsion through increasing goblet cell mucus production and by promoting intestinal smooth muscle contractions in conjunction with enteric nerve stimulation, resulting in the mechanical expulsion of worms (183, 184).

The recent identification of ILC1s as a distinct population from cNK cells means that their specific functions, separate to cNK cells, within inflammation are still currently being investigated (135). Upon infection with *Salmonella*, *Toxoplasma gondii* and *Clostridium difficile* ILC1s are suggested to be the main contributors of early IFN- γ production (27, 130, 185). It is, however, difficult to determine the individual roles of ILC1s, cNK cells and plastic ex-ILC3s contribution to IFN- γ production due to overlapping phenotypic markers. Klose et al., established the identification of an ILC1 subset distinct from cNK cells and ex-ILC3s, however when determining their functionality upon *Toxoplasma gondii* infection, due to the lack of transgenic mice solely lacking ILC1s, T-bet deficient mice were examined concluding that ILC1s provided protection against infection (27). Although *Tbx21*^{-/-} mice lack ILC1s, they also have reduced numbers of cNK cells and T-bet is required for the efficient production of IFN- γ and

development of NCR⁺ ILCs and ex-ILC3s, presenting a caveat to these findings (27, 130, 186). Within the gut, IFN- γ production provides protection against *Salmonella* infections, with exogenous administration of IFN- γ preventing death upon mice being challenged with a lethal dose of *Salmonella* (187). IFN- γ elicits its protective functions by playing an important role in the stimulation of other immune cells such as macrophages, enhancing their phagocytotic abilities (187, 188).

Under certain conditions the functional properties of ILCs can contribute to the development of inflammatory bowel disease (IBD). Inappropriate activation of ILCs can result in their unwanted production of cytokines, driving inflammation and autoimmunity. IBD affects around 2.5 million people and includes Crohn's disease and ulcerative colitis (UC) (189, 190). It can be caused by many genetic and environmental factors resulting in a dysregulated immune response leading to chronic inflammation of the gastrointestinal tract (189-191). Gastrointestinal ILCs have also been associated with the development of IBD with genome-wide association studies identifying genes related to ILCs, mainly the ILC3 subset, as a risk of loci for IBD, suggesting a role of ILCs in its pathogenesis (190).

The increased production of IFN- γ has been associated in many studies with the development of human Crohn's disease (192). It is currently under debate, within the field, as to the exact source of innate IFN- γ , with Crohn's disease patients having increased numbers of cNK cells and ILC1s (104, 193). To examine the role of ILC1s in Crohn's disease, the murine anti-CD40 IBD model was established in *Rag*^{-/-} mice, examining the innate contribution to development of disease (104). An increase in ILC1s and their production of IFN- γ was observed and the development of colitis was prevented upon blocking ILC1s with anti-NK1.1 (104). As discussed

previously the identification between ILC1s, ex-ILC3s, NCR⁺ ILC3s and cNK cells is blurred and anti-NK1.1 will also deplete these described cells (101, 104, 194). Furthermore, lacking adaptive immunity may exaggerate the contribution of ILCs (194).

ILC3s have also been implicated in the development of IBD, with increased production of IL-22 by ILC3s being detected in human IBD patients (195). Dysregulated production of IL-22 leads to the increase in the permeability of the intestinal epithelial barrier, a hallmark of IBD, resulting in decreased protection against pathogen invasion (168, 196). Powell et al., conclude that in *Rag2*^{-/-} mice lacking T-bet expression, *Helicobacter typhlonius* drives the development of UC in an ILC3 dependent manner (197, 198). Increased levels of IL-23 and DCs were shown to contribute to the activation of ILC3s and their production of IL-17 and IL-22, with *in vivo* blocking of these cytokines reducing the development of colitis (197, 198). Furthermore, within the murine UC model induced by anti-CD40 in *Rag*^{-/-} mice, ILC3s, in an IL-23 dependent manner, produce IL-22, with *in vivo* neutralisation of IL-22 protecting the mice from developing colitis (199). Although these studies both indicate a role for IL-22 producing ILC3s in the development of IBD, similar to the previous *in vivo* studies assessing ILCs role in IBD, *Rag*^{-/-} mice were used. As well as exaggerating the ILC response, it has been established that the homeostasis of ILCs is perturbed in *Rag*^{-/-} mice with increased numbers of ILC2, ILC3 and their respective cytokine production (106, 200). This is potentially due to the excess of cytokines, which would normally be involved in T cell proliferation and survival, such as IL-7, influencing ILCs (201, 202).

Another model of IBD, induced in *Rag*^{-/-} mice by *Helicobacter hepaticus*, is characterised by the IL-23 dependent production of IL-17 and IFN- γ by ILC3s (175). This study combines the

importance of ILC1 and ILC3 cytokine production in IBD, with ILC3s developing into an ILC1 phenotype, producing IFN- γ , but maintaining the ability to produce IL-17 (175). Although *Rag*^{-/-} mice are not the most appropriate model to assess IBD development by ILCs, these *in vivo* models do suggest that disturbances in ILC regulation and function may contribute to the development of chronic inflammation.

ILC1s and ILC3s both seem to play an important role in the development of inflammation via their production of IFN γ , IL-17 and IL-22. Interestingly, the new subgroup of ILCs, termed ILCregs, are shown to regulate intestinal inflammation (113). Inflammatory signals driven by the infection with *Salmonella typhimurium* and *Citrobacter Rodentium* induces ILCregs to produce TGF- β 1, which maintains their own expansion during inflammation, and the production of IL-10 (113). IL-10 suppresses the activation and cytokine production of ILC1s and ILC3s, protecting against the development of inflammation (113). As discussed previously, there is currently debate within the literature surrounding the source of ILC derived IL-10 and the functionality of these described ILCregs (140).

1.6.2 Lung

ILCs reside within the lungs of humans and mice, with ILC2 being the dominant subset playing a role in the repair and remodelling of damaged tissue (28, 110, 203). Under homeostatic conditions ILC2s contribute to the maintenance of the epithelial barrier, expressing multiple genes associated with tissue remodelling, including amphiregulin, which were comparatively not expressed in splenic ILC2s (110). Influenza viral infection elicits damage to the epithelium, resulting in the release of alarmins including IL-33, which in turn stimulates ILC2s production of amphiregulin (110, 204). Depleting ILCs with anti-CD90 resulted in a decrease in epithelial

integrity and an impairment in tissue remodelling, which was reversed upon administration of amphiregulin (110).

The initial descriptions of ILC2s identified that both nuocytes and innate helper 2 cells played a role in the expulsion of helminth infections from the lung (25, 103, 108). Helminths such as *Nippostrongylus brasiliensis*, stimulate epithelial cells, macrophages and DCs to produce IL-25 and IL-33, which in turn induces the recruitment, expansion and activation of ILC2s (108, 205, 206). Mice lacking IL-25 and/or IL-33 are unable to efficiently clear *Nippostrongylus brasiliensis* infections due to a decrease in ILC2s and therefore type2 cytokine production (25, 205). IL-13 production by ILC2s, is essential for the expulsion of helminth infections and it has been established, through the transfer of nuocytes into mice deficient in IL-4 and IL-13, that even if ILC2s are the only source of IL-13, helminth clearance still occurs (25). Even with ILC2s providing the main source of IL-13, effective expulsion is still dependent on the presence of the adaptive immune system, with *Rag2^{-/-}* mice being unable to clear infection, suggesting ILC2s interact directly or indirectly with T or B cells, promoting their production of IL-13 (25, 103). Lung ILC2s may communicate with T cells through the expression of MHCII (164). They possess the ability to uptake and process antigen *in vitro*, however, when cultured with T cells, were unable to elicit T cell proliferation (164). Other type 2 cytokines produced by ILC2s, such as IL-5 and IL-9, are important in the recruitment of eosinophils alongside IL-4 and IL-13 which contribute to the initial hyperplasia of goblet cells and therefore the increase in mucus production and effective expulsion of helminth infections (103, 184, 207-211). The production of IL-9, alongside having an autocrine function in promoting cytokine production also promotes B cell survival (212-215).

ILC1s and ILC3s are much smaller populations within the lung compared to ILC2s, with ILC3s contributing roughly 2% of total lung ILCs (216). Furthermore, as discussed previously, ILC1s role in inflammation is currently being investigated, partly due to the lack of clarity in the discrimination between cNK cells and other IFN- γ producing cells. Consequently, little is known about ILC1s function within the lung. However, under infection with influenza virus ILC2s are able to develop into IFN- γ producing ILC1s (142). IFN- γ production is important in the clearance of pathogens by activating macrophage phagocytosis, as shown in *Mycobacterium bovis* infected lungs (126). Although ILC3s are a small population within the healthy lung within obese murine models, mice developed airway hyperreactivity which was linked to an increase in LTi-like cells within the lung, contributing to IL-17A production (217). LTi-like cell activation was driven by IL-1 β , produced by macrophages, which upon blockage reduced the number of LTi-like cells and obesity induced airway hyperreactivity (217). Furthermore, ILC3s residing within the lung also play a role in combating bacterial infections such as *Streptococcus pneumoniae*, by producing large amounts of IL-22 (107). Interestingly, within human lungs Carrega et al., identified IL-22 producing NCR⁺ ILC3s in being important in the development of tertiary lymphoid structures, which are important in the early stages of protection against tumours (218).

The lung is continuously exposed to airborne antigens, some being pathogenic and others being allogenic which unnecessarily stimulates an immune response in the lung, driving the inflammatory lung disease, allergic asthma (219, 220). Asthma is characterised by airway hyperreactivity and can be activated upon viral or fungal challenge (110, 221-224). Under these conditions ILC2s can be activated in a similar manner to helminth infections, via alarmin

release from epithelial cells, however, this unwanted activation results in the development of airway hyperreactivity (219, 221-224). Fungal, allergen and viral induced airway hyperreactivity has been shown to be independent of the adaptive immune system with eosinophil recruitment and mucus hyperproduction being induced by papain administration in *Rag*^{-/-} mice but not *Rag*^{-/-} mice lacking ILCs (110, 219, 221).

1.6.3 Skin

The skin provides a thick mechanical and chemical barrier to the outside world, preventing the entry of pathogens whilst controlling the colonisation of commensal bacteria (1). It is comprised of an outer epidermis layer and an inner dermis layer, each containing a plethora of immune cells (1). ILCs play an important role in the homeostasis of the skin barrier, with ILC2s continuously producing IL-13 which is involved in the anti-inflammatory functions via the suppression of mast cells trafficking through the skin (200). IL-13 also functions in the repair and maintenance of the epithelial barrier with mice lacking IL-13 being more susceptible to epithelial carcinogens (225). ILCs have also recently been discovered to be important in the maintenance of Tregs within the skin with a select group of CCR10⁺ skin ILCs being required for the effective reconstitution of Tregs into the skin in *Rag*^{-/-} host wild type (WT) BM chimeras (226).

ILCs are also involved in the maintenance of the skin epithelial barrier, with ILC2s being activated in an IL-33 dependent manner, upon skin damage, promoting wound repair via the production of amphiregulin (227, 228). In the absence of ILCs, using anti-CD90 depleting antibodies, the skin showed delayed wound healing, however, due to the deletion of all ILCs, this cannot be solely attributed to ILC2s (228). Upon skin injury, Notch1 signalling drives the

production of TNF- α by epithelial cells recruiting CCR6⁺ NKp46^{low/-} ILC3s to dermis of the skin (229). Increased levels of IL-17 and IL-22 are also involved in skin repair and maintenance and were detected at skin damage sites with wound closure being delayed in *Rorc*^{-/-} mice (79, 229, 230).

Dysregulation of ILCs has also been reported to cause unwanted inflammation within the skin. ILC2s are found within the lesions of atopic dermatitis (AD) patients and AD murine models potentiating the type 2 response via cytokine production (227, 231). *Ror* α ^{-/-} BM reconstituted WT hosts failed to develop induced AD, compared to controls, suggesting the importance of ILC2s in disease development (227). Psoriatic lesions within patients show an enrichment in ILC3s, similar again to murine models, contributing to the development of psoriasis through the production of IL-22 and IL-17 alongside $\gamma\delta$ T cells (232-234). These diseases will be discussed in more detail later within this investigation.

1.6.4 Secondary lymphoid tissue

During embryogenesis, LT_i cells are required for the formation of LNs (111, 235). They are recruited to the LN anlagen early in embryonic development providing essential signals to LT β R⁺ mesenchymal cells via surface LT $\alpha_1\beta_2$ for further LN development, with *LT β R*^{-/-} and *LT β* ^{-/-} mice being unable to develop LNs or PP (137, 161, 236). *Id2*^{-/-} and *Rorc*^{-/-} mice, lacking ILCs and ILC3s respectively, have a deficiency in the development of both LNs and PP, supporting that LT_i cells are the key cellular provider of LT $\alpha_1\beta_2$ (237-239). The interactions between LT_i and mesenchymal cells are further enhanced by the expression of receptor activator of nuclear factor κ B Ligand (RANKL) on LT_i cells, which interacts with receptor activator of nuclear factor κ B (RANK), expressed on mesenchymal cells (240, 241). RANK

signalling in LTi cells increases their expression of $LT\alpha_1\beta_2$ required for the accumulation of LTi cells at the LN anlagen with *Rank*^{-/-} mice lacking the development of peripheral LNs (240-242). LTi cells stimulate mesenchymal cells to upregulate vascular cell adhesion molecule 1 (VCAM-1) and intercellular adhesion molecule 1 (ICAM-1) which are important in the recruitment and arrangement of cells, including monocytes, T cells and B cells, enabling the full development of the LN (235, 240). $LT\alpha_1\beta_2$ signals are also required for the organisational development of the spleen, with mice lacking these signals losing normal T cell and B cell segregation (161, 236).

Within the adult, an LTi-like cell population is identified clustered within the interfollicular areas between T cell and B cell zones and contributes to the repair and maintenance of SLTs (243, 244). Upon lymphocytic choriomeningitis virus (LCMV) infection stromal cells are destroyed within the spleen, disrupting T and B cell zones, however, LTi-like cells provide a source of $LT\alpha_1\beta_2$ signalling which contributes to the rebuilding of the SLT stromal framework (244). This suggests that LTi-like cells function in promoting the repair of tissues, with restoration being delayed within *Rorc*^{-/-} mice (244). Furthermore, ILC3s play an important role in the maintenance and function of LNs in an IL-7 dependent manner, with the absence of IL-7 signalling resulting in a decrease in ILC3 numbers and impaired migration of T and B cells into the LN (245).

Although ILC3s within the gut have an inhibitory effect on CD4⁺ T cells, controversially within the spleen ILC3s have been suggested to prime CD4⁺ T cell responses (114, 162). Von Burg et al., show that upon IL-1 β and TLR stimulation ILC3s upregulate cytokine production, MHCII, CD40, CD80 and CD86 expression (114). Therefore, upon antigen presentation ILC3s induced

CD4⁺ T cell activation and proliferation, with mice lacking MHCII on ROR γ t expressing cells observing reduced proliferation of ovalbumin (OVA) specific T cells upon OVA immunization (114). The comparison between MHCII⁺ NCR⁻ ILC3s within the spleen and gut suggest a differential role for these subgroups depending on location and potentially a further subdivision in the MHCII⁺ NCR⁻ ILC3 subgroup into cells that possess the ability to upregulate co-stimulatory molecules and those that don't. However, within the publication by von Burg et al., the florescent activated cell sorting (FACS) data, showing an increase in CD80, CD86 and CD40, is dubious (114). Further experiments would need to be conducted to determine whether ILCs required CD80, CD86 and CD40 to efficiently activate T cells, potentially through the use of genetically modified mice lacking the expression of these co-stimulatory molecules exclusively on ILC3s.

Similar to intestinal and splenic ILC3s, a population of ILC2s within the mesenteric LN (mLN) has been identified to express MHCII (25, 164). Alongside MHCII they also express CD80, CD86 and possess the ability to process and present antigen (25, 164). *In vitro* studies showed that MHCII-antigen TCR-CD3 complex mediated interactions between ILC2s and CD4⁺ T cells mutually supports both populations, promoting ILC2 proliferation and production of IL-13 alongside T cell maintenance and cytokine production (164). The importance of this cross talk was demonstrated *in vivo* with mice lacking ILC2s being unable to effectively clear *Nippostrongylus brasiliensis* worm burden (164). This supports previous publications by Neill et al., who showed that although IL-13 production by ILC2s was important in the expulsion of helminth infections, mice lacking adaptive immunity were unable to efficiently expel *Nippostrongylus brasiliensis* infections (25). In comparison to B cells, mLN ILC2s have a lower expression of MHCII which is lost upon short term culture (164). This raises the debate as to

whether ILC2s are true professional APCs or whether they just provide additional signals promoting T cell and their own maintenance. As discussed previously the strength of TCR interactions can influence the development of Th cells. It is suggested that this lower expression of MHCII, CD80 and CD86 may be important in skewing CD4⁺ T cells towards a Th2 response (246). Together this indicates a mutual relationship between the innate and adaptive immune system with ILC2s and ILC3s within SLT promoting T cell responses.

In conjunction with cell surface protein interactions, ILCs are able to elicit their functions through the productions of cytokines within SLTs. Upon enteric pathogen infections, alongside increased activation and accumulation of ILCs at the site of infection, some reports have identified an increase in ILCs within the mLN (185). *Clostridium difficile* infections did not only induce ILC1s and ILC3 cytokine production, in the small intestine (SI) but also in the mLN (185). Similarly, in *Heligmosomoides polygyrus* infected mice, ILC2s and their production of IL-4 was increased within the SI and mLN (182). Through the use of BM chimeras Pelly et al., showed that mice lacking ILC2s or IL-4 producing ILC2s had fewer Th 2 cells within the mLN and spleen (182). Although it was not determined whether this was a direct or indirect effect of ILC2s, it indicates a relationship for ILCs in promoting Th cell development, potentially via cytokine production (182). Supporting this, circulatory cNK cells have been shown by Martin-Fontecha et al., to migrate into LNs in a C-X-C chemokine receptor (CXCR) 3 dependent manner on activation via mature DCs (116). cNK cells were shown to provide an early source of IFN γ , promoting the differentiation of effector Th1 cells (116). As discussed earlier, Th differentiation can be skewed dependent on the cytokine environment, together, these publications suggests a role for cNK cells and helper ILCs in the direct regulation of the adaptive immune system (116, 182, 185).

1.7 MIGRATORY PROPERTIES OF ILCs

The positioning of ILCs at barrier sites allows for the efficient early production of effector cytokines upon pathogen invasion and in the regulation of epithelial barriers. Within SLTs ILCs cytokine production is involved in the structural repair post infection and is also believed to influence the differentiation of Th cells. More recently ILCs have been shown to express antigens via MHCII, with the largest MHCII expression being located on ILCs residing within SLT, posing the question as to how ILCs are able to gain access to antigen from the site of infection and present it within the draining LN (114, 164). Oliphant et al., has shown the ability of ILC2s to acquire MHCII expression via trogocytosis, so potentially ILCs gain their antigen expression from migratory APCs such as DCs. However, another potential mechanism is that helper ILCs may be able to acquire antigen at the site of infection and then migrate to lymphoid tissues in a similar manner to DCs (247). This raises the question as to whether ILCs are tissue-resident or possess migratory abilities, similar to cNK cells (116). Currently the prevailing view on helper ILCs migratory properties within the field is that they are tissue-resident within lymphoid, including the spleen and mLN, and non-lymphoid tissue evident by the inability of ILC exchange within parabiotic mice (248, 249). Gasteiger et al., suggests that ILCs are replenished through local differentiation from progenitor populations rather than seeding with mature ILCs that have migrated from the BM (249). Upon acute helminth infection ILC populations expanded via proliferation within the tissue and not via migration from the blood (249). cNK cells are a well-established migratory ILC population, surveying tissues via migration from blood into LNs occurring in a similar manner to T cells (116, 249). Within the blood cNK cells express L-selectin (CD62L) and CCR7, which are required for the exit of lymphocytes from the blood and into the LN, with intravenously injected splenic cNK

cells migrating to the draining LN within 12 hours (116, 250, 251). It is, however, becoming apparent that cNK cells may not be the only migratory ILC population, with recent publications arguing against a solely tissue-resident helper ILC population (226, 243, 252). Although it was concluded, using parabiotic mice, that helper ILCs were tissue-resident within the assessed tissues, ILC1s were present within the blood and were found to equilibrate between the parabiotic mice, although they didn't enter the assessed tissues (249, 253). The migration of ILCs from barrier sites to draining LNs was also not assessed within the parabiotic mice (249). Supporting the theory of a migratory population of helper ILCs, Mackley et al., used Kaede transgenic mice to show that ILC3s possess the ability to migrate from the gut to the draining mLN in a CCR7 dependent manner (243). Further ILC migration within the gut and gut associated LNs was suggested by Kim et al., who indicated that helper ILCs possessed the ability to migrate to the gut upon the upregulation of gut homing molecules, such as $\alpha 4\beta 7^+$, in a retinoic acid dependent manner with ILC1s and ILC3s originating from SLT and ILC2s from the BM (252). Injected ILCs into the skin draining LNs are able to acquire expression of the skin homing receptor CCR10 and migrate into the skin to promote the homeostasis of skin resident T cells (226). A recent publication has further explored the migratory abilities of the iILC2 population detected initially within the intestine (108, 254). Through the use of parabiotic mice and *Nippostrongylus brasiliensis* infections they show that iILC2s are able to undergo proliferation within the intestine, upon IL-25 stimulation, drain into the lymph and then blood in a sphingosine-1-phosphate (S1P) dependent manner and disseminate into peripheral tissues including the lung, spleen, liver and mLN (254). These studies clearly challenge the theory of a solely tissue-resident ILC population, however, the relationship of ILCs between non-lymphoid and lymphoid tissues is still unclear.

1.8 AIMS OF THIS INVESTIGATION

The aim of this investigation was to explore and compare ILCs across lymphoid and non-lymphoid tissues and to develop a clearer understanding of the relationship between these different cellular compartments. Although ILC function has been investigated in multiple non-lymphoid tissues their function within LNs and their communication with the adaptive immune response remains unclear. Furthermore, ILCs express co-stimulatory molecules that are critical for interactions between cells of the adaptive immune system such as members of the B7 family. Thus, it was sought to investigate the requirement for key co-stimulatory molecules for ILC function in both lymphoid and non-lymphoid tissue. It was hypothesised that ICOS:ICOSL interactions were required for normal ILC2 homeostasis. To further assess whether the ILC populations within non-lymphoid tissue and the SLT that drain them were related, novel models of cellular migration were used to directly test the hypothesis that ILCs migrate from non-lymphoid to lymphoid tissue.

In summary, the key aims of this investigation were:

1. Characterise and compare ILCs within lymphoid and non-lymphoid, determining whether ILC subgroups phenotype differs depending on location.
2. Explore the importance of the co-stimulatory molecule ICOS expression on the homeostasis of ILC2s and ILC3s within lymphoid and non-lymphoid tissue.
3. Investigate whether ILCs are a solely tissue-resident population within peripheral LNs, or whether they are able to migrate into, or egress from the SLT and the mechanisms behind this.

4. Begin to explore the migration of ILCs between the skin and draining LN under steady state or inflammatory conditions and the mechanisms behind ILC retention or migration.

Chapter 2. MATERIALS AND METHODS

2.1 MICE STRAINS

The mice models used in this project were maintained at the University of Birmingham Biomedical Serviced Unit (BMSU) and used in accordance with Home Office guidelines (Table 2.1). Within these experiments' WT mice and conditional knock outs were used to assess ILCs under normal and genetically manipulated conditions, respectively, in a variety of tissues. Photoconvertible Kaede mice were used to track the migration of cells *in vivo* from sight specific labelled areas and Kaede conditional knock outs used to assess the mechanisms controlling migration. In all experiments mice were age matched between 6-11 weeks of age.

Table 2.1. Mouse strains used within this investigation

Strain	Formal strain name	Background	Phenotype	Source
C57BL/6		C57BL/6J	Used as a WT control	BMSU
<i>Ccr6</i> ^{-/-}	B6.129P2- <i>Ccr6</i> ^{tm1Dgen} /J	C57BL/6J	CCR6 knock out; Absence of CCR6:CCL20 interactions	JAX (original reference not provided by JAX)
<i>Ccr7</i> ^{-/-}	<i>Ccr7</i> ^{tm1Rfor} /J	C57BL/6J	CCR7 knock out; Absence of CCR7:CCL21 and CCR7:CCL19 interactions	JAX (255)
<i>Icos</i> ^{-/-}	B6.129P2- <i>Icos</i> ^{tm1Shr}	C57BL/6J	ICOS knock out; Absence of ICOS expression and ICOS:ICOSL interactions	MedImmune (256)
<i>Icosl</i> ^{-/-}	B6.129P2- <i>Icosl</i> ^{tm1Mak} /J	C57BL/6J	ICOSL knock out; Absence of ICOSL expression and ICOS:ICOSL interactions	JAX (257)
Id2 GFP	Id2 ^{tm1Gtbz}	C57BL/6J	eGFP was inserted into the 3' UTR of Id2 generating a reporter mouse	Gabrielle Belz (258)
IL-13 GFP	Il13 ^{tm3.1Anjm}	C57BL/6J	These mice are an eGFP knock in at exon 1 of IL-13, generating a reporter mouse	Andrew McKenzie (164)
Kaede	Tg(CAG-Kaede)15Kgua	C57BL/6J	Ubiquitous expression of a photoconvertible Kaede green protein	University of Glasgow (53)

2.2 MEDIUMS AND REAGENTS

2.2.1 Mediums

These mediums were used throughout various experiments.

Table 2.2. Staining buffer

Media and Reagents	Manufacture	Final Concentration
Dulbecco's Phosphate-Buffered Saline (DPBS) [+] MgCl (1000 mg/L) and CaCl (100 mg/L)	Life technologies	
Ethylenediaminetetraacetic Acid Solution (EDTA)	Sigma-Aldrich	2.5 mM
Foetal Bovine Serum (FBS) Heat Inactivated	Sigma-Aldrich	2%

Table 2.3. Culture media

Media and Reagents	Manufacture	Final Concentration
Roswell Park Memorial Institute 1640 Medium [+] L-Glutamine	Life Technologies	
Penicillin Streptomycin Solution	Invitrogen (Life Tech)	0.98%
L-Glutamine	Sigma-Aldrich	0.98%
FBS Heat Inactivated	Sigma-Aldrich	9.80%

Table 2.4. Staining solution for immunofluorescence microscopy

Media and Reagents	Manufacture	Final Concentration
PBS	Sigma-Aldrich	
Bovine Serum Albumin (BSA) Heat Inactivated	Sigma-Aldrich	1%

2.2.2 Gey's solution

Gey's solution is a red cell lysis buffer made within the laboratory (Table 2.5) samples are incubated in Gey's solution to lyse and remove red blood cells. Solution A and B are made up

to 1 L within distilled water and autoclaved. Gey's solution consists of 10 mL of Solution A, 2.5 mL of Solution B, 2.5 mL of Solution C and 35 mL of distilled water and kept at 4°C. Gey's solution is then run through a 0.2 µm filter to use in sterile conditions.

Table 2.5. Gey's solution

Solution	Additive	Quantity
A	NH ₄ Cl	35 g
	KCl	1.85 g
	Na ₂ HPO ₄ .12H ₂ O	1.5 g
	KH ₂ PO ₄	0.119 g
	Glucose	5.0 g
	Gelatin	25.0 g
	1% Phenol red	1.5 mL
B	MgCl ₂ .6H ₂ O	4.2 g
	MgSO ₄ .7H ₂ O	1.4 g
	CaCl ₂	3.4 g
C	NaHCO ₅	22.5 g

2.3 PREPARING CELL SUSPENSIONS

Tissues were prepared similar to methods previously published by Dutton et al., and Mackley et al. (216, 243).

2.3.1 Lymph nodes and spleen

Tissue was isolated from the mouse and cleaned using a dissection microscope and forceps, removing the fat and blood vessels, in Roswell Park Memorial Institute (RPMI) 1640 Medium (Life Technologies). Where large amounts of fat were removed, the tissue was transferred into 3 mL of fresh RPMI before being teased apart using forceps. For digestion, collagenase dispase (final concentration, 0.25 mg/ml) (Roche Life Sciences) and DNase (0.025 mg/ml) (Roche Diagnostics) were added and the cells were incubated at 37°C for 20 minutes. Digestion was

stopped through the addition of EDTA (0.01 M) (Sigma-Aldrich) and the tissues were crushed through a 70 µm filter into a falcon tube using a 2 mL syringe plunger. Samples were centrifuged (5 minutes, 1,500 revolutions per minute (rpm), 4°C) and the supernatant removed. Lymph nodes (LN) were resuspended in an appropriate amount of staining buffer, however, spleen samples were resuspended in 5 mL of Gey's red blood cell lysis buffer and incubated for 5 minutes on ice. Spleens were diluted with RPMI, centrifuged and re-suspended in the appropriate amount of staining buffer.

2.3.2 Lung

To isolate the lungs, mice were perfused with Dulbecco's Phosphate-Buffered Saline (DPBS) (Life Technologies), the right atrium of the heart was pierced with a needle and the left ventricle was forcefully injected with 10 mLs of DPBS. This causes inflating of the lungs and the blood to be flushed out. The lung was removed and cleaned in a petri dish containing culture media, teased apart with dissection forceps and transferred to a falcon tube. Lungs were agitated at 37°C for 45 minutes in an overall volume of 5 mL of culture media containing Liberase thermolysin medium concentration (TM) (42.4 µg/ml) (Roche Life Sciences) and DNase1 (0.02 mg/ml). Samples were then crushed through a 70 µm filter, washed with culture media, centrifuged and incubated on ice for 2 minutes in Gey's solution. Lungs were then washed with RPMI and re-suspended in an appropriate amount of staining buffer.

2.3.3 Small intestine lamina propria

The dissection of the SI LP needed to occur within a short time frame to prevent cell death. It was dissected from below the stomach to above the caecum and then placed in Hank's Balanced Salt Solution (HBSS, Sigma-Aldrich) containing 2% FCS. Within the solution, dissection forceps and scissors were used to remove the fat and PP before longitudinal cutting

of the SI, washing out the contents. The SI was cut into small pieces, roughly 2 cm longitudinally, and placed in a falcon tube containing HBSS and shaken vigorously. The SI was removed from the solution by being filtered through nitex mesh. The SI underwent a sequence of incubations with various medias; it was placed in a specific media, shaken vigorously for 20 seconds, agitated at 37°C for 15/20 minutes, removed from the current media via being filtered, resuspended in HBSS and vigorously shaken for 20 seconds before final filtering and then resuspension and incubation in another media. This process was carried out with the first specific media being HBSS 2 mM EDTA (20 minutes), which was repeated twice and the second media being pre-warmed culture media containing 1 mg/mL collagenase VIII (Sigma-Aldrich) (15 minutes). After digestion the SI was filtered twice through 100 µm and 70 µm cell strainers before being centrifuged and re-suspended in an appropriate amount of staining buffer.

2.3.4 Ear skin

The ear was removed, cutting along the hairline of the ear, placed in a 1.5 mL eppendorf and cut into small sections. Samples were incubated at 37°C for 30 minutes in 1 mL of Dulbecco's Modified Eagle Medium (DMEM) containing Liberase TM (6.25 mg/mL) and DNase1 (0.25 mg/mL), whilst being agitated in a thermomixer (Eppendorf). The tissue was filtered and washed, with DMEM, allowing the digested skin cells within the supernatant to be collected. The digestion and washing process was repeated two more times with the remaining undigested ear. Following the third incubation, using a 2 mL syringe plunger, the remaining undigested ear skin was crushed through the filter and washed with DMEM. Samples were centrifuged and re-suspended in an appropriate amount of staining buffer.

2.3.5 Blood

1-2 mLs of blood was harvested, via cardiac puncture, in an eppendorf containing 300 μ L of EDTA, to prevent clotting. Samples were then centrifuged (5 minutes, 2,000 rpm), supernatant removed, resuspended in 500 μ L of Gey's solution and incubated on ice for 5 minutes. This was repeated two more times, before samples were resuspended in appropriate amount of staining buffer.

2.3.6 Lymph node stromal digestion

To specifically isolate stromal cells from LNs, instead of lymphocytes, a different digestion protocol to previous was used. LNs were removed, the fat and blood vessels removed, placed in a 1.5 mL eppendorf and cut into small pieces. Samples were resuspended in culture media with DNase1 (0.01 mg/mL) and Collagenase D (2.5 mg/mL) (Roche Life Sciences) and agitated at 37°C in a thermomixer. Every 5 minutes each sample was vigorously pipetted until it was fully digested (30-40 minutes) then EDTA (0.25 mM) was added to each sample. Samples were then filtered through a 70 μ m cell strainer and resuspended in a desired amount of staining buffer.

2.4 MAGNETIC-ACTIVATED CELL SORTING

2.4.1 CD45⁺ enrichment

Single cell suspensions were incubated with anti-CD45 MicroBeads (MACS) diluted in staining buffer for 40 minutes on ice. Samples were then directly run through pre-washed (with staining buffer) LS columns (MACS) and the negative fraction of CD45⁻ cells collected (Table 2.6). Staining buffer was forced through the LS column with a syringe plunger eluting the

positive fraction of CD45⁺ cells. The desired fraction was washed and re-suspended in an appropriate amount of staining buffer.

2.4.2 ILC enrichment

Single cell suspensions were incubated with anti B220, CD3 and CD5 antibodies conjugated to APC, diluted in staining buffer for 30 minutes on ice (Table 2.7). Samples were washed twice with staining buffer and resuspended in anti-APC MicroBeads (MACS) diluted in staining buffer for 15 minutes (Table 2.6). Samples were washed again and run through LD columns (MACS) pre-washed with staining buffer. The negative fraction was collected, and staining buffer was used to elute the positive fraction, using a syringe plunger.

Table 2.6. Microbeads used in cell separation

MicroBeads	Dilution	Manufacture
anti-CD45	1:60	MACS Miltenyi Biotec
anti-APC	1:5	MACS Miltenyi Biotec

2.5 FLOW CYTOMETRY

2.5.1 Extracellular staining

Cells were prepared for flow cytometry following the same protocol as Mackley et al and Dutton et al (216, 243). Antibodies used for flow cytometric analysis are shown in Table 2.7. All staining was conducted in a 96-well plate (Thermo Scientific) with cells being suspended in 100 µL of antibody diluted in staining buffer, unless stated otherwise. The proportion of sample stained varied depending on the size of the tissue (Table 2.8). All tissues were initially stained with an APC-eFluor780 viability dye (1:1000, eBioscience), diluted in DPBS for 20 minutes on ice. Following each incubation, 100µL of staining buffer was added to each sample prior to centrifugation (1,500 rpm, 2 minutes). Samples were then washed with 200 µL of

staining buffer twice before continuing with the subsequent staining step. All extracellular staining occurred in the dark at 4°C for 30 minutes, unless stated otherwise. Samples which extracellular staining panel included anti-CCR7 were incubated at 37°C for 30 minutes. Staining for lineage markers was either conducted using the same fluorochrome for all markers, or individual fluorochromes for separate markers.

Stains consisting of a primary and biotinylated antibody required a further 30 minute incubation step before incubation with secondary antibody, shown in Table 2.9. The secondary antibody for example, fluorochrome-conjugated streptavidin (SA), shown in Table 2.10 was then incubated for a further 30 minutes. Samples which included the S1P receptor 1 (S1PR1) primary antibody required the initial staining with the primary S1PR1 antibody followed by anti-Rat IgG1k biotin. A rat serum block was then applied for 15 minutes at 4°C to prevent any unspecific binding (Table 2.11).

2.5.2 Intracellular staining

Post extracellular staining, cells were permeabilised using the Foxp3 TF staining buffer kit (Foxp3 kit, BD Biosciences), following manufacture instructions. Each sample was resuspended in 100 µL of Foxp3 fixation/permeabilisation buffer (1:3 concentrate:diluent) and incubated for 30 minutes, 4°C. Post-permeabilisation all samples were washed with 200 µL Permeabilisation buffer (1:10 10x Permeabilisation buffer:dH₂O) (BD Biosciences) and stained in 100 µL of intracellular staining antibody diluted in Permeabilisation buffer at room temperature for 45 minutes. Samples were then washed twice with Permeabilisation buffer and twice with staining buffer, before being filtered through 50 µm CellTrics filters (Sysmex) into fluorescence-activated cell sorting (FACS) tubes in 300 µL of staining buffer.

2.5.3 Intracellular staining in Kaede mice

Intracellular staining via the Foxp3 kit resulted in the loss of Kaede protein from the cytoplasm and therefore Kaede Red and Kaede Green cells were unable to be identified. However, the Kaede protein was not lost when cells were fixed with the BD Cytotfix/Cytoperm kit (BD kit) and stained in the Foxp3 kit which was used to stain for the intracellular marker Ki-67. The TF T-bet, GATA-3 and ROR γ t were not efficiently identified upon using the BD kit. Kaede cells were only analysed for the intracellular marker Ki-67 using a combination of the BD kit and Foxp3 kit. Post extracellular staining, samples were resuspended in 100 μ L of BD kit Fixation/Permeabilisation solution and incubated for 1 hour at 4°C. Samples were then washed with Foxp3 kit Permeabilisation buffer twice before being resuspended in antibody diluted in 100 μ L of Foxp3 kit Permeabilisation buffer for 45 minutes room temperature. Samples were then washed twice with Permeabilisation buffer and twice with staining buffer, before being filtered through 50 μ m CellTrics filters (Sysmex) into fluorescence-activated cell sorting (FACS) tubes in 300 μ L of staining buffer.

2.5.4 Flow cytometry analysis

Samples were run on the BD LSRFortessa™ X-20 (BD Biosciences), the data collected using BD FACSDiva Software (BD Biosciences) and analysed using Flow Jo software (Treestar). 10,000 counting beads (Spherotech) were added to the samples prior to being run on the LSRFortessa™ X-20 to enable the total number of cells per sample to be calculated. Upon running the sample and analysing the data, the number of beads (x bead count) and the number of cells (y cell count) run in one sample were used to calculate the total cell number per sample (z total cell number), as shown below.

$$\frac{10,000 \text{ beads}}{x \text{ bead count}} = \frac{z \text{ total cell number}}{y \text{ cell count}}$$

Table 2.7. Fluorescent activated cell labelling reagents used for flow cytometry

Antibody Specificity	Conjugate (working dilution)	Clone	Manufacture
B220 (CD45R)	FITC (1:300)	RA3-6B2	eBioscience
	PECy7 (1:200)	RA3-6B2	eBioscience
	APC (1:200)	RA3-6B2	BioLegend
CCR6 (CD196)	BV605 (1:100)	29-2L17	BioLegend
CCR7	PE (1:100)	4B12	eBioscience
CD3 ϵ	FITC (1:100)	145-2C11	eBioscience
	AF700 (1:100)	eBio500A2	eBioscience
	PECy7 (1:200)	145-2C11	eBioscience
	APC (1:100)	145-2C11	eBioscience
	BV650 (1:100)	145-2C11	BD Horizon
	BV605 (1:100)	17A2	BioLegend
CD4	BV785 (1:100)	RM4-5	BioLegend
CD5	FITC (1:100)	53-7.3	eBioscience
	APC (1:100)	53-7.3	eBioscience
	PECy7 (1:200)	53-7.3	eBioscience
CD8	BV711 (1:200)	53-6.7	BioLegend
CD11b	FITC (1:300)	M1/70	eBioscience
	PECy7 (1:200)	M1/70	eBioscience
CD11c	FITC (1:300)	N418	eBioscience
	BV785 (1:200)	N418	BioLegend
	PECy7 (1:200)	N418	eBioscience
CD19	PECy7 (1:200)	eBio1D3	eBioscience
	FITC (1:200)	eBio1D3	eBioscience
CD25	BV650 (1:200)	PC61	BioLegend
	AF700 (1:50)	PC61	eBioscience
CD31	APC (1:400)	eBio390/390	eBioscience
CD45	BV785 (1:100)	30-F11	BioLegend
CD45.2	eFluor450 (1:200)	104	eBioscience
	BV785 (1:100)	104	BioLegend

Antibody Specificity	Conjugate (working dilution)	Clone	Manufacture
CD49b	PECy7 (1:200)	DX5	eBioscience
	AF700 (1:200)	DX5	eBioscience
	FITC (1:200)	DX5	eBioscience
CD62L	BV711 (1:100)	MEL/14	BioLegend
	PECy7 (1:500)	MEL/14	eBioscience
	APC (1:1500)	MEL/14	eBioscience
CD69	BV711 (1:100)	H1.2F3	eBioscience
CD103	PECy7 (1:200)	2E7	BioLegend
CD123	FITC (1:500)	5B11	eBioscience
CD207 (Langerin)	APC (1:100)	4C7	BioLegend
c-kit	BV711 (1:100)	H57-597	eBioscience
EOMES	PECy7 (1:50)	Dan11mag	eBioscience
F4/80	PECy7 (1:200)	BM8	eBioscience
	FITC (1:200)	BM8	eBioscience
FceRI	PECy7 (1:200)	MAR-1	eBioscience
	FITC (1:200)	MAR-1	eBioscience
GATA-3	PerCP710 (1:75)	TWAI	eBioscience
gp38	PECy7 (1:1000)	8.1.1	BioLegend
Gr-1	PECy7 (1:2000)	RB6-8C5	eBioscience
	FITC (1:2000)	RB6-8C5	eBioscience
ICOS	APC (1:200)	C398.4A	BioLegend
	PeCy7 (1:200)	C398.4A	BioLegend
IL-7R α (CD127)	BV421 (1:50)	A7R34	BioLegend
Ki-67	PECy7 (1:400)	SolA15	eBioscience
	AF700 (1:50)	SolA15	eBioscience
KLRG1	BV605 (1:200)	2F1	BioLegend
	APC (1:200)	2F1	eBioscience
MHCII (I-A/I-E)	BV510 (1:500)	M5/114.15.2	BioLegend
	AF700 (1:100)	M5/114.15.2	eBioscience
NK1.1	PECy7 (1:200)	PK136	eBioscience
	BV650 (1:100)	PK136	BD Horizon
NKp46 (CD335)	BV711 (1:50)	29A1.4	BioLegend
	PeCy7 (1:100)	29A1.4	eBioscience
ROR γ t	PE (1:100)	AFKJS-9	eBioscience
ST2 (IL-33R α)	PE (1:50)	DIH9	BioLegend
T-bet	eF660 (1:50)	eBio4B10	eBioscience

Antibody Specificity	Conjugate (working dilution)	Clone	Manufacture
	PE-Cy7 (1:50)	eBio4B10	eBioscience
TCR β	AF700 (1:100)	H57-597	BioLegend
TCR $\gamma\delta$	APC (1:100)	GL3	BioLegend
	BV711 (1:200)	GL3	BD Horizon
TCR V γ 1.1	BV421 (1:100)	2.11	BD Horizon
TCR V γ 2 (V γ 4)	PECy7 (1:200)	UC3-10A6	eBioscience
TCR V γ 3 (V γ 5)	APC (1:200)	536	BioLegend
TER-119	PECy7 (1:200)	TER-119	eBioscience
	FITC (1:100)	TER-119	eBioscience
	AF700 (1:200)	TER-119	BioLegend

Table 2.8. Minimal proportions of tissues stained

Total counts were performed with count beads, therefore a known proportion of the cellular suspension was used during flow cytometric analysis, which was then used to calculate the total numbers.

Tissue	Minimum proportion stained
mesenteric LN	1/3
Small Intestine	1/5
Lung	1/8
auricular LN	1/2
Ear	1/2
brachial LN	1/2
Spleen	1/15

Table 2.9. Primary and biotinylated antibodies

Antibody Specificity	Conjugate (dilution)	Clone	Host	Anti-	Manufacture
anti-Rat IgG1k	Biotin (1:100)	MRG2a-83	Mouse	Rat	BioLegend
KLRG1	Biotin (1:100)	2F1	Syrian Hamster	Mouse	eBioscience
S1PR1	Purified (1:10)	713412	Rat	Mouse	R&D Systems

Table 2.10. Fluorochrome-conjugated streptavidin

Streptavidin	Manufacture
SA-PECy7 (1:500)	eBioscience

Table 2.11. Blocking serums used in flow cytometry

Serum	Diluted in	Concentration
Rat	Staining Buffer	10%

2.6 IMMUNOFLUORESCENCE MICROSCOPY

2.6.1 Preparation of frozen tissue slides

Human tissues were supplied by MedImmune and murine samples were collected in Birmingham. Murine LN sections were cleaned and snap frozen on optimal cutting temperature (OCT) to aid sectioning. The SI LP was collected, the fat removed in HBSS 2% FCS and the lumen flushed with staining buffer before being tightly curled and snap frozen. Tissues were stored at -80°C until they were ready for sectioning. Samples were cut into 6 µm thick sections using the cryostat and positioned onto a 4-spotted glass slide (LNs) or clear glass slide

(SI LP). The slides were air dried before being fixed in acetone at 4°C for 20 minutes and then left to dry overnight. Dry tissue sections were stored at -20°C until use.

2.6.2 Immunofluorescence staining of tissue

Immunofluorescent staining requires a series of steps in which the tissue undergoes multiple incubations with specific serums and antibodies. All incubations occurred at room temperature in a humidified chamber and after each incubation the tissue was washed, a process in which excess antibody solution was removed from the slides before the tissue was suspended in PBS for 10 minutes. PBS/1% Bovine Serum Albumin (BSA) (Table 2.4) was used as a diluent for the antibodies and serums that were used during this process (Table 2.12-2.14).

Slides mounted with tissue were removed from storage and left to air dry for 20 minutes before being hydrated in PBS for 10 minutes. Initially the avidin/biotin block kit (Vector Laboratories) was used, according to manufacturer instructions, to block non-specific binding to biotin receptors or avidin binding sites. Following a 2 minute wash, a series of incubations were conducted, after each incubation containing an antibody mix the slides were washed, as described above, however, after incubation with a serum the serum was aspirated off of the slide with a pipette, not washed and the following solution applied to the tissue.

A horse serum block was initially applied for 15 minutes, blocking non-specific protein binding sites, aspirated and then followed by the application of appropriate primary antibodies, which were incubated for 40 minutes (Table 2.12). The subsequent incubations with additional antibodies occurred for 30 minutes.

To provide a signal strong enough to be effectively detected, multiple amplification steps were required for the identification of TFs. Initially the purified primary ROR γ t and GATA-3

antibodies were applied, followed by the secondary antibody donkey anti-rat-IgG FITC, which bound to the purified primary TF antibodies, due to the primary antibodies being raised within a rat. To further amplify the signal additional tertiary and quaternary antibodies were applied including rabbit anti-FITC AF488 and donkey anti-rabbit-IgG AF488, respectively (Table 2.13). To prevent any unspecific binding of tertiary and quaternary antibodies to the primary antibodies a rat serum block was applied and incubated for 15 minutes after secondary antibody incubation.

Prior to secondary, tertiary and quaternary incubations the antibodies used were cross-absorbed for 30 minutes with 10% human or mouse serum, depending on whether human or murine samples were being used. SA antibodies were used to detect biotinylated primary antibodies.

Following this, samples were counterstained with 4',6-diamidino-2-phenylindole (DAPI) for 30 seconds, then washed in fresh PBS 3 times. Prolong gold mounting media (Life Technologies) was applied to semi-dried slides to preserve the tissue sections. A cover slip was gently lowered onto the slide, avoiding bubbles and left to semi-dry before the coverslip was sealed with clear nail varnish. Post overnight drying in the dark at room temperature, slides were stored at 4°C until analysis.

2.6.3 Analysis of immunofluorescence stained tissue

Stained tissue samples were analysed using the Zeiss 780 Zen microscope (Zeiss). Automatic stitching via the Zen software (Zeiss) was used on tile-scanned images. The location of IL-7R α ⁺ ROR γ t⁺ CD3⁻ ILCs was analysed on Zen software.

Table 2.12. Immunofluorescence primary antibodies

Primary Antibody	Conjugate (working dilution)	Clone	Host	Anti-	Manufacture
CD3	AF594 (1:25)	UCHT1	Rat	Human	eBioscience
CD3	Biotin (1:25)	UCHT1	Mouse IgG1	Human	BioLegend
CD3	Biotin (1:100)	eBio500A2	Syrian Hamster	Mouse	eBioscience
CD161	AF647 (1:25)	HP-3G10	Mouse IgG1	Human	BioLegend
GATA3	Purified (1:25)	TWAI	Rat	Human Mouse	eBioscience
HLA-DR (MHCII)	AF647 (1:25)	LN3	Mouse IgG2	Human	BioLegend
ICOS	BV647 (1:25)	C398.4A	Armenian Hamster	Human Mouse Rat	BioLegend
IL-7R α (CD127)	ef660 (1:25)	A7R34	Rat	Mouse	eBioscience
IL-7R α (CD127)	Biotin (1:25)	eBioRDR5	Mouse	Human	eBioscience
IL-7R α (CD127)	AF647 (1:25)	A019D5	Mouse IgG1	Human	BioLegend
ROR γ t	Purified (1:25)	AFKJS-9	Rat	Human Mouse	eBioscience

Table 2.13. Immunofluorescence secondary and streptavidin antibodies

Secondary Antibodies	Conjugate (working dilution)	Category Number	Manufacture
Affinity Pure Donkey α Rat IgG (H+L)	FITC (1:150)	712-095-153	Jackson Immunoresearch
Rabbit IgG fraction α fluorescein/Oregon Green [®]	AF488 (1:200)	A-11090	Molecular Probes
Donkey α Rabbit IgG (H+L)	AF488 (1:200)	A-21206	Molecular Probes
SA	AF555 (1:500)	S-21381	Molecular Probes

2.7 PHOTOCONVERTIBLE KAEDE MICE

2.7.1 Photoconvertible Kaede mice

Photoconvertible Kaede mice ubiquitously express a gene, cloned from stony coral, which encodes a green fluorescent protein (GFP) called Kaede (53, 259). A tripeptide, His-Try-Gly, is what acts as the green chromophore within the Kaede protein and when exposed to ultraviolet (UV) light, ranging between 350 – 400 nm, is converted to Kaede red (53, 259, 260). The UV light induces a peptide cleavage and formation of a double bond within the Kaede chromophore (53, 260). The proteins excitation and emission wavelengths changes so it is now perceived as red, this photoconversion does not affect the reproduction, growth or migration of cells (53). The Kaede Green and Kaede Red fluorescence can be detected using flow cytometry, which does not induce photoconversion (53, 259). During cell proliferation, the photoconverted Kaede Red protein is diluted out and replaced with newly synthesised Kaede Green protein, however in lymphocytes the photoconverted Kaede Red protein has a

long biological half-life (53). Therefore, these mice can be used to track the migration of cells *in vivo*.

2.7.2 Violet light conversion of the brachial lymph node

Mice were administered with a subcutaneous injection of buprenorphine (Tamgesic, Animal Care UK) 1 hour prior to the administration of anaesthetic, gaseous isoflurane (Zoetis), with oxygen as a carrier fluid. The brachial LN (bLN) was exposed to UV light 365 nm light using a light emitting diode (LED), via a small incision in the arm, for 3 and a half minutes before single interrupted sutures were used to close the incision. Mice were subcutaneously injected with 500 μ L of pre-warmed saline solution and allowed to recover.

2.7.3 Violet light conversion of the ear

Mice were anaesthetised with gaseous isoflurane and the ear exposed to UV 405 nm light using a light amplification by stimulated emission of radiation (LASER), which is a more intense beam of light. The LASER light source was used instead of the LED light source due to LED light being insufficient in photoconversion of the ear. To prevent damage the violet light exposure was applied in a swaying movement and given in doses; 1 x 20 seconds and 2 x 10 seconds with 10 second intervals. Black card was used to shield the rest of the body from UV light, preventing unspecific UV exposure. The mice recovered from anaesthetic and were culled a maximum of 72 hours after UV light conversion.

2.7.4 Violet light conversion of the head

Mice were anaesthetised with gaseous isoflurane, the forehead shaved and then exposed to UV 405 nm light. To prevent damage the violet light exposure was applied in a swaying movement for 2 minutes. Black card was used to shield both ears preventing their violet light

exposure, allowing for the assessment of cellular migration into the ear. The mice recovered from anaesthetic and were culled a maximum of 72 hours after violet light conversion.

2.8 EAR INFLAMMATION MODELS

2.8.1 Calcipotriol topical application to the ear

Calcipotriol (MC903), a vitamin D3 analogue (Tocris), was used to induce AD-like inflammation on the ears of mice. MC903 was dissolved in absolute ethanol (VWR Chemicals) to achieve a final concentration of 200 μ M. 20 μ L (4 nmol) of MC903 or 20 μ L of absolute ethanol, termed the vehicle control (VC), 10 μ L on the dorsal and 10 μ L on the ventral ear, was then applied to the ear. This was repeated on consecutive days for varying time periods reaching a maximum of 5 days.

2.8.2 Aldara topical application to the ear

Aldara (Imiquimod) 5% cream (Meda) was used to induce psoriasis-like inflammation on the ears of mice. 30 mg of Aldara 5% cream was applied, 15 mg to the dorsal and 15 mg to the ventral segment of the ear and repeated on consecutive days for varying time periods reaching a maximum of 5 days.

2.9 FTY720 MOUSE MODELS

2.9.1 FTY720 administration

Mice were intraperitoneally injected (i.p) with 200 μ L of FTY720 (1 mg/mL) (Sigma) dissolved in H₂O or with H₂O as a vehicle control. FTY720 was prepared in sterile conditions and filtered through a 0.2 μ m filter prior to injection. Injections were repeated on consecutive days up to

6 days in conjunction with other procedures. FTY720 is an S1PR inhibitor and prevents the egress of cells from tissue in an S1P dependent manner (261).

2.9.2 FTY720 in combination with previous models

FTY720 was administered in combination with the bLN violet light conversion surgery protocol and the MC903 model. Administration started one day prior to the start of the protocols and injections were given every consecutive day during the procedure.

2.10 ETHICAL APPROVAL

All human tissue samples (whole FFPE tissue blocks or TMA's) used in this study were sourced from donors whom provided full informed consent for the use of their samples in research. All samples were sourced through various commercial human biological samples vendors and this study performed under the MedImmune Research Tissue Bank Ethical Review REC reference 16/EE/0334 as approved by the East of England NRES committee.

2.11 STATISTICAL ANALYSIS

Data was collected using Flow Jo software (Treestar) and was statistically analysed using the computer program GraphPad Prism 7. When comparing two sets of data statistical significance was tested using an unpaired Mann Whitney t-test. Upon comparing more than two sets of data a Kruskal-Wallis one-way ANOVA with post hoc Dunn's test was performed. For each of these test * = <0.05 , ** $p = < 0.01$ and *** $p = < 0.005$. Where a p value is not indicated, no statistical difference is observed. Due to the nature of the data the percentage of Kaede Green cells cannot be statistically compared to Kaede Red cells within a population, therefore no statistics are conducted on these data.

Chapter 3. CHARACTERISATION OF ILCs

3.1 INTRODUCTION

ILCs are a recently characterised subset of lymphoid cells belonging to the innate immune system, with the initial discovery of cNK cells in 1975 and LTI-like cells in 1997 (111, 117). These cells were later included within the ILC population upon the proposal of a uniformed nomenclature in 2013 (101).

IL-7R α and CD90, are common markers expressed on ILCs, used either in conjunction or interchangeably in the identification of ILCs (107, 108, 243, 262). ILCs lack the expression of certain lineage markers which are expressed by and used in the identification of myeloid cells, DCs, T cells and B cells and is therefore another distinct feature of ILCs (101, 107). Despite a proposed method of ILC identification, current publications differ on lineage markers used in their identification, ranging from markers identifying T cells, B cells, DCs and neutrophils to the inclusion of eosinophil, erythrocyte, monocyte and macrophage markers (108, 110, 221, 243). Through the use of flow cytometry and whole mouse genome arrays, ILCs were divided into 3 well characterised groups, similar to effector Th cell subgroups (28, 101). Group 1 ILCs express T-bet and produce Th1 cytokines, group 2 ILCs which express GATA-3 secrete Th2 cytokines and thirdly ROR γ t dependent group 3 ILCs, which produce Th17 cytokines (101, 221, 263).

Within the current literature the TF ROR γ t is frequently used to identify ILC3s in the SI, lung, skin and mLN, enabling consistent identification and characterisation between tissues (107, 114, 162, 229, 243, 264). In comparison, many publications identify ILC2s based on the

expression of cell surface markers and cytokine production. ILC2s within the lung have been identified based on the expression of ST2, KLRG1, ICOS and CD25 along with the cytokines IL-5 and IL-13 (108, 164, 221, 265). A caveat in the identification of ILC2s via surface markers, is that expression may be expected to vary between different tissues, which could result in inefficient ILC2 identification. For example, Kim et al., use ST2, which was originally shown on ILC2s within the lung, to identify ILC2s within the skin, without supporting evidence that ILC2s within the skin express ST2 (25, 231, 265). Different research groups use a variety of methods to identify ILC2s within different tissues, making it difficult to compare ILC2 functions across publications. For example, KLRG1 has been used within the gut, compared to other studies which have used GATA-3 (181, 182). ST2 is mainly used within the lung and skin, however ICOS has been targeted to induce ILC2 depletion alongside ROR α (164, 231, 265). As discussed previously, ILC2s are comprised of ST2⁻ iILC2s and ST2⁺ nILC2s, suggesting that previous publications using ST2 to identify ILC2s may have missed the identification of iILC2s within their analysis (108).

Group 1 ILCs are identified by their expression of T-bet, production of IFN- γ and co-expression of NK1.1 and Nkp46 (135, 263). This group is comprised of ILC1s and cNK cells, the latter being well documented cytotoxic cells. cNK cells are distinct from ILC1s as they also express CD49b and EOMES which is required for their development (135, 263). cNK cells IL-7 independent and EOMES dependent maturation enables efficient separation of ILC1s and cNK cells (127, 128, 156). However, compared to cNK cells ILC1s are a relatively new identified population suggesting that previous publications investigating the functions of cNK cells may not have excluded ILC1s from their analysis. Furthermore, cNK cells and ILC1s are not the only subgroup

of ILCs to express T-bet. As previously discussed, NCR⁻ ILC3s can upregulate T-bet expression becoming NCR⁺ ILC3s, contributing to the production of IFN- γ (130, 141). This level of plasticity between ILC3s developing into ILC1s poses a problem in identifying the main sources of IFN- γ in different infections, suggesting that the expression of multiple TFs may be needed to ensure accurate identification of ILC subgroups (27, 130, 185).

Varying protocols are used to prepare different tissues, with specific enzymes, temperatures and incubation periods required to achieve efficient tissue digestion and preparation of single cell suspensions (216, 243, 254). Furthermore, digestion protocols used for the same tissue may vary across different labs, with different use of equipment, enzymes and concentrations (243, 254). This again introduces a level of variation across publications especially when the conditions in which tissues are digested may influence the level of expression of surface proteins. Liu et al., have demonstrated the importance of digestion protocols by showing that different incubation lengths, alongside different types of enzymes, dramatically changes the detectable level of CD62L on splenic CD4⁺ T cells (266). This further suggests that using surface markers alone may not be the most efficient means of identifying ILCs.

Human ILCs are similar to murine ILCs and are defined as IL-7R α ⁺ Lineage⁻ and sub grouped into ILC1s, ILC2s and ILC3s (267). Alongside IL-7R α expression, CD161 is also expressed on human ILCs and is commonly used in their identification (267, 268). Several further markers, not used in mice, have also been well established in identifying different human ILC subsets. CRTH2 is a common ILC2 marker and alongside c-Kit and NKp44 staining enables the identification of NCR⁻ ILC3s (CRTH2⁻ c-Kit⁺ NKp44⁻), NCR⁺ ILC3s (CRTH2⁻ c-Kit⁺ NKp44⁺) and ILC1s (CRTH2⁻ c-Kit⁻ NKp44⁻) (267-269). ILCs have currently been located within multiple human

tissues with their main analysis being conducted within human blood and tonsils. Due to ILCs being a rare population in tissue analysed, such as human blood, their analysis is normally conducted through the use of surface markers. (267-269).

3.1.1 Project Aims

The inconsistency across publications in the identification methods used to analyse ILCs makes it difficult to compare subgroups across different tissues. This chapter aimed to identify and compare ILC subsets and their phenotype in a consistent manner across lymphoid and non-lymphoid tissues. This was achieved using flow cytometry or confocal imaging with ILCs being identified based on their expression of IL-7R α , due to the functional relevance of IL-7 signalling in ILC development and maintenance being well documented (101, 270). In comparison to CD90 in which the function in ILC biology is unknown.

3.2 RESULTS

The results within this chapter have been published by Dutton et al., in Wellcome Open Research in 2017; Characterisation of innate lymphoid cell populations at different sites in mice with defective T cell immunity (216).

3.2.1 ILC populations are identified within lymphoid and non-lymphoid tissues

ILCs reside in non-lymphoid and lymphoid tissues and are identified by the lack of expression of lineage markers; B220 (identifies B cells and plasmacytoid DCs), CD3 ϵ , CD5 (identifies T cells), CD11c and CD11b (identifies DCs and neutrophils) (112, 271). All helper ILCs express IL-7R α and lack intracellular CD3 ϵ (iCD3 ϵ), which is expressed by immature T cells (Figure 3.1a-e) (243). The largest percentage of ILCs, as a proportion of Live CD45⁺ cells, which will here on be referred to as CD45⁺ cells, was located within the ear and SI LP, however,

numerically ILCs were most abundant in the lung and SI LP, partially due to tissue size (Figure 3.2a). Within the LNs ILCs were numerically less abundant and proportionally much reduced, largely contributed to by the presence of a large naïve lymphocyte population (243).

Due to the inconsistency within the current literature of phenotypic markers used to identify ILC subsets in different tissues and disease models, ILC subsets were analysed based on their expression of TFs (Figure 3.1a-e). T-bet, GATA-3 and ROR γ t were used to identify ILC1s (ROR γ t⁻ T-bet⁺ GATA-3⁻), ILC2s (ROR γ t⁻ GATA-3⁺ T-bet⁻) and ILC3s (ROR γ t⁺ GATA-3⁻), providing a consistent identification method and therefore comparison across all lymphoid and non-lymphoid tissues. Out of these three subgroups ILC1s were dominant in the ear and auricular LN (auLN), ILC3s within the SI LP, mLN and auLN and ILC2s within the lung (Figure 3.2b). Categorising ILC subgroups based on TF expression lead to the identification of a putative fourth ILC population, triple negative (TrN) ILCs, so called because this population lacked expression of T-bet, GATA-3 and ROR γ t. TrN ILCs were detected in all tissues analysed but were most prevalent in the ear and lung.

3.2.2 ILC3 subsets are not evenly distributed between assessed tissues

The recent identification of ILC1s as a distinct group from cNK cells and the lack of lineage markers identified to clearly separate ILC1s from cNK cells and NCR⁺ ILC3s has meant that ILC1s phenotype and functions are less characterised within the literature compared to ILC2s and ILC3s (130, 135, 263, 272). Therefore, within this study characterisation and phenotyping of the ILC subsets was restricted to ILC2s and ILC3s, which were assessed and compared across the Ear, auLN, SI LP, lung and mLN. Within adult mice ILC3s can be divided into 3 subgroups

Figure 3.1. Characterisation of ILCs in lymphoid and non-lymphoid tissue

Cells were isolated from ear, auLN, SI LP, lung and mLN from WT mice as described in methods. When identifying ILCs the lineage markers include; B220, CD11c, CD11b, CD3 and CD5. ILCs were gated negatively for iCD3 ϵ .

Each data point represents 2 ears, 2 auLNs, 1 SI LP, 1 lung and 1 mLN from one mouse. Data pooled a minimum of 3 experiments. Values on flow cytometry plots represent percentages of ILC as a proportion of Live CD45⁺ cells and ILC subsets as a proportion of total ILCs.

- a) Representative flow cytometry plots, previously gated on Live CD45⁺ cells, showing ILCs (Lineage⁻ IL-7R α ⁺ iCD3 ϵ ⁻), ILC1s (Lineage⁻ IL-7R α ⁺ iCD3 ϵ ⁻ GATA-3⁻ ROR γ t⁻ T-bet⁺), ILC2 (Lineage⁻ IL-7R α ⁺ iCD3 ϵ ⁻ GATA-3⁺ ROR γ t⁻ T-bet⁻), ILC3 (Lineage⁻ IL-7R α ⁺ iCD3 ϵ ⁻ GATA-3⁻ ROR γ t⁺) and TrN ILCs (Lineage⁻ IL-7R α ⁺ iCD3 ϵ ⁻ GATA-3⁻ ROR γ t⁻ T-bet⁻) within the ear.
- b) Representative flow cytometry plots, previously gated on Live CD45⁺ cells, showing ILCs, ILC1s, ILC2, ILC3 and TrN ILCs within the auLN.
- c) Representative flow cytometry plots, previously gated on Live CD45⁺ cells, showing ILCs, ILC1s, ILC2, ILC3 and TrN ILCs within the SI LP.
- d) Representative flow cytometry plots, previously gated on Live CD45⁺ cells, showing ILCs, ILC1s, ILC2, ILC3 and TrN ILCs within the Lung.
- e) Representative flow cytometry plots, previously gated on Live CD45⁺ cells, showing ILCs, ILC1s, ILC2, ILC3 and TrN ILCs within the mLN.

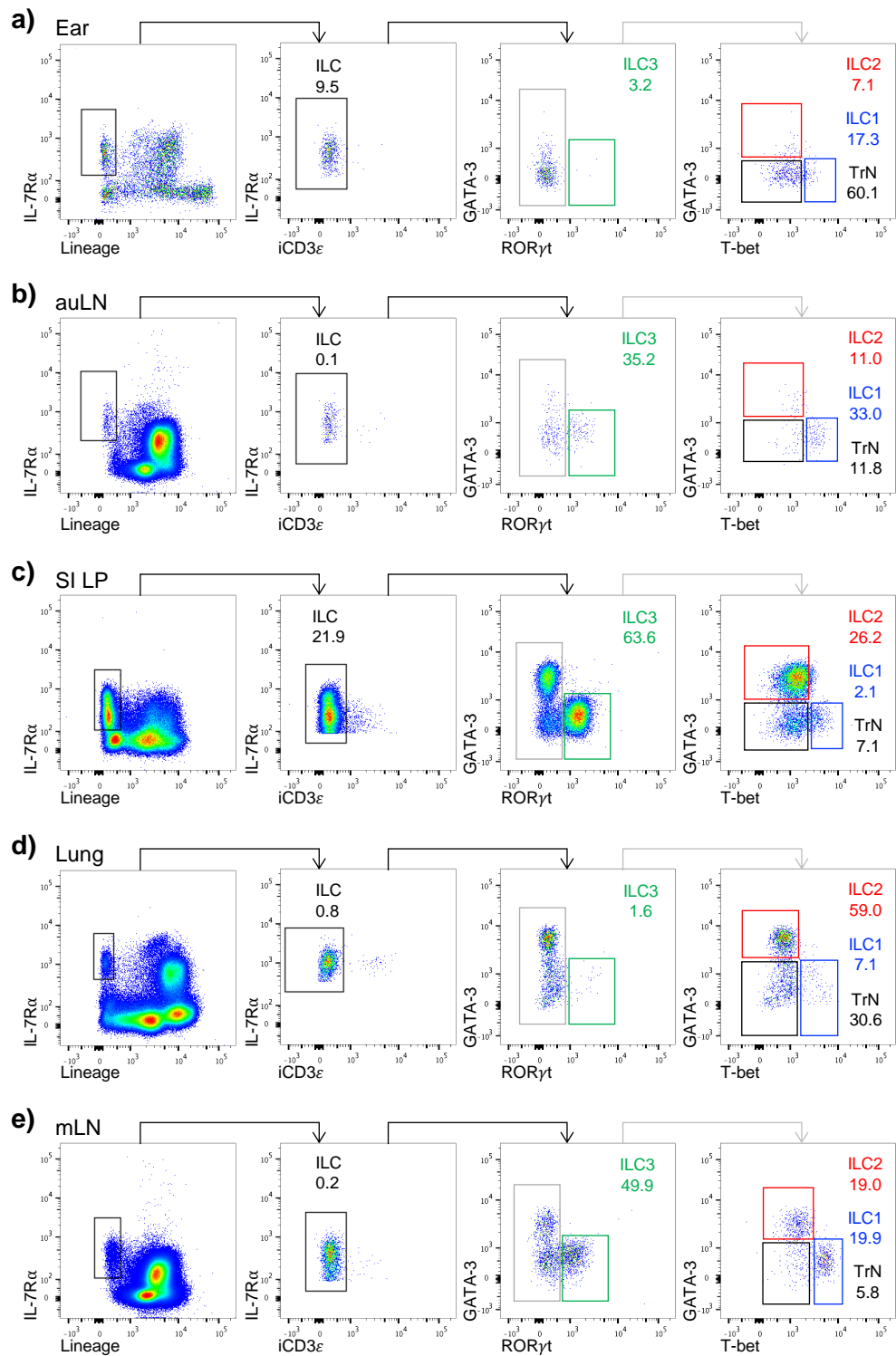
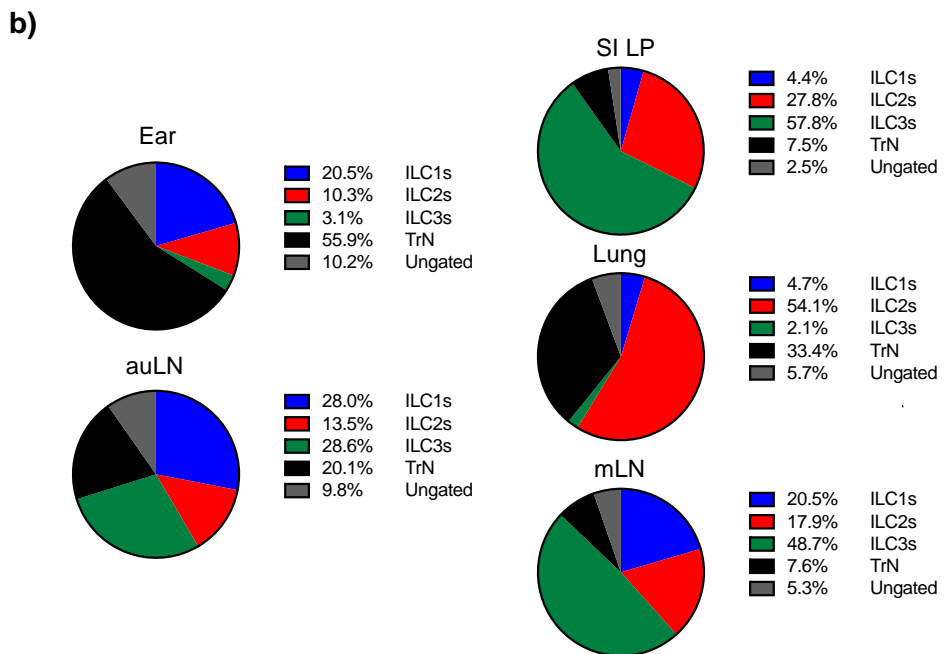
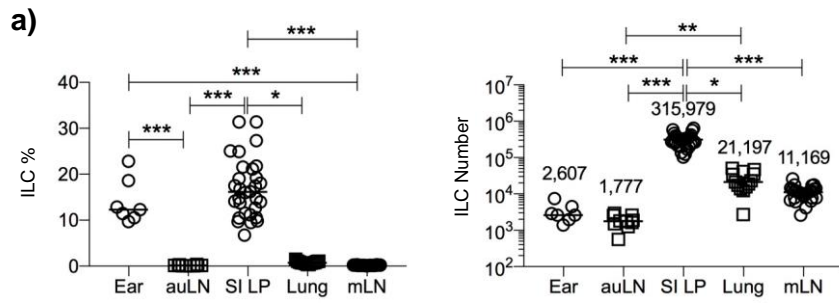


Figure 3.2. Quantification of ILCs in lymphoid and non-lymphoid tissue

Cells were isolated from ear, auLN, SI LP, lung and mLN from WT mice as described in methods. When identifying ILCs the lineage markers include; B220, CD11c, CD11b, CD3 and CD5. ILCs were gated negatively for iCD3 ϵ .

Each data point represents 2 ears, 2 auLNs, 1 SI LP, 1 lung and 1 mLN from one mouse. Data pooled a minimum of 3 experiments. Values on flow cytometry plots represent percentages, bars on scatter plots represents the median, which is also shown numerically. Statistical significance was tested using Kruskal-Wallis one-way ANOVA with post hoc Dunn's test: * $p \leq 0.05$, ** $p \leq 0.01$, *** $p \leq 0.001$.

- a) Percentage, as a proportion of Live CD45⁺ (left), and number (right) of ILCs (Live CD45⁺ Lineage⁻ IL-7R α ⁺ iCD3 ϵ ⁻) cells within the ear (n=6), auLN (n=10), SI (n=30), lung (n=13) and mLN (n=26).
- b) Pie charts showing the mean percentage of ILC1s (Live CD45⁺ Lineage⁻ IL-7R α ⁺ iCD3 ϵ ⁻ GATA-3⁻ ROR γ t⁻ T-bet⁺), ILC2s (Live CD45⁺ Lineage⁻ IL-7R α ⁺ iCD3 ϵ ⁻ GATA-3⁺ ROR γ t⁻ T-bet⁻), ILC3s (Live CD45⁺ Lineage⁻ IL-7R α ⁺ iCD3 ϵ ⁻ GATA-3⁻ ROR γ t⁺), TrN ILCs (Live CD45⁺ Lineage⁻ IL-7R α ⁺ iCD3 ϵ ⁻ GATA-3⁻ ROR γ t⁻ T-bet⁻) and ungated cells (Live CD45⁺ Lineage⁻ IL-7R α ⁺ iCD3 ϵ ⁻) as a proportion of total ILCs in the ear (n=6), auLN (n=10), SI (n=30), lung (n=13) and mLN (n=26).



based on their expression of NKp46 and CCR6; NKp46⁻ CCR6⁺ LTi-like cells, NKp46⁺ CCR6⁻ NCR⁺ ILC3s and NKp46⁻ CCR6⁻ NCR⁻ ILC3s, as discussed previously (130, 139). The ability to compare ILC3s consistently across different tissues shows that the ILC3 subsets are not evenly distributed between these analysed sites (Figure 3.3a-c). Within the SI LP all three ILC3 populations were clearly identified, consistent with the requirement for LTi-like cells in promoting epithelial repair and maintenance, NCR⁻ ILC3s in providing regulatory signals to CD4⁺ T cells and NCR⁺ ILC3s function in the protection against extracellular pathogens (26, 162, 168, 187). In comparison LTi-like cells are the clear dominant population within the assessed lymphoid tissues and are important in the regulation of adaptive responses and maintenance of LN structure (114, 243, 244). ILC3s are the smallest subgroup of ILCs within the ear and the lung, shown in Figure 3.2, however, this population clearly consists of NCR⁻ ILC3s and LTi-like cells in both tissues. Within the lung ILC3s play a role in the protection against extracellular bacterial infections and within the skin are important in wound repair (107, 229). Therefore, ILC3 subsets seem to be distributed according to their functional requirement in different tissues.

3.2.3 ILC2s phenotype differs between assessed tissues

The plethora of ILC2 surface makers associated with their phenotype has caused inconsistencies in ILC2 identification across the literature. Therefore, within these studies ILC2s were identified via the expression of GATA-3, which is required for their full maturation and function, to enable the assessment and comparison of common ILC2 surface markers across the ear, SI LP, Lung and mLN (136). Lineage⁺ IL-7R α ⁻ cells were used as a control as these mainly represent APCs, such as B cells, DCs and macrophages which have very low, if

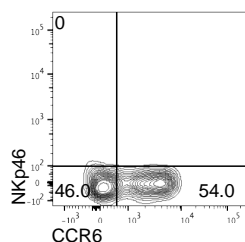
Figure 3.3. Analysis of ILC3 subsets isolated from different tissues

Cells were isolated from ear, auLN, SI LP, lung and mLN as described in methods. Lineage markers include; B220, CD11c, CD11b, CD3 and CD5. Cells were previously gated on ILC3s (Live CD45⁺ Lineage⁻ iCD3ε⁻ IL-7Rα⁺ GATA-3⁻ RORγt⁺). ILC3s were identified using differential expression of CCR6 and NKp46.

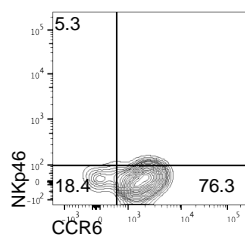
Each data point represents 2 ears, 2 auLNs, 1 SI LP, 1 lung and 1 mLN from one mouse. Data pooled from a minimum of 3 experiments. Values on flow cytometry plots represent percentages, bars on scatter plots represents the median, which is also shown numerically. Statistical significance was tested using Kruskal-Wallis one-way ANOVA with post hoc Dunn's test: *p≤0.05, **p≤0.01, ***p≤0.001.

- a) Representative flow cytometry plots showing expression of CCR6 and NKp46 on ILC3s within the ear, auLN, SI LP, lung and mLN.
- b) Percentage of ILC3s expressing CCR6 and NKp46 within the ear (n=7), auLN (n=10), SI LP (n=28), lung (n=13) and mLN (n=26).
- c) Number of ILC3s expressing CCR6 and NKp46 within the ear (n=7), auLN (n=10), SI (n=28), lung (n=13) and mLN (n=26).

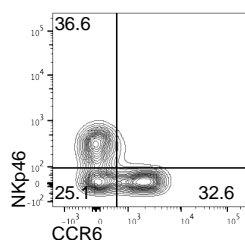
a) Ear



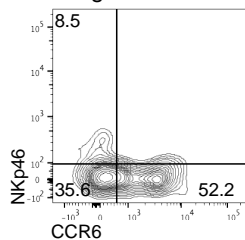
auLN



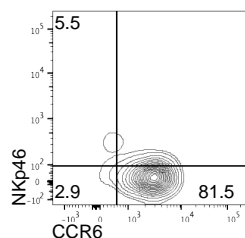
SI LP



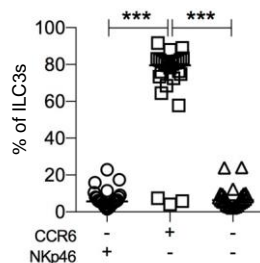
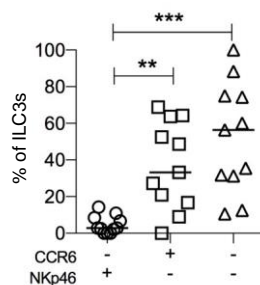
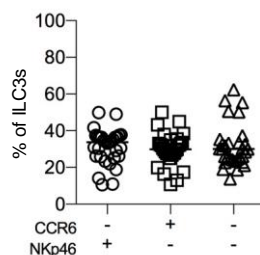
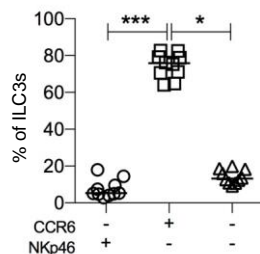
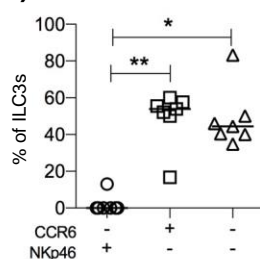
Lung



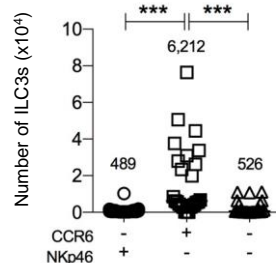
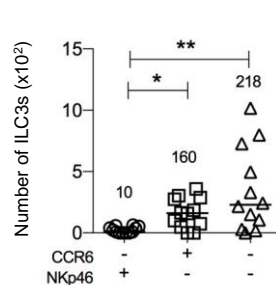
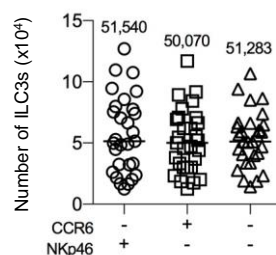
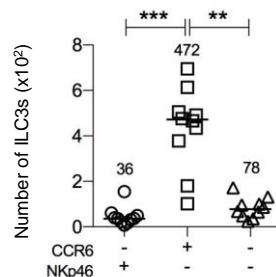
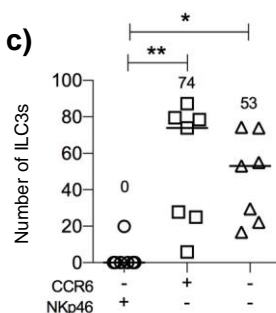
mLN



b)



c)



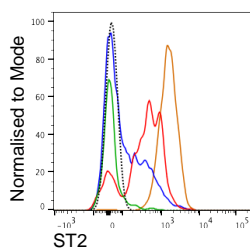
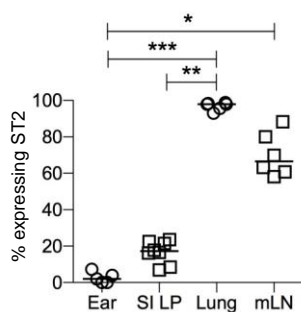
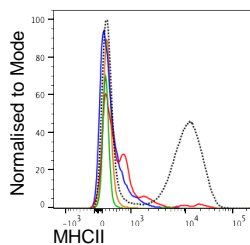
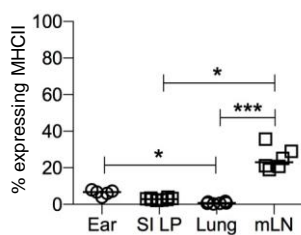
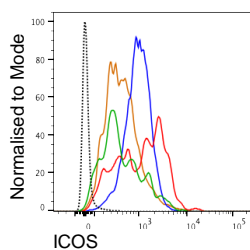
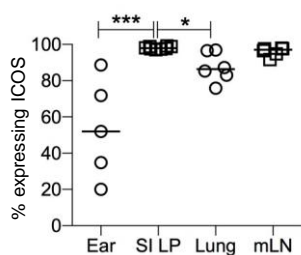
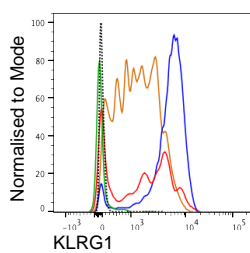
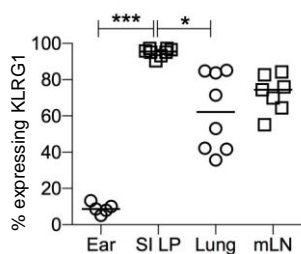
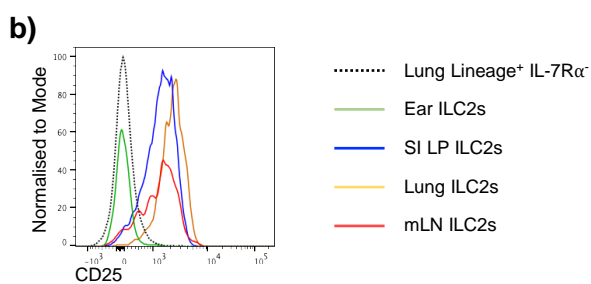
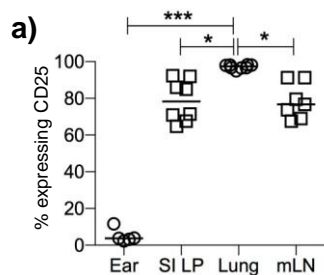
any, expression of the key ILC2 phenotypic markers assessed within these studies (273). Markers commonly associated with ILC2 identification, in previous studies, include CD25, KLRG1 and the co-stimulatory molecule ICOS which are highly expressed on ILC2s with the SI LP, Lung and mLN (Figure 3.4a-b) (25, 108, 142, 274). In comparison ILC2s within the ear lacked CD25 and KLRG1 expression with variable levels of ICOS. CD25 and KLRG1 are both activation markers expressed on activated T cells, suggesting that within the ear ILC2s had a low activation status (275, 276). As previously discussed, ILC2s within the mLN express MHCII, although at lower levels compared to APC B cells, which enables their interactions with CD4⁺ T cells (164). MHCII expression was also detected on lung ILC2s, although at a reduced frequency in comparison to mLN ILC2s (164). Consistent with this study, a proportion of ILC2s within the mLN express MHCII, with the frequency of expression being comparably lower than APCs. Lung ILC2s, on the other hand, alongside ear and SI LP ILC2s had negligible levels of MHCII. ST2 is one of the most common markers used in ILC2 identification across a variety of tissues including the ear skin, mLN and lung and is important in the activation of ILC2s via IL-33 stimulation (164, 221, 231). Controversially, ST2 expression was only highly expressed within the lung and mLN, with lower levels detected in the ear and SI LP. This may suggest that ST2 cannot be uniformly used across different tissues in the identification of ILC2s, showing the importance of establishing the phenotype of ILC2s in a specific tissue, in which GATA-3 is a useful tool, to enable efficient and correct identification of ILC subsets.

Figure 3.4. Characterisation of ILC2s isolated from different tissues

Cells were isolated from ear, SI LP, lung and mLN as described in methods. Lineage markers include; B220, CD11c, CD11b, CD3 and CD5. Cells were previously gated on ILC2s (Live CD45⁺ Lineage⁻ iCD3⁻ IL-7R α ⁺ GATA-3⁺) and their phenotype assessed.

Each data point represents 2 ears, 1 SI LP, 1 lung and 1 mLN from one mouse. Data pooled from a minimum of 3 experiments. Within scatter plots the bar represents the median. Statistical significance was tested using Kruskal-Wallis one-way ANOVA with post hoc Dunn's test: *p \leq 0.05, **p \leq 0.01, ***p \leq 0.001.

- a) Percentage of ILC2s expressing CD25, KLRG1, ICOS, MHCII and ST2 normalised to mode within the ear (n=5), SI LP (n=8), lung (n=6-8) and mLN (n=6).
- b) Representative histograms showing the expression of CD25, KLRG1, ICOS, MHCII and ST2 on ILC2s or Lineage⁺ IL-7R α ⁺ cells within the ear (green line), SI LP (blue line), lung ILC2s (orange line) and mLN (red line), using lung Lineage⁺ IL-7R α ⁻ (black dotted line) as a control.



3.2.4 Lineage⁻ IL-7R α ⁺ cells lacking classical ILC TF expression are a true ILC population

Until recently, publications contained little information on the presence or function of ILCs lacking the three TFs, T-bet, GATA-3 and ROR γ t. A study by Wang et al., published in 2017, has identified a fourth subgroup of ILCs, termed ILCregs that lack T-bet, GATA-3 and ROR γ t expression (113). They have been termed regulatory due to their ability to suppress intestinal inflammation through the production of IL-10 (113). To confirm that the TrN ILC population identified within these studies was a true ILC population and was not being contaminated by IL-7R α ⁺ non ILCs the current lineage channel was extended to include antibodies that recognise cells expressing CD19 (identifying B cells), Ter119 (identifying erythrocytes), Gr1 (identifying macrophages, monocytes and eosinophils), CD123 (identifying DCs), F4/80 (identifying macrophages and eosinophils), CD49b (identifying cNK cells) and Fc ϵ RI (identifying basophils and mast cells) (112, 164, 271, 274, 277-282). TrN ILCs were analysed within the ear due to this tissue containing the largest proportion of this population. Even with the extended lineage channel, the TrN population still remained to be the largest subset of ILCs within the ear (~50%), suggesting that this population is not comprised of IL-7R α ⁺ non-ILCs (Figure 3.5a-b).

To provide further evidence that the TrN ILCs resembled ILCs, expression of Id2 using Id2 GFP mice was undertaken. Id2 is paramount in the development of all ILC populations, suppressing the developmental pathway towards the T or B cell lineage (127, 136, 152, 153). Expression has been identified in mature cNK cells, all ILC3 subsets and ILC2s and not within mature T or B cells (127, 136). However, ILCs Id2 dependent development is not unique, with other lineages such as DCs expressing Id2 in their mature state (258). Using WT mice as a control for

Id2 GFP gating, it was observed that within Id2 GFP reporter mice ~90% of ILCs within the ear express Id2, although their expression was weaker than cNK cells, which are a known population to express Id2 (Figure 3.5c-d) (127). The extended lineage used to identify ILCs confirmed that other populations expressing Id2 were not included within this analysis. This further supports the hypothesis that the TrN ILCs were likely to be an ILC population that doesn't fit within the existing nomenclature.

3.2.5 ILC identification via TF is affected by digestion protocols

The lack of common ILC2 markers expressed within the ear, raised the concern that the ear digestion protocol (EDP) was downregulating or cleaving surface proteins during the preparation of the ear. This has been shown within previous studies which report that different digestion protocols can result in the reduced ability to identify certain surface markers, affecting analysis (266). If IL-7R α ⁺ Lineage⁺ hematopoietic cells were losing the expression of their lineage markers this could lead to their identification as IL-7R α ⁺ Lineage⁻ ILCs. This would contaminate the ILC population and result in incorrect identification of ILC populations, potentially included within the TrN ILC gate. To test this hypothesis the lung was prepared under the normal lung digestion protocol (LDP) and compared to preparation under the EDP. These two protocols were compared due to them sharing the same digestion enzymes, Liberase TM and DNase, but at different concentrations. Within the EDP the enzymes were used at a higher concentration than the LDP, roughly x150 and x13 higher, respectively, and incubated at 37°C for twice as long. Thus, the EDP is a much harsher digestion to that of the LDP, but there are similarities in the enzymes used. Notably, isolating

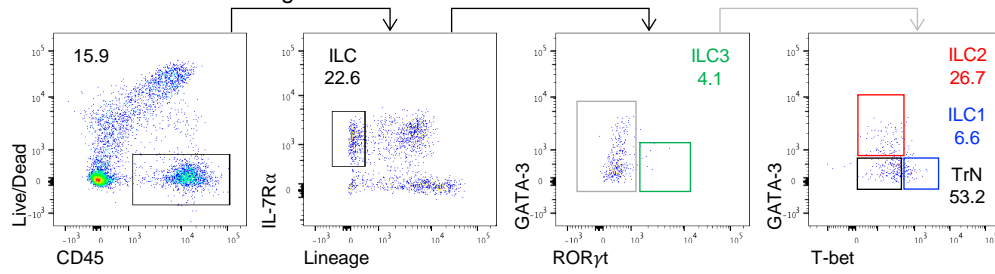
Figure 3.5. Evidence that Lineage⁻ IL-7Rα⁺ GATA-3⁻ RORγt⁻ T-bet⁻ cells are ILCs

Cells were isolated from the ear and spleen of WT mice and Id2 GFP reporter mice as described in methods. When identifying ILCs lineage markers include; B220, CD11c, CD11b, CD3, CD5, CD19, Ter119, Gr1, CD123, CD49b, F4/80 and FcεRI.

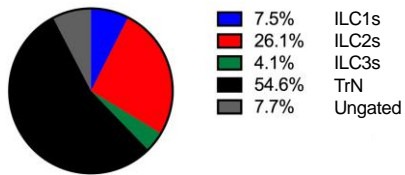
Each data point represents 2 ears and 1 spleen from one mouse. Data pooled from a minimum of 2 experiments. Values on flow cytometry plots represent percentages of ILC as a proportion of Live CD45⁺ cells and ILC subsets as a proportion of total ILCs. Bars on scatter plots represents the median, which is also shown numerically.

- a) Representative flow cytometry plots showing Live CD45⁺ cells, ILCs (Live CD45⁺ Lineage⁻ IL-7Rα⁺ iCD3ε⁻) and ILC1s (Live CD45⁺ Lineage⁻ IL-7Rα⁺ iCD3ε⁻ GATA-3⁻ RORγt⁻ T-bet⁺), ILC2s (Live CD45⁺ Lineage⁻ IL-7Rα⁺ iCD3ε⁻ GATA-3⁺ RORγt⁻ T-bet⁻), ILC3s (Live CD45⁺ Lineage⁻ IL-7Rα⁺ iCD3ε⁻ GATA-3⁻ RORγt⁺) and TrN ILCs (Live CD45⁺ Lineage⁻ IL-7Rα⁺ iCD3ε⁻ GATA-3⁻ RORγt⁻ T-bet⁻) in the ear with the extended lineage. ILCs were gated negatively for iCD3ε (gating strategy not shown).
- b) Pie chart showing mean percentage of ILC1s, ILC2s, ILC3s, TrN and ungated cells (Live CD45⁺ Lineage⁻ IL-7Rα⁺ iCD3ε⁻), as a total proportion of ILCs in the ear (n=6)
- c) Representative flow cytometry plots previously gated on Live CD45⁺ cells showing ILCs (Live CD45⁺ Lineage⁻ IL-7Rα⁺) expression of Id2 GFP in Id2 GFP reporter mice (top) and WT controls (bottom) within the ear.
- d) Representative flow cytometry plots previously gated on Live CD45⁺ cells, showing cNK cell (Live CD45⁺ NK1.1⁺ NKp46⁺) expression of Id2 GFP in Id2 GFP reporter mice (top) and WT controls (bottom) within the spleen.

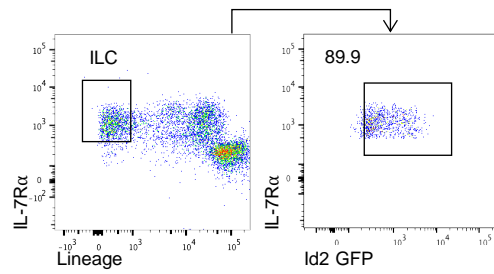
a) Ear – Extended Lineage



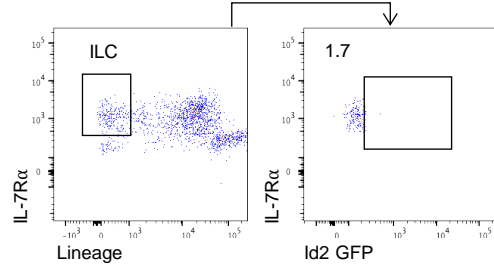
b) Ear – Extended Lineage



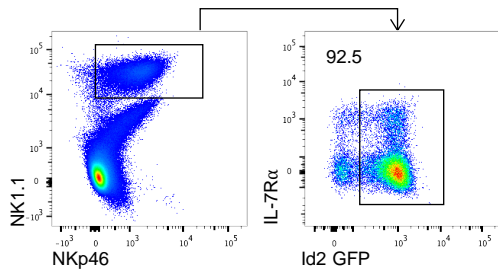
c) Id2 GFP Ear



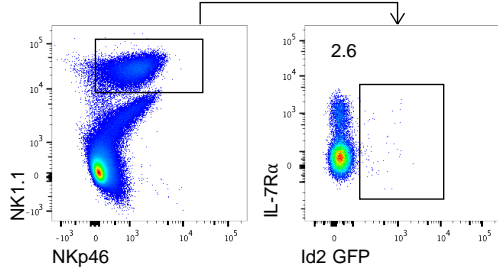
WT Ear – Control for Id2 GFP



d) Id2 GFP Spleen



WT Spleen – Control for Id2 GFP



cells from the lung using the EDP rather than the LDP, resulted in a significant 2-fold increase in CD45⁺ hematopoietic cells, and 4-fold increase in ILCs, based on Lineage⁻ IL-7R α ⁺ gating, revealing that greater yields of cells could be isolated with harsher digestion of the lung tissue (Figure 3.6a-b). Even though numerically there were more ILCs within the EDP, the proportion of CD45⁺ cells and ILCs were comparable between digestions, suggesting that ILC gating was not being contaminated. To further ensure that Lineage⁺ cells were not becoming Lineage⁻, expression the lineage markers that are identified on IL-7R α ⁺ hematopoietic populations, CD3 ϵ , CD5, CD49b, F4/80 and Fc ϵ RI were assessed on CD45⁺ cells within the lung. All markers were not downregulated under the EDP, proposing that IL-7R α ⁺ Lineage⁺ populations are not 'artificially' becoming IL-7R α ⁺ Lineage⁻ due to digestion (Figure 3.7a-b).

Harsher digestion of the lung tissue with the EDP appeared to release a higher yield of ILCs. To look in more detail at the ILCs isolated through digestion of the lung under the LDP or the EDP, TF expression by ILCs was assessed. Considering an increase in total ILCs under the EDP, TrN ILCs and ILC3s were the only subsets to increase numerically, suggesting that the EDP may affect the identification of ILC1 and ILC2 subsets (Figure 3.8a-b). A potential mechanism for this is that harsher digestion conditions, may affect the expression of signature TFs used to identify the ILC subsets, potentially resulting in the 'artificial' identification of TrN ILCs. To explore this further, TF expression was assessed in CD45⁺ cells from the lung under LDP or EDP. The EDP caused a significant decrease in the expression of T-bet and GATA-3 but not ROR γ t on CD45⁺ cells within the lung (Figure 3.8c-d). This suggests that the TrN population may be comprised of ILC1s and ILC2s that have lost their expression of T-bet and GATA-3, respectively. Whilst some TrN ILCs may exist and are apparent in tissues that have had a much

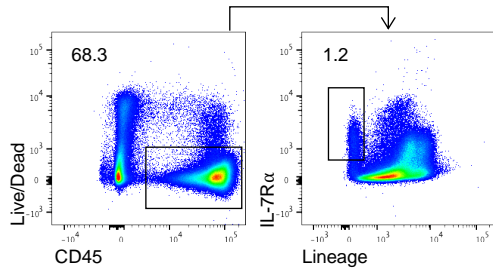
Figure 3.6. Identification of the ILC population is unaffected by the ear digestion protocol

Cells were isolated from the ear using the ear digestion protocol (EDP) and the lung using either the normal lung digestion protocol (LDP) as described in methods of WT mice. When identifying ILCs lineage markers include; B220, CD11c, CD11b, CD3, CD5, CD19, Ter119, Gr1, CD123, CD49b, F4/80 and FcεRI. ILCs were gated negatively for iCD3ε (gating strategy not shown).

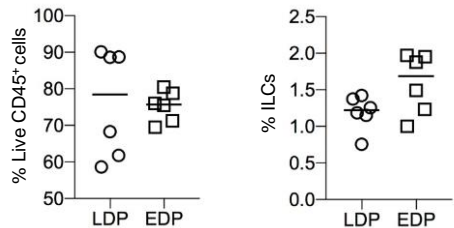
Each data point represents 2 ears and 1 lung from one mouse. Data pooled from a minimum of 2 experiments. Values on flow cytometry plots represent percentages, bars on scatter plots represents the median, which is also shown numerically. Statistical significance was tested using an unpaired, non-parametric, Mann-Whitney two tailed T test: * $p \leq 0.05$, ** $p \leq 0.01$, *** $p \leq 0.001$.

- a) Representative flow cytometry plots showing Live CD45⁺ cells and ILCs (Live CD45⁺ IL-7Rα⁺ Lineage⁻) populations within the lung under LDP (top) and lung under EDP (bottom).
- b) Percentage (top) and number (bottom) of Live CD45⁺ cells (left) and ILCs (right) within the lung under LDP (n=6) and lung under EDP (n=6).

a) Lung – Lung Digestion Protocol (LDP)



b)



Lung – Ear Digestion Protocol (EDP)

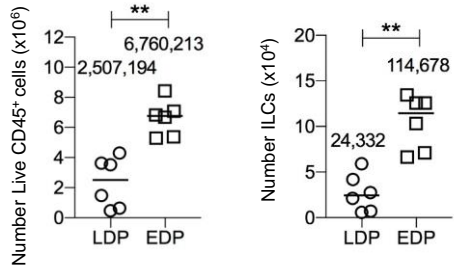
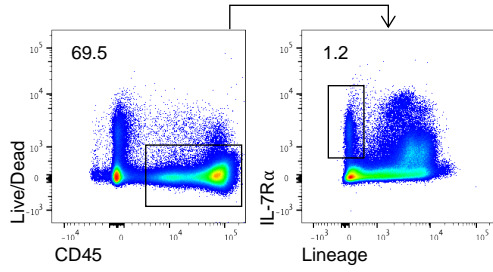


Figure 3.7. Expression of lineage markers used to identify ILCs was not decreased under the ear digestion protocol

Cells were isolated from the ear of WT mice using the EDP and the lung using either the normal LDP or the EDP as described in methods.

Each data point represents 2 ears and 1 lung from one mouse. Data pooled from a minimum of 2 experiments. Values on flow cytometry plots represent percentages, bars on scatter plots represents the median. Statistical significance was tested using an unpaired, non-parametric, Mann-Whitney two tailed T test: * $p \leq 0.05$, ** $p \leq 0.01$, *** $p \leq 0.001$.

- a) Representative flow cytometry plots showing Live CD45⁺ cells expression of CD3 ϵ , CD5, CD49b, F4/80 and Fc ϵ RI within the ear – EDP (left), lung – LDP (middle) and lung – EDP (right).
- b) Percentage of Live CD45⁺ cells expressing CD3 ϵ , CD5, CD49b, F4/80 or Fc ϵ RI within the lung under the LDP (n=6) or the EDP (n=6).

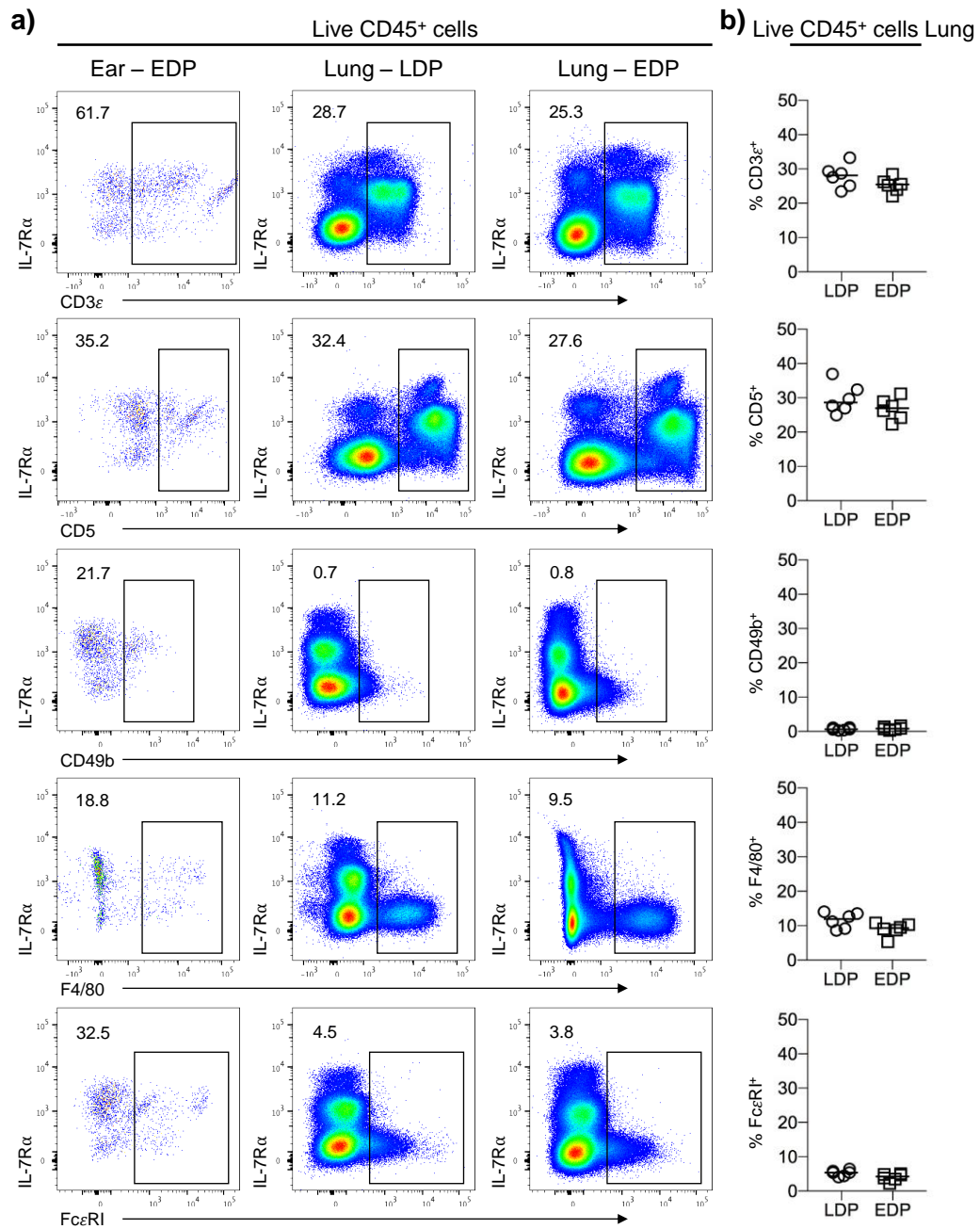


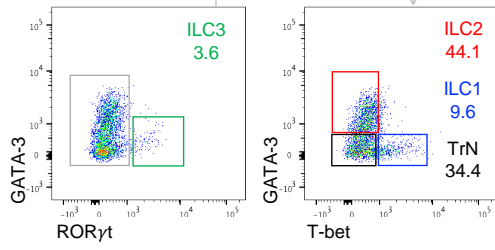
Figure 3.8. ILC transcription factor expression is reduced under the EDP

Cells were isolated from the ear using the EDP and the lung using either the normal LDP or the EDP as described in methods in WT mice. When identifying ILCs lineage markers include; B220, CD11c, CD11b, CD3, CD5, CD19, Ter119, Gr1, CD123, CD49b, F4/80 and FcεRI. ILCs were gated negatively for iCD3ε (gating strategy not shown).

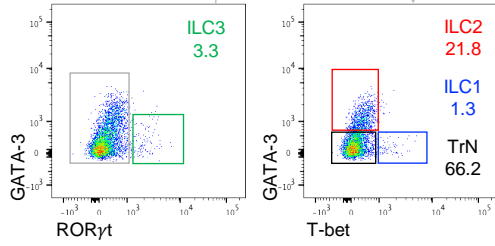
Each data point represents 2 ears and 1 lung from one mouse. Data pooled from a minimum of 2 experiments. Values on flow cytometry plots represent percentages, bars on scatter plots represents the median, which is also shown numerically. Statistical significance was tested using an unpaired, non-parametric, Mann-Whitney two tailed T test: * $p \leq 0.05$, ** $p \leq 0.01$, *** $p \leq 0.001$.

- a) Representative flow cytometry plots, previously gated on ILCs, showing ILC1s (Live CD45⁺ Lineage⁻ IL-7Rα⁺ iCD3ε⁻ GATA-3⁻ RORγt⁻ T-bet⁺), ILC2s (Live CD45⁺ Lineage⁻ IL-7Rα⁺ iCD3ε⁻ GATA-3⁺ RORγt⁻ T-bet⁻), ILC3s (Live CD45⁺ Lineage⁻ IL-7Rα⁺ iCD3ε⁻ GATA-3⁻ RORγt⁺) and TrN ILCs (Live CD45⁺ Lineage⁻ IL-7Rα⁺ iCD3ε⁻ GATA-3⁻ RORγt⁻ T-bet⁻), as a proportion of total ILCs within the lung under LDP (top) and lung under EDP (bottom).
- b) Percentage (top) and number (bottom) of ILC subsets within the lung under LDP (n=6) and lung under EDP (n=6).
- c) Representative flow cytometry plots showing Live CD45⁺ cells expression of RORγt, T-bet, and GATA-3 by Live CD45⁺ cells within the ear – EDP (left), lung – LDP (middle) and lung – EDP (right).
- d) Percentage of Live CD45⁺ cells expressing RORγt, T-bet, or GATA-3 within the lung under the LDP (n=6) or the EDP (n=6).

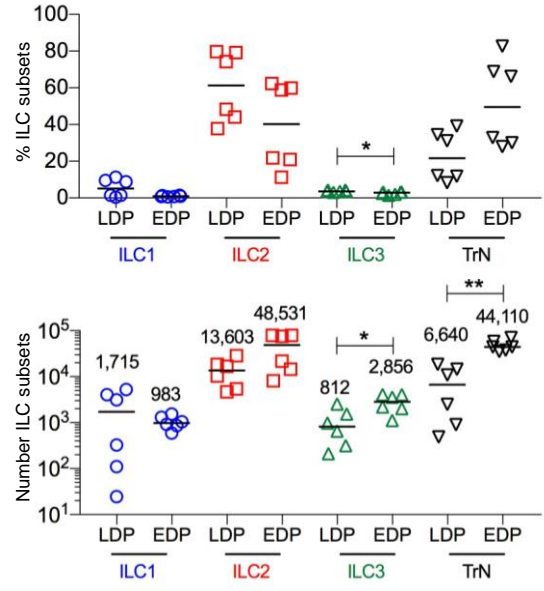
a) Lung – Lung Digestion Protocol (LDP)



Lung – Ear Digestion Protocol (EDP)

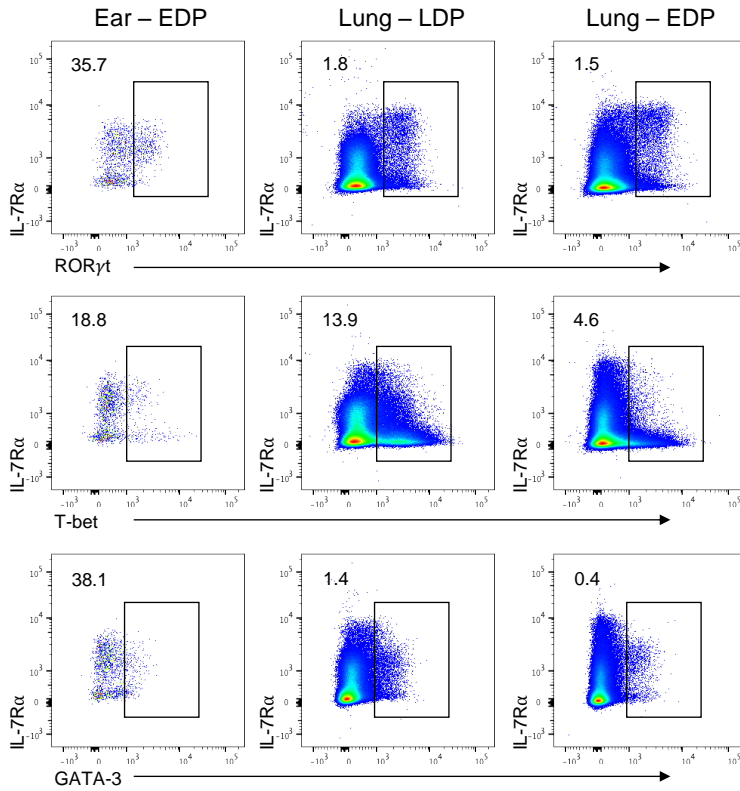


b)



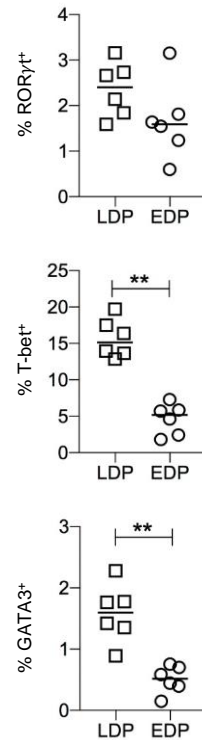
c)

Live CD45⁺ cells



d)

Live CD45⁺ cells Lung



milder digestion (see figure 3.2), these data argue that this population is at least in part an artefact of how the cells are isolated.

3.2.6 Various surface markers are downregulated under a harsh digestion protocol

Comparing the two digestion protocols and observing the effect of the harsher digestion on the expression of T-bet and GATA-3 raised the possibility that other markers previously analysed may also be affected. Therefore, the expression of the markers that were previously chosen as key to characterising ILC2 were compared between the LDP and the EDP. The expression of CD25 and KLRG1 was downregulated under the EDP, however ICOS, MHCII and ST2 were not (Figure 3.9a-b). This suggests that previous phenotyping of ILC2s within the ear may be skewed as ILC2s were identified to lack expression of CD25 and KLRG1 which may just be a result of the digestion. Expanding this analysis, markers required for identifying T cell and ILC3 populations (CD4 and CD8), cellular migration (CD62L, CD69) and, given the impact on TF expression, the proliferation marker Ki-67 were also tested (42, 49, 243, 283). The expression of CD62L, CD4 and CD8 were downregulated under the EDP whereas CD69 and Ki-67 expression were not (Figure 3.9c-d). This suggests that certain surface proteins are cleaved or downregulated during the EDP, which should be taken into consideration upon characterisation of ILCs and other populations such as T cells. These observations are summarised within table 3.1. These results emphasise the importance of digestion protocols and how they can affect the phenotype of the cell upon analysis. To determine whether the LDP was more appropriate in isolating cells from the ear the ear was digested using the EDP and compared to the LDP (Figure 3.10a-b). The decrease in number of CD45⁺ cells and ILC along with ILC percentage suggests that the LDP is insufficient in obtaining a significant yield

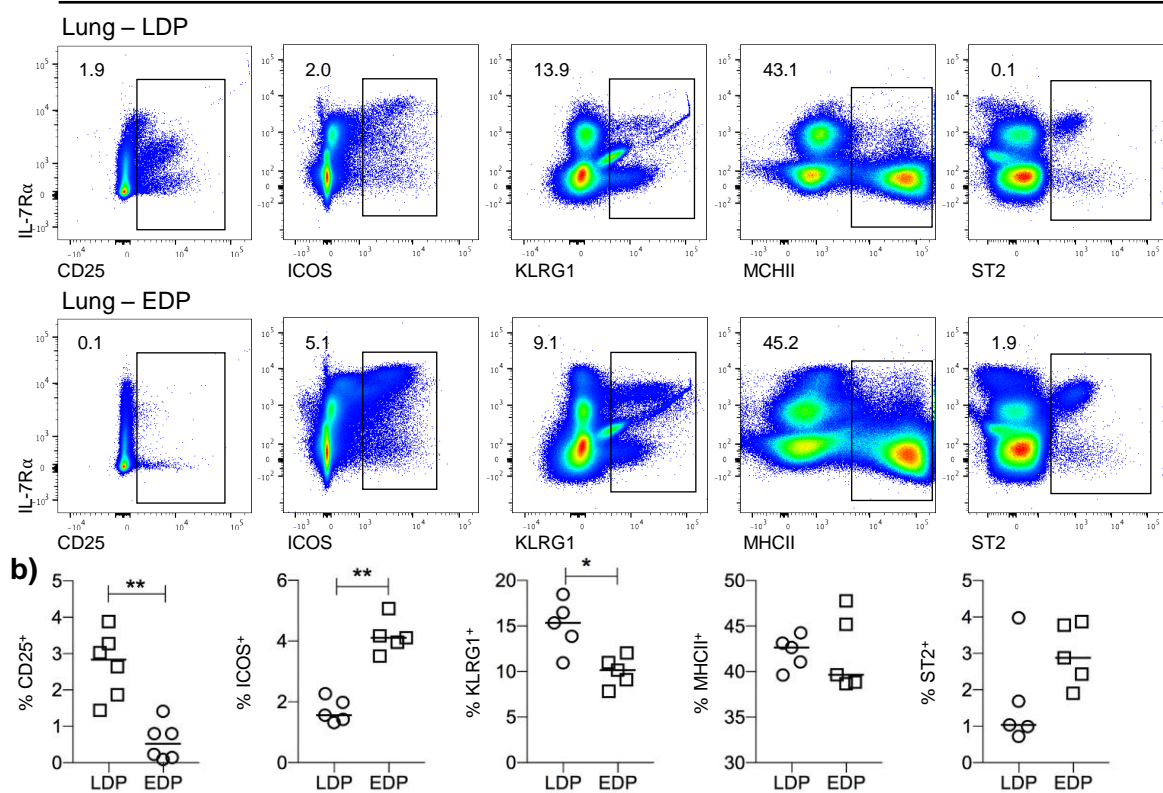
Figure 3.9. Identification of various markers used to phenotype ILCs have decreased expression under the ear digestion protocol

Cells were isolated from the ear using the EDP and the lung using either the normal LDP or the EDP as described in methods in WT mice.

Each data point represents 2 ears and 1 lung from one mouse. Data pooled from a minimum of 2 experiments. Values on flow cytometry plots represent percentages, bars on scatter plots represents the median. Statistical significance was tested using an unpaired, non-parametric, Mann-Whitney two tailed T test: * $p \leq 0.05$, ** $p \leq 0.01$, *** $p \leq 0.001$.

- a) Representative flow cytometry plots showing Live CD45⁺ cells expression of CD25, ICOS, KLRG1, MHCII and ST2 within the lung – LDP (top) and lung – EDP (bottom).
- b) Percentage of Live CD45⁺ cells expressing CD25, ICOS, KLRG1, MHCII or ST2 within the lung under the LDP (n=5-6) or the EDP (n=5-6).
- c) Representative flow cytometry plots showing Live CD45⁺ cell expression of CD62L, CD69, CD4, CD8 and Ki-67 within the lung – LDP (top) and lung – EDP (bottom).
- d) Percentage of Live CD45⁺ cells expressing CD62L, CD69, CD4, CD8 or Ki-67 within the lung under the LDP (n=5-6) or the EDP (n=5-6).

a)

Live CD45⁺ cells

c)

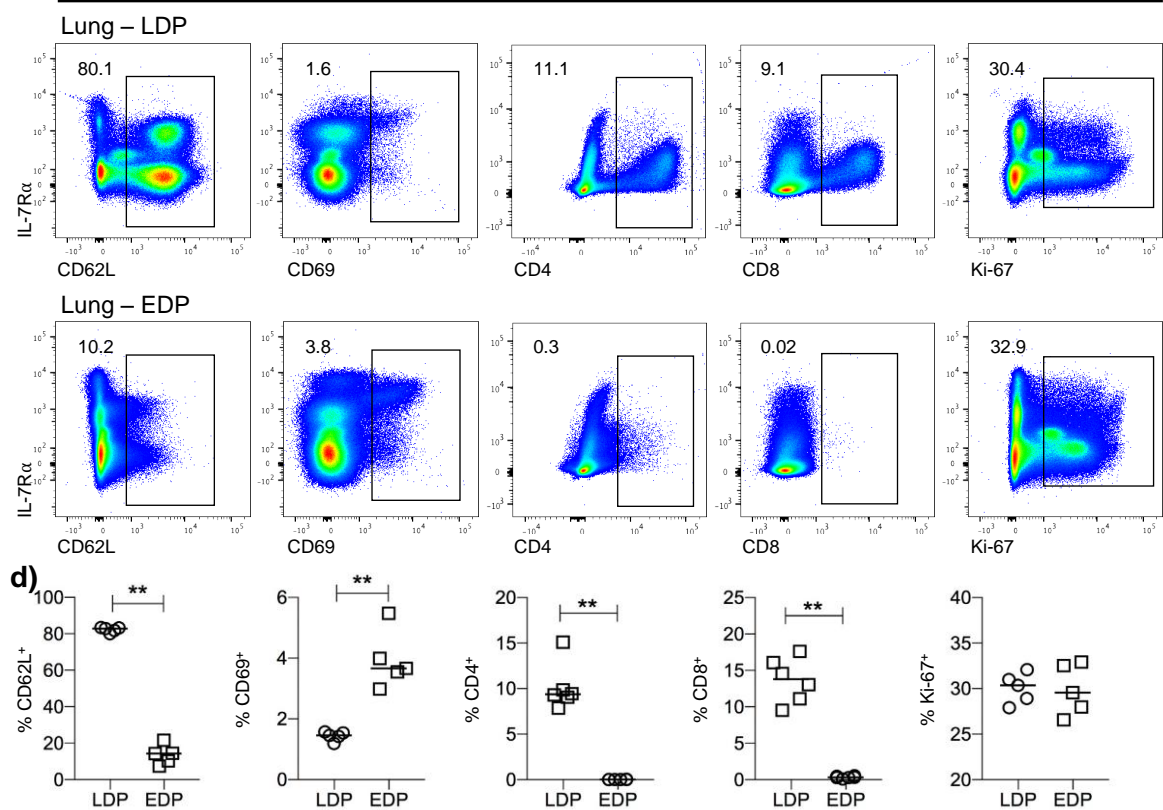
Live CD45⁺ cells

Table 3.1. Summarising table of markers expression compared between the EDP and LDP

A summarising table showing whether the marker expression on Live CD45⁺ cells within the lung were reduced when the lung underwent the EDP compared to the LDP.

Marker		Decreased expression under EDP compared to LDP
Lineage Markers	CD3 ϵ	No
	CD5	No
	CD49b	No
	F4/80	No
	Fc ϵ RI	No
TF	GATA-3	Yes
	ROR γ t	No
	T-bet	Yes
ILC2 Surface Markers	CD25	Yes
	ICOS	No
	KLRG1	Yes
	MHCII	No
	ST2	No
Other Key Markers	CD4	Yes
	CD8	Yes
	CD62L	Yes
	CD69	No
	Ki-67	No



Expression decreased



Expression not decreased

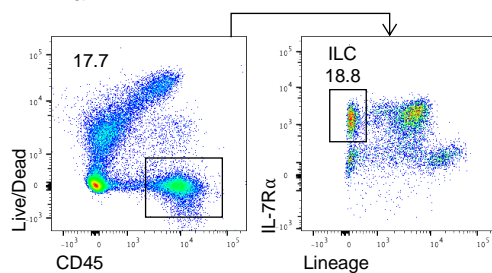
Figure 3.10. Poor ILC isolation from ear skin using milder enzymatic digestion

Cells were isolated from the ear using the ear digestion protocol (EDP) or the lung digestion protocol (LDP) as described in methods in WT mice. When identifying ILCs lineage markers include; B220, CD11c, CD11b, CD3, CD5, CD19, Ter119, Gr1, CD123, CD49b, F4/80 and FcεRI. ILCs were gated negatively for iCD3ε (gating strategy not shown).

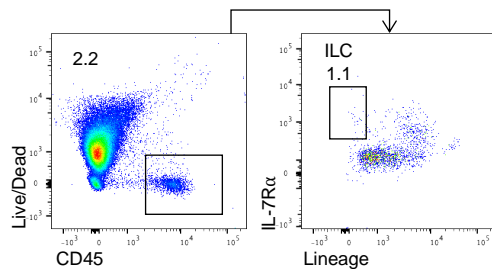
Each data point represents 2 ears from one mouse. Data pooled from a minimum of 2 experiments. Values on flow cytometry plots represent percentages, bars on scatter plots represents the median, which is also shown numerically. Statistical significance was tested using an unpaired, non-parametric, Mann-Whitney two tailed T test: * $p \leq 0.05$, ** $p \leq 0.01$, *** $p \leq 0.001$.

- a) Representative flow cytometry plots showing Live CD45⁺ cells and ILCs within the ear under EDP (top) and ear under LDP (bottom).
- b) Percentage (top) and number (bottom) of Live CD45⁺ cells and ILCs within the ear under EDP (n=6) or LDP (n=5).

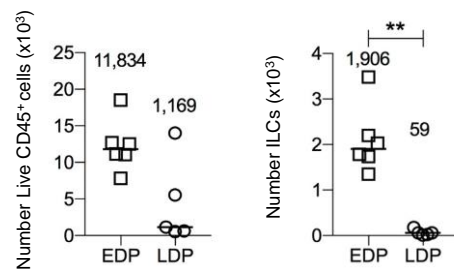
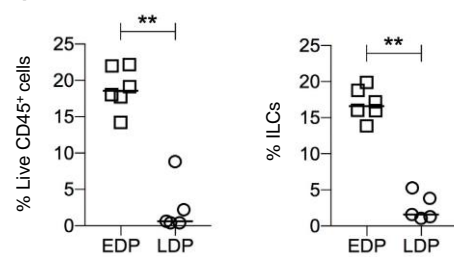
a) Ear – EDP



Ear – LDP



b)



of ILCs from the ear. This indicates that in some cases a harsh digestion is needed to obtain a significant cell yield, however the caveats associated with this should be taken into consideration.

3.2.7 ILCs are located within secondary lymphoid tissues within mouse and human

Flow cytometry is a useful technique used to quantify ILC populations within tissues, however, it is unable to pinpoint the location of cells within the microenvironment. Immunofluorescent imaging enables the visualisation of ILCs, locating the areas in which they reside and potentially which cells they interact with. Building on recently published methods, the location of ILCs within tissues was assessed (243). The stromal network of the mLN provides and maintains a niche microenvironment, supporting cellular interactions and the successful activation of the adaptive immune response (49). Similar to previous reports ILC3s are located within the interfollicular areas positioned at the edge of the B cell zones and T cell follicles (Figure 3.11a) (243). Within the aLN, the microenvironment and organisation of T and B cells is comparable with the mLN, alongside the positioning of ILC3s (Figure 3.11b). This location is key for interactions between T cells and B cells, in the initial stages of the adaptive immune response, suggesting ILC3s may have a role in influencing either T or B cell development (243). To compare the location of ILC3s within lymphoid tissue to non-lymphoid tissues the SI LP was assessed (Figure 3.11c). Comparable to other reports ILC3s were identified within clusters termed CP located near the luminal wall (284).

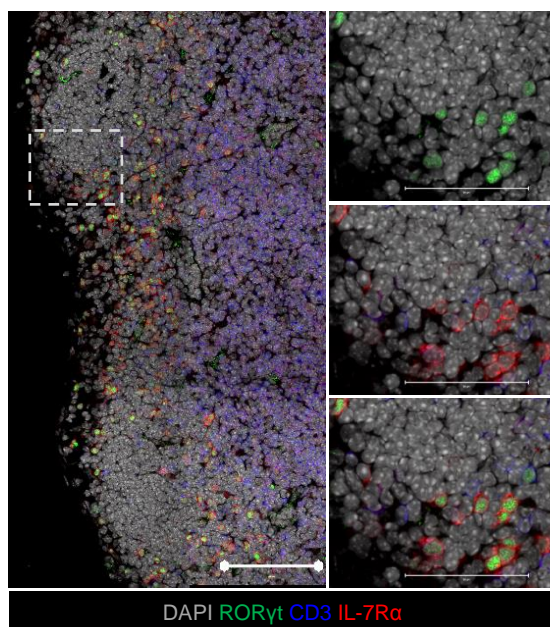
Having identified murine ILCs in lymphoid tissue and due to the cross reactivity of the antibodies used in the murine samples with human tissue, the location of human ILCs was

Figure 3.11. Identification of ILC3s in murine lymphoid and non-lymphoid tissues

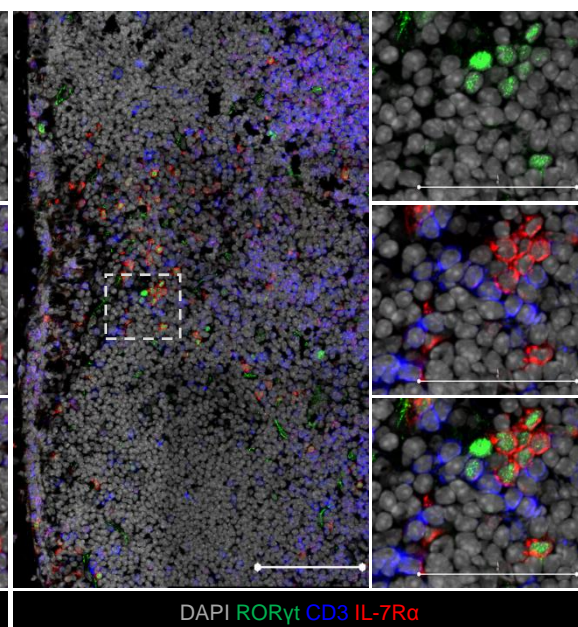
Representative immunofluorescent microscopy images of WT mouse mLN, auLN and SI LP. Sections were stained for ROR γ t, CD3 ϵ and IL-7R α then counterstained with DAPI, to identify ILC3s. Tiled image is positioned on the left, the region of interest (ROI) is highlighted by a white dashed box and the 3 images on the right are zoomed in areas of the ROI. Larger images scale bar represents 100 μ m and smaller images represents 50 μ m. Information regarding the health of the patient, from which the sample was obtained, was not provided.

- a) Tiled image of mLN section (n=4).
- b) Tiled image of auLN section (n=3).
- c) Tiled image of SI LP section (n=3).

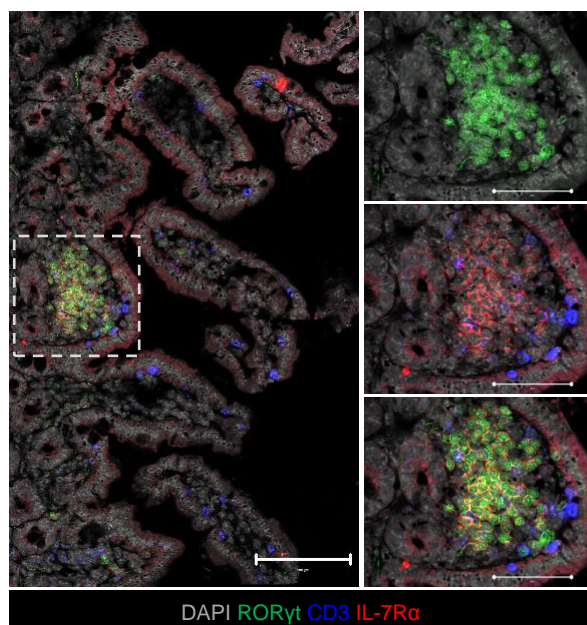
a) mouse mLN – ILC3s



b) mouse auLN – ILC3s



c) mouse SI LP – ILC3s



investigated to provide a basic description of their location and phenotype. Initially the location of ILCs was determined within human adult mLN, to compare to the positioning within mice. ILC3s were located within the interfollicular areas of adult human mLN, similar to murine models and previous publications (Figure 3.12a) (285-287). Within murine models, ILC2s have been located in a similar position to ILC3s in the interfollicular areas (243). This positioning within the mLN supports the function of ILC2s in interacting with T cells, directing the development of the adaptive immune response (164). In contrast to ILC3s, ILC2s within the human mLN were observed at a different location than their position within the murine model (Figure 3.12b). ILC2s were instead located within the B cell follicles, suggesting a potential difference between the function of murine ILC2s and human ILC2s.

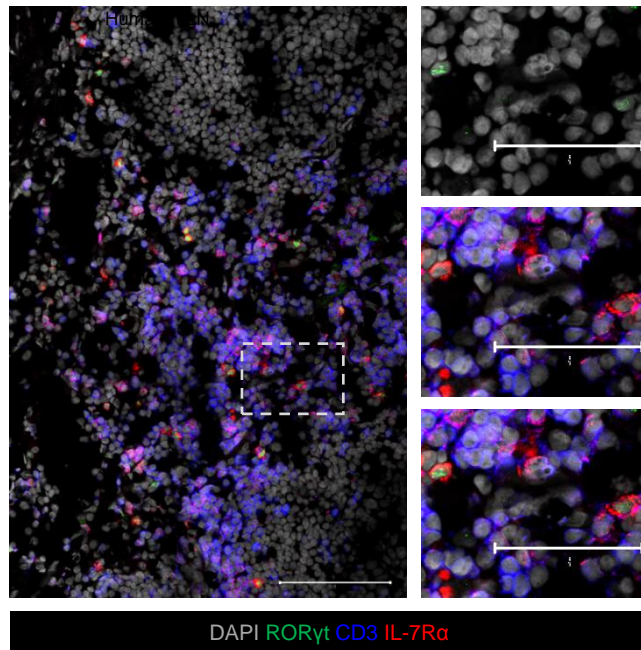
To further characterise human ILCs *in situ* the staining panel was developed to include a 5th colour, enabling the identification and then phenotyping of ILCs. The current literature on human ILCs within SLTs is mainly derived from the adult palatine tonsils (286). All three ILC subsets are located within the tonsil, however studies have focused on characterising ILC3s, with recent publications suggesting their involvement in regulating the proliferation and survival of innate B cells (268, 288-290). The palatine tonsil is histologically similar to the human and mouse mLN, containing B cell follicles surrounded by T cell areas and similar to the mLN, ILC3s were located within the T cell zone, situated between B cell follicles (Figure 3.13a) (291, 292). A common phenotypic marker of ILCs within human tissue is CD161 which is expressed by ILC3s within the tonsil (268, 293). Upon the introduction of CD161 as a 5th colour within the staining panel it was clear that the majority of ILC3s expressed CD161 (Figure 3.13b). MHCII expression on ILCs, as discussed previously, is important in the regulation of CD4⁺ T cells within the spleen and SI (114, 162, 163). ILCs within the tonsil have also been

Figure 3.12. Identification of ILC2s and ILC3s in adult human mLN

Representative immunofluorescent microscopy images of adult human mLN. Sections were counterstained with DAPI. Tiled image is positioned on the left, the ROI is highlighted by a white dashed box and the 3 images on the right are zoomed in areas of the ROI. Larger images scale bar represents 100µm and smaller images represents 50µm. Information regarding the health of the patient, from which the sample was obtained, was not provided.

- a) Tiled image of mLN section, stained for RORγt, CD3ε and IL-7Rα (n=9), identifying ILC3s.
- b) Tiled image of mLN section stained for GATA-3, CD3ε and ICOS (n=5), identifying ILC2s.

a) Human mLN – ILC3s



b) Human mLN – ILC2s

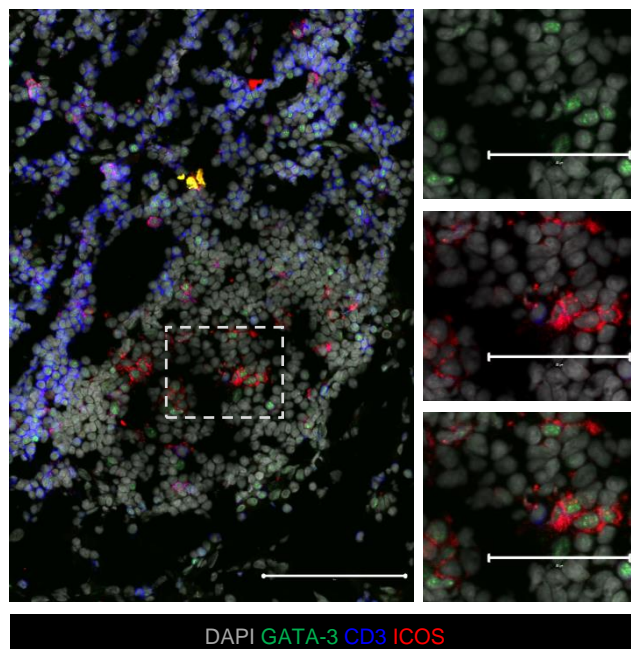
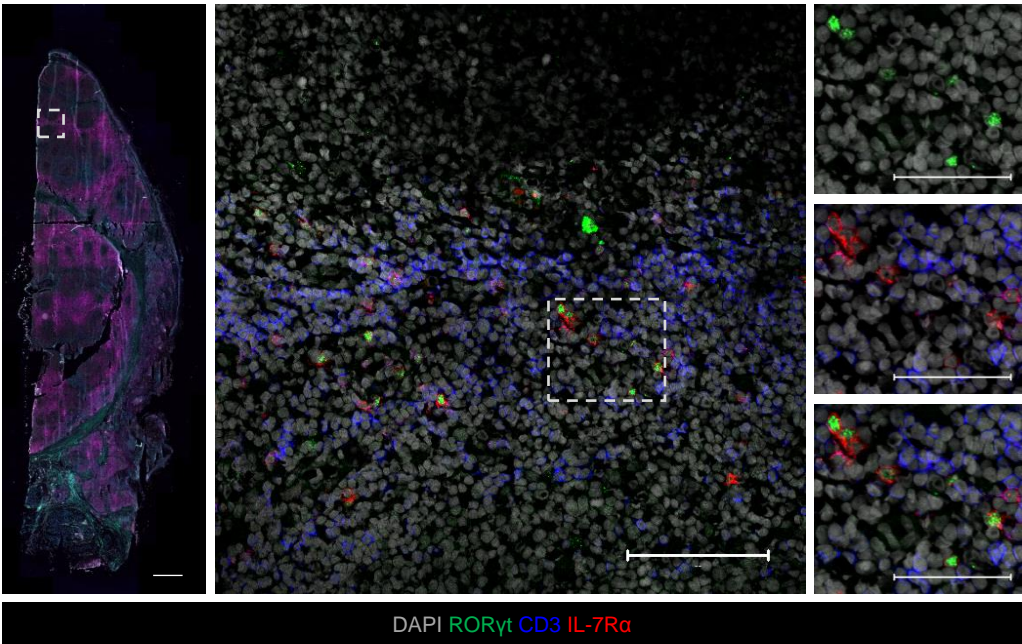


Figure 3.13. Phenotyping of ILC3s within human adult tonsil

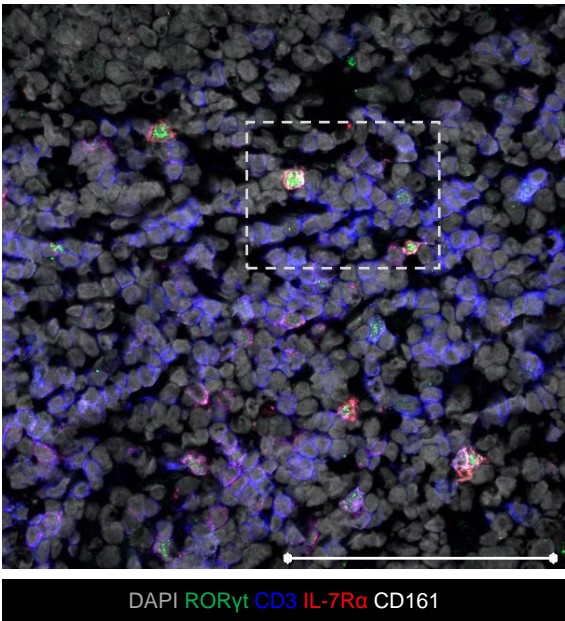
Representative immunofluorescent microscopy images of adult human tonsil. Sections were counterstained with DAPI. Information regarding the health of the patient, from which the sample was obtained, was not provided.

- a) Slide scanned image of whole tonsil section stained for expression of ROR γ t, CD3 ϵ and IL-7R α (left). An interfollicular area is highlighted by a white dashed box. Tile-scanned showing human tonsil interfollicular area stained for expression of ROR γ t, CD3 ϵ and IL-7R α (middle). ROI is highlighted by a white dashed box, the smaller 3 images are zoomed in areas of the ROI. Larger image scale bar represents 100 μ m and smaller images represent 50 μ m (n=4).
- b) Image showing human tonsil interfollicular area stained for expression of ROR γ t, CD3 ϵ , IL-7R α and CD161. ROI is highlighted by a white dashed box, the smaller 3 images are zoomed in areas of the ROI. Larger image scale bar represents 100 μ m and smaller images represent 50 μ m (n=4).
- c) Image showing human tonsil interfollicular area stained for expression of ROR γ t, CD3 ϵ , IL-7R α and MHCII. ROI is highlighted by a white dashed box, the smaller 3 images are zoomed in areas of the ROI. Larger image scale bar represents 100 μ m and smaller images represent 50 μ m (n=4).

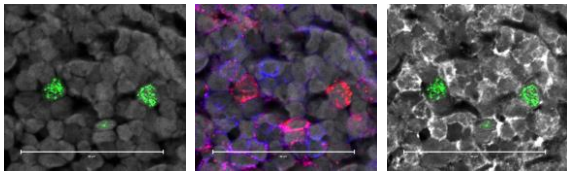
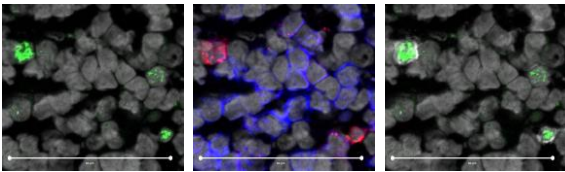
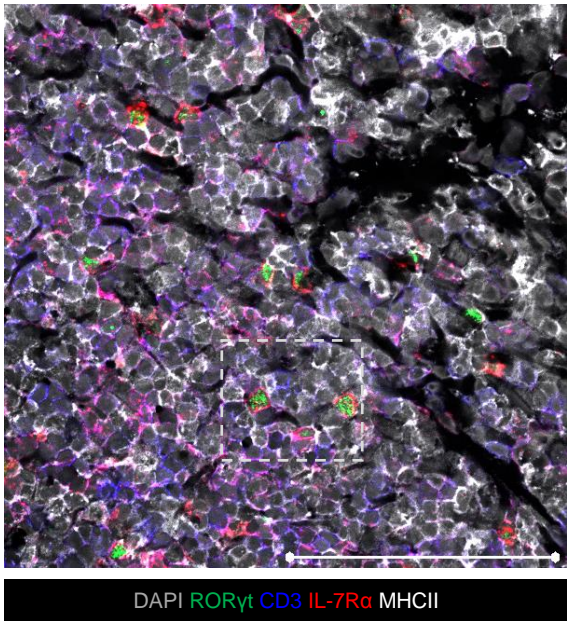
a) Human tonsil - ILC3s



b) Human tonsil – ILC3s CD161 expression



c) Human tonsil – ILC3s MHCII expression



identified to express MHCII by flow cytometry, which can be visualised by immunofluorescent microscopy within this study (Figure 3.13c) (289, 293).

Through a consistent characterisation method, ILCs were identified and compared between murine lymphoid and non-lymphoid tissues, with further analysis of the ILC2 population revealing that their phenotype differed between tissues. The importance of specific digestion protocols was emphasised within this chapter, with TFs and surface protein expression being affected by certain protocols, affecting the accuracy of their analysis. Finally, some initial data was provided comparing the location and phenotype of ILCs within murine and human SLTs.

3.3 SUMMARY

Within this chapter characterisation of the ILC populations in lymphoid and non-lymphoid tissues, through the utilisation of TF expression, enabled the simple and robust identification of ILC subsets. Such analysis facilitated the comparisons of ILC groups between different tissues. These data observed that ILC2s phenotype varies within different tissues alongside the identification of a potentially novel population of ILCs lacking TFs. Further analysis of this population demonstrated that the manner in which the tissue is digested can have substantial effects, both on ILC surface marker expression but also, unexpectedly, the detectability of TF expression. Finally, within this chapter ILC2s and ILC3s locations within SLTs were compared across murine and human mLN, alongside human tonsil samples revealing that ILC3s were consistently located within the interfollicular area with ILC2s interestingly being identified within B cell follicles.

Consistent characterisation of ILCs via TF expression enabled their comparison across the ear, auLN, SI LP, lung and mLN (25, 108, 243). ILC3 subsets were observed to be dispersed in

different proportions within the tissues assessed and ROR γ t staining was important in the identification of the ILC3 subset which was identified based on the lack of markers, CCR6 $^{-}$ NKp46 $^{-}$. Furthermore, the phenotype of ILC2s between the different tissues was observed not to be consistent. The main contradicting observation from these studies was the lack of ST2 on ILC2s within the ear, which has previously been used to identify ILC2s within this tissue (112). As previously discussed ST2 $^{-}$ iILC2s reside within the SI LP and proliferate upon IL-25 stimulation, and due to the lack of ST2 expression within the ear, it is possible that these cells also reside here (108, 254). However, iILC2s also express high levels of KLRG1, which is identified within the SI LP, but not the ear (108). Further analysis of IL-25R may identify whether ILC2s within the ear are similar to iILC2s being more responsive to IL-25 rather than IL-33 (108). The variation in the levels of ILC2 markers detected on ILCs within these different tissues emphasises that surface markers are not as accurate in identifying subgroups compared to staining for TFs or using TF-reporter mice.

Analysis of ILC subsets through the use of TFs revealed the presence of a novel population of TrN ILCs. Extending the lineage markers used to identify ILCs, in accordance with other publications, confirmed that the ILC gating strategy was not contaminated by other hematopoietic cells (221). Furthermore, ~90% of the ILC population express Id2 within the ear, as TrN ILCs comprise of over half of total ILCs within the ear this indicates that TrN ILCs express Id2. It was also clear that lineage markers expressed by IL-7R α $^{+}$ Lineage $^{+}$ cells were not downregulated under the EDP, indicating that TrN ILCs were not a contamination of non-ILCs due to the digestion protocol, suggesting that TrN ILCs are a true ILC population. Further characterisation of these cells would be useful to further confirm their ILC phenotype, such as

CD90 expression. Currently within the literature little is published on the function and characterisation of ILCs which lack expression of T-bet, GATA-3 and ROR γ t apart from recent publication which has seemingly identified a group of TrN ILCs which also lack Foxp3 expression, called ILCregs (113). ILCregs as well as requiring Id2 for their development also depended on the expression of DNA-binding protein inhibitor 3 (Id3) (113). These cells are described to reside mainly within the SI and abrogate intestinal inflammation via IL-10 production (113). TrN ILCs may belong within the ILCreg population with further analysis of the TrN ILCs phenotype, including IL-10 production and Id3 expression, being required to confirm this (113). Although the TrN ILCs share similarities with the ILCregs, the localisation of these two populations are not comparable. ILCregs are abundant in the SI, and scarce within the lung, unlike TrN ILCs which along with the ear skin are most abundant within the lung (113). This suggests that ILCregs may contribute to a proportion of the identified TrN ILCs, however, it is unlikely that the entire population can be attributed to by ILCregs.

It is further possible that the TrN population may also consist of ILC precursors, for example the CHILP population (Lineage⁻ IL-7R α ⁺ α ₄ β ₇⁺ CD25⁻ Id2⁺ GATA-3⁻) (27, 98). ILC progenitors (Lineage⁻ IL-7R α ⁺ α ₄ β ₇⁺) are a rare population mainly studied within the foetal liver, foetal gut and adult BM with little being reported on their presence in adult tissue (155, 294). However, similar to ILCregs, given that ILC precursors are a rare population in adult tissue, it is unlikely that they contribute largely to the TrN ILCs.

The importance in digestion protocols used for certain tissue preparations was elaborated upon the down regulation of T-bet and GATA-3 expression, under the EDP, diminishing the ability to identify ILC1s and ILC2s. This may result in ILC1s and ILC2s inclusion within the TrN

population gate, which may explain why it is such a large population in the ear. Therefore, although TrN ILCs are a true ILC population they may also contain ILC1 or ILC2 subgroups. The decrease of expression of a variety of surface markers on hematopoietic cells under the EDP, highlights the importance of digestion protocols on the analysis of surface markers used in the identification and characterisation of cellular populations.

Interestingly TrN ILCs are most abundant within the lung and the ear with these tissues, compared to other tissue analysed, being the only digestion protocols that both include an enzymatic digestion involving Liberase TM enzyme. Previous reports have shown that certain enzymes can affect the expression of surface molecules, therefore, Liberase TM may be responsible for the loss of protein expression (266). However, the auLN and mLN undergo the same digestion protocol, which doesn't require Liberase TM, and still contains TrN ILCs. The auLN in fact contains a larger proportion of TrN ILCs compared to the mLN, suggesting that the digestion protocol is not responsible for the entire TrN population, but that this TrN population still exists as true ILC subset, and is just altered by the digestion protocol. The LDP was unable to obtain a sufficient cell yield from the ear, and due to a more appropriate digestion protocol for the ear has not been established the EDP was continuously used when analysing ear skin. Through the assessment of different concentrations of Liberase TM and different incubation periods a more efficient EDP may be established, with a balance between obtaining an appropriate cell yield without affecting protein analysis.

Comparisons between human and murine SLT microenvironments revealed the similarities and differences between ILC locations. Within the human mLN and tonsil and the murine LNs, ILC3s are situated within the interfollicular areas and expression of CD161 and MHCII can be

detected by immunofluorescent imaging in the tonsil. CD161 is not a marker specific for ILCs and is also identified on T cells (295). The initial identification of ILCs as CD3⁻ supports that the ILC3s identified are true ILCs, however a caveat of immunofluorescent microscopy is the lack of markers able to be used. This is a problem when assessing ILCs as a plethora of lineage markers are normally used in their identification. The location of ILC2s within murine and human mLNs differs, with human ILCs being located within the B cell follicle (243). This suggests that there may be differences between human and mouse ILC2s within the mLN. On the other hand, murine samples are taken from an animal where the immunological history is known and monitored. This is compared to human patients in which all immunological responses are not documented. A multitude of past infections may shape the microenvironment of human LNs and immune cell characteristics and functions. It is therefore interesting to observe that human ILC2s have the capability to enter B cell follicles and potentially interact with B cells, with IL-9 being an important cytokine in promoting B cell survival, which may also occur in murine samples (212). This identification method of ILC2s only involves ILCs being gated negatively for T cells and does not contain the extensive lineage marker pool used previously in flow cytometry analysis. This suggests, the identified ILCs may potentially be a different non-ILC IL-7R α ⁺ GATA-3⁺ ICOS⁺ CD3⁻ population. Using phenotypic markers more commonly used in human staining, such as CRTH2 may be a more accurate method of detecting ILC2s (267-269). Within these studies the characterisation of ILCs was not continued further. This was mainly due to the unavailability of fresh tissue and the low impact factor of phenotyping ILCs in human tissue within the field.

Overall these data are important in addressing the fundamental issues in the identification of ILCs within a range of lymphoid and non-lymphoid tissues. ILC2s do not consistently express

the same surface markers across different tissues, suggesting that TF staining is a more robust method of identification. Digestion protocols can, however, effect the identification of extracellular and intracellular proteins, used in the analysis of different populations. Therefore, understanding the effects of the digestion protocol is essential in the efficient analysis of cellular populations. ILCs were identified and phenotyped in human and murine SLT sections showing their location within the niche microenvironment of the mLN and tonsil. This initial characterisation of ILCs within human tissues, establishes a platform in which the position of ILCs across different tissues can be located and phenotyped.

Chapter 4. DETERMINING THE ROLE OF ICOS AND ICOSL

INTERACTIONS IN ILC HOMEOSTASIS

4.1 INTRODUCTION

SLTs, such as LNs, provide a unique microenvironment which supports interactions between the innate and adaptive immune system paramount in the development of an effective immune response. Upon entry into the LN T cells crawl along fibroblastic reticular cells (FRCs), part of the stromal network, refining their movement to T cell zones and enabling their scanning of MHCII presented antigen on APCs, such as DCs, which are colocalised to the FRCs (50). Upon recognition of cognate antigen, via the TCR complex, naïve CD4⁺ T cells undergo a series of steps, involving co-stimulatory molecule interactions, leading to their full activation and development into a cytokine producing effector Th cell (54-57). These co-stimulatory interactions are essential for controlled activation of naïve CD4⁺ T cells and begins with CD28, which is upregulated on T cells upon TCR stimulation, interacting with CD80/CD86 enhancing T cell proliferation. CD28:CD80/CD86 interactions also leads to the upregulation of CTLA-4 and ICOS. CTLA-4 competes with CD28 for CD80/CD86, inhibiting and controlling T cell proliferation, whereas, ICOS:ICOSL interactions support T cell activation, survival and proliferation alongside OX40 and OX40L interactions (57, 60, 63, 64).

ICOS is the third member of the CD28 superfamily, following CD28 and CTLA-4, and is upregulated on activated T cells upon CD28:CD80/CD86 interactions (296). Its ligand, ICOSL is located within a range of tissues, including lymphoid and non-lymphoid and its expression varies on different antigen presenting cells (297, 298). ICOSL is constitutively expressed on

naïve B cells, DCs, macrophages and splenocytes, however expression is induced by TNF- α and other inflammatory stimuli on fibroblasts and in non-lymphoid tissues (60, 61, 297, 299). *Icos*^{-/-} mice have been previously used to understand the importance of ICOS:ICOSL interactions in T cell activation (62, 300). Under steady conditions T and B cell biology in *Icos*^{-/-} mice are comparable to WT mice, showing that ICOS is not required for the development of these populations (300). However, *in vitro* studies observed that ICOS was necessary for stimulated naïve T cells to efficiently proliferate and produce T effector cell cytokines such as IL-4, IFN- γ and IL-10 (62, 296). This was supported *in vivo* by keyhole limpet hemocyanin (KLH) immunisations showing that ICOS:ICOSL interactions were paramount in the expansion of primed T cells within the LN and their ability to produce effector cytokines including IL-4, IL-5 and IL-10 (57, 62, 301). ICOS:ICOSL interactions initiate a series of intracellular steps, including the recruitment of phosphatidylinositol 3-kinase (P13K) and subsequent activation of mitogen-activated protein (MAP) kinases which in turn regulates the cellular response (302).

ICOS:ICOSL interactions are important in directing T cell differentiation, enhancing the development into Th2 and Tfh cells (302, 303). Studies originally explored the role of ICOS in the differentiation between Th1 and Th2 responses and suggested that signalling through ICOS:ICOSL interactions lead to the development and support of a Th2 response (57, 296). This was shown by blocking ICOS interactions *in vitro*, skewing Th effector development to favour Th1 cells (296). Furthermore, Coyle et al., have also shown that within a lung infection model ICOS is paramount in the activation of antigen-specific Th2 but not Th1 effector cells (57). Tfh cell development, maintenance and function was also shown to be dependent on ICOS as ICOS deficient mice had reduced numbers of Tfh cells and therefore impaired germinal centre

formation and class switching of IgA, IgE and IgG (57, 303). Furthermore, the migration of Tfh cells towards the B cell zone was reduced due to diminished expression of CXCR5 upon ICOSL blockade (304). Lack of ICOS:ICOSL interactions therefore resulted in the decreased ability of Tfh cells to communicate with B cells and the subsequent formation of normal germinal centres (304). The importance of ICOS:ICOSL interactions in the development of a normal B cell response was also shown upon immunisation with KLH, in which *Icos*^{-/-} mice had a reduced production of KLH-specific IgG1 and IgG2, alongside a decrease in the number and size of germinal centres within the spleen (300). Similar to CD28 inhibition by CTLA-4, ICOS:ICOSL interactions are also regulated by a negative feed-back loop as transgenic mice that highly express ICOS on all T cells, showed that overstimulation resulted in reduced expression of ICOSL (305). Together, these studies determine a role for ICOS:ICOSL interactions in the proliferation, survival and maturation of effector Th2 and Tfh cells and the efficient induction of the B cell response.

ILC2s have previously been shown to express ICOS within the lung, supported by data in Chapter 3, and also within the SI LP and mLN (25, 216, 221). The original focus of this PhD was to explore the role of co-stimulatory molecules within ILC biology and their cross-talk with the adaptive immune system, focusing principally on ICOS:ICOSL interactions. However, studies by Maazi et al., and Paclik et al., published in 2015, showed that ILC2s were dependent upon ICOS:ICOSL interactions for their homeostatic and inflammatory functions within the lung (262, 306). The data presented within this Chapter were collected in 2014-2015, before these publications, and focuses on the role of ICOS:ICOSL interactions in the development and maintenance of ILCs under steady state conditions.

4.1.1 Project Aims

Within T cell biology ICOS:ICOSL interactions are important in the differentiation of Th2 cells, Tfh cells and the development of an effective B cell response. However, the role of ICOS on ILCs is still unclear. Due to the expression of ICOS on ILC2s and ILC3s, the aim of this chapter was to explore the impact in the deficiency of ICOS:ICOSL interactions on ILC2 and ILC3 populations in the different tissues assessed in Chapter 3 (25, 216, 221).

4.2 RESULTS

The data within this chapter have been recently published by Dutton et al., in Wellcome Open Research in 2017 (216).

4.2.1 ILC populations are not perturbed in the absence of ICOSL expression

Co-stimulatory molecules are paramount in the activation of T cells upon recognition of cognate antigen providing proliferation and survival signals enabling naïve cells to mature into functional T helper cells (55-57). ICOS:ICOSL interactions aid cell proliferation, cytokine production alongside Th2 and Tfh cell differentiation (57, 62). ICOS is expressed on ILC2s, within the lung, mLN and SI LP, as shown in Chapter 3, and on a subset of ILC3s within the SI LP (216, 221). However, the role of ICOS:ICOSL interactions in ILCs biology is unknown. (216, 221).

To investigate the role of ICOS:ICOSL interactions in normal ILC biology under steady state conditions, ILC populations isolated from *Icosl*^{-/-} mice were compared to those isolated from WT mice. Due to previous data showing high expression of ICOS on ILC2s within the SI LP, mLN and lung, the composition of ILC subsets was explored in detail within these tissues. Within the SI LP, WT and *Icosl*^{-/-} mice had comparable percentages and numbers of CD45⁺

hematopoietic cells and ILCs (Figure 4.1a-c). Interestingly, there was a modest, but significant decrease in the percentage of ILC2s and an increase in the percentage of ILC3s, suggesting that the two ILC subgroups known to express ICOS were perturbed in the absence of ICOS:ICOSL interactions. However, the total number of all ILC subsets, including ILC2s and ILC3s, was comparable between mice (Figure 4.1a-c). Within the mLN only an increase in percentage of CD45⁺ cells was detected in *Icosl*^{-/-} mice (Figure 4.2a-c). This increase may be determined by alterations in the amount of cell death induced as part of the cell digestion protocol. All other populations were comparable between WT and *Icosl*^{-/-} mice. Within the lung the percentage of ILCs was decreased within *Icosl*^{-/-} mice which may be a result of alterations in the number of other (non-ILC) immune cells within the lung, due to there being no change in ILC number observed. All other populations were comparable between the WT and *Icosl*^{-/-} mice apart from an increase in the percentage of ILC1s in *Icosl*^{-/-} mice (Figure 4.3a-c). Within these results modest differences in proportions of ILCs was observed between WT and *Icosl*^{-/-} mice, however, these differences were not observed within the enumeration of ILCs. It would be assumed that changes in numbers would support differences between the two mice, indicating a clear role for ICOS:ICOSL interactions in ILC biology. Therefore, these data suggest that under steady state ICOSL expression is not required for the development and maintenance of ILC populations.

4.2.2 Minimal impact of ICOS:ICOSL on the phenotype of ILC2s

Currently ICOS or ICOSL expression has not been identified on ILC1s, therefore, this study will focus on the homeostasis of ILC2s and ILC3s in the absence of ICOS:ICOSL interactions.

Figure 4.1. Minimal impact on ILC populations in the SI LP of *Icosl*^{-/-} mice

Tissues from WT mice were compared to *Icosl*^{-/-} mice. Cells were isolated from SI LP as described in methods. Lineage markers include; B220, CD11c, CD11b, CD3 and CD5. ILCs were gated negatively for iCD3ε (gating not shown).

Each data point represents 1 SI LP from one mouse. Data pooled from 7 experiments. Values on flow cytometry plots represent percentages, ILCs as a proportion of Live CD45⁺ cells and ILC subsets as a proportion of total ILCs. Bars on scatter plots represents the median, which is also shown numerically. Statistical significance was tested using an unpaired, non-parametric, Mann-Whitney two tailed T test: *p≤0.05, **p≤0.01, ***p≤0.001.

- a) Representative flow cytometry plots showing Live CD45⁺ cells, ILCs (Live CD45⁺ IL-7Rα⁺ Lineage⁻) and ILC1s (Lineage⁻ IL-7Rα⁺ iCD3ε⁻ GATA-3⁻ RORγt⁻ T-bet⁺), ILC2 (Lineage⁻ IL-7Rα⁺ iCD3ε⁻ GATA-3⁺ RORγt⁻ T-bet⁻), ILC3 (Lineage⁻ IL-7Rα⁺ iCD3ε⁻ GATA-3⁻ RORγt⁺) and TrN ILCs (Lineage⁻ IL-7Rα⁺ iCD3ε⁻ GATA-3⁻ RORγt⁻ T-bet⁻) within the WT SI LP or *Icosl*^{-/-} SI LP.
- b) Percentage of Live CD45⁺ cells, ILCs and ILC subsets compared between the WT SI LP (n=13) and *Icosl*^{-/-} SI LP (n=11).
- c) Number of Live CD45⁺ cells, ILCs and ILC subsets compared between the WT SI LP (n=13) and *Icosl*^{-/-} SI LP (n=11).

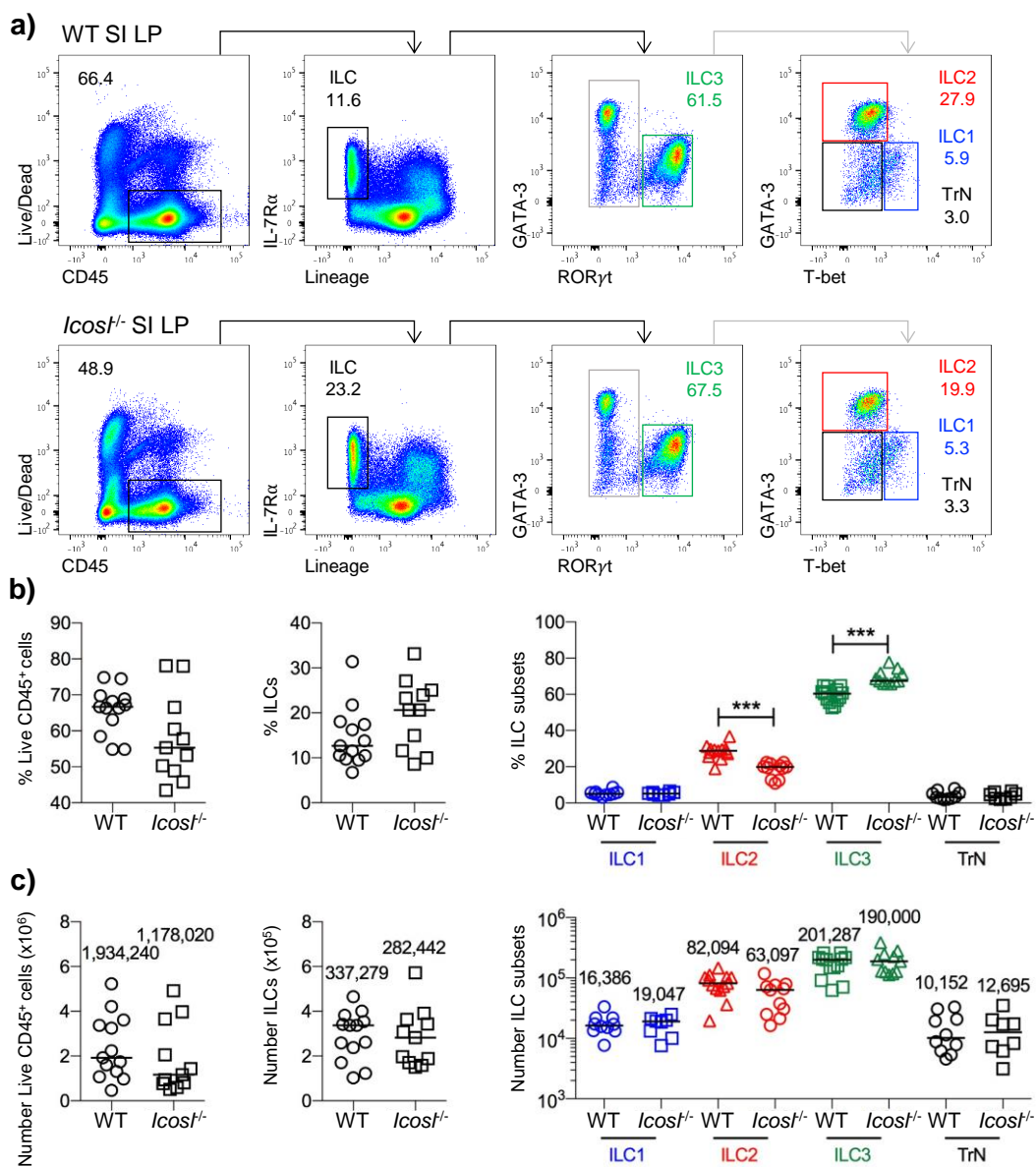


Figure 4.2. No impact on ILC populations within the mLN of *Icosl*^{-/-} mice

Tissues from WT mice were compared to *Icosl*^{-/-} mice. Cells were isolated from mLN as described in methods. Lineage markers include; B220, CD11c, CD11b, CD3 and CD5. ILCs were gated negatively for iCD3ε (gating not shown).

Each data point represents 1 mLN from one mouse. Data pooled from 5 experiments. Values on flow cytometry plots represent percentages, ILCs as a proportion of Live CD45⁺ cells and ILC subsets as a proportion of total ILCs. Bars on scatter plots represents the median, which is also shown numerically. Statistical significance was tested using an unpaired, non-parametric, Mann-Whitney two tailed T test: *p≤0.05, **p≤0.01, ***p≤0.001.

- a) Representative flow cytometry plots showing Live CD45⁺ cells, ILCs (Live CD45⁺ IL-7Rα⁺ Lineage⁻) and ILC1s (Lineage⁻ IL-7Rα⁺ iCD3ε⁻ GATA-3⁻ RORγt⁻ T-bet⁺), ILC2 (Lineage⁻ IL-7Rα⁺ iCD3ε⁻ GATA-3⁺ RORγt⁻ T-bet⁻), ILC3 (Lineage⁻ IL-7Rα⁺ iCD3ε⁻ GATA-3⁻ RORγt⁺) and TrN ILCs (Lineage⁻ IL-7Rα⁺ iCD3ε⁻ GATA-3⁻ RORγt⁻ T-bet⁻) within the WT mLN or *Icosl*^{-/-} mLN.
- b) Percentage of Live CD45⁺ cells, ILCs and ILC subsets compared between the WT mLN (n=7) and *Icosl*^{-/-} mLN (n=7).
- c) Number of Live CD45⁺ cells, ILCs and ILC subsets compared between the WT mLN (n=7) and *Icosl*^{-/-} mLN (n=7).

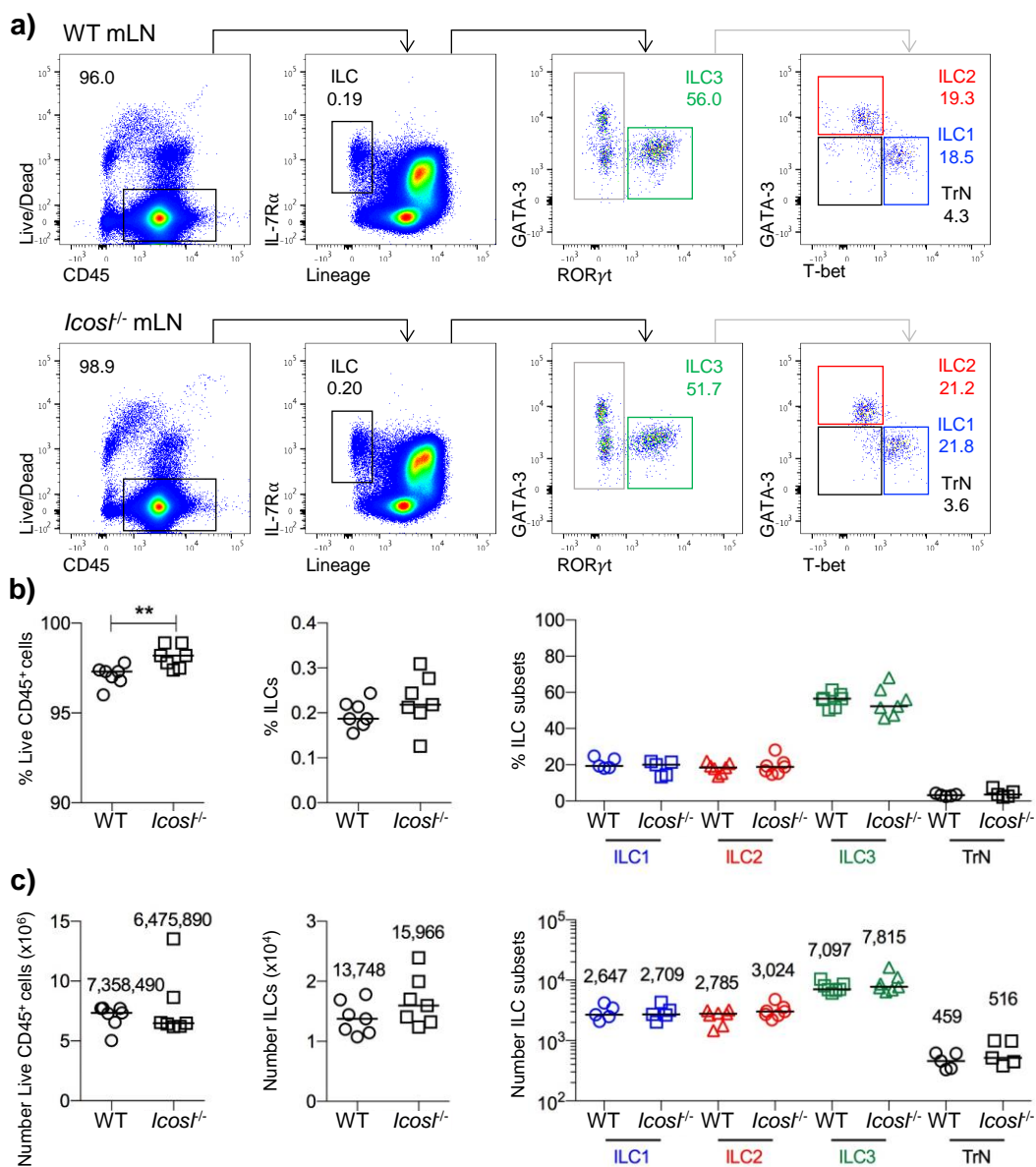
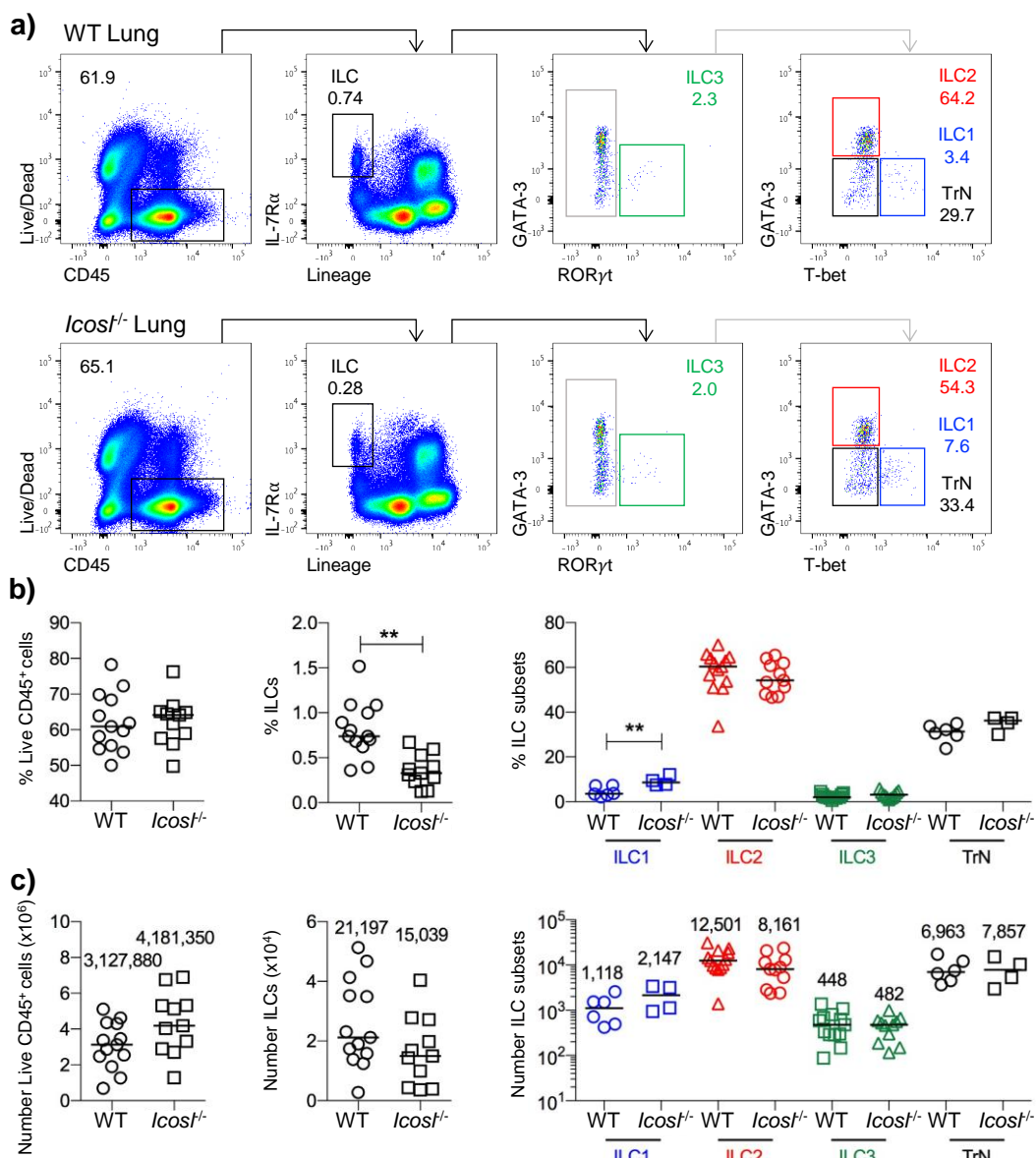


Figure 4.3. Minimal impact on ILC populations in the lungs of mice lacking ICOSL expression

Tissues from WT mice were compared to *Icosl*^{-/-} mice. Cells were isolated from the lung as described in methods. Lineage markers include; B220, CD11c, CD11b, CD3 and CD5. ILCs were gated negatively for iCD3ε (gating not shown).

Each data point represents 1 lung from one mouse. Data pooled from 7 experiments. Values on flow cytometry plots represent percentages, ILCs as a proportion of Live CD45⁺ cells and ILC subsets as a proportion of total ILCs. Bars on scatter plots represents the median, which is also shown numerically. Statistical significance was tested using an unpaired, non-parametric, Mann-Whitney two tailed T test: *p≤0.05, **p≤0.01, ***p≤0.001.

- a) Representative flow cytometry plots showing Live CD45⁺ cells, ILCs (Live CD45⁺ IL-7Rα⁺ Lineage⁻) and ILC1s (Lineage⁻ IL-7Rα⁺ iCD3ε⁻ GATA-3⁻ RORγt⁻ T-bet⁺), ILC2 (Lineage⁻ IL-7Rα⁺ iCD3ε⁻ GATA-3⁺ RORγt⁻ T-bet⁻), ILC3 (Lineage⁻ IL-7Rα⁺ iCD3ε⁻ GATA-3⁻ RORγt⁺) and TrN ILCs (Lineage⁻ IL-7Rα⁺ iCD3ε⁻ GATA-3⁻ RORγt⁻ T-bet⁻) within the WT lung or *Icosl*^{-/-} lung.
- b) Percentage of Live CD45⁺ cells, ILCs and ILC subsets compared between the WT lung (n=13) and *Icosl*^{-/-} lung (n=11).
- c) Number of Live CD45⁺ cells, ILCs and ILC subsets compared between the WT lung (n=13) and *Icosl*^{-/-} lung (n=11).



Although numerically ILC2s were comparable in *Icosl*^{-/-} and WT mice, their phenotype and therefore function may have been altered. In Chapter 3, ILC2s within the SI LP, mLN and lung were shown to all express high levels of CD25, ICOS and KLRG1. MHCII was refined to ILC2s within the mLN and ST2 to the mLN and lung. ICOS:ICOSL interactions have been associated with an increase in T cell activation, increased CD25 expression, downregulation of ICOSL and skewing of T effector cell differentiation towards the Th2 fate (296, 301, 305). Therefore, to determine whether the lack of ICOS:ICOSL interactions effects the expression of CD25, ICOS, ST2, the activation marker KLRG1, as well as MHCII, ILC2s were analysed in detail within WT and *Icosl*^{-/-} mice (108, 275). ILC2s were assessed within the SI LP, mLN and lung, using Lineage⁺ IL-7R α ⁻ cells for a gating strategy control. Within the SI LP an increase in percentage of ILC2s expressing CD25 and ICOS was observed (Figure 4.4a-c). ICOS expression may be increased potentially due to the absence of ligand and therefore reduced binding and internalisation. An increase in percentage of MHCII and ST2 expression was observed within *Icosl*^{-/-} mice, however, a decrease in the percentage of KLRG1⁺ ILC2s (Figure 4.4a-c) (305). Although these differences were significant, they were very modest in nature making it difficult to convincingly conclude much about the biological relevance of such data. Importantly, no differences in the number of CD25⁺, ICOS⁺, KLRG1⁺, MHCII⁺ or ST2⁺ ILC2s was observed between WT and *Icosl*^{-/-} mice, further suggesting that slight changes in the proportions of cells expressing a given marker may not be biologically relevant (Figure 4.4d). Within the mLN the percentage and number of ILC2s expressing each marker was comparable between WT and *Icosl*^{-/-} mice, suggesting that the ILC2 phenotype was not perturbed in the absence of ICOSL (Figure 4.5a-d). ILC2s within the lung were similar to that in the mLN with the percentages and numbers being comparable between the two mice, apart from an increase in the percentage

Figure 4.4. Minimal impact on ILC2 phenotype in the absence of ICOSL in the SI LP

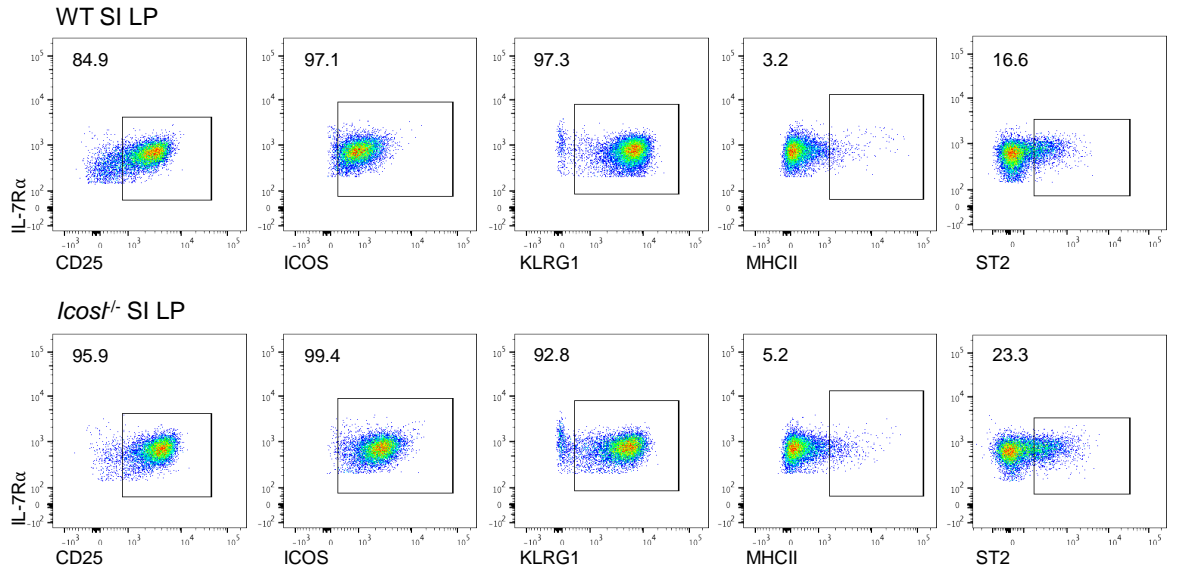
Tissues from WT mice were compared to *Icosl*^{-/-} mice. Cells were isolated from SI LP as described in methods. Lineage markers include; B220, CD11c, CD11b, CD3 and CD5. ILC2s were previously gated on Live CD45⁺ Lineage⁻ IL-7R α ⁺ iCD3 ϵ ⁻ GATA-3⁺.

Each data point represents 1 SI LP from one mouse. Data pooled from 4 experiments. Values on flow cytometry plots represent percentages, bars on scatter plots represents the median, which is also shown numerically. Statistical significance was tested using an unpaired, non-parametric, Mann-Whitney two tailed T test: *p \leq 0.05, **p \leq 0.01, ***p \leq 0.001.

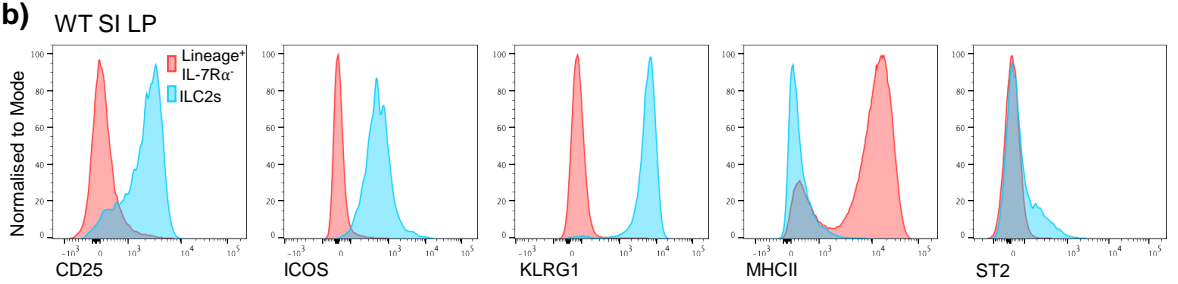
- a) Representative flow cytometry plots of CD25, ICOS, KLRG1, MHCII and ST2 expression on ILC2s in the WT SI LP and *Icosl*^{-/-} SI LP.
- b) Representative histograms, normalised to mode, showing the expression of CD25, ICOS, KLRG1, MHCII and ST2 by ILC2s or Lineage⁺ IL-7R α ⁻ cells within the WT SI LP, which were used to help identify gating methods.
- c) Percentage of ILC2s expressing CD25, ICOS, KLRG1, MHCII and ST2 within WT SI LP (n= 8) and *Icosl*^{-/-} SI LP (n=6).
- d) Number of ILC2s expressing CD25, ICOS, KLRG1, MHCII and ST2 within WT SI LP (n= 8) and *Icosl*^{-/-} SI LP (n=6).

a)

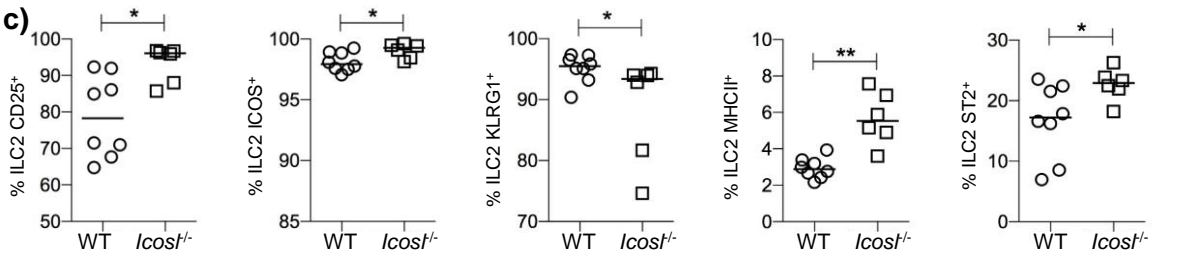
ILC2s



b)



c)



d)

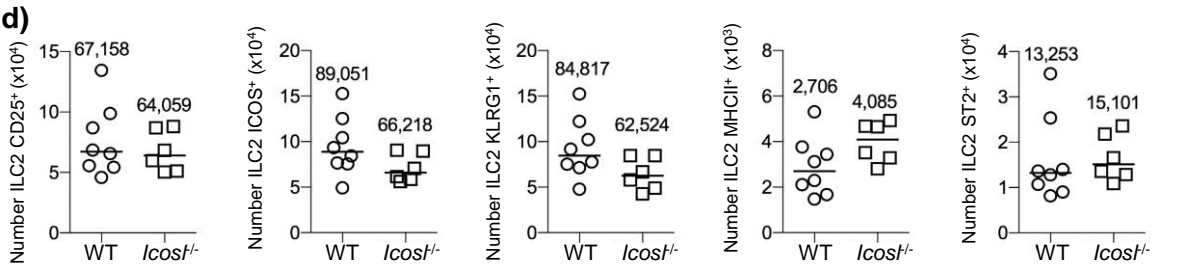


Figure 4.5. No impact on ILC2 phenotype in the absence of ICOSL in the mLN

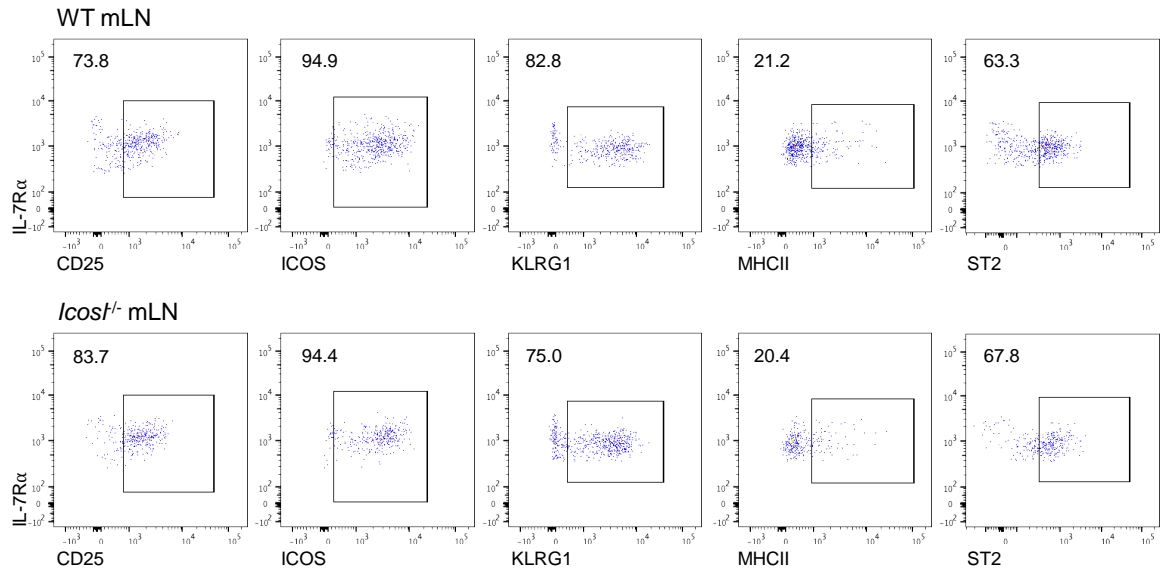
Tissues from WT mice were compared to *Icosl*^{-/-} mice. Cells were isolated from mLN as described in methods. Lineage markers include; B220, CD11c, CD11b, CD3 and CD5. ILC2s were previously gated on Live CD45⁺ Lineage⁻ IL-7R α ⁺ iCD3 ϵ ⁻ GATA-3⁺.

Each data point represents 1 mLN from one mouse. Data pooled from 4 experiments. Values on flow cytometry plots represent percentages, bars on scatter plots represents the median, which is also shown numerically. Statistical significance was tested using an unpaired, non-parametric, Mann-Whitney two tailed T test: *p \leq 0.05, **p \leq 0.01, ***p \leq 0.001.

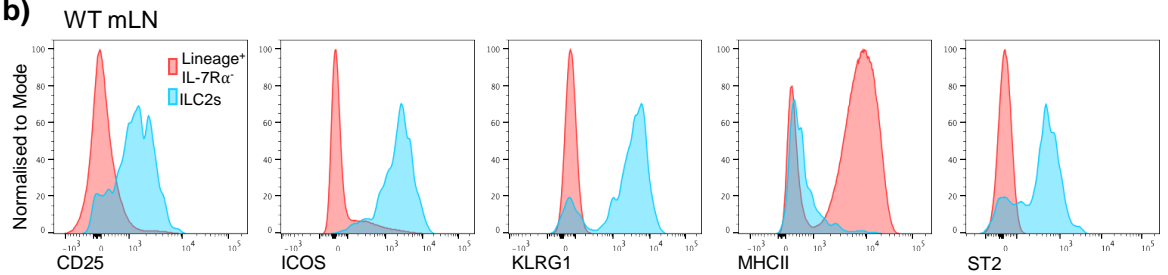
- a) Representative flow cytometry plots of CD25, ICOS, KLRG1, MHCII and ST2 expression on ILC2s in the WT mLN and *Icosl*^{-/-} mLN.
- b) Representative histograms, normalised to mode, showing the expression of CD25, ICOS, KLRG1, MHCII and ST2 by ILC2s or Lineage⁺ IL-7R α ⁻ cells within the WT mLN, which were used to help identify gating methods.
- c) Percentage of ILC2s expressing CD25, ICOS, KLRG1, MHCII and ST2 within WT mLN (n= 6-7) and *Icosl*^{-/-} mLN (n=4-5).
- d) Number of ILC2s expressing CD25, ICOS, KLRG1, MHCII and ST2 within WT mLN (n= 6-7) and *Icosl*^{-/-} mLN (n=4-5).

a)

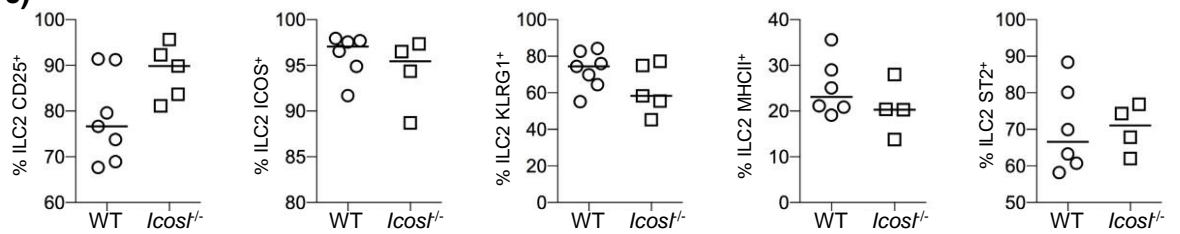
ILC2s



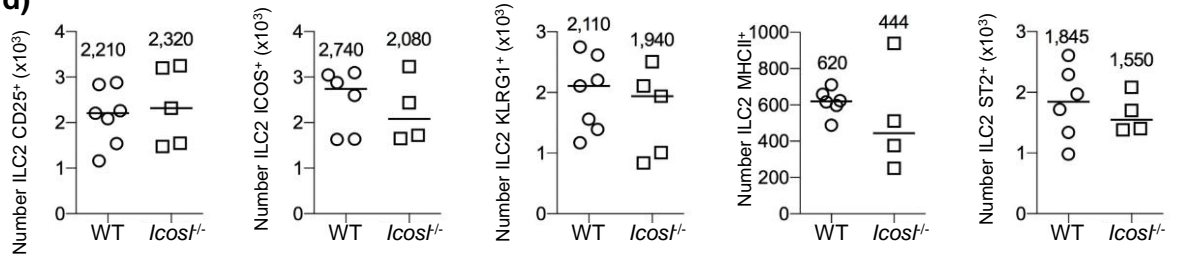
b)



c)



d)



of ILC2s expressing CD25 (Figure 4.6a-d). Together these data suggest that the phenotype of ILC2 in terms of expression of the molecules CD25, ICOS, KLRG1, MHCII and ST2 was not greatly affected by the absence of ICOSL interactions.

4.2.3 Minimal impact on ILC3 subgroups in the absence of ICOSL

ILC3s within the SI LP, similar to ILC2s, also express ICOS (216, 296). Although the total number of ILC3s are unchanged in *Icosl*^{-/-} mice compared to WT mice, the individual ILC3 subgroups have not been assessed. ILC3s are subdivided into 3 groups based on their expression of NKp46 and CCR6, NCR⁺ ILC3s (NKp46⁺ CCR6⁻), LTi-like ILC3s (NKp46⁻ CCR6⁺) and NCR⁻ ILC3s (NKp46⁻ CCR6⁻). To determine whether specific subsets of ILC3s are altered in the absence of ICOS:ICOSL interactions the three subgroups were analysed within the SI LP, mLN and lung of WT and *Icosl*^{-/-} mice. Within the SI LP and the mLN the percentage and number of NCR⁺, LTi-like and NCR⁻ ILC3s was comparable between WT and *Icosl*^{-/-} mice (Figure 4.7 & 4.8). ILC3s are the smallest subgroup of ILCs within the lung and although NCR⁻ and LTi-like ILC3s were comparable between WT and *Icosl*^{-/-} mice, there was a significant increase in the number of NCR⁺ ILC3s within *Icosl*^{-/-} mice (Figure 4.9a-b). This may suggest that ICOS:ICOSL interactions suppress the development of NCR⁻ ILC3s into NCR⁺ ILC3s, however, due to such small numbers of ILC3s within the lung, and NCR⁺ cells making up under 10% of lung ILC3s, this is also potentially due to sample variability. Combined, these data provide further evidence that ILC2 and ILC3 populations are fairly normal in the absence of ICOSL, arguing that ICOS:ICOSL interactions are not critical for normal homeostasis of ILCs.

Figure 4.6. Minimal impact on ILC2 phenotype within the lung of *Icosl*^{-/-} mice

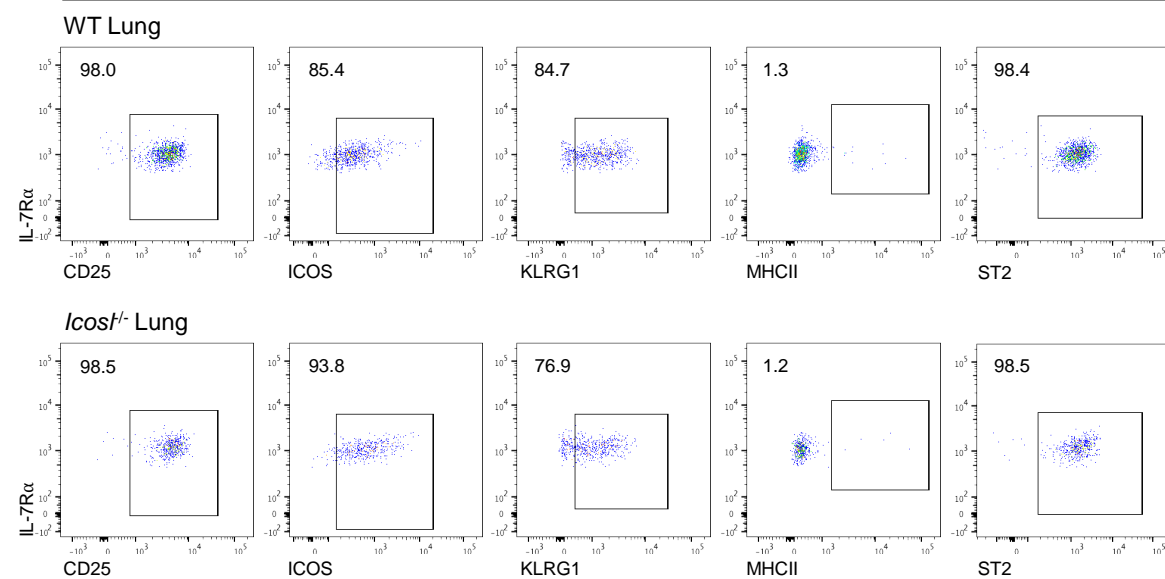
Tissues from WT mice were compared to *Icosl*^{-/-} mice. Cells were isolated from lung as described in methods. Lineage markers include; B220, CD11c, CD11b, CD3 and CD5. ILC2s were previously gated on Live CD45⁺ Lineage⁻ IL-7R α ⁺ iCD3 ϵ ⁻ GATA-3⁺.

Each data point represents 1 lung from one mouse. Data pooled from 4 experiments. Values on flow cytometry plots represent percentages, bars on scatter plots represents the median, which is also shown numerically. Statistical significance was tested using an unpaired, non-parametric, Mann-Whitney two tailed T test: *p \leq 0.05, **p \leq 0.01, ***p \leq 0.001.

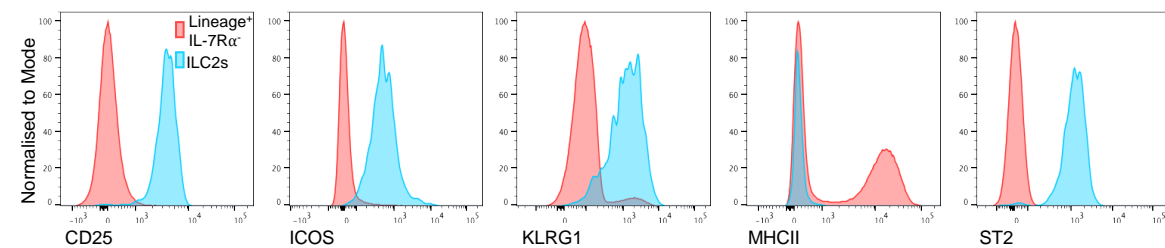
- a) Representative flow cytometry plots of CD25, ICOS, KLRG1, MHCII and ST2 expression on ILC2s in the WT lung and *Icosl*^{-/-} lung.
- b) Representative histograms, normalised to mode, showing the expression of CD25, ICOS, KLRG1, MHCII and ST2 by ILC2s or Lineage⁺ IL-7R α ⁻ cells within the WT lung, which were used to help identify gating methods.
- c) Percentage of ILC2s expressing CD25, ICOS, KLRG1, MHCII and ST2 within WT lung (n= 6-8) and *Icosl*^{-/-} lung (n=4-6).
- d) Number of ILC2s expressing CD25, ICOS, KLRG1, MHCII and ST2 within WT lung (n= 6-8) and *Icosl*^{-/-} lung (n=4-6).

a)

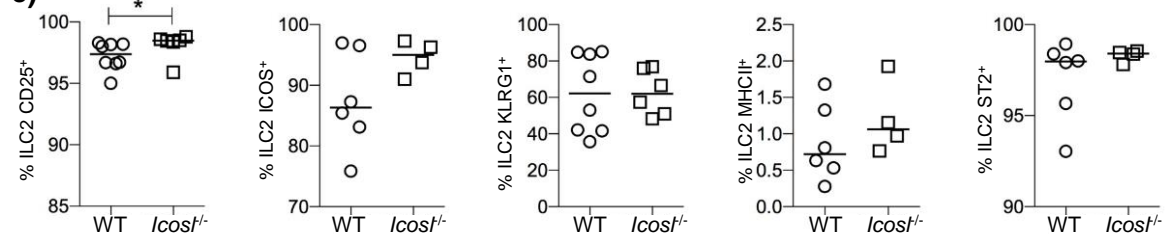
ILC2s



b) WT Lung



c)



d)

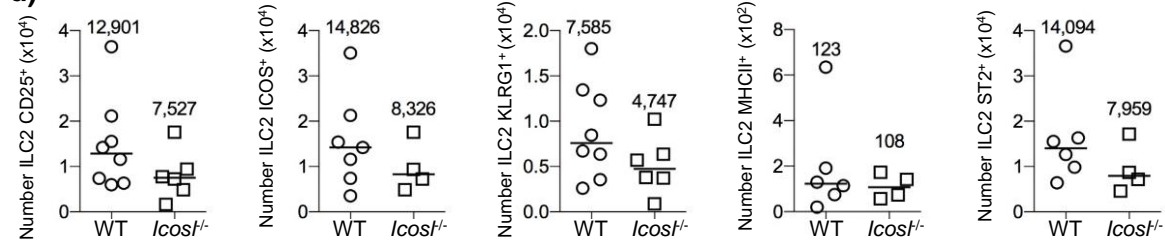


Figure 4.7. ILC3 subsets are not perturbed in the absence of ICOSL in the SI LP

Tissues from WT mice were compared to *Icosl*^{-/-} mice. Cells were isolated from SI LP as described in methods. Lineage markers include; B220, CD11c, CD11b, CD3 and CD5. ILC3s were previously gated on Live CD45⁺ Lineage⁻ IL-7Rα⁺ iCD3ε⁻ GATA-3⁻ RORγt⁺.

Each data point represents 1 SI LP from one mouse. Data pooled from 7 experiments. Values on flow cytometry plots represent percentages, bars on scatter plots represents the median, which is also shown numerically. Statistical significance was tested using an unpaired, non-parametric, Mann-Whitney two tailed T test: *p≤0.05, **p≤0.01, ***p≤0.001.

- a) Representative flow cytometry plots showing expression of CCR6 and NKp46 on ILC3s within the WT SI LP compared to the *Icosl*^{-/-} SI LP.
- b) Percentage (left) and numbers (right) of ILC3s that are CCR6⁻ NKp46⁺, CCR6⁺ NKp46⁻ and CCR6⁺ NKp46⁺ within WT SI LP (n=13) compared to *Icosl*^{-/-} SI LP (n=11).

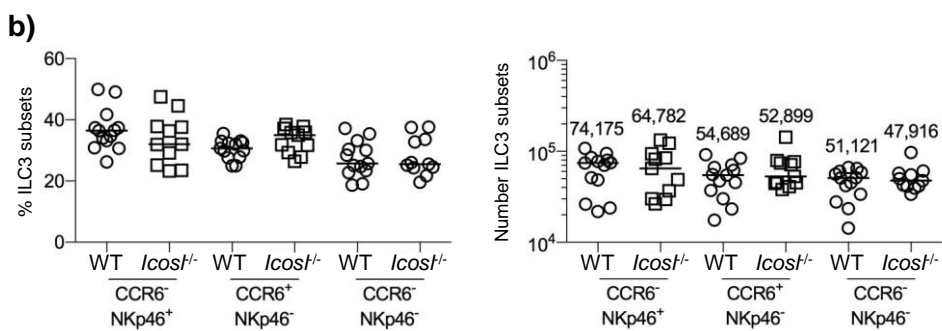
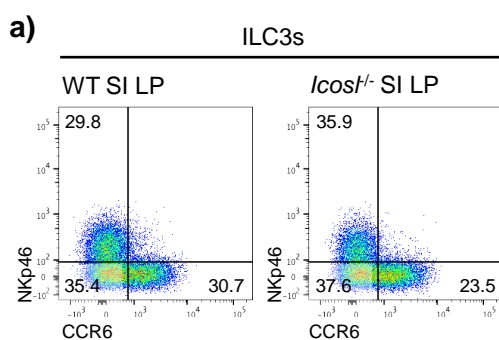


Figure 4.8. ILC3 subsets are not perturbed in the mLN of *Icosl*^{-/-} mice

Tissues from WT mice were compared to *Icosl*^{-/-} mice. Cells were isolated from the mLN as described in methods. Lineage markers include; B220, CD11c, CD11b, CD3 and CD5. ILC3s were previously gated on Live CD45⁺ Lineage⁻ IL-7R α ⁺ iCD3 ϵ ⁻ GATA-3⁻ ROR γ t⁺.

Each data point represents 1 mLN from one mouse. Data pooled from 5 experiments. Values on flow cytometry plots represent percentages, bars on scatter plots represents the median, which is also shown numerically. Statistical significance was tested using an unpaired, non-parametric, Mann-Whitney two tailed T test: *p \leq 0.05, **p \leq 0.01, ***p \leq 0.001.

- a) Representative flow cytometry plots showing expression of CCR6 and NKp46 on ILC3s within the WT mLN compared to the *Icosl*^{-/-} mLN.
- b) Percentage (left) and numbers (right) of ILC3s that are CCR6⁻NKp46⁺, CCR6⁺ NKp46⁻ and CCR6⁺ NKp46⁺ within WT mLN (n=7) compared to *Icosl*^{-/-} mLN (n=7).

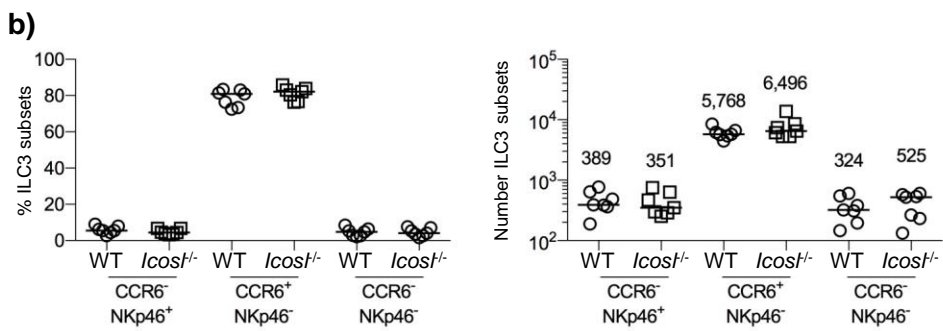
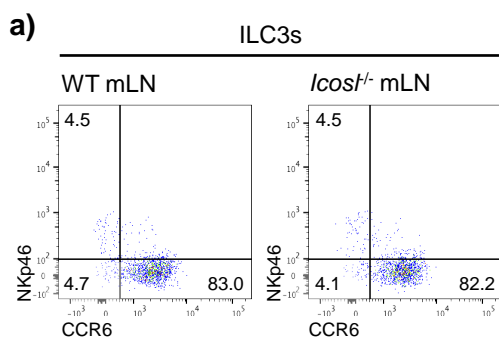
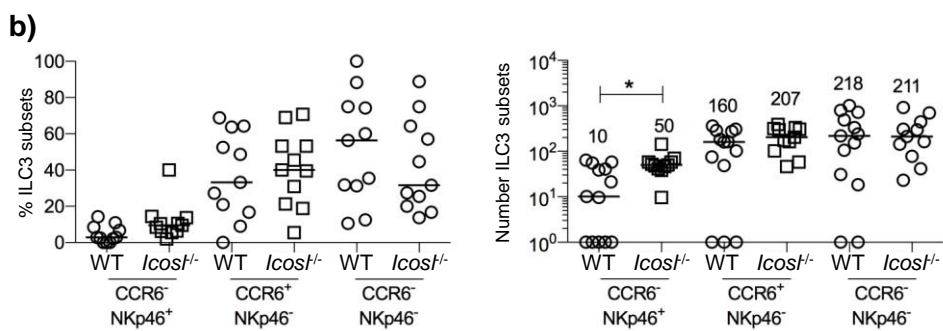
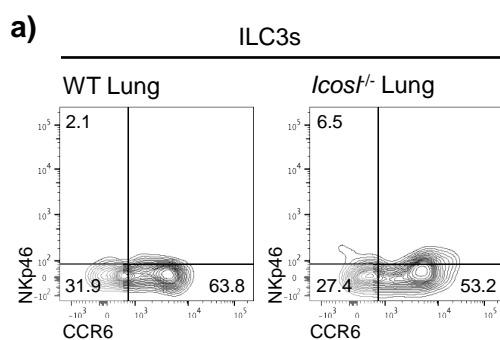


Figure 4.9. Minimal impact on ILC3 subsets in ICOSL deficient lungs

Tissues from WT mice were compared to *Icosl*^{-/-} mice. Cells were isolated from the lung as described in methods. Lineage markers include; B220, CD11c, CD11b, CD3 and CD5. ILC3s were previously gated on Live CD45⁺ Lineage⁻ IL-7R α ⁺ iCD3 ϵ ⁻ GATA-3⁻ ROR γ t⁺.

Each data point represents 1 lung from one mouse. Data pooled from 7 experiments. Values on flow cytometry plots represent percentages, bars on scatter plots represents the median, which is also shown numerically. Statistical significance was tested using an unpaired, non-parametric, Mann-Whitney two tailed T test: *p \leq 0.05, **p \leq 0.01, ***p \leq 0.001.

- a) Representative flow cytometry plots showing expression of CCR6 and Nkp46 on ILC3s within the WT lung compared to the *Icosl*^{-/-} lung.
- b) Percentage (left) and numbers (right) of ILC3s that are CCR6⁻ Nkp46⁺, CCR6⁺ Nkp46⁻ and CCR6⁺ Nkp46⁺ within WT lung (n=13) compared to *Icosl*^{-/-} lung (n=11). Due to the range of numbers of ILC3s data is presented on a logarithmic scale where values equal to 0 are represented as 1.



4.2.4 Perturbations of ILC3 subgroups in the absence ICOS

Publications studying the role of ICOS have previously analysed ICOS:ICOSL interactions in *Icos*^{-/-} mice or ICOS-transgenic mice, where ICOS is expressed on all T cells, instead of focusing on *Icosl*^{-/-} mice (62, 300, 305). Therefore, to further confirm that ICOS:ICOSL interactions were not required for normal ILC biology, ILCs within WT and *Icos*^{-/-} mice were assessed in the SI LP and the mLN. The composition of CD45⁺ cells, ILCs and ILC subsets within the SI LP was similar to observed in the *Icosl*^{-/-} SI LP. Modest but significant differences were observed within the percentages of ILC2s and ILC3s, however, the total numbers of these cells were not different (Figure 4.10a-c). Similarly, ILC3 subgroups were comparable between WT and *Icos*^{-/-} mice (Figure 4.11a-b). Within the mLN the percentage of ILC1s and ILC2s was modestly but significantly increased within *Icos*^{-/-} mice, however, again this was not reflected in the total numbers (Figure 4.12a-c). Within the *Icos*^{-/-} mice there was a significant decrease in the number of ILC3s, which was not observed within the *Icosl*^{-/-} mice and the decrease in ILC3 was observed within the two dominant ILC3 subgroups within the mLN, the LTI-like and the NCR⁺ ILC3 cell fraction (Figure 4.13a-b). This may suggest different requirements of ILC3s for ICOS over ICOSL.

In summary, the data provided here, assessing ILC populations in both *Icosl*^{-/-} and *Icos*^{-/-} mice, has revealed no substantial differences in ILC number or phenotype within the lung and SI LP, with only occasional modest differences, mostly in the proportions of different ILC subsets. Consequently, the data strongly support the contention that the normal homeostasis of ILC2 and ILC3 populations in mucosal tissues do not require ICOS:ICOSL interactions. Interestingly a requirement for ICOS over ICOSL in the establishment of a normal ILC3 population was required within the mLN, suggesting difference between *Icos*^{-/-} and *Icosl*^{-/-} mice.

Figure 4.10. Normal ILC populations in the SI LP of *Icos*^{-/-} mice

Tissues from WT mice were compared to *Icos*^{-/-} mice. Cells were isolated from the SI LP as described in methods. Lineage markers include; B220, CD11c, CD11b, CD3 and CD5. ILCs were gated negatively for iCD3ε (gating not shown).

Each data point represents 1 SI LP from one mouse. Data pooled from 4 experiments. Values on flow cytometry plots represent percentages, ILCs as a proportion of Live CD45⁺ cells and ILC subsets as a proportion of total ILCs. Bars on scatter plots represents the median, which is also shown numerically. Statistical significance was tested using an unpaired, non-parametric, Mann-Whitney two tailed T test: *p≤0.05, **p≤0.01, ***p≤0.001.

- a) Representative flow cytometry plots showing Live CD45⁺ cells, ILCs (Live CD45⁺ IL-7Rα⁺ Lineage⁻) and ILC1s (Lineage⁻ IL-7Rα⁺ iCD3ε⁻ GATA-3⁻ RORγt⁻ T-bet⁺), ILC2 (Lineage⁻ IL-7Rα⁺ iCD3ε⁻ GATA-3⁺ RORγt⁻ T-bet⁻), ILC3 (Lineage⁻ IL-7Rα⁺ iCD3ε⁻ GATA-3⁻ RORγt⁺) and TrN ILCs (Lineage⁻ IL-7Rα⁺ iCD3ε⁻ GATA-3⁻ RORγt⁻ T-bet⁻) within the WT SI LP or *Icos*^{-/-} SI LP.
- b) Percentage of Live CD45⁺ cells, ILCs and ILC subsets compared between the WT SI LP (n=10) and *Icos*^{-/-} SI LP (n=10).
- c) Number of Live CD45⁺ cells, ILCs and ILC subsets compared between the WT SI LP (n=10) and *Icos*^{-/-} SI LP (n=10).

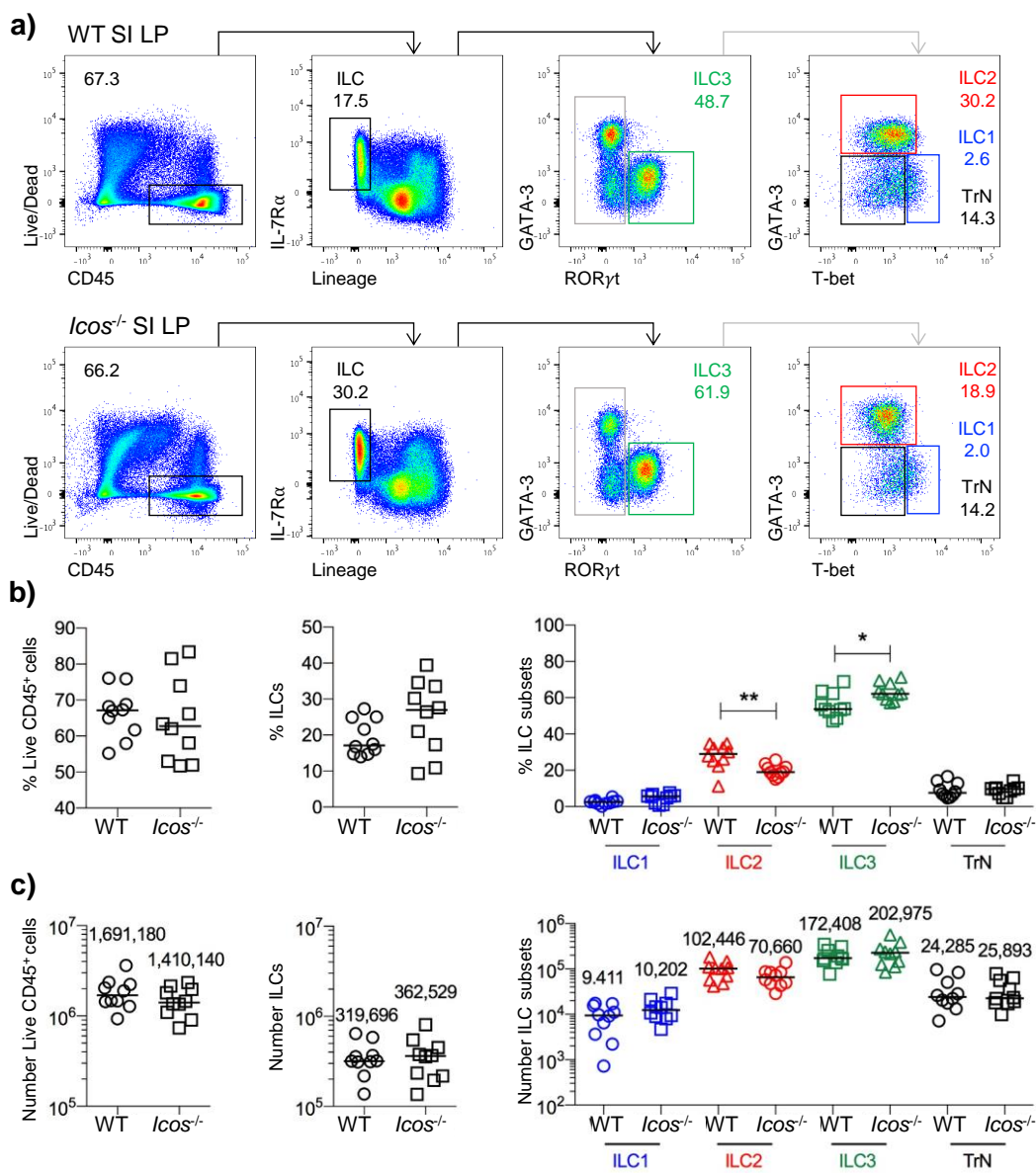


Figure 4.11. ILC3 subsets are not perturbed in the SI LP of *Icos*^{-/-} mice

Tissues from WT mice were compared to *Icos*^{-/-} mice. Cells were isolated from the SI LP as described in methods. Lineage markers include; B220, CD11c, CD11b, CD3 and CD5. ILC3s were previously gated on Live CD45⁺ Lineage⁻ IL-7R α ⁺ iCD3 ϵ ⁻ GATA-3⁻ ROR γ t⁺.

Each data point represents 1 SI LP from one mouse. Data pooled from 4 experiments. Values on flow cytometry plots represent percentages, bars on scatter plots represents the median, which is also shown numerically. Statistical significance was tested using an unpaired, non-parametric, Mann-Whitney two tailed T test: *p \leq 0.05, **p \leq 0.01, ***p \leq 0.001.

- a) Representative flow cytometry plots showing expression of CCR6 and NKp46 on ILC3s within the WT SI LP compared to the *Icos*^{-/-} SI LP.
- b) Percentage (left) and numbers (right) of ILC3s that are CCR6⁻NKp46⁺, CCR6⁺ NKp46⁻ and CCR6⁺ NKp46⁺ within WT SI LP (n=10) compared to *Icos*^{-/-} SI LP (n=10).

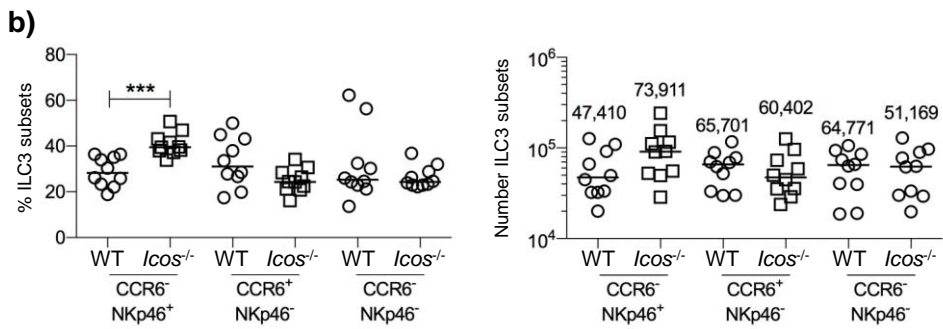
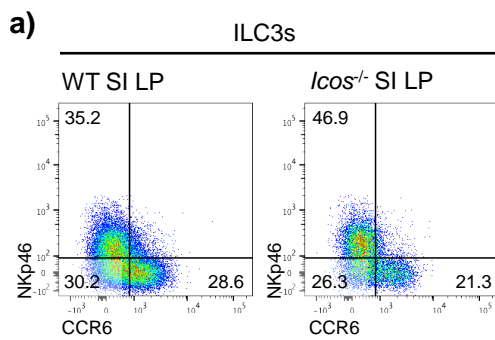


Figure 4.12. Reduced numbers of ILC3s in the mLN of *Icos*^{-/-} mice

Tissues from WT mice were compared to *Icos*^{-/-} mice. Cells were isolated from the mLN as described in methods. Lineage markers include; B220, CD11c, CD11b, CD3 and CD5. ILCs were gated negatively for iCD3ε (gating not shown).

Each data point represents 1 mLN from one mouse. Data pooled from 4 experiments. Values on flow cytometry plots represent percentages, ILCs as a proportion of Live CD45⁺ cells and ILC subsets as a proportion of total ILCs. Bars on scatter plots represents the median, which is also shown numerically. Statistical significance was tested using an unpaired, non-parametric, Mann-Whitney two tailed T test: *p≤0.05, **p≤0.01, ***p≤0.001.

- a) Representative flow cytometry plots showing Live CD45⁺ cells, ILCs (Live CD45⁺ IL-7Rα⁺ Lineage⁻) and ILC1s (Lineage⁻ IL-7Rα⁺ iCD3ε⁻ GATA-3⁻ RORγt⁻ T-bet⁺), ILC2 (Lineage⁻ IL-7Rα⁺ iCD3ε⁻ GATA-3⁺ RORγt⁻ T-bet⁻), ILC3 (Lineage⁻ IL-7Rα⁺ iCD3ε⁻ GATA-3⁻ RORγt⁺) and TrN ILCs (Lineage⁻ IL-7Rα⁺ iCD3ε⁻ GATA-3⁻ RORγt⁻ T-bet⁻) within the WT mLN or *Icos*^{-/-} mLN.
- b) Percentage of Live CD45⁺ cells, ILCs and ILC subsets compared between the WT mLN (n=10) and *Icos*^{-/-} mLN (n=10).
- c) Number of Live CD45⁺ cells, ILCs and ILC subsets compared between the WT mLN (n=10) and *Icos*^{-/-} mLN (n=10).

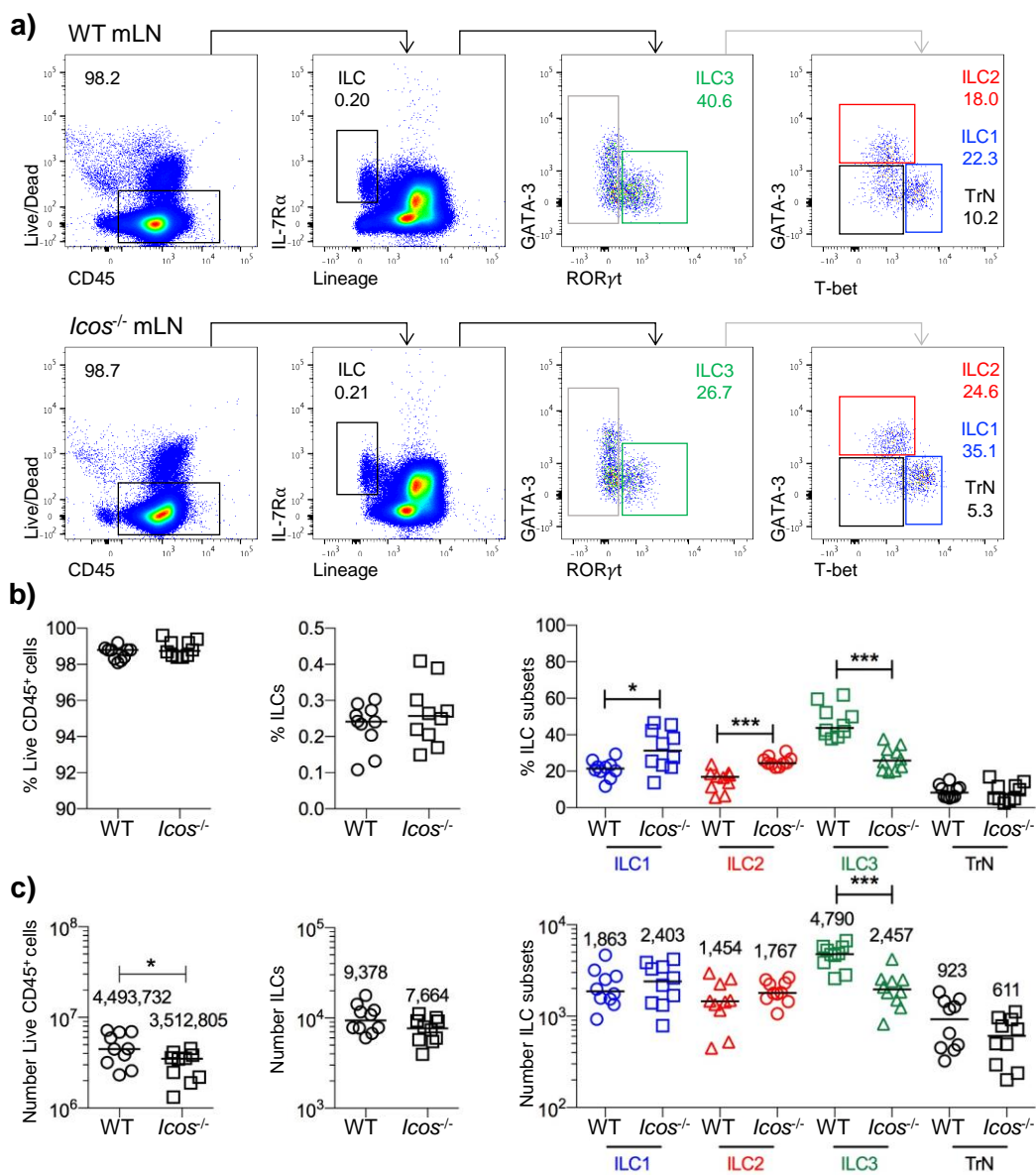
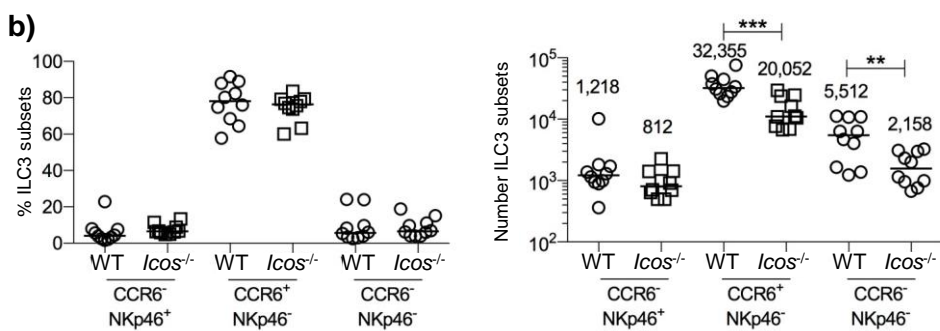
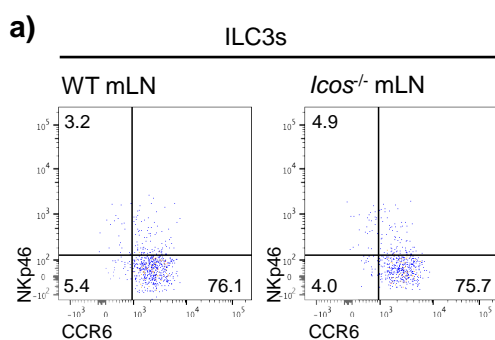


Figure 4.13. Reduced numbers of all ILC3 populations in the mLN of *Icos*^{-/-} mice

Tissues from WT mice were compared to *Icos*^{-/-} mice. Cells were isolated from the mLN as described in methods. Lineage markers include; B220, CD11c, CD11b, CD3 and CD5. ILC3s were previously gated on Live CD45⁺ Lineage⁻ IL-7R α ⁺ iCD3 ϵ ⁻ GATA-3⁻ ROR γ t⁺.

Each data point represents 1 mLN from one mouse. Data pooled from 4 experiments. Values on flow cytometry plots represent percentages, bars on scatter plots represents the median, which is also shown numerically. Statistical significance was tested using an unpaired, non-parametric, Mann-Whitney two tailed T test: *p \leq 0.05, **p \leq 0.01, ***p \leq 0.001.

- a) Representative flow cytometry plots showing expression of CCR6 and NKp46 on ILC3s within the WT mLN compared to the *Icos*^{-/-} mLN.
- b) Percentage (left) and numbers (right) of ILC3s that are CCR6⁻NKp46⁺, CCR6⁺ NKp46⁻ and CCR6⁺ NKp46⁺ within WT mLN (n=10) compared to *Icos*^{-/-} mLN (n=10).



4.3 SUMMARY

In the absence of studies exploring the role of ICOS in ILC biology, ILCs were assessed in both mucosal and lymphoid tissues of *Icosl*^{-/-} and *Icos*^{-/-} mice to determine whether ICOS:ICOSL interactions were required in the development and maintenance of ILCs under steady state conditions. This investigation showed that within the SI LP, lung and mLN of *Icosl*^{-/-} mice, although the proportion of ILCs varied compared to WT mice, upon enumeration no differences were observed. Changes in ILC numbers would clearly support a role of ICOS:ICOSL interactions in the development or maintenance of ILCs. Therefore, upon the observation that no ILC subset was numerically altered in *Icosl*^{-/-} mice compared to WT mice there seemed to be little requirement for ICOS:ICOSL interactions under steady state conditions within the tissues analysed. It was then explored whether the phenotype of ILC2s or ILC3s was perturbed. For ILC2s this involved looking at the expression of known surface markers commonly used in the identification of ILC2s, as described in Chapter 3, and for ILC3s, where there are several subsets, it was explored whether the importance of ICOS:ICOSL interactions were subset dependent. The number of CD25⁺, ICOS⁺, KLRG1⁺, MHCII⁺ and ST2⁺ ILC2s was comparable between WT and *Icosl*^{-/-} mice, alongside the number of NCR⁺, LTi-like and NCR⁻ ILC3s within the SI LP, mLN and lung. This suggests that lacking ICOSL has minimal impact on the phenotype and subgroups of ILC2s and ILC3s, respectively. Similarly, within the *Icos*^{-/-} SI LP the number of ILCs was comparable to WT mice. Although the comparison of WT and *Icosl*^{-/-} mice suggested no defect in ILC homeostasis within the mLN, upon comparing WT to *Icos*^{-/-} mice, a decrease in LTi-like and NCR⁻ ILC3s, was observed. These data indicate that ICOS:ICOSL interactions are not required for the development and maintenance of ILCs within the lung

and SI LP. Within the mLN, the differences in ILC3s requirement for ICOS over ICOSL suggests other ligands or receptors may be involved in these interactions.

ILC biology seems to be unaffected in the absence of ICOSL within the SI LP, mLN and lung within naive mice. This suggests that, similar to T cells, ILCs do not require ICOS:ICOSL interactions in their development and homeostasis (300). Whilst these data were being collected two studies were published on ILC2s requirement for ICOS:ICOSL interactions by Maazi et al., and Paclik et al., (262, 306). Paclik et al., identified ILC2s based on their expression of GATA-3 and demonstrated that under steady state at least a 50% reduction in the number of ILC2s within the lung and SI LP of *Icos*^{-/-} and *Icosl*^{-/-} mice was observed (306). Results published by Paclik et al., are not comparable to the results obtained within this Chapter. Due to similarities within the gating strategies and a clear decrease being observed within Paclik et al., data it may be suggested that the differences observed, compared to this investigation, reflect variations in the animal facilities used to breed and house mice. An increase in the understanding of gut microbiota has brought to attention its effect on the health and immune system of the animal (307, 308). Microbiota are known to vary between animal facilities due to different husbandry related factors and may in turn have an impact on the analysis of immune cell populations (307). For example, C57BL/6 mice from different external suppliers had different abilities of the APC subsets to induce Tregs vs Th17 cells (307, 309). This may suggest why results within this investigation compared to Paclik et al., do not show similar effects on the ILC2 population in the absence of ICOS:ICOSL interactions.

T cells dependency on ICOS:ICOSL interactions for efficient activation is only observed under immunological challenge, for example in KLH immunised mice (62). Therefore, the role of

ICOS:ICOSL interactions in the function of ILCs upon activation was planned to be further assessed under inflammatory conditions via intra nasal administration of IL-33, however, these experiments were conducted in the two papers discussed previously (262, 306). Maazi et al., and Paclik et al., both showed that under IL-33 driven airway hyperactivity ICOS:ICOSL interactions were important in the survival, proliferation and IL-13 production of ILC2s within the lung, with the absence of these interactions resulting in a reduced expansion of ILC2s and a reduction in inflammation (262, 306). Maazi et al., further discovered that ILC2s also express ICOSL and suggests that ILC2s are able to communicate with each other via ICOS:ICOSL interactions, promoting their survival and function through the STAT5 signalling pathway (262).

Within the SI LP and lung total numbers of ILC3s were comparable between WT mice and mice lacking ICOS:ICOSL interactions, suggesting that these interactions play a redundant role in their development and maintenance under steady state conditions. These data were supported by Paclik et al., who also demonstrate that ILC3s were comparable between WT, *Icos*^{-/-} and *Icosl*^{-/-} mice within these tissues (306). However, Paclik et al., did not explore the role of ICOS:ICOSL interactions in lymphatic tissues, in which these studies determined a different requirement for ICOS compared to ICOSL on ILC3 subset numbers within the mLN. Currently within the literature it is believed that ICOS and ICOSL only interact with one another, however, these results showing differences between *Icos*^{-/-} and *Icosl*^{-/-} mice may be explained by a potential binding of ICOS, or ICOSL to another ligand or receptor. It would be interesting to determine whether this is specific to the mLN or whether ILC populations in other SLTs also exhibit a dependence on ICOS or ICOSL.

In summary, a lack of substantial differences between genetically depleted mice compared to WT mice suggests it is unlikely that ICOS:ICOSL interactions play a critical role in normal ILC homeostasis. Studies could be extended to test under inflammatory conditions, however, with the reports already published the value of such further work was questionable. The lack of substantial effects indicates that the ICOS:ICOSL pathway was not key, therefore, these studies were focused towards exploring other aspects of ILC biology, focusing on the relationship between non-lymphoid tissue and SLTs such as LNs.

Chapter 5. DETERMINING THE MIGRATORY PROPERTIES OF ILCs WITHIN PERIPHERAL LNS

5.1 INTRODUCTION

The movement of lymphocytes and myeloid cells around the body is regulated by chemokines and integrins (49). These interactions control the directional migration or retention of populations within lymphoid or non-lymphoid tissues and is therefore, an essential feature of the immune system and fundamental for cell function. The cellular composition and structure of SLTs, including LNs, provides a niche microenvironment for naïve T cells and B cells to survey for antigen presented via MHCII on APCs (49, 310). Upon encountering cognate antigen T cells are activated through the TCR and develop into Th cells, which are important in the development of an effective immune response (310). Therefore, it is important to understand the mechanisms of leukocyte entry into the LN, via high endothelial venules (HEVs) or lymphatic vessels, and egress. The migratory properties of naïve lymphocytes within the immune system are well studied within the literature, however other populations, such as ILCs, migratory abilities are not clear.

5.1.1 Lymphocyte entry into the LNs via HEVs

Under homeostatic conditions naïve T and B cells migrate from primary lymphoid tissue into the blood, with naïve T cells searching for cognate antigen on APCs including DCs in SLTs (48). Entry into LNs occurs via HEVs, which are small blood vessels protruding into the LN and are paramount in the high input of naïve T cells and B cells from the blood (49, 311). Lymphocytes enter the LN, through HEVs, via a ‘tethering, rolling, sticking and transmigration’ mechanism

(49, 312). Within the blood, lymphocytes express CD62L which initiates tethering to the luminal wall of high endothelial cells (HECs). CD62L binds to a 6-sulpho sialyl-Lewis X motif on the type 1 transmembrane protein, sialomucin, which is expressed on the luminal facing side of HECs (49, 312-314). These interactions cause the cells to 'roll' along the luminal surface of HEVs before entry into the LN, in which CD62L is downregulated and only upregulated upon exit into the blood (49, 312, 315). To enable lymphocyte transmigration through HEVs the cells have to arrest and 'stick' to the luminal wall which occurs via chemokine activation of integrins on lymphocytes (316). CCL21, which is highly expressed by HEVs and in the T cell zone of LNs by FRCs, activates lymphocytes via its receptor CCR7, which is expressed on naïve lymphocytes and a subgroup of DCs (316, 317). CCL21 cell stimulation causes the upregulation and activation of integrin lymphocyte function-associated antigen 1 (LFA-1), which adheres to ICAM-1 expressed on the luminal side of HECs (316-318). This adhesion is efficient to arrest the 'rolling' phase of the cell, causing 'sticking' and eventually transmigration across the HEVs into the LN (318). This mechanism reflects the entry of lymphocytes into peripheral LNs, however, interactions between the integrin $\alpha 4\beta 7$, on lymphocytes and mucosal addressin cell adhesion molecule 1 (MADCAM1) on HEVs, is required for the entry of lymphocytes into gut associated lymphoid tissue, such as the mLN (319-321) Mice deficient in CCL21 and CCL19, which also binds CCR7, (*plt/plt* mice) exhibited reduced LFA-1 mediated T cell adhesion to the HEVs, which was restored upon CCL21 but not CCL19 intracutaneous injections (316). Furthermore, *Ccr7*^{-/-} mice and *Cd62l*^{-/-} mice exhibit a decrease in lymphocytes within the LNs and within *Ccr7*^{-/-} mice an increase in lymphocytes within the blood is observed (255, 313). These data support the importance of lymphocytes within the blood expressing CD62L and

CCR7 to enable their entry into the LN. Entry from the blood via HEVs into the LN is the main mechanism for T cells, including naïve, memory and Tregs, naïve B cells and cNK cells (49, 116).

5.1.2 Lymphocyte migration into the LV via the lymphatics system

The entry of lymphocytes into the LN also occurs via the lymphatics and is the main mechanism of entry for DCs (49). Lymph consists of immune cells and tissue-derived antigens and enters into the LN via afferent lymphatic vessels at the subcapsular sinus (35). Upon entry into the LN the lymph percolates from the subcapsular sinus through the medullary sinuses and the cortical sinuses before exiting via the efferent lymphatic vessel (35). DCs and T cells are both able to enter the LN parenchyma in a CCR7 dependent manner during this period, DCs through the base of the subcapsular sinus and T cells via the cortical or medullary sinuses (35).

Upon entry into the LN, via HEVs or the afferent lymphatic vessel, naïve T cells investigate the LN for cognate antigen presentation by DCs (310). If this encounter does not occur T cells are able to leave through the efferent lymphatic vessel (310). From the efferent lymph lymphocytes enter the thoracic duct and can then re-enter the blood to recirculate around the body (322). Efficient egress of lymphocytes requires the expression of the G protein-coupled, S1P receptor (322-325). There are 5 subgroups of S1P receptors with T cells and B cells expressing S1PR1 and S1PR4 and cNK cells expressing S1PR5 (324-326). S1P is generated *in vivo* by sphingosine kinase 1 and 2 and is highly concentrated in the blood and lymph (322, 323). Through the use of sphingosine kinase 1 and 2 conditional knock outs, Pappu et al., and Pham et al., showed erythrocytes to be the major source of S1P in the blood and lymphatic

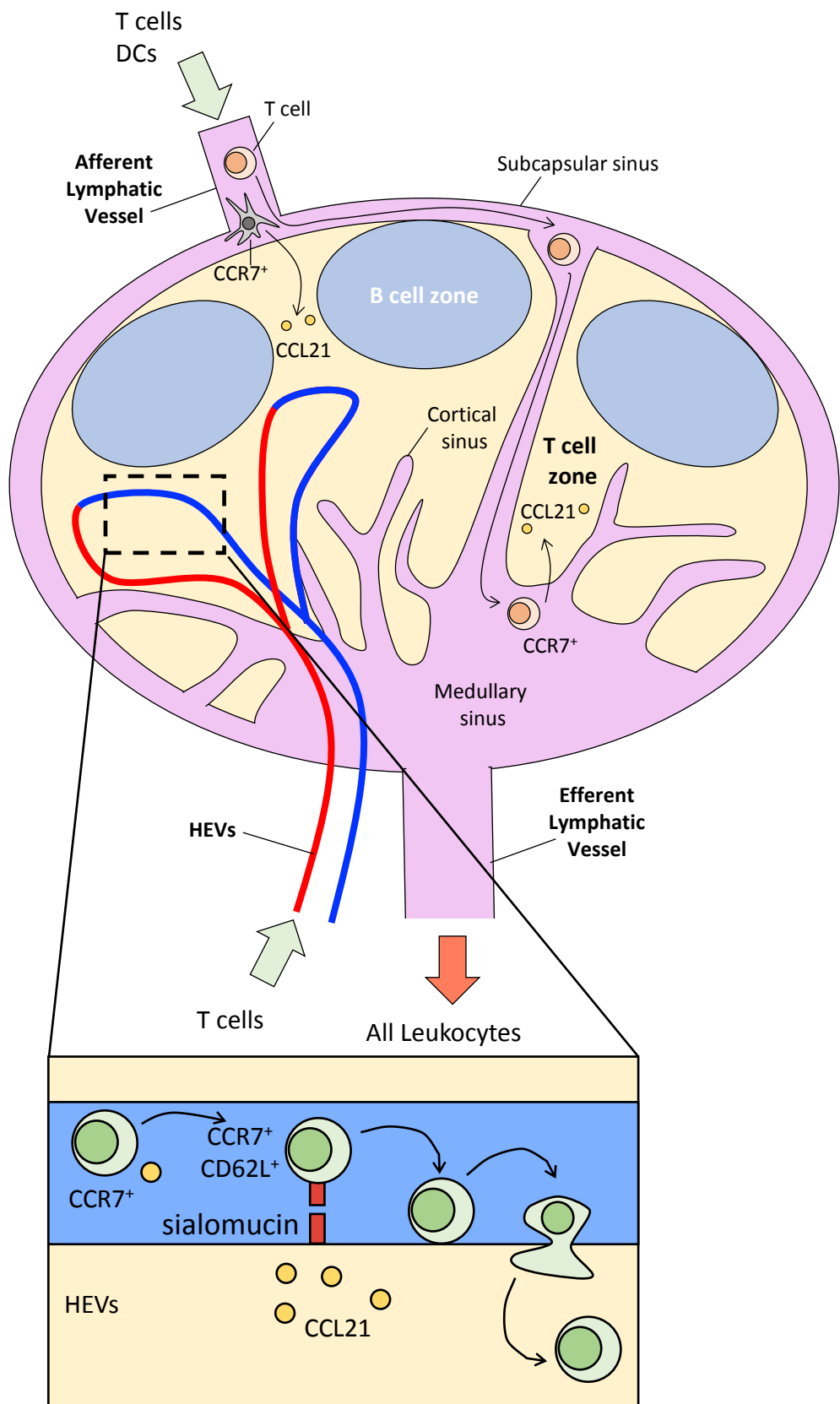
endothelial cells in the lymph (322, 323). The migration of innate and adaptive immune cells into the LN via either the blood or afferent lymphatic vessel is summarised within Figure 5.1.

5.1.3 Lymphocyte egress from LNs occurs in an S1P dependent manner

S1PR:S1P interactions are paramount in the egress of lymphocytes from the LN parenchyma via cortical and medullary sinuses, where they are transported into the lymph and then into blood, both of which have high concentrations of S1P (261, 322, 323, 327). The immunosuppressant drug FTY720 is an S1P receptor agonist, with lowest affinity to S1PR2 and S1PR5, and upon binding causes its downregulation (254, 261). Mandala et al., showed that administration of FTY720 prevents the egress of lymphocytes from SLTs, resulting in peripheral blood lymphopenia and a decrease in lymphocytes within the thoracic duct (261, 325). Furthermore, lymphocytes were found clustered within T cell and B cell zones, with the medullary and cortical sinuses containing very few lymphocytes (261). S1P degradation by S1P lyase is paramount in creating a low extracellular concentration of S1P in SLTs (328). This enables the maintenance of an S1P concentration gradient between the LN and the blood and lymph, promoting efficient egress of lymphocytes (49, 328). Inhibition of S1P lyase consequently results in the sequestration of lymphocytes within SLT, shown by Schwab et al., (328). Upon the entry of lymphocytes into the lymph and blood, high extracellular concentrations of S1P results in the internalisation of S1PR1 (329). This eventually enables the re-entry of lymphocytes into the LN in a CCR7:CCL21 dependent manner (329). However, once back in the LN, where there are low levels of S1P, S1PR1 is upregulated to overcome CCR7:CCL21 interactions, allowing lymphocyte egress (329). This enables the recirculation of T cells through SLTs (35, 53, 330). T cells can either migrate directly from a primary LN to a secondary LN without entering the blood, shown by Braun et al., by injecting T cells into the

Figure 5.1. Lymphocyte entry into the LN

Diagram of a LN which provides a niche microenvironment in which innate and adaptive immune cells are concentrated, facilitating their interactions. Cells are able to migrate into the LN via the blood, or the lymphatics. The main method of entry for DCs is through the afferent lymphatic vessel in which they migrate through the subcapsular sinus in a CCR7 dependent manner. T cells are also able to enter through the afferent lymphatic vessel, however, they migrate into the medullary sinus before migrating into the T cell zone in a CCR7 dependent mechanism. Ingress through the blood is the main route of entry into the LN for naïve T cells. Entry requires cells within the blood to undergo a 'tethering, rolling, sticking and transmigration' mechanism along the luminal wall of the HEV, in which CCR7 and CD62L expression is required. Naïve T cells express CD62L, which binds to sialomucin on the surface of the HECs required for cells to 'roll' along HEVs. CCR7 and CCL21, which are at high concentrations within the T cell zone, interactions increases the expression of integrins on T cells and subsequently the 'sticking phase' which eventually results in transmigration across the HEVs into the LN. Upon exit all hematopoietic cells egress via the efferent lymphatic vessel.



afferent lymphatic vessel of the popliteal LN and locating them within the iliac LN, which is downstream of the popliteal LN (35). T cells are also able to migrate to contralateral LNs through the blood shown by Tomura et al., who uses photoconvertible Kaede mice to show the migration of lymphocytes from the inguinal LN (iLN) through to blood into other peripheral LNs, which was dramatically reduced under FTY720 treatment (35, 53, 330, 331).

5.1.4 Retention of lymphocytes within the LN

During particular immune responses lymphocyte egress from the LN is blocked in an IFN- α/β dependent manner (332). T cell and B cell activation through the IFN- α/β receptor strongly induces the expression of the activation marker CD69, a C-type lectin receptor (332, 333). A role for CD69 in regulating the migration of lymphocytes was suggested when overexpression of CD69 resulted in a decrease in the egress of single positive thymocytes from the thymus (333, 334). Furthermore, the adoptive transfer of WT and *Cd69*^{-/-} lymphocytes into WT ploy(I:C), synthetic RNA which activates an immune response, treated hosts, by Shiow et al., revealed that WT lymphocytes were unable to efficiently egress from the LN into lymph compared to *Cd69*^{-/-} cells which were (332). CD69 inhibits the egress of cells via forming cross-interactions with S1PR1, in turn resulting in its downregulation and inhibition of function (332, 335).

5.1.5 Models used to track migration in vivo

Cellular migration has been tracked using methods such as two-photon microscopy, parabiotic models and injections of labelled cells or fluorescent substrates (35, 50, 249). These methods, however, all have their limitations and inhibit the observation of cellular movement in a homeostatic environment. Within recent years, the development of fluorescent proteins has

enhanced the ability to assess *in vivo* cell migration (336). Phototransformable fluorescent proteins change structure and therefore emission spectra permanently upon photoconversion with unique wavelengths of light (336). One of the first discovered Phototrasformable fluorescent proteins was the Kaede protein, a GFP fluorescent protein, which has been used to design photoconvertible fluorescence protein Kaede transgenic mice (53, 336). These Kaede mice were designed by Tomura et al., and ubiquitously express the Kaede protein, cloned from stony coral, within the cytoplasm of all cells (53, 259). After synthesis the protein emits bright green fluorescence, however, when exposed to UV or violet light, between the wavelengths of 350-410 nm, it is converted to emit a bright red fluorescence (259, 260). Within the Kaede protein, the peptide sequence His⁶²-Try⁶³-Gly⁶⁴ acts as the green chromophore and upon photoconversion, peptide cleavage occurs near the green chromophore, resulting in a change in the emission wavelength and excitation of the protein (260). The Kaede protein is now perceived as Kaede Red instead of Kaede Green and can be detected using fluorescence microscopes and flow cytometry (53, 260). The Kaede Red protein has a long biological half-life in lymphocytes *in vivo*, however, due to the location of the Kaede protein in the cytoplasm, after conversion of Kaede Green to Kaede Red, the Kaede Red protein can become diluted upon several cell divisions, so tracking of cells is limited to small time frames (53, 260). Kaede mice have previously been used to track the migration of T cells and B cells within peripheral LNs, the migration of DCs from skin to draining LN, retention of antigen-specific memory CD4⁺ T cells and ILC migration from gut to mLN (53, 92, 243, 247).

5.1.6 Migratory properties of ILCs

Through studies using parabiotic models, helper ILCs were established as tissue-resident, being replenished through local progenitor populations with minimal contribution of migratory mature ILCs (248, 249). cNK cells, on the other hand, are a well-known migratory population being able to enter LNs from the blood, with similar properties to cytotoxic CD8⁺ T cells (115-117). A limitation of the parabiotic models is the inability to assess migration through the lymphatics or the migration of cells within one mouse. Furthermore, ILC migration was not assessed in peripheral LN tissues, with the studies by Gasteiger et al., focusing on assessing ILC migration within the spleen and mLN (249). Evidence that ILCs move from the intestine to the mLN has been published, however, this involved substantial *in vivo* manipulation that may generate artefacts (243). Other studies propose the migration of ILCs from LN to tissues, however, these lacked any direct evidence of unmanipulated *in vivo* migration (226, 252). Huang et al., on the other hand has directly shown that iILC2s are able to respond to IL-25 stimulation within the gut and clearly disseminate to other tissues including the lung and mLN (254). Gasteiger et al., have also reported the presence of ILC1 within the blood and their ability to equilibrate between the blood of parabiotic mice, but not to be able to enter the assessed tissue.

5.1.7 Project Aims

ILC migration between lymphoid and non-lymphoid tissue is still unclear, therefore the aim of this investigation was to use transgenic photoconvertible mice to directly assess the *in vivo* migration of ILCs within the peripheral LNs. Using a previously established Kaede bLN model, in which leukocyte migration could be observed, the hypothesis that ILCs were not solely a tissue-resident population within peripheral LNs was assessed.

5.2 RESULTS

5.2.1 ILCs consist of migratory and tissue-resident populations within the bLN

LNs provide a niche microenvironment for the interactions between innate and adaptive cells important in the activation of the adaptive immune system and therefore in the induction of an effective immune response (49). Under homeostatic conditions T cells, B cells, DCs and cNK cells, enter LNs through HEVs and/or afferent lymphatic vessels (49, 53, 337). Through the use of photoconvertible Kaede mice Tomura et al., have shown the rapid migratory kinetics of T cells, B cells and DCs in the iLN over 24 hours, demonstrating that photoconvertible mice are a unique model, enabling the direct visualisation of lymphocytes migratory patterns (53). Due to the migratory properties of ILCs currently being unclear between non-lymphoid and lymphoid tissues, Kaede mice were used to assess the migratory kinetics of ILCs in the peripheral bLN (53, 92). Marriott et al., previously established a Kaede model to track the migration of antigen-specific CD4⁺ memory T cells from the bLN (92). The bLN was photoconverted, labelling all of the cells within the LN from Kaede Green to Kaede Red. This enabled the assessment of the bLN at various time points post photoconversion, with Kaede Red cells remaining in the LN being termed 'resident' and new Kaede Green cells termed 'migratory'. This model also enabled the tracking of Kaede Red cells out of the bLN into other tissues (92). Using these methods, the bLN was fully converted from Kaede Green to Kaede Red and the Kaede expression assessed 0 hours and 72 hours post photoconversion (Figure 5.2a-d) (92). The median percentage of cells expressing Kaede Red within the bLN was 99.7% at 0 hours, suggesting that the bLN was successfully photoconverted. Due to the nature of the data statistical significance could not be assessed between the percentage of Kaede Green and Kaede Red expressing cells within a population. Migration was observed 72 hours post

photoconversion due to it being anticipated that ILCs would be less migratory than naïve lymphocytes therefore leaving sufficient time to detect potential migration. Furthermore, Tomura et al., identifies Kaede Red expression in HeLa cells up to 72 hours post photoconversion and Marriott et al., shows the retention of Kaede Red antigen-specific CD4⁺ T cells in the bLN 120 hours post photoconversion, suggesting that this time scale was appropriate to assess migration without the potential issues of loss of Kaede Red signal (53, 92). After 72 hours >90% of the CD45⁺ cells, in the bLN, were Kaede Green, suggesting that cells within the bLN undergo dynamic changes over 3 days (Figure 5.2c-d) (53). The composition of the CD45⁺ Kaede Green 'migratory' population was mainly comprised of $\alpha\beta$ T cells, which although not directly phenotyped, were believed to mainly consist of naïve T cells which are highly migratory, trafficking through the blood and LNs spending up to 12 hours searching for cognate antigen within LNs (Figure 5.2e-f) (53). Smaller populations of $\gamma\delta$ T cells, ILCs and LCs also contributed to the Kaede Green population. ILC migration was compared to the migratory properties of T cells and LCs due these populations having different trafficking routes, blood vs lymph, and representing known migratory adaptive and innate populations, therefore a sensible comparison to ILCs for which the migratory properties are unknown (53, 247, 337, 338). Similar proportions of $\alpha\beta$, $\gamma\delta$ T cells, ILCs and LCs were found within the Kaede Red 'residential' population as the Kaede Green (Figure 5.2g-h). These data indicate that the ILC population, within the bLN, changes over time and whilst some ILCs are likely tissue-resident, migratory ILC populations exist.

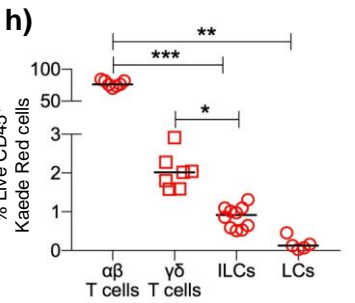
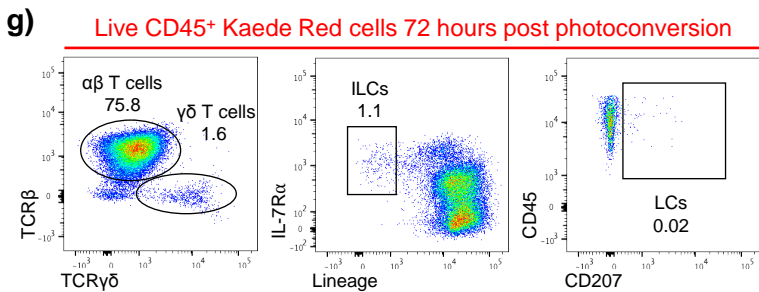
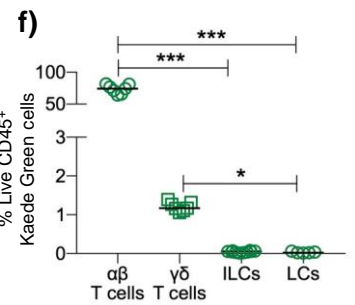
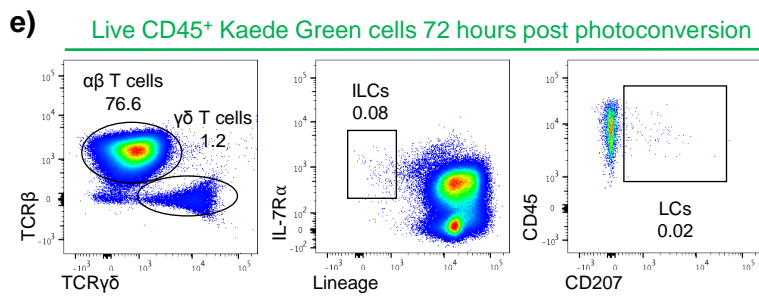
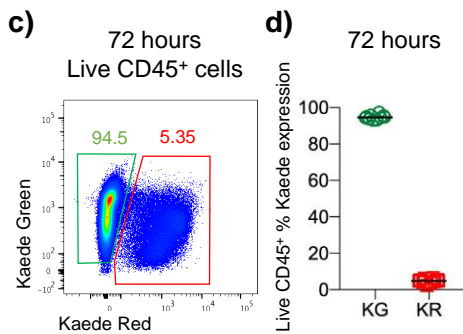
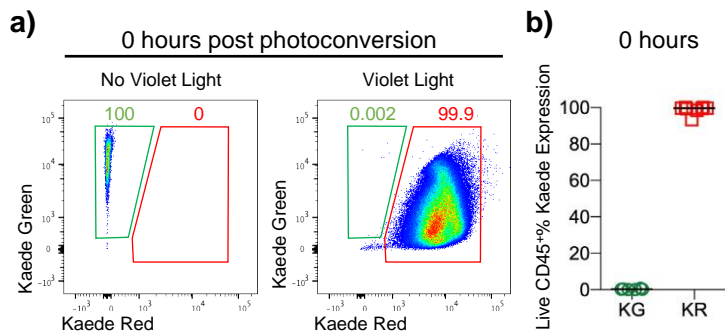
LNs have a highly complex and organised structure composed of stromal cells. They provide a mesh network for movement of lymphocytes, alongside the production of cytokines to aid

Figure 5.2. Tracking dynamic changes in immune cell composition of a peripheral LN

Violet light photoconversion of the bLN and cell isolation conducted as described in methods.

Each data point represents 1 bLN from one mouse. Data pooled from a minimum of 2 experiments. Values on flow cytometry plots represent percentages, bars on scatter plots represents the median. Samples were statistically tested using Kruskal-Wallis one-way ANOVA with post hoc Dunn's test: * $p \leq 0.05$, ** $p \leq 0.01$, *** $p \leq 0.001$. When gating on ILCs lineage markers include; B220, CD11c, CD11b, CD3, CD5, CD19, Ter119, Gr1, F4/80, Fc ϵ RI and F4/80.

- a) Representative flow cytometry plots showing Kaede Green (KG) and Kaede Red (KR) expression of the bLN with no violet light photoconversion (left) and violet light photoconversion (right) 0 hours post photoconversion.
- b) Percentage of Live CD45⁺ cells that express Kaede Green or Kaede Red in the bLN 0 hours post photoconversion (n=8).
- c) Representative flow cytometry plot showing Kaede Green and Kaede Red expression of Live CD45⁺ cells within the bLN 72 hours post photoconversion.
- d) Percentage of Live CD45⁺ cells that express Kaede Green or Kaede Red in the bLN 72 hours post photoconversion (n=10).
- e) Representative flow cytometry plots of Live CD45⁺ Kaede Green cells, identifying $\alpha\beta$ T cells (CD3 ϵ ⁺ TCR β ⁺ TCR $\delta\gamma$ ⁻), $\delta\gamma$ T cells (CD3 ϵ ⁺ TCR β ⁻ TCR $\delta\gamma$ ⁺), ILCs (Lineage⁻ IL-7R α ⁺) and LCs (MHCII⁺ CD11c⁺ CD207⁺) in the bLN 72 hours post photoconversion. The percentages represent that population as a proportion of Live CD45⁺ Kaede Green cells.
- f) Percentage of Kaede Green Live CD45⁺ cells that are $\alpha\beta$ T cells (n=7), $\delta\gamma$ T cells (n=7), ILCs (n=10) or LCs (n=5).
- g) Representative flow cytometry plots of Live CD45⁺ Kaede Red cells, identifying $\alpha\beta$ T cells, $\delta\gamma$ T cells, ILCs and LCs in the bLN 72 hours post photoconversion. The percentages represent that population as a proportion of Live CD45⁺ Kaede Red cells.
- h) Percentage of Kaede Red Live CD45⁺ cells that are $\alpha\beta$ T cells (n=7), $\delta\gamma$ T cells (n=7), ILCs (n=10) or LCs (n=5).



directional migration (49, 50). To contrast the highly migratory populations within an anticipated resident population, testing that the model works in identifying Kaede Red cells as tissue-resident, Kaede expression was analysed within the bLN stromal cells, 72 hours post photoconversion (Figure 5.3a-f) (50, 339). Few CD45⁺ stromal cells expressed Kaede Green, with a median of 4.1% Kaede Green stromal cells, similar to its sub populations; blood endothelial cells (BECs), FRCs and lymphatic endothelial cells (LECs) (Figure 5.3b-f). These data indicate that tissue-resident stromal cells maintain their Kaede Red expression over 72 hours, supporting the ability of the Kaede model to discriminate between resident and migratory populations.

5.2.2 Migration into the bLN is dependent on CCR7

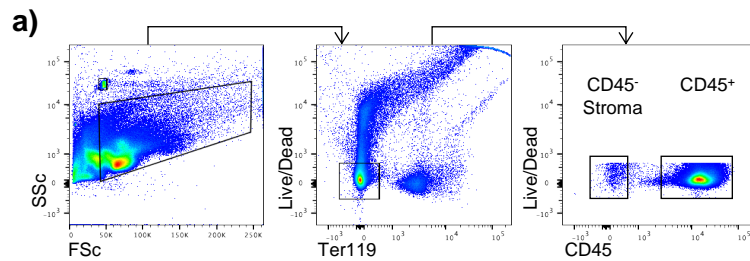
Upon the identification of a new Kaede Green ILC population within the bLN, suggesting that ILCs migrate into the tissue rather than remaining in the LN as purely resident cells, the mechanism behind their entry was investigated. CCR7 is paramount in the recruitment of lymphocytes into LNs, with *Ccr7*^{-/-} mice having significantly reduced numbers of T cells, B cells and DCs in the mLN and peripheral LNs (243, 255). Furthermore, CCR7 was shown to be directly involved in the migration of LT α i-like ILC3s from the intestine to the mLN (243). To further explore this *Ccr7*^{-/-} Kaede mice were made and compared to WT Kaede mice and the migration of lymphocytes, including ILCs assessed. Compared to WT Kaede, all populations, including ILCs were substantially decreased in number within *Ccr7*^{-/-} Kaede mice, suggesting a dependency on CCR7 for ILC homeostasis (Figure 5.4a). Upon analysing the proportion of Kaede Green vs Kaede Red in all populations within WT Kaede, it was clear that T cells and LCs contain a high percentage of Kaede Green cells, consistent with these populations being highly migratory. In comparison ILCs have a more equal ratio of Kaede Green and Kaede Red

Figure 5.3. Stromal populations within the bLN remain Kaede Red 72 hours after photoconversion

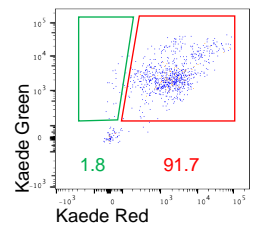
Violet light photoconversion of the bLN of WT Kaede mice and cell isolation of the stromal population were conducted as described in methods.

All data shown are 72 hours post photoconversion. Each data point represents 1 bLN from one mouse. Data pooled from a minimum of 2 experiments. Values on flow cytometry plots represent percentages, bars on scatter plots represents the median.

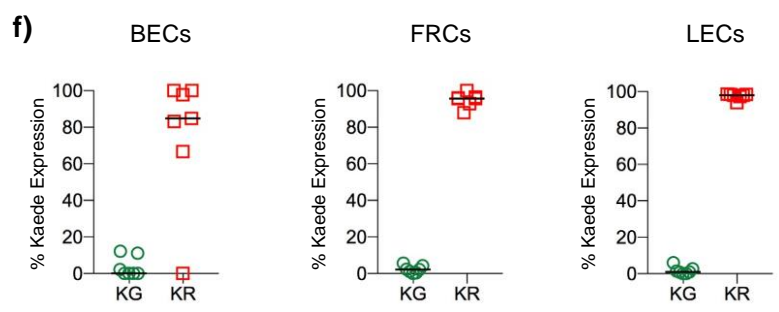
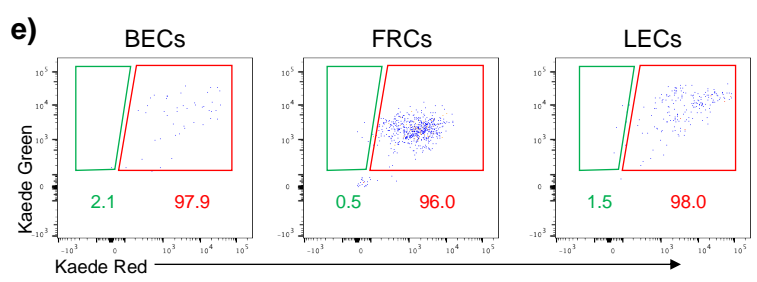
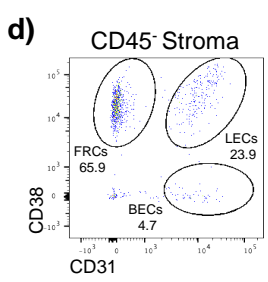
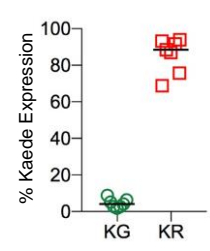
- a) Representative flow cytometry plots showing the gating mechanism used to identify stromal cells (Live Ter119⁻ CD45⁻).
- b) Representative flow cytometry plot showing Kaede Green and Kaede Red expression of stromal cells.
- c) Percentage of Kaede Green and Kaede Red stromal cells (n=7), 72 hours post photoconversion.
- d) Representative flow cytometry plots of stromal cell subsets, blood endothelial cells (BECs) (Live Ter119⁻ CD45⁻ CD31⁺ CD38⁻), fibroblastic reticular cells (FRCs) (Live Ter119⁻ CD45⁻ CD31⁻ CD38⁺) and lymphatic endothelial cells (LECs) (Live Ter119⁻ CD45⁻ CD31⁺ CD38⁺).
- e) Representative flow cytometry plots showing Kaede Green and Kaede Red expression of BECs, FRCs and LECs 72 hours post photoconversion.
- f) Percentage of Kaede Green and Kaede Red BECs, FRCs and LECs (n=7).



b) CD45⁻ Stroma 72 hours post photoconversion



c)



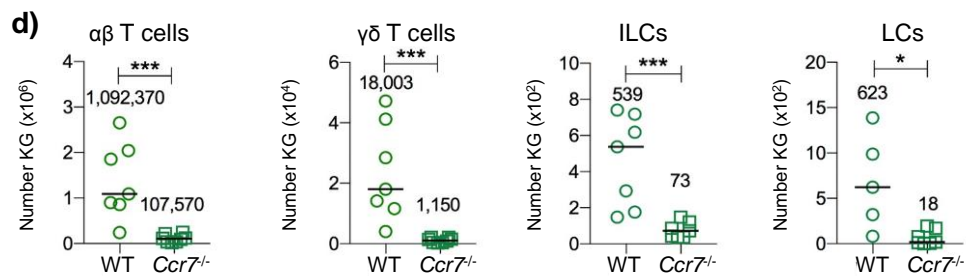
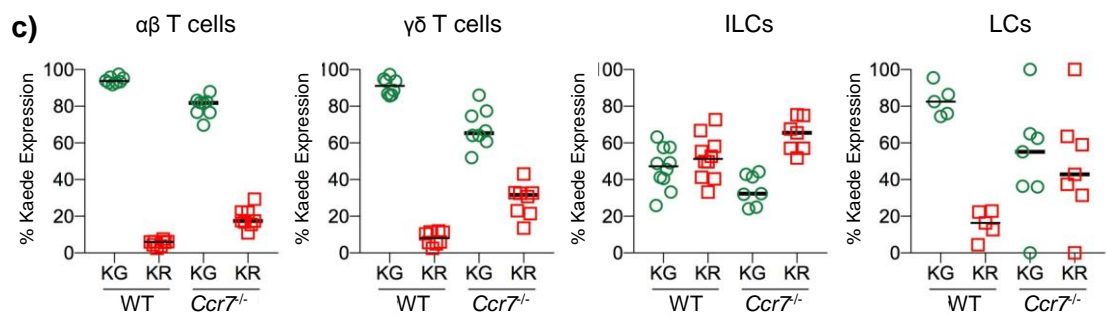
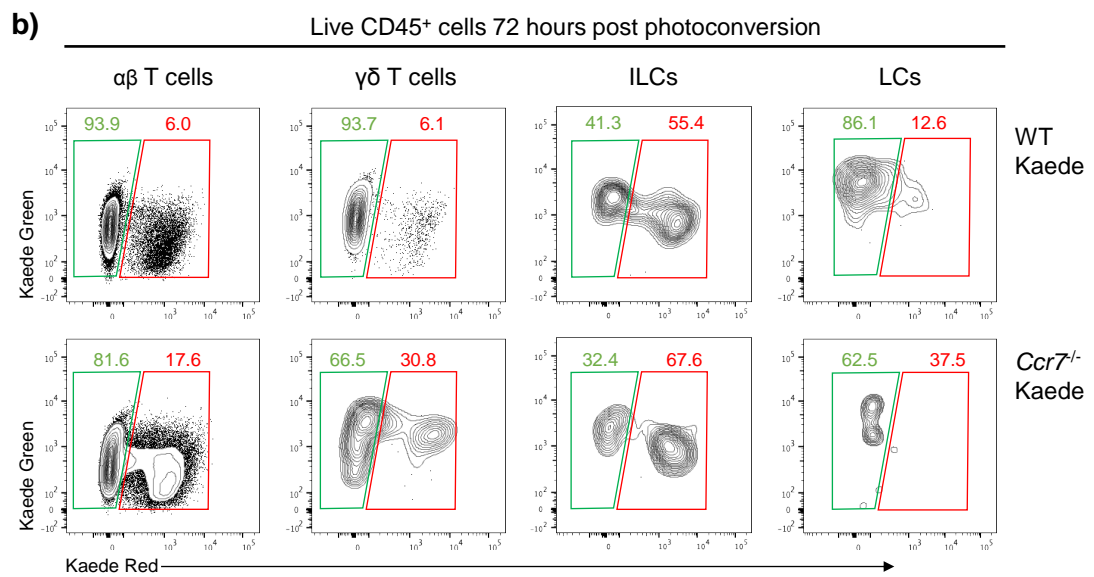
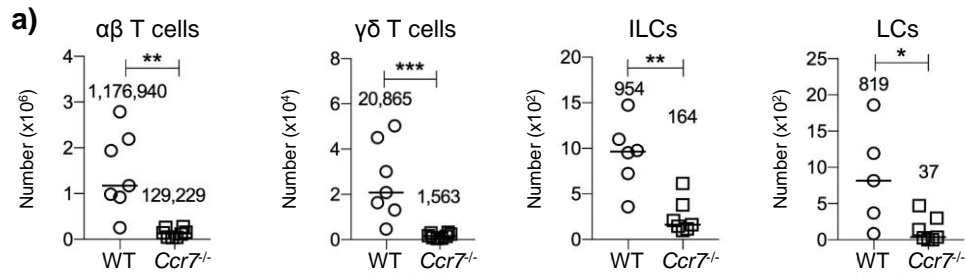
expression suggesting that although they contain a proportion of migratory cells, there is still the presence of a clear resident population (Figure 5.4b-c). To assess whether migration was perturbed in the absence of CCR7, Kaede expression of each population was assessed in *Ccr7*^{-/-} Kaede mice and the Kaede Green cells were enumerated to determine if ILC migration specifically into the LN was dependent on CCR7 expression (Figure 5.4b-d). All populations observed a decreased in Kaede Green cells entering into the bLN within the 72 hour assessed period, indicating that ILC migration into the peripheral LN is dependent on CCR7 (Figure 5.4d) (243, 255, 337). $\gamma\delta$ T cells share similarities with ILCs, given that they are lymphocytes but are considered more of an innate population than $\alpha\beta$ T cells, with a less diverse TCR and ability to provide a quick source of cytokine upon activation (338, 340, 341). Within the skin they are subdivided into three populations, dendritic epidermal T cells (DETCs) which express V γ 5, dermal V γ 4⁺ and dermal V γ 4⁻ T cells. DETCs are a tissue-resident population with dermal V γ 4⁺ T cells possessing the ability to migrate into draining LNs upon skin inflammation (338, 341). Considering that $\gamma\delta$ T cells were the second largest population of cells entering the bLN, their subsets were further assessed within the Kaede model. V γ 1 T cells were also assessed as these mainly reside within lymphatic tissues (338, 342). All subtypes of $\gamma\delta$ T cells were decreased in number in *Ccr7*^{-/-} mice (Figure 5.5a). Upon analysis of Kaede expression V γ 1 and V γ 4 T cells had a high >80% Kaede Green expression, suggesting that they were highly migratory populations, consistent with previous publications studying the migratory properties of V γ 4⁺ T cell (338). Although V γ 5 T cells are a skin-resident population, the presence of Kaede Green V γ 5 T cells suggests that a small proportion of these cells are able to migrate into the LN (341). Within the *Ccr7*^{-/-} Kaede mice, V γ 1 and V γ 4 $\gamma\delta$ T cell population had a larger percentage of Kaede Green expressing cells to Kaede Red, similar to WT Kaede mice, however due to the

Figure 5.4. Migration of ILCs is CCR7 dependent

Tissues from WT Kaede mice were compared to *Ccr7*^{-/-} Kaede mice. Violet light photoconversion of the bLN and cell isolation were conducted as described in methods. All data shown are 72 hours post photoconversion.

Each data point represents 1 bLN from one mouse. Data pooled from a minimum of 2 experiments. Values on flow cytometry plots represent percentages, bars on scatter plots represents the median, which is also shown numerically. Statistical significance was tested using an unpaired, non-parametric, Mann-Whitney two tailed T test: *p≤0.05, **p≤0.01, ***p≤0.001. When gating on ILCs lineage markers include; B220, CD11c, CD11b, CD3, CD5, CD19, Ter119, Gr1, F4/80, FcεRI and F4/80.

- a) Total numbers of $\alpha\beta$ T cells (Live CD45⁺ CD3 ϵ ⁺ TCR β ⁺ TCR $\gamma\delta$ ⁻), $\gamma\delta$ T cells (Live CD45⁺ CD3 ϵ ⁺ TCR β ⁻ TCR $\gamma\delta$ ⁺), ILCs (Live CD45⁺ Lineage⁻ IL-7R α ⁺) and LCs (Live CD45⁺ MHCII⁺ CD11c⁺ CD207⁺) in WT Kaede (n=5-7) and *Ccr7*^{-/-} Kaede (n=7-8) mice.
- b) Representative flow cytometry plots showing Kaede Green and Kaede Red expression of $\alpha\beta$ T cells, $\delta\gamma$ T cells, ILCs and LCs in the bLN of WT Kaede (top) and *Ccr7*^{-/-} Kaede (bottom) mice.
- c) Percentage of Kaede Green and Kaede Red expression by $\alpha\beta$ T cells, $\gamma\delta$ T cells, ILCs and LCs in WT Kaede (n=5-10) and *Ccr7*^{-/-} Kaede (n=7-8) mice.
- d) Number of Kaede Green $\alpha\beta$ T cells, $\gamma\delta$ T cells, ILCs and LCs in WT Kaede (n=5-7) and *Ccr7*^{-/-} Kaede (n=7-8) mice.



reduced numbers of V γ 5 T cells, their Kaede expression was extremely varied between samples (Figure 5.5b-c). All subsets observed decreased numbers of Kaede Green cells entering the bLN within 72 hours in *Ccr7*^{-/-} mice compared to the WT Kaede mice (Figure 5.5d). These data are consistent with published migratory properties of dermal V γ 4⁺ T cells but also suggest a migratory population of V γ 1 T cells alongside a small V γ 5 population, that all migrate into the bLN in a CCR7 dependent manner (338).

5.2.3 Photoconversion does not result in the accumulation of cells within the bLN

The photoconversion approach required a small incision to be made in the skin to expose the bLN. Since new Kaede Green ILCs moving into the tissue were detected it was a concern that the skin damage caused in this procedure resulted in the recruitment and accumulation of cells in the skin draining bLN. To assess the effect of surgery on the bLN, control mice, which had no surgical procedure, were compared to mice which underwent the violet light surgical procedure and were left to recover for 72 hours (Figure 5.6a). Upon comparison there was no difference in CD45⁺ cells, ILCs or ILC subsets, apart from an increase in number of TrN cells, within the bLN (Figure 5.6b). This suggests that the surgical procedure does not cause an increase and accumulation of cells within the bLN. Repeating this experiment in Kaede mice, showed that the increase in number of Kaede Green ILCs in the violet light mouse is accompanied by a loss of Kaede Red ILCs (Figure 5.6c-d). These data suggest that the ingress of ILCs is balanced by the loss of Kaede Red ILCs, either through egress or death.

5.2.4 ILCs egress from the bLN in an S1P dependent manner

For efficient egress from the LN, lymphocytes require the expression of S1PR and high levels of S1P in the blood and lymph (261, 322, 323). T cell and B cells express S1PR1 and S1PR4 and

Figure 5.5. CCR7 dependent trafficking of $\gamma\delta$ T cell subsets

Tissues from WT Kaede mice were compared to *Ccr7*^{-/-} Kaede mice. Violet light photoconversion of the bLN and cell isolation were conducted as described in methods. All data shown are 72 hours post photoconversion.

Each data point represents 1 bLN from one mouse. Data pooled from a minimum of 2 experiments. Values on flow cytometry plots represent percentages, bars on scatter plots represents the median, which is also shown numerically. Statistical significance was tested using an unpaired, non-parametric, Mann-Whitney two tailed T test: * $p \leq 0.05$, ** $p \leq 0.01$, *** $p \leq 0.001$.

- a) Total numbers of $\gamma\delta$ T cells V γ 1, $\gamma\delta$ T cells V γ 4 and $\gamma\delta$ T cells V γ 5s in WT Kaede (n=7) and *Ccr7*^{-/-} Kaede (n=8) mice.
- b) Representative flow cytometry plots showing Kaede Green and Kaede Red expression of $\delta\gamma$ T cell subsets, $\gamma\delta$ T cells V γ 1 (Live CD45⁺ CD3 ϵ ⁺ TCR $\gamma\delta$ ⁺ V γ 1⁺), $\gamma\delta$ T cells V γ 4 (Live CD45⁺ CD3 ϵ ⁺ TCR $\gamma\delta$ ⁺ V γ 4⁺) $\gamma\delta$ T cells V γ 5 (Live CD45⁺ CD3 ϵ ⁺ TCR $\gamma\delta$ ⁺ V γ 5⁺) in WT Kaede (top) and *Ccr7*^{-/-} Kaede (bottom) mice.
- c) Percentage of Kaede Green and Kaede Red expression by $\gamma\delta$ T cells V γ 1, $\gamma\delta$ T cells V γ 4 and $\gamma\delta$ T cells V γ 5s in WT Kaede (n=7) and *Ccr7*^{-/-} Kaede (n=8) mice.
- d) Number of Kaede Green $\gamma\delta$ T cells V γ 1, $\gamma\delta$ T cells V γ 4 and $\gamma\delta$ T cells V γ 5s in WT Kaede (n=7) and *Ccr7*^{-/-} Kaede (n=8) mice.

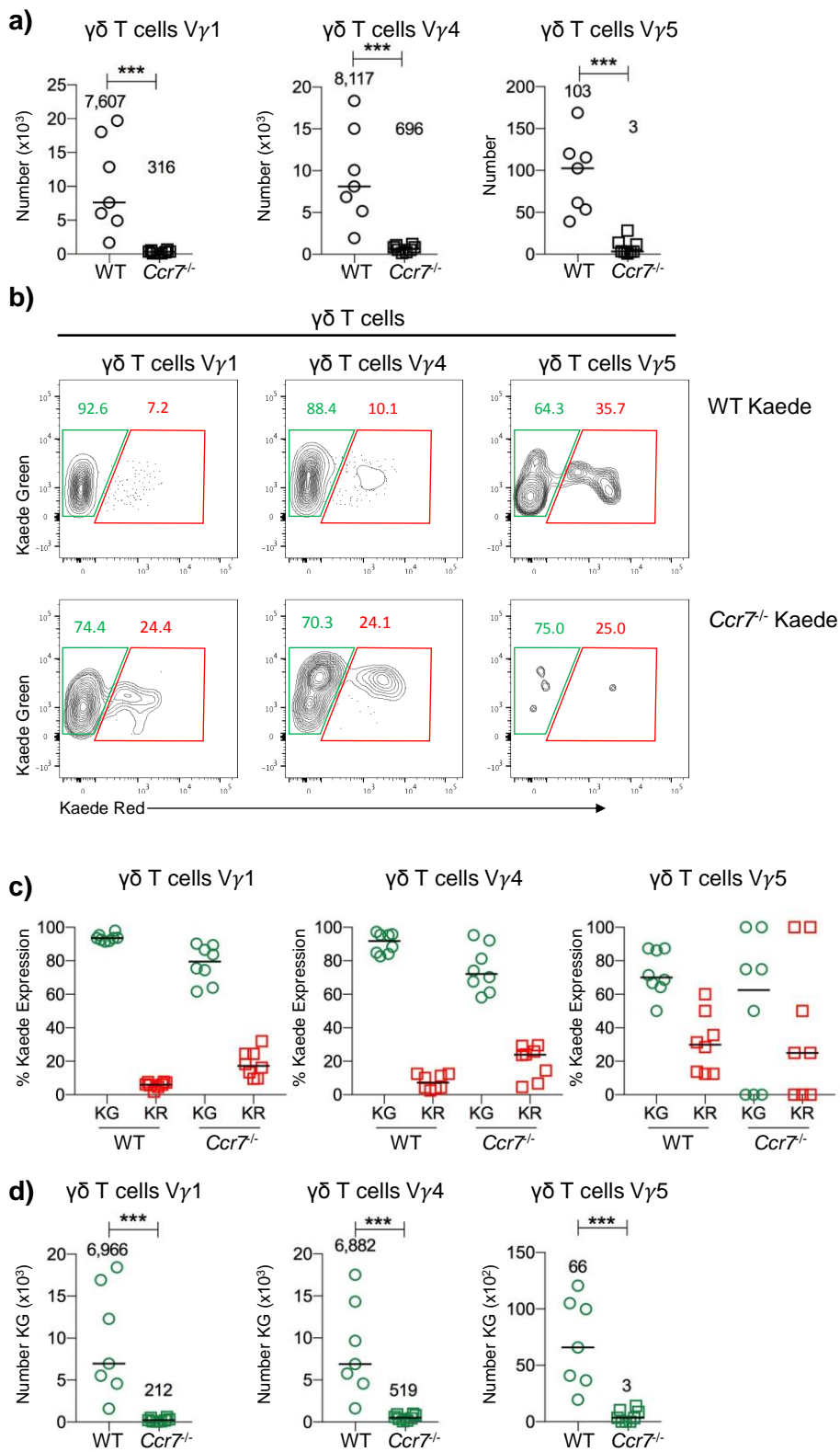
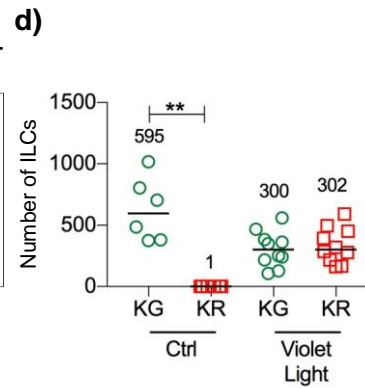
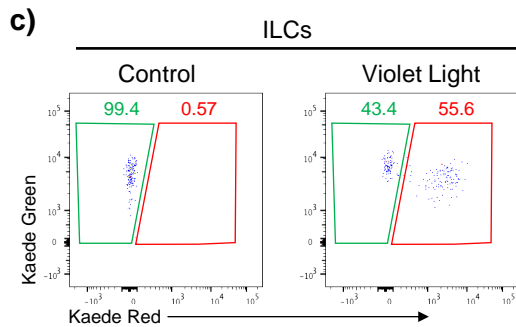
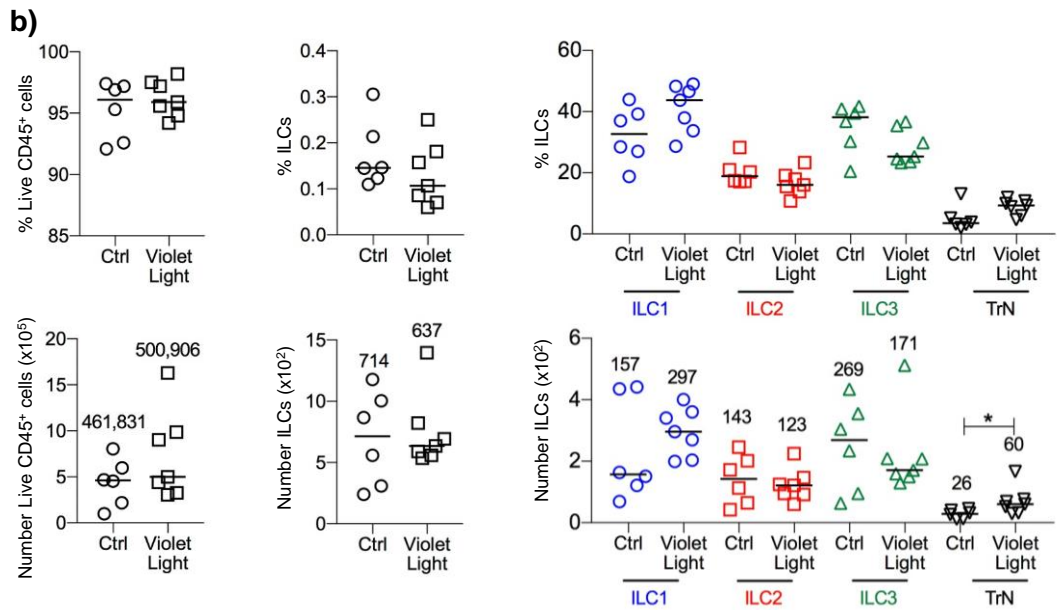
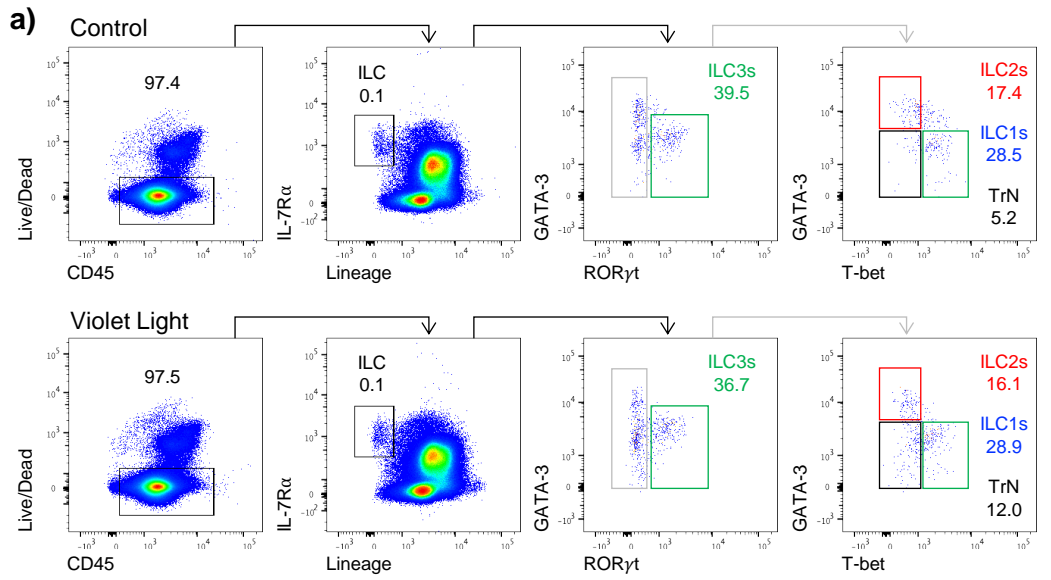


Figure 5.6. Photoconversion does not result in the accumulation of ILCs within the LN

Mice either underwent photoconversion surgery (violet light) or did not (control), as described in methods. All data shown are 72 hours post photoconversion. Cell isolation of the bLN was conducted as described in methods.

Each data point represents 1 bLN from one mouse. Data pooled from a minimum of 3 experiments. Values on flow cytometry plots represent percentages, ILCs as a proportion of Live CD45⁺ cells and ILC subsets as a proportion of total ILCs. Bars on scatter plots represents the median, which is also shown numerically. Statistical significance was tested using an unpaired, non-parametric, Mann-Whitney two tailed T test: *p≤0.05, **p≤0.01, ***p≤0.001. When gating on ILCs in WT Kaede mice lineage markers include; B220, CD11c, CD11b, CD3, CD5, CD19, Ter119, Gr1, F4/80, FcεRI and F4/80. In non Kaede mice, the additional lineage marker CD123 was used and ILCs were gated on negatively for iCD3ε.

- a) Representative flow cytometry plots of WT mice showing Live CD45⁺ cells, ILCs (Live CD45⁺ Lineage⁻ IL-7Rα⁺ iCD3ε⁻), ILC1s (Live CD45⁺ Lineage⁻ IL-7Rα⁺ iCD3ε⁻ RORγt⁻ GATA-3⁻ T-bet⁺), ILC2s (Live CD45⁺ Lineage⁻ IL-7Rα⁺ iCD3ε⁻ RORγt⁺ GATA-3⁺ T-bet⁻), ILC3s (Live CD45⁺ Lineage⁻ IL-7Rα⁺ iCD3ε⁻ RORγt⁺) and TrN cells (Live CD45⁺ Lineage⁻ IL-7Rα⁺ iCD3ε⁻ RORγt⁻ GATA-3⁻ T-bet⁻) in control (top) and violet light (bottom) mice.
- b) Percentage (top) and number (bottom) of WT mice Live CD45⁺, ILCs and ILC subsets in control (n=6) and violet light (n=7) mice.
- c) Representative flow cytometry plots showing WT Kaede mice Kaede Green and Kaede Red expression in ILCs in control (left) and violet light (right) mice.
- d) Number of WT Kaede mice Kaede Green and Kaede Red ILCs in control (n=6) and violet light (n=10) mice.



ILCs have recently been shown to express S1PR1, S1PR4 and S1PR5, however, the majority of literature focuses on the role of S1PR1 in lymphocyte egress (254, 261). To determine whether ILCs had the capability to egress from the bLN in a similar manner to lymphocytes, their expression of S1PR1 was assessed. S1PR1 expression was observed on all ILC subgroups, with the highest expression on ILC3s (Figure 5.7a-b). This suggests that ILCs might exit the LN utilising S1PR1 in a similar manner to T cells.

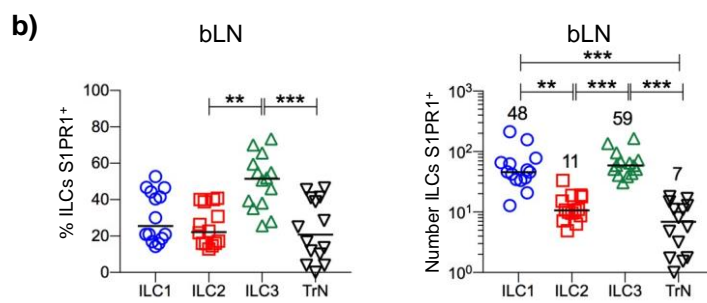
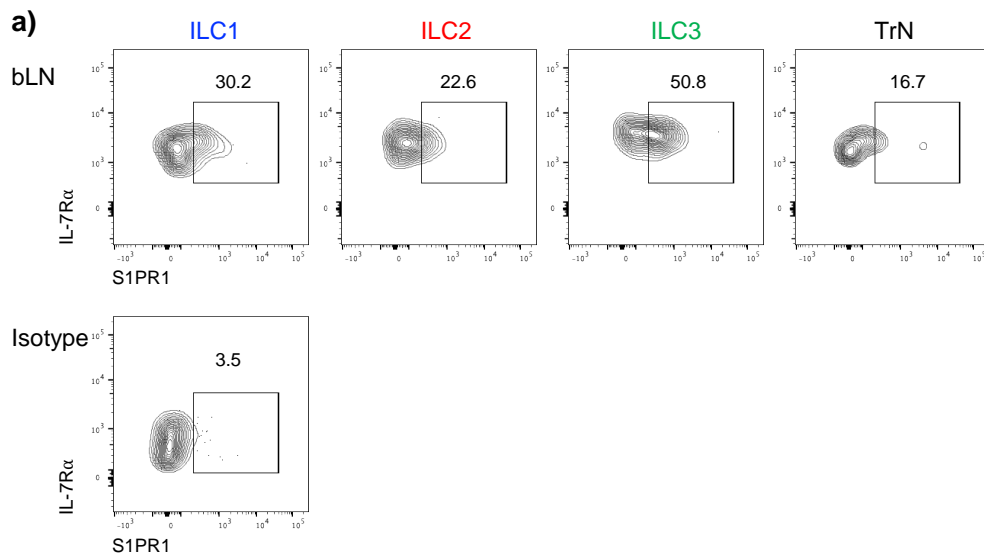
To formally test the hypothesis that ILC egress in an S1PR dependent manner FTY720, an S1PR agonist, which has previously been used in multiple studies to show the importance of S1PR:S1P interactions in the egress of lymphocytes from SLTs, was utilised (53, 261, 343). FTY720, however, does not efficiently block all S1PRs, including S1PR2 and S1PR5 and has therefore been mainly used to assess the S1PR1 and S1PR4 dependent migration of lymphocytes (254, 344). Tomura et al., administered FTY720 to Kaede mice and observed an increase in Kaede Red cells within the iLN 24 hours post photoconversion, showing that lymphocytes that normally egress via S1P mechanisms were sequestered in the LN (53). Therefore, within these studies, Kaede mice were injected with FTY720 one day prior to bLN photoconversion and everyday throughout the protocol. Blocking the S1PR-mediated egress of cells resulted in no difference in the number of CD45⁺ hematopoietic cells or T cells, however an increase in the number of ILCs, within the bLN was observed (Figure 5.8a-b). Naïve T cells recirculate through the blood entering and exiting LNs in search of cognate antigen and blocking their egress from LNs halts this recirculation suggesting why comparable numbers of T cells in control and FTY720 mice was observed (53). This is evident when assessing Kaede Green and Kaede Red expression, with an accumulation of Kaede Red T cells observed within the bLN of FTY720 mice, represented by a statistical decrease in number of Kaede Green T

Figure 5.7. ILCs express S1PR1 in the peripheral LN

Cell isolation of the bLN from WT mice was conducted as stated in the methods. ILCs identified and their expression of S1PR1 analysed.

Each data point represents 1 bLN from one mouse. Data pooled from a minimum of 2 experiments. Values on flow cytometry plots represent percentages, bars on scatter plots represents the median, which is also shown numerically. Statistical significance was tested using Kruskal-Wallis one-way ANOVA with post hoc Dunn's test: * $p \leq 0.05$, ** $p \leq 0.01$, *** $p \leq 0.001$. When gating on ILCs lineage markers include; B220, CD11c, CD11b, CD3, CD5, CD19, Ter119, Gr1, F4/80, FcεRI and F4/80.

- a) Representative flow cytometry plots showing the expression of S1PR1 on ILC1s (Live CD45⁺ Lineage⁻ IL-7Rα⁺ iCD3ε⁻ RORγt⁻ GATA-3⁻ T-bet⁺), ILC2s (Live CD45⁺ Lineage⁻ IL-7Rα⁺ iCD3ε⁻ RORγt⁻ GATA-3⁺ T-bet⁻), ILC3s (Live CD45⁺ Lineage⁻ IL-7Rα⁺ iCD3ε⁻ RORγt⁺) and TrN cells (Live CD45⁺ Lineage⁻ IL-7Rα⁺ iCD3ε⁻ RORγt⁻ GATA-3⁻ T-bet⁻) in the bLN, compared to an isotype control.
- b) Percentage (left) and total number (right) of ILC subsets expressing S1PR1 in the bLN. Due to the range of numbers within the data it is presented on a logarithmic scale where values equal to 0 are represented as 1.



cells and increase in number of Kaede Red within the FTY720 treated mice (Figure 5.8c-e). Similar to T cells, blocking S1P-dependent egress of cells from the LN resulted in an increased number of Kaede Red ILCs, suggesting that under normal conditions ILCs egress from the tissue in an S1P dependent manner (Figure 5.8f-h). Interestingly there was no difference in the number of Kaede Green ILCs entering the bLN. Since FTY720 doesn't efficiently block all S1PR, it is possible that some ILCs still egress from other tissues, dependent on either S1PR2 or S1PR5, which in turn could explain normal numbers of Kaede Green ILC being able to enter the LN from circulation. Furthermore, the reduction in number and percentage of Kaede Red T cells in the contralateral LNs is consistent with a block in T cell recirculation (Figure 5.8i-j).

Sequestration of ILCs within the bLN upon FTY720 administration indicates that ILCs, under homeostatic conditions, are able to leave the bLN within the 72 hour period assessed. Upon leaving the LN, naïve T cells recirculate through lymphoid tissue in the search for antigen. To determine whether ILCs recirculate through contralateral LNs, the bLN was photoconverted and 72 hours later, the presence of Kaede Red ILCs within a pool of contralateral LNs including the mLN, auLN, iLN, cervical LN (cLN), axillary LN (axLN), bLN was assessed. The cell suspension from the contralateral LNs was depleted of B cells and T cells through magnetic-activated cell sorting (MACS)-enrichment for B220, CD3 and CD5, to try to increase the proportion of ILCs, helping to track rare Kaede Red cells. Kaede Red T cells were identified in contralateral LNs and supporting their CCR7-dependent migration were reduced in *Ccr7*^{-/-} Kaede mice (Figure 5.9a-b) (53). In the depleted cell fraction a small proportion of Kaede Red ILCs were detected, including within *Ccr7*^{-/-} Kaede mice, consistent with ILCs being a recirculatory population (Figure 5.9c-d). The low numbers of Kaede Red ILCs that could be detected may represent the

Figure 5.8. Inhibition of S1P mediated egress directly results in the accumulation of ILCs

WT Kaede mice were administered i.p injections of 1 mg/mL FTY720 in H₂O (FTY720) (n=7) or H₂O (control) (n=4) one day prior to surgery and then every day after surgery as described in methods. All data shown are 72 hours post photoconversion. Cell isolation from bLN, mLN, iLN, auLN, axLN and cLN were conducted as discussed in methods.

Each data point represents 1 bLN or 1 pool of contralateral LNs from one mouse. Data pooled from a minimum of 2 experiments. Values on flow cytometry plots represent percentages, bars on scatter plots represents the median, which is also shown numerically. Statistical significance was tested using an unpaired, non-parametric, Mann-Whitney two tailed T test: *p≤0.05, **p≤0.01, ***p≤0.001. When gating on ILCs lineage markers include; B220, CD11c, CD11b, CD3, CD5, CD19, Ter119, Gr1, F4/80, FcεRI and F4/80.

- a) Representative flow cytometry plots showing Live CD45⁺ cells, T cells (Live CD45⁺ CD3ε⁺) and ILCs (Live CD45⁺ Lineage⁻ IL-7Rα⁺) in control (top) and FTY720 (bottom) mice.
- b) Number of Live CD45⁺ cells, T cells and ILCs in control and FTY720 mice.
- c) Representative flow cytometry plots showing Kaede Green and Kaede Red expression of T cells in control (left) and FTY720 (right) mice.
- d) Percentage of Kaede Green and Kaede Red T cells in control and FTY720 mice.
- e) Number of Kaede Green (left) and Kaede Red (right) T cells in control and FTY720 mice.
- f) Representative flow cytometry plots showing Kaede Green and Kaede Red expression of ILCs in control (left) and FTY720 (right) mice.
- g) Percentage of Kaede Green and Kaede Red ILCs in control and FTY720 mice.
- h) Number of Kaede Green (left) and Kaede Red (right) ILCs in control and FTY720 mice.
- i) Representative flow cytometry plots showing Kaede Green and Kaede Red expression of T cells in contralateral LNs in control (left) and FTY720 (right) mice.
- j) Percentage (right) and number (left) of Kaede Red T cells in contralateral LNs of control and FTY720 mice.

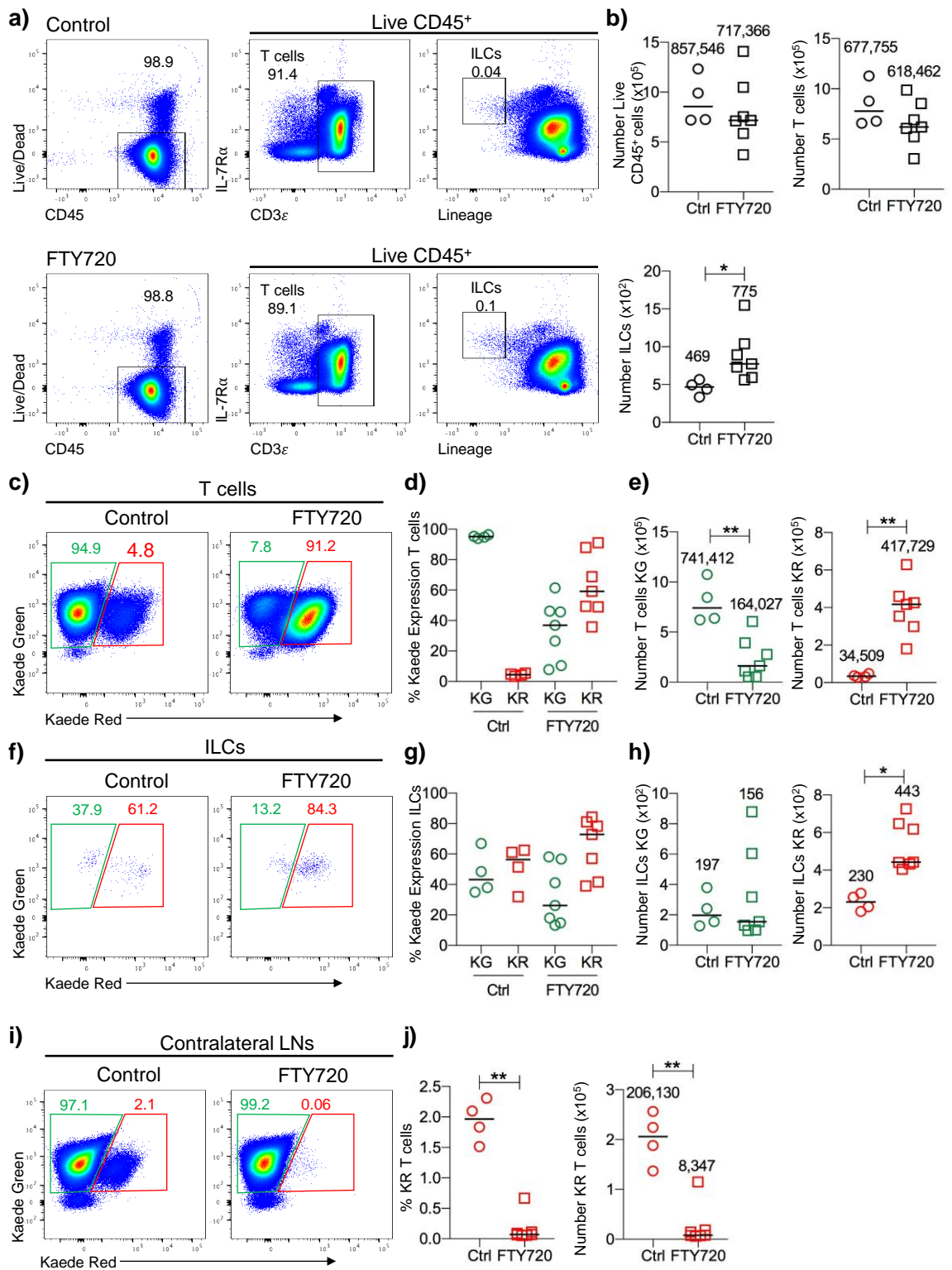


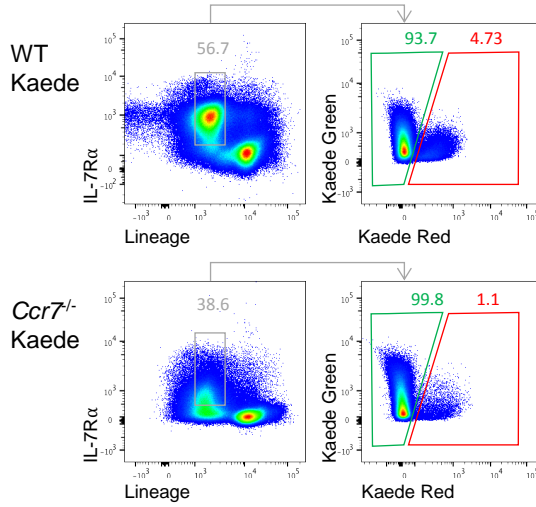
Figure 5.9. ILCs recirculate into contralateral LNs

A pool of contralateral LNs from WT Kaede mice were compared to *Ccr7*^{-/-} Kaede mice. Violet light photoconversion of the bLN and cell isolation of contralateral LNs were conducted as stated in methods. All data shown are 72 hours post photoconversion.

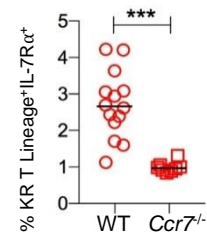
Each data point represents 1 bLN or 1 pool of contralateral LNs (mLN, iLN, auLN, axLN and cLN) from one mouse. Data pooled from a minimum of 2 experiments. Values on flow cytometry plots represent percentages, bars on scatter plots represents the median, which is also shown numerically. Statistical significance was tested using an unpaired, non-parametric, Mann-Whitney two tailed T test: * $p \leq 0.05$, ** $p \leq 0.01$, *** $p \leq 0.001$. When gating on ILCs lineage markers include; B220, CD11c, CD11b, CD3, CD5, CD19, Ter119, Gr1, F4/80, FcεRI and F4/80.

- a) Representative flow cytometry plots of T cells (Live CD45⁺ Lineage⁺ IL-7Rα⁺) (left) and their expression of Kaede Green and Kaede Red (right) in B220, CD3 and CD5 enriched fraction of contralateral LNs of WT Kaede (top) and *Ccr7*^{-/-} Kaede (bottom) mice.
- b) Percentage of Kaede Red T cells in contralateral LNs of WT Kaede (n=14) and *Ccr7*^{-/-} Kaede (n=8) mice.
- c) Representative flow cytometry plots of ILCs (Live CD45⁺ Lineage⁻ IL-7Rα⁺) (left) and their expression of Kaede Green and Kaede Red (right) in B220, CD3 and CD5 depleted fraction of contralateral LNs of WT Kaede (top) and *Ccr7*^{-/-} Kaede (bottom) mice.
- d) Percentage of Kaede Red ILCs in contralateral LNs of WT Kaede (n=14) and *Ccr7*^{-/-} Kaede (n=8) mice.

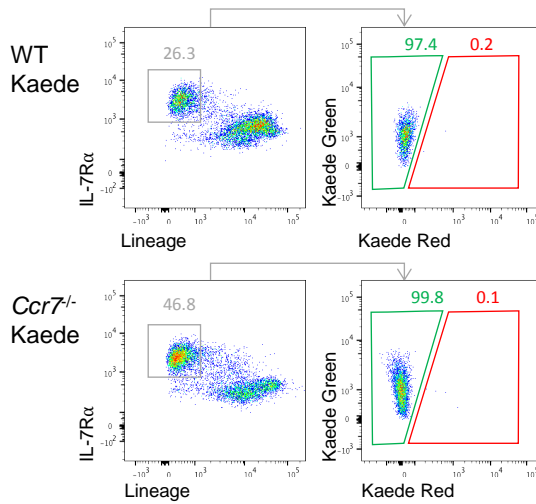
a) Contralateral LNs
B220, CD3, CD5 Enriched cell fraction



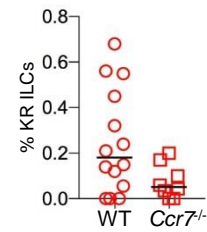
b)



c) Contralateral LNs
B220, CD3, CD5 Depleted cell fraction



d)



challenges of trying to track very small populations *in vivo* and potentially ILC may leave LNs and go to other locations that were not assessed. These data do suggest that at least some ILCs leave the peripheral LNs and then recirculate back through these tissues.

In addition to the role of CCR7 and S1P, the molecules CD62L and CD69 play critical roles in the movement of lymphocytes into and out of LNs (312, 315, 332, 334). CD62L is paramount in the mechanistic entry of lymphocytes into the LN from the blood, enabling cells to 'tether' and 'roll' along the HEVs before transmigrating into the LN parenchyma where it is downregulated immediately (49, 312, 315). CD69, on the other hand, is involved in the retention of activated lymphocytes in the LN via downregulating S1PR1 (332, 335). To further investigate the mechanisms controlling ILC migration into and out of LNs, CD62L and CD69 expression was assessed. Migratory Kaede Green ILCs express higher levels of CD62L compared to resident Kaede Red which is consistent with these cells migrating in from the blood (Figure 5.10a-b). In comparison, CD69 levels are increased on Kaede Red resident ILCs compared to Kaede Green (Figure 5.10c-d). This differential expression of CD69 is consistent with the cells staying within the LN and not egressing. These data further support that Kaede Green ILCs are migratory and Kaede Red ILCs are a resident population.

5.2.5 ILC1s are the most migratory subset of ILCs within the bLN

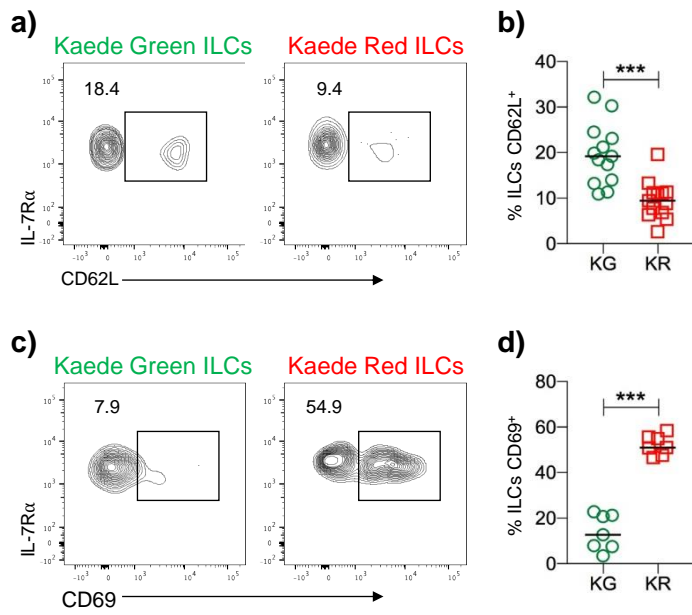
In some situations, there is evidence that ILC subsets show differing abilities to migrate into or out of LNs. iILC2s are the dominant migratory population under IL-25 administration and *Nippostrongylus brasiliensis* infections, migrating through the lymph and blood into the lung, spleen, liver and mLN (254). Mackley et al shows the migration of ILC3s from the gut to the

Figure 5.10. Kaede Green and Kaede Red ILCs express migratory and resident markers, respectively

WT Kaede mice underwent photoconversion of the bLN as described in methods. All Kaede data was analysed 72 hours post photoconversion. Isolation of cells from the bLN were conducted as in shown in methods.

Each data point represents 1 bLN from one mouse. Data pooled from a minimum of 2 experiments. Values on flow cytometry plots represent percentages, bars on scatter plots represents the median. Statistical significance was tested using an unpaired, non-parametric, Mann-Whitney two tailed T test: * $p \leq 0.05$, ** $p \leq 0.01$, *** $p \leq 0.001$. When gating on ILCs lineage markers include; B220, CD11c, CD11b, CD3, CD5, CD19, Ter119, Gr1, F4/80, Fc ϵ RI and F4/80.

- a) Representative flow cytometry plots of Kaede Green (left) and Kaede Red (right) ILCs (Live CD45⁺ IL-7R α ⁺ Lineage⁻) expression of CD62L in the bLN.
- b) Percentage of Kaede Green and Kaede Red ILCs expressing CD62L (n=13).
- c) Representative flow cytometry plots of Kaede Green (left) and Kaede Red (right) ILCs expression of CD69 in the bLN.
- d) Percentage of Kaede Green and Kaede Red ILCs expressing CD69 (n=7).



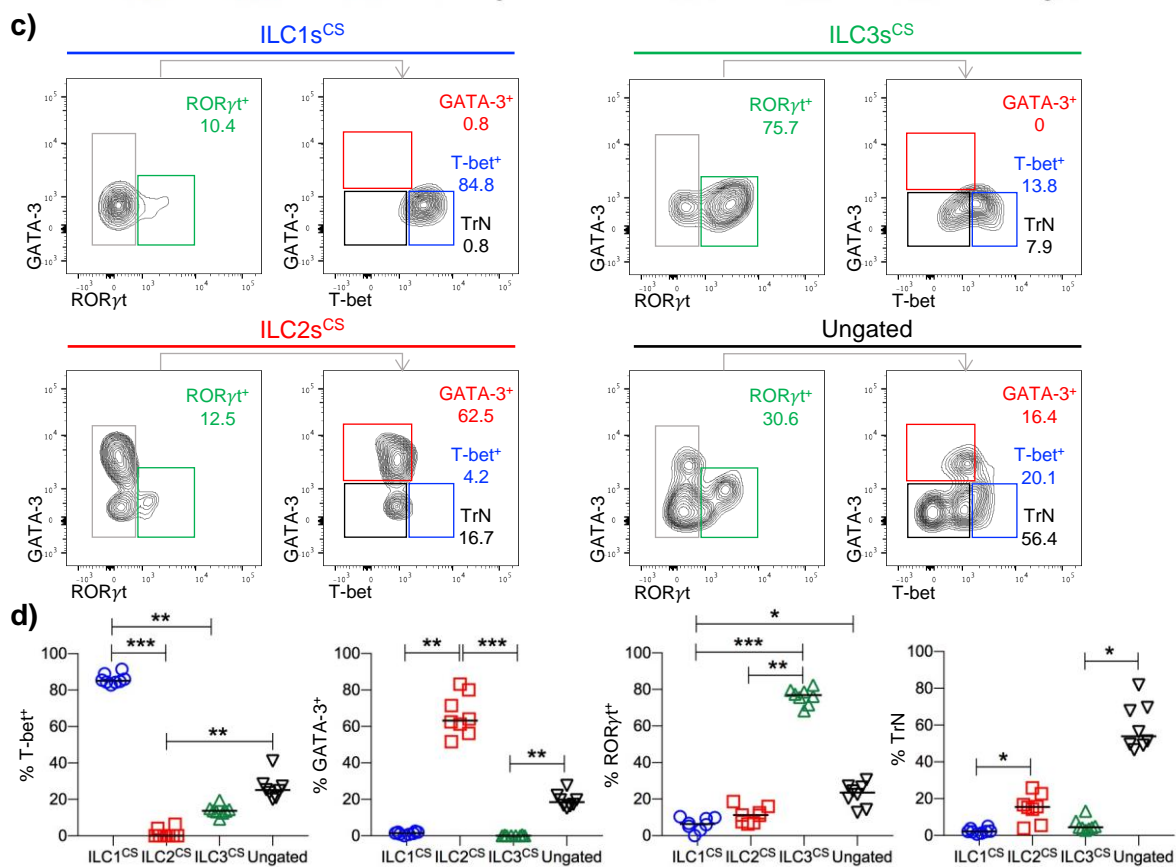
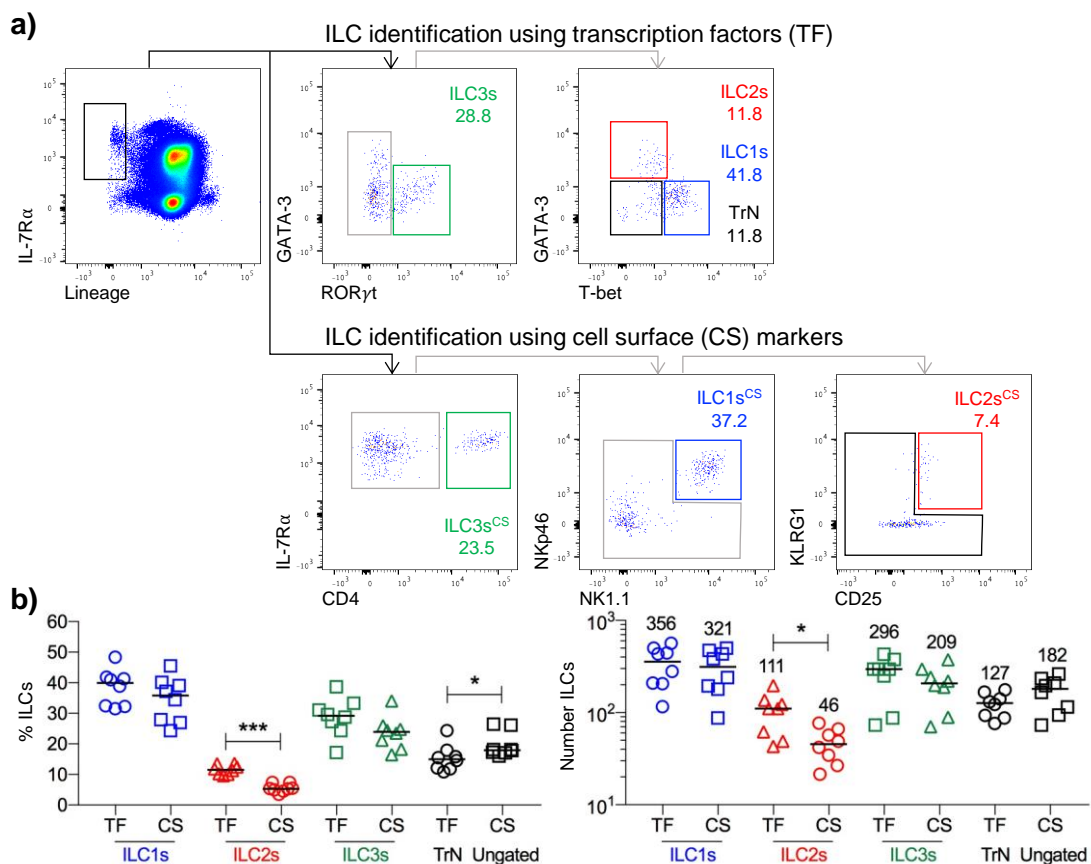
mLN and Kim et al., have shown ILC1s and ILC3s migrating from the mLN to the gut and ILC2s from the BM to the gut, supporting that ILC subsets have different migratory kinetics (243, 252). It is therefore important to determine whether these data within this study are explained by the partial migration of all subsets, or whether particular subsets in the LN are more migratory vs resident. Due to the Kaede protein being located within the cytoplasm, intracellular staining through cell permeabilisation, via the Foxp3 BD kit or BD kit, was not efficient at labelling for TFs whilst maintaining optimal Kaede protein expression. This made it difficult to accurately identify ILC subsets through the use of TFs in Kaede mice. Consequently, a staining panel including TFs, alongside an array of ILC specific cell surface (CS) markers was used to determine a method to identify ILC subgroups solely on the use of CS markers. CS markers identified a population CD45⁺ Lineage⁻ IL-7R α ⁺ ILCs that were subgrouped into ILC1s^{CS} (CD4⁻ (NK1.1 NKp46)⁺), ILC2s^{CS} (CD4⁻ (NK1.1 NKp46)⁻ (KLRG1 CD25)⁺), ILC3s^{CS} (CD4⁺) and ungated cells (CD4⁻ (NK1.1 NKp46)⁻ (KLRG1 CD25)⁻) (Figure 5.11a). Upon comparing the percentage and number of ILC subsets identified by either TFs or CS markers, a decrease in ILC2s identified via the CS marker method was observed (Figure 5.11b). This suggests that although using CS markers enables the identification of ILC subsets, it is not as efficient as TFs, with some ILCs remaining unidentified. To further determine that CS identified ILCs were gated into the correct subgroup, their expression of T-bet, GATA-3 and ROR γ t was assessed. The majority of ILC1s^{CS} (>80%), ILC2s^{CS} (>60%), ILC3s^{CS} (>70%) and ungated cells (>40%), express T-bet, GATA-3, ROR γ t, and no TFs, respectively (Figure 5.11c-d). However, this gating mechanism has not managed to identify all of the ILC subsets, with the ungated population being comprised of ~20% of T-bet⁺ ILC1s, GATA-3⁺ ILC2s, and ROR γ t⁺ ILC3s. This suggests that the CS marker gating mechanism is able to identify ILC1s, ILC2s and ILC3s, however, doesn't

Figure 5.11. Identification of ILC subsets in the bLN using cell surface markers

bLN from WT mice were isolated and ILCs identified using TF or cell surface (CS) markers (n=8), within the same staining panel. ILCs identified by CS markers are marked with ^{CS}.

Each data point represents 1 bLN from one mouse. Data pooled from a minimum of 2 experiments. Values on flow cytometry plots represent percentages, bars on scatter plots represents the median, which is also shown numerically. Paired samples were statistically tested using an unpaired, non-parametric, Mann-Whitney two tailed T test, when comparing more than two sets of data statistical significance was tested using Kruskal-Wallis one-way ANOVA with post hoc Dunn's test: *p≤0.05, **p≤0.01, ***p≤0.001. When gating on ILCs lineage markers include; B220, CD11c, CD11b, CD3, CD5, CD19, Ter119, Gr1, F4/80, FcεRI and F4/80.

- a) Representative flow cytometry plots showing gating mechanism to identify (Live CD45⁺ Lineage⁻ IL-7Rα⁺) ILC subsets using TFs (top) and CS proteins (bottom). TF gated ILC subsets; ILC1s (RORγt⁻ GATA-3⁻ T-bet⁺), ILC2s (RORγt⁻ GATA-3⁺ T-bet⁻), ILC3s (GATA-3⁻ RORγt⁺) and TrN cells (RORγt⁻ GATA-3⁻ T-bet⁻). ILCs identified with CS proteins; ILC1s* (CD4⁻ (NK1.1 NKp46)⁺), ILC2s* (CD4⁻ (NK1.1 NKp46)⁻ (KLRG1 CD25)⁺), ILC3s* (CD4⁺) and ungated (CD4⁻ (NK1.1 NKp46)⁻ (KLRG1 CD25)⁻).
- b) Percentage (left) and number (right) of ILC subsets identified by TF compared to CS proteins.
- c) Representative flow cytometry plots showing TF expression of RORγt, GATA-3 and T-bet by ILCs identified by CS markers, ILC1s^{CS} (top left), ILC2s^{CS} (bottom left), ILC3s^{CS} (top right) and ungated (bottom right).
- d) Percentage of ILC1s^{CS}, ILC2s^{CS}, ILC3s^{CS} and ungated cells that express T-bet (left), GATA-3 (middle left), RORγt (middle right) or no TFs (right).



include all of the individual subgroups within the bLN, with some ILC1s, ILC2s and ILC3s lying within the ungated population. To determine whether ILC subsets in the LN show equal abilities to enter and leave the LN, the subsets were identified with the surface markers described above and Kaede Green versus Kaede Red expression assessed 72 hours post photoconversion. (Figure 5.12a-d). Upon comparing the percentage of Kaede Green cells within each subset, ILC1s^{CS} had the highest proportion of Kaede Green expressing cells and were the only subset to have a greater proportion of Kaede Green cells than Kaede Red (Figure 5.12c-e). This would suggest that ILC1s are more migratory than ILC2s and ILC3s which were more tissue-resident over the 72 hour time frame. It was a concern that the ILC1 population was being contaminated by cNK cells, which are known to efficiently enter and exit LNs (116, 251, 326, 345). To determine that they were not included in this gating strategy, cNK cells were identified as T-bet⁺ GATA-3⁻ RORγt⁻ EOMES⁺ within the lineage⁻ IL-7Rα⁺ ILC population (Figure 5.12f-g). Due to the lineage dump channel containing CD49b, a phenotypic marker of cNK cells, cNK cells were a very small fraction of the ILC population, excluding them from this analysis, concluding that the identified ILC1s were comprised of helper ILC1s.

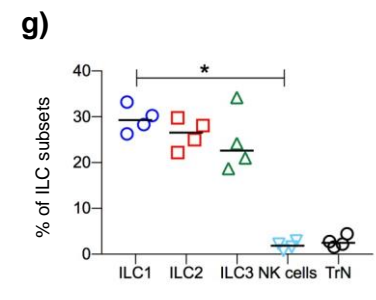
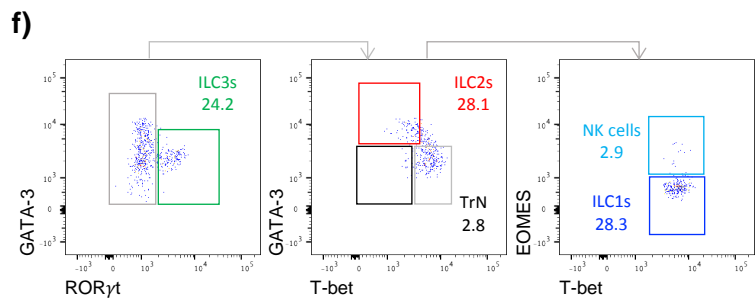
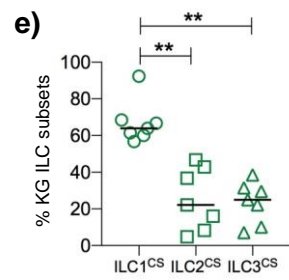
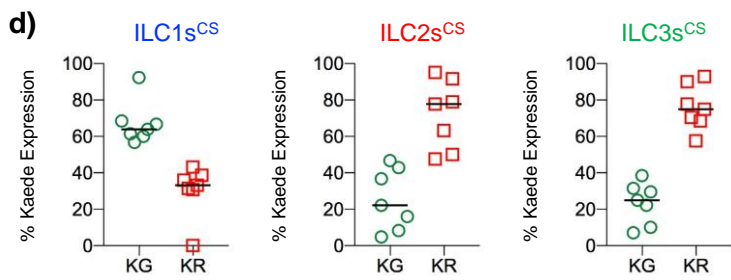
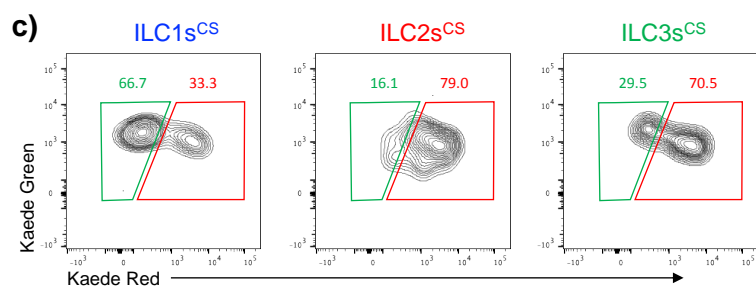
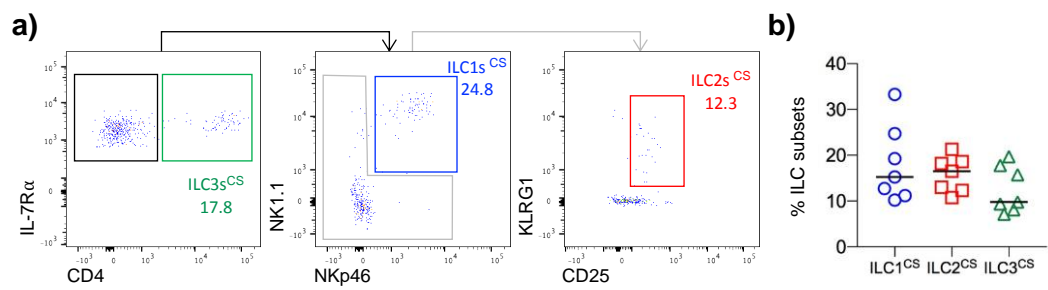
cNK cells are able to recirculate through the blood and SLT, being able to be primed by DCs in LNs (115-117, 346). To compare cNK cell recirculation to ILC1 recirculation, cNK cells Kaede expression was analysed within the bLN 72 hours post photoconversion. Within the lab it was confirmed that the cNK cells (NK1.1⁺ CD3ε⁻ TCRβ⁻ CD49b⁺ IL-7Rα⁺) gated within the bLN are T-bet⁺ EOMES⁺ (Withers lab unpublished observations). The majority of cNK cells expressed Kaede Green ~90%, consistent with their ability to rapidly migrate through the LN (Figure 5.13a-b)(116, 249). Furthermore, analysing the contralateral LNs for the expression of Kaede

Figure 5.12. The majority of ILC migration at 72 hours are ILC1s

WT Kaede mice underwent violet light photoconversion as described in methods. All Kaede data shown are 72 hours post photoconversion. Isolation of cells from the bLN were conducted as in shown in methods.

Each data point represents 1 bLN or from one mouse. Data pooled from a minimum of 2 experiments. Values on flow cytometry plots represent percentages, bars on scatter plots represents the median. Statistical significance was tested using Kruskal-Wallis one-way ANOVA with post hoc Dunn's test: * $p \leq 0.05$, ** $p \leq 0.01$, *** $p \leq 0.001$. When gating on ILCs in WT Kaede mice lineage markers include; B220, CD11c, CD11b, CD3, CD5, CD19, Ter119, Gr1, F4/80, Fc ϵ RI and F4/80. In non Kaede mice, the additional lineage marker CD123 was used and ILCs were gated on negatively for iCD3 ϵ .

- a) Representative flow cytometry plots of ILC subset identification using cell surface (CS) markers. ILC1s^{CS} (Live CD45⁺ Lineage⁻ IL-7R α ⁺ CD4⁻ (NK1.1 NKp46)⁺), ILC2s^{CS} (Live CD45⁺ Lineage⁻ IL-7R α ⁺ CD4⁻ (NK1.1 NKp46)⁻ (KLRG1 CD25)⁺) and ILC3s^{CS} (Live CD45⁺ Lineage⁻ IL-7R α ⁺ CD4⁺).
- b) Percentage of ILC subsets identified using CS markers (n=7).
- c) Representative flow cytometry plots showing Kaede Green and Kaede Red expression of ILC1s^{CS}, ILC2s^{CS} and ILC3s^{CS}.
- d) Percentage of Kaede Green and Kaede Red expressing ILC1s^{CS}, ILC2s^{CS} and ILC3s^{CS} (n=7).
- e) Percentage of Kaede Green ILC1s^{CS}, ILC2s^{CS} and ILC3s^{CS} within the bLN 72 hours post photoconversion (n=7).
- f) Representative flow cytometry plots in WT mice showing ILC1s (Live CD45⁺ Lineage⁻ IL-7R α ⁺ ROR γ t⁻ GATA-3⁻ T-bet⁺ EOMES⁻), ILC2s (Live CD45⁺ Lineage⁻ IL-7R α ⁺ ROR γ t⁻ GATA-3⁺ T-bet⁻), ILC3s (Live CD45⁺ Lineage⁻ IL-7R α ⁺ ROR γ t⁺), NK cells (Live CD45⁺ Lineage⁻ IL-7R α ⁺ ROR γ t⁻ GATA-3⁻ T-bet⁺ EOMES⁺) and TrN cells (Live CD45⁺ Lineage⁻ IL-7R α ⁺ ROR γ t⁻ GATA-3⁻ T-bet⁻) in the bLN.
- g) Percentage of ILC1s, ILC2s, ILC3s, NK cells and TrN cells in the bLN (n=4).



Red cNK cells supported their ability to recirculate through draining LNs (Figure 5.13c-d). Due to ILC1s being the main migratory population out of the three ILC subgroups, their ability to recirculate was also assessed and a small population of Kaede Red ILC1s was identified (Figure 5.13c-d). Together, this suggests that ILC1s are similar to their closely related cNK cells and able to traffic into LNs from the blood via HEV and recirculate through LNs after their egress.

This chapter has shown that ILCs traffic into and out of a peripheral LN and although in small numbers, recirculate to contralateral LNs within 72 hours. Furthermore, the data indicate that it is really the ILC1 subset that likely accounts for most of the migration observed when the total ILC population is assessed. Whilst ILC in human blood have been extensively characterised and studied, the ILC composition of murine blood is poorly understood, although Gasteiger et al described ILC1 being present in the circulation (249, 267). Therefore, to investigate whether ILC migrating into the LN may traffic direct from the circulation, ILC populations in murine blood were assessed (Figure 5.14a-b). The percentage of ILCs was assessed due to an inability to harvest the exact same volume of blood per mouse. With hindsight analysing a set volume of blood from each mouse would enable cells to be enumerated and compared across mice, however, due to ILCs being a rare population as much blood as possible was collected. Consistent with previous reports ILC1s were the most abundant subgroup of ILCs within the blood, alongside a few ILC2s (249, 347). Combining the blood of 3 mice, and enriching for CD45⁺ cells via MACS-enrichment, enabled a high yield of cells to be obtained and therefore ILC1s were identified via T-bet expression as the dominant ILC population within the blood (Figure 5.14c-d). For efficient egress out of the blood and into the LN dual expression of CD62L and CCR7 is required, therefore T-bet⁺ ILC1s were analysed

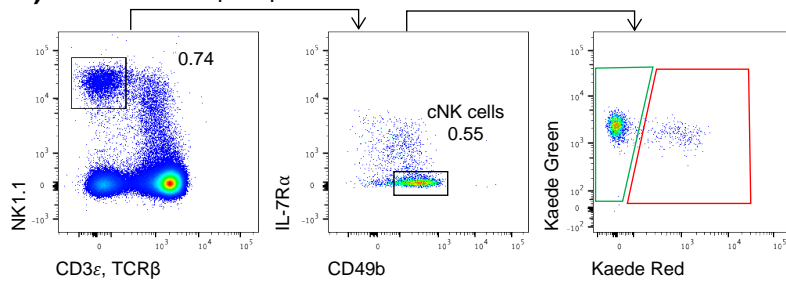
Figure 5.13. cNK cells are able to recirculate through draining LNs

Kaede mice underwent violet light photoconversion as described in methods. The photoconverted bLN and a pool of contralateral LNs were analysed 72 hours post photoconversion. cNK cells and ILC1s were identified within Kaede mice. Cell isolation of the bLN and contralateral LNs were conducted as stated in methods.

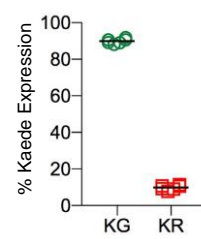
Each data point represents 1 bLN or 1 pool of contralateral LNs (mLN, iLN, auLN, axLN and cLN) from one mouse. Data pooled from a minimum of 2 experiments. Values on flow cytometry plots represent percentages, bars on scatter plots represents the median, which is also shown numerically. Statistical significance was tested using an unpaired, non-parametric, Mann-Whitney two tailed T test: * $p \leq 0.05$, ** $p \leq 0.01$, *** $p \leq 0.001$. When gating on ILCs lineage markers include; B220, CD11c, CD11b, CD3, CD5, CD19, Ter119, Gr1, F4/80, Fc ϵ RI and F4/80.

- a) Representative flow cytometry plots of cNK cells (Live CD45⁺ CD3⁻ TCR β ⁻ NK1.1⁺ IL-7R α ⁻ CD49b⁺) and their expression of Kaede Green and Kaede Red in the bLN.
- b) Percentage of Kaede Green and Kaede Red cNK cells (n=6).
- c) Representative flow cytometry plots of cNK cells and ILC1s (Live CD45⁺ CD3⁻ TCR β ⁻ NK1.1⁺ IL-7R α ⁺ CD49b⁻) Kaede Green and Kaede Red expression in contralateral LNs of Kaede mice.
- d) Number of Kaede Red cNK cells and ILC1s in contralateral LNs of Kaede mice (n=6).

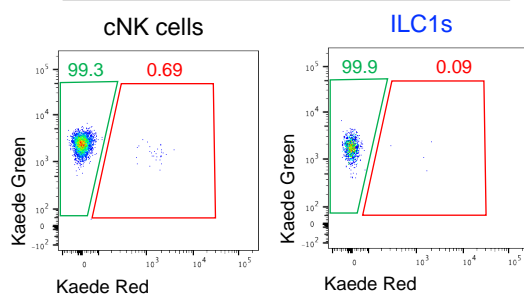
a) bLNs 72 hours post photoconversion



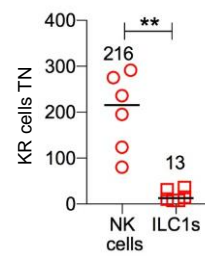
b) cNK cells



c) Contralateral LNs



d)



for the expression of these two markers (49, 255, 315). It was observed that ILC1s contain a population which are CCR7⁺ CD62L⁺, suggesting that they possess the ability to enter LNs, alongside a population of CCR7⁺ CD62L⁻ cells, suggesting that some ILC1s possess the ability to enter the LN and others do not (Figure 5.14 e-g).

Within this chapter it was observed that ILCs were not solely comprised of a tissue-resident population, with a proportion of ILCs being able to migrate into peripheral LNs in a CCR7 dependent manner. Furthermore, egress of ILCs from LNs in an S1PR dependent manner and ability to circulate through draining LNs was observed. ILC1s were discovered to be the dominant ILC migratory population, sharing similar abilities with cNK cells, located within the blood expressing surface proteins consistent with the requirement to enter LNs.

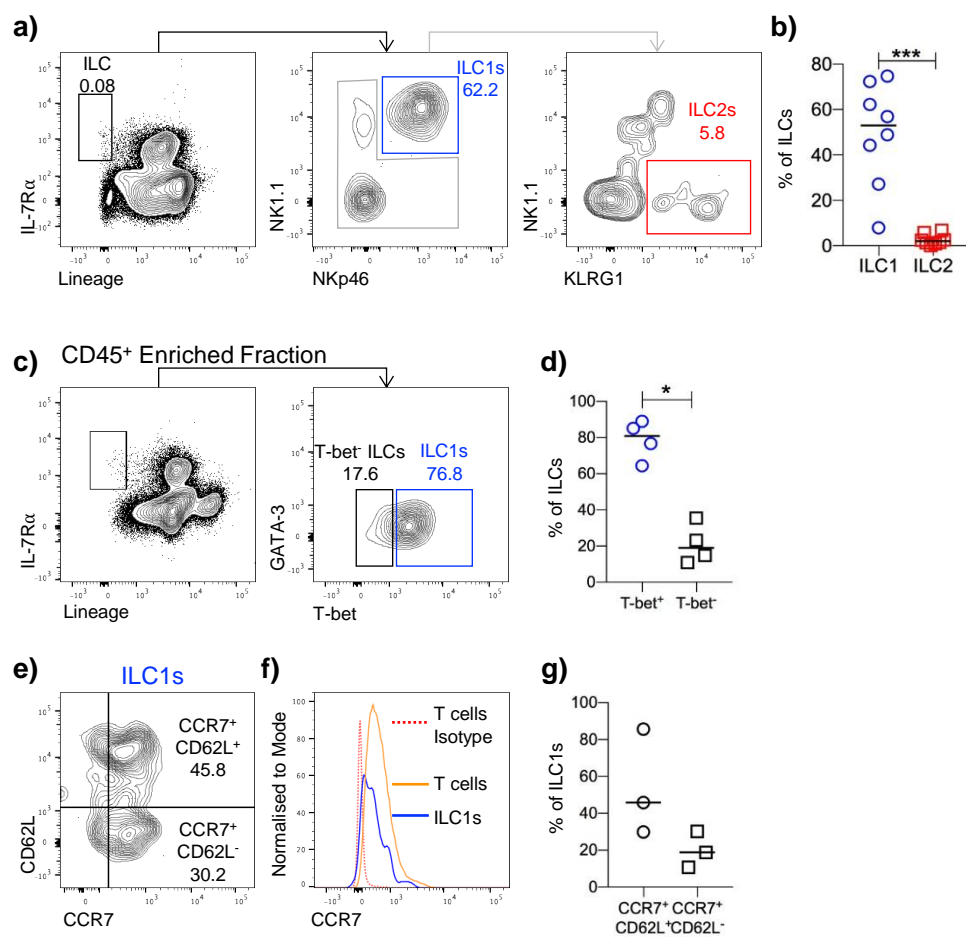
5.3 SUMMARY

With new publications within the literature, challenging the original consensus that ILCs were strictly a tissue-resident population, this chapter aimed to determine whether there is evidence that ILCs are able to move in and out of peripheral LNs. Complete photoconversion of all the cells within the bLN from Kaede Green to Kaede Red fluorescence has enabled the *in vivo* visualisation of cell migration both into and out of the bLN. This model led to the identification of a tissue-resident and CCR7 dependent migratory ILC population. Furthermore, the data provided clear evidence that ILCs normally egress from the LN in an S1P dependent manner and that they are able to recirculate through peripheral LNs. Within the blood ILC1s express a phenotype which suggests they are able to enter LNs from the blood, therefore, it was concluded that migratory ILCs, which were mainly comprised of ILC1s, are able to recirculate through LNs in a similar manner to cNK cells. The findings within this

Figure 5.14. CCR7⁺ CD62L⁺ ILC1s are located within the blood

Each data point represents blood collected from (a-b) one WT mouse (c-g) three WT mice. Data pooled from a minimum of 3 experiments. Values on flow cytometry plots represent percentages. Statistical significance was tested using an unpaired, non-parametric, Mann-Whitney two tailed T test: * $p \leq 0.05$, ** $p \leq 0.01$, *** $p \leq 0.001$. When gating on ILCs lineage markers include; B220, CD11c, CD11b, CD3, CD5, CD19, Ter119, CD123, Gr1, F4/80, Fc ϵ RI and F4/80.

- a) Representative flow cytometry plots showing ILC1s (Live CD45⁺ Lineage⁻ IL-7R α ⁺ (NK1.1 NKp46)⁺) and ILC2s (Live CD45⁺ Lineage⁻ IL-7R α ⁺ (NK1.1 NKp46)⁻ KLRG1⁺) and ILC2s within the blood.
- b) Percentage of ILC subsets in the blood (n=8).
- c) Representative flow cytometry plots of CD45 enriched blood fractions showing ILC1s (Live CD45⁺ Lineage⁻ IL-7R α ⁺ T-bet⁺) and T-bet⁻ ILCs (Live CD45⁺ Lineage⁻ IL-7R α ⁺ T-bet⁻).
- d) Percentage of T-bet expression by ILCs within the blood (n=4).
- e) Representative flow cytometry plots showing expression of CCR7 and CD62L on T-bet⁺ ILC1s.
- f) Representative histogram showing expression of CCR7, normalised to mode, of T cells isotype control (pink dashed line), T cells (orange line) and ILC1s (blue line) (n=3).
- g) Percentage of ILC1s that are CCR7⁺ CD62L⁺ or CCR7⁺ CD62L⁻ (n=3).



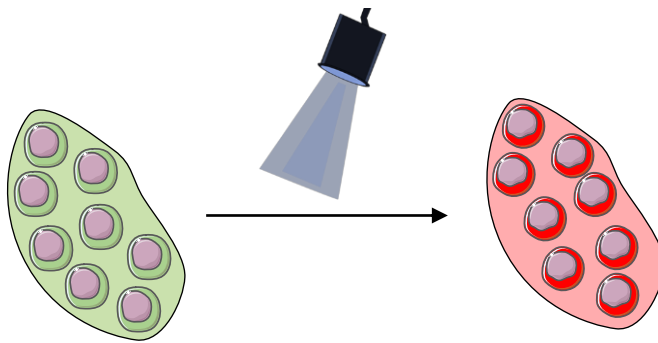
Chapter, using photoconvertible Kaede mice to further understand ILC migration within the peripheral LN is summarised in Figure 5.15. Furthermore, a suggested model of specific ILC subset migration is proposed in Figure 5.16.

At the heart of this chapter is a photoconversion approach which has utilised a model of temporal labelling of all cells within a LN to interrogate migration into and out of the tissue. This model enables the visualisation of cell migration *in vivo* through photoconversion via violet light exposure, which does not affect the function of the cell (53). Within these studies the retention of Kaede Red expression within CD45⁻ stromal cells and the large influx of Kaede Green CD45⁺ T cells within the bLN provides strong evidence that this model can be used to distinguish between cells that are migratory and others that are tissue-resident. Upon the deletion of a key molecule integral in the migration of lymphocytes into the LNs, such as CCR7 in the migration of T cells, the differences observed in Kaede Green ‘migratory’ cells entering the bLN is entirely consistent with the differences being migratory related. Similarly, blocking the S1P dependent egress of lymphocytes, via FTY720 administration, caused the accumulation of Kaede Red labelled cells providing strong evidence that under normal conditions these cells exit the tissue. Combined this evidence clearly argues that the temporal labelling of the LN is a robust means of assessing movement into and out of the LN and this approach demonstrates the ingress and egress of ILC from peripheral LNs. The main caveat of the Kaede model is the ability for proliferating Kaede Red cells to dilute out Kaede Red expression and replace it within Kaede Green. To combat this, analysis of migration was assessed a maximum of 72 hours post photoconversion as previously shown by Tomura et al., and Marriott et al., as discussed previously (53, 92). Furthermore, work within the lab has revealed a low Ki-67 expression by ILCs in the LN under steady state (Withers lab unpublished

Figure 5.15. Summary Diagram of ILC migration within bLN Kaede model

All of the cells within the bLN can be photoconverted from Kaede Green to Kaede Red upon exposure to violet light. 72 hours post photoconversion a migratory population of Kaede Green ILCs was observed within the bLN, suggesting to have entered from the lymphatics or through HEVs, with this migration being dependent on CCR7. ILCs are present within the blood with dual expression of CD62L and CCR7, which are required for the migration of cells from the blood into the LN. Kaede Red resident ILCs are shown to express high levels of CD69, consistent with their retention in the LN. ILCs were shown to egress from the bLN in an S1P dependent manner and recirculate through the blood into contralateral LNs.

bLN Photoconversion



ILC Migration within Peripheral LNs

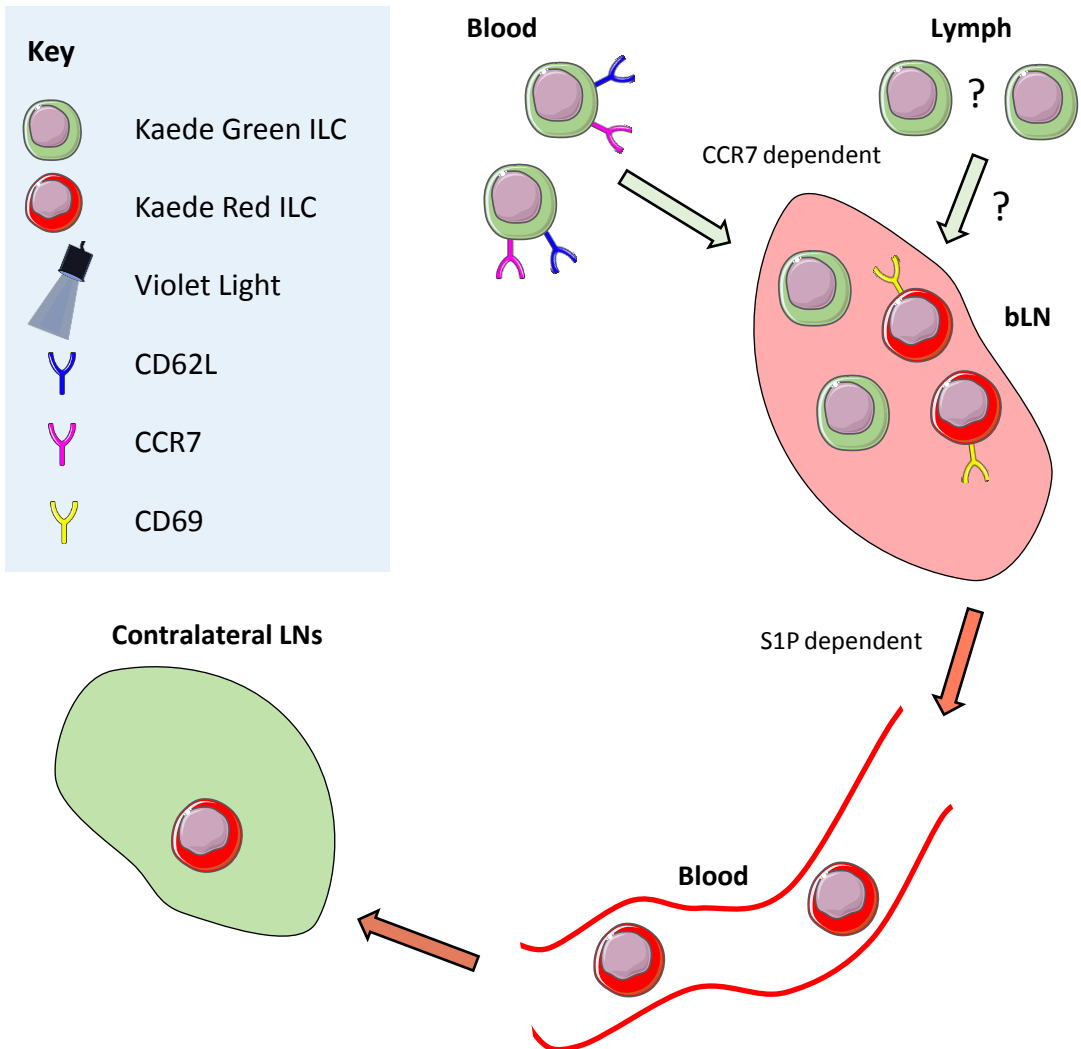



Figure 5.16. Summary Diagram of proposed model of ILC subset migration

ILC1s and cNK cells are able to travel through the blood, entering and exiting peripheral LNs in a manner dependent on CD62L and CCR7 expression for entry and S1PR expression for egress. ILC2s and ILC3s are a more resident population, remaining within peripheral LNs under steady state conditions.


This diagram simplifies the migratory properties of ILC subsets, with the presence of a smaller population of resident ILC1s and migratory ILC2s and ILC3s not being represented within this diagram.

Proposed ILC Migration


Key




ILC1



ILC2



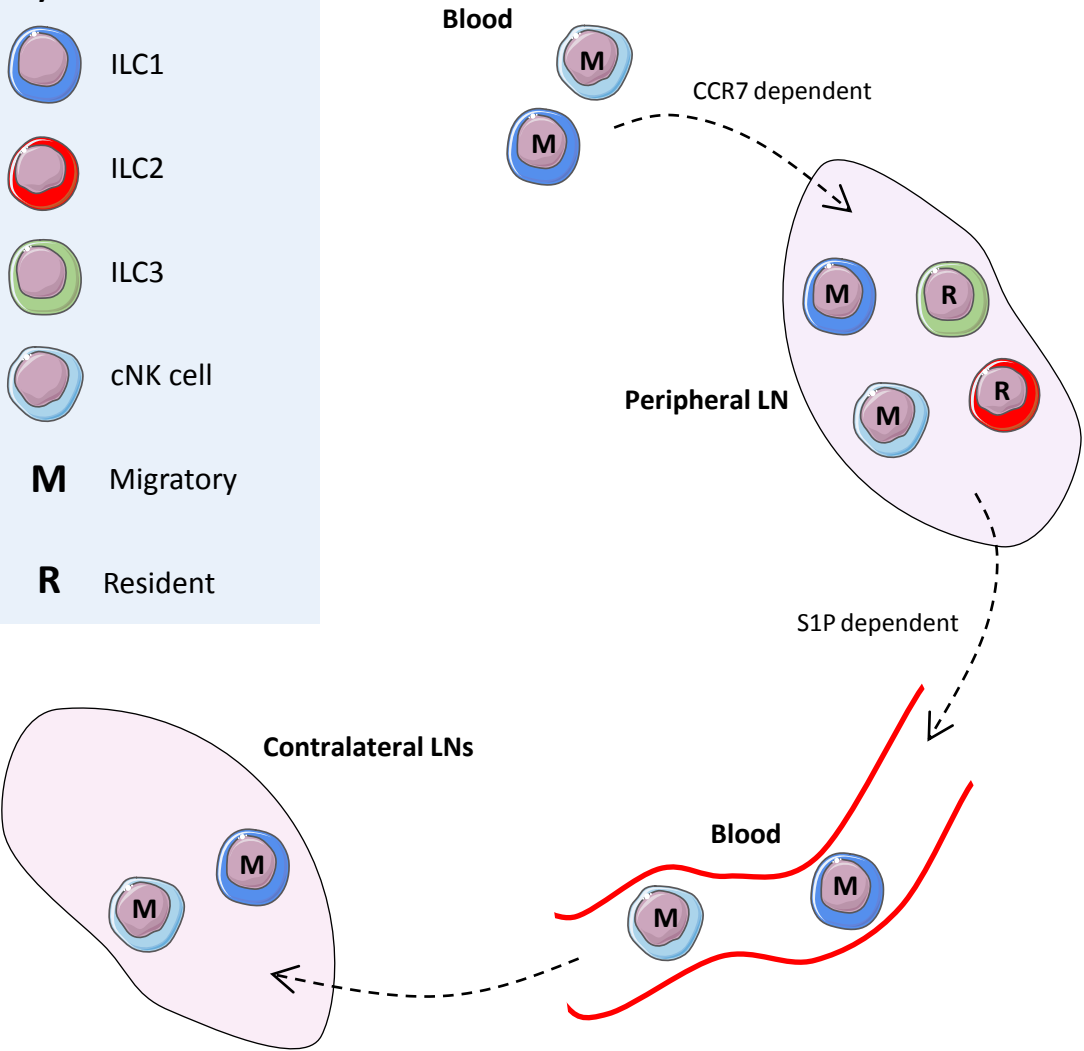
ILC3



cNK cell

M Migratory

R Resident



observations).

Within this model Kaede Red cells have been termed tissue-resident cells, however, these cells may not be permanently resident. Migration was only observed over a 72 hour period, therefore, Kaede Red expression is suggestive of a resident population, but does not take into account the potential for Kaede Red cells to leave the LN after the 72 hour time frame, identifying migratory cells that have much slower kinetics than assessed here. Longer time periods would need to be assessed to determine whether Kaede Red ILCs are a long-lasting resident population. Although the Kaede protein has a long half-life, observing migration beyond 72 hours is not ideal. Dendra mice are a new photoconvertible mouse model used to track the migration of cells (336, 348-350). Similar to Kaede mice the photoactivatable GFP Dendra2 is converted into a red fluorescence upon exposure to violet light (348, 349, 351). However, the Dendra2 protein is fused to histones, which are important in the structure and organisation of nucleosomes (348, 349). This increases protein stability allowing the tracking of converted cells over a longer period of time, with reports identifying populations remaining resident for up to 4 weeks (348-350). These mice would therefore be useful to test whether 'resident' ILCs within the bLN remain over several weeks. From these results, a further hypothesis could be proposed that tissue-resident ILCs are permanently resident within the LN.

These studies alongside showing the ability of ILCs to enter peripheral LNs have also provided evidence that ILCs are able to exit in an S1P dependent manner. Clear evidence supporting this conclusion was shown via blocking S1P receptors resulting in the accumulation of ILCs within the bLN. S1PR1 was detected on a proportion of cells within the bLN, suggesting its

involvement in ILC egress, however, other reports have also shown iILC2s within the lung and mLN, under certain conditions, have inducible expression of S1PR1 and S1PR4, alongside mLN ILC2s expressing S1PR5 (254). Further analysis of differential receptor expression across the ILC subsets would be required to further explore the mechanism of ILC egress. FTY720 selectively blocks S1PR1, S1PR3 and S1PR4, suggesting that if ILC egress also depends on S1PR5, this would not be inhibited within these experiments using FTY720 (254, 261, 345). It is therefore reasonable to assume that there may be tissues from which ILCs egress in an S1PR5 dependent manner, enabling them to reach the blood or lymph and still enter the LN. This may potentially explain the Kaede Green ILC population observed migrating into the bLN of mice administered with FTY720. Supporting this, Huang et al., reports that under FTY720 administration iILC2 migration was blocked from the intestine into the lung, where iILC2s only express S1PR1 and S1PR4, but only partially blocked migration to the mLN, where they additionally express S1PR5 (254). Furthermore, cNK cells egress from the LN in an S1PR5 dependent manner which is also unable to be blocked via FTY720 administration (344). This suggests that the ILCs observed migrating into the bLN under FTY720 administration might migrate within an S1PR5 dependent mechanism and that additional blocking with a substance specific to S1PR5 may completely block ILC recirculation and therefore Kaede Green ILCs entering the bLN. Altogether this would suggest that ILC egress is partly dependent on S1PR1 or S1PR4, due to FTY720 causing accumulation of ILCs within the LN and bLN ILCs expressing S1PR1, but may also be dependent on S1PR5, as suggested by other publications exploring ILC and cNK cell migration.

ILC egress was accompanied by their recirculation into other LNs, evident by the detection of Kaede Red ILCs being identified within contralateral LNs. This identified population was

modest but significant and surprisingly, comparable to *Ccr7*^{-/-} Kaede mice. This may suggest a redundancy in CCR7 for ILCs to recirculate into contralateral LNs, unlike T cells, contradicting data showing ILCs dependency on CCR7 to enter LNs. On the other hand, it is most likely due to a reduced ability in identifying a rare lymphocyte population and sample size, suggesting further work is needed to confidently conclude whether ILCs recirculate in a CCR7 independent manner. ILCs are sparse within SLTs, comprising of roughly 1,000 cells within the bLN, therefore locating small numbers of Kaede Red ILCs in the contralateral LNs is unsurprising. The additional conversion of the iLN and axLN alongside the bLN would increase the number of converted ILCs, and therefore the number of Kaede Red ILCs able to be tracked within the contralateral LNs, increasing the chance of identifying a more substantial population of migratory ILCs. A further method to identify the location of where ILCs migrate to would be to assess the migration into ipsilateral LNs. The efferent lymphatic vessel of the bLN drains directly to the axLN, if ILCs are able to egress through the efferent lymphatic vessel in a similar manner to T cells then they may be able to directly drain into the secondary LN without entering the blood (35, 331). Previously when Marriott et al., established photoconversion of the bLN it was a concern that the axLN occasionally underwent partial photoconversion (92). This prevented the ability to analyse Kaede Red ILCs within the axLN as it could not be determined whether they had migrated from the bLN or were converted upon initial violet light exposure. With a refined labelling protocol, it is possible that this caveat could be removed and the migration of ILCs from a primary to a secondary LN assessed.

The migration of ILCs into the bLN within the 72 hours was shown to be reduced within *Ccr7*^{-/-} Kaede mice, suggesting that similar to T cells, ILCs depend on CCR7 for their entry into the LN (316). However, these experiments do not specifically identify whether ILCs directly express

CCR7 and require CCR7:CCL21/CCL19 interactions or whether a separate cell type, which is required for ILC entry, is dependent on CCR7. Assessing the expression of CCR7 on ILCs within the bLN would help to determine whether ILCs directly or indirectly require CCR7 for their ingress into the peripheral LNs.

Initially within this investigation the migration of ILC as a total population was assessed. To better understand whether all ILCs were equally migratory or had distinct migratory properties ILC subgroups migration needed to be assessed. However, due to the need to preserve Kaede expression, using a fixation and permeabilisation staining method to enable detection of TFs was an issue. The solution was a compromise, using surface markers to clearly identify some, but not all ILC subsets with some ILC1s, ILC2s and ILC3s falling within the ungated population. For example, a subset of ILC1s and ILC3s are both CD4⁻ NKp46⁺ NK1.1⁻, meaning with this staining panel they are unable to be identified separately and therefore were included within the ungated cells. A more efficient staining panel was unable to be established, so the current panel was used to identify that ILC1s are the main subgroup of migratory ILCs. Within photoconvertible Dendra mice the Dendra2 protein is fused to histones and not present within the cytoplasm, suggesting that these cells may be able to undergo intracellular TF staining, therefore they may be useful in the accurate identification of ILC subsets through the use of T-bet, GATA-3 and RORγt (349).

ILC1s were identified as the dominant population of ILCs migrating into the bLN and the source of ILC1s was investigated. They were located within the blood to have dual expression of CD62L and CCR7, in which a simple explanation of this data is that ILC1s move via HEVs into LNs, in a similar manner to cNK cells (49, 116). This is supported by their ability to recirculate

into other peripheral LNs. Upon entry into LNs CD62L is promptly downregulated which may explain why CD62L expression is low on Kaede Green ILCs within the bLN (~20%) (315). A further similarity between the closely related ILC1s and cNK cells is their ability to migrate into contralateral LNs. Kaede Red ILC2s and ILC3s were not individually analysed within the pool of contralateral LNs and therefore their ability to recirculate was not assessed. It would be interesting to determine whether ILC1s were the only helper ILC subset able to recirculate through LNs, which could be determined using the CS panel described earlier, however, due to a small number of recirculatory ILCs being identified, this could be problematic.

These data identified within this chapter add to the understanding of the migratory properties of ILCs. The identification of a migratory ILC population entering the bLN is consistent with the identification of ILCs entering the mLN from the intestine (243, 252, 254). However, this investigation shows the ingress into peripheral LNs rather than the mLN. This migratory population was potentially not observed within the parabiotic mice used by Gasteiger et al., as they only assessed entry into the mLN and spleen lymphoid tissues and not the peripheral lymphoid tissues (249). Consistent with Gasteiger et al., and Huang et al., ILCs were identified within the blood, mainly ILC1s, with these data identifying the expression of CD62L and CCR7 on ILC1s essential for their entry into LNs (249, 254). ILC2s were not observed to be abundant within the blood as shown by Huang et al., however this was only observed after i.p. injection of IL-25 or infection with *Nippostrongylus brasiliensis* (254). It would therefore be interesting to observe the migratory properties of ILCs under different inflammation models. Furthermore, ILC1s which are closely related to cNK cells seem to have a similar migratory ability to previously published reports on cNK cell migration (116). Currently within the literature ILC migration is mainly assessed from non-lymphoid tissue into draining LNs and

with ILC migration not being assessed within parabiotic mice, it is therefore suggested that they can migrate within the lymphatic system. This raises the question of whether the ILCs entering the peripheral LNs are originating from non-lymphoid tissue and draining through the lymph into the LN.

Chapter 6. ASSESSING THE MECHANISMS OF ILC MIGRATION BETWEEN SKIN AND DRAINING PERIPHERAL LN

6.1 INTRODUCTION

Within Chapter 5 direct evidence was provided showing that ILCs, can recirculate through LNs. Thus, a clear pathway through which ILC1 migrate would appear to be from the blood into the LN. Another method of hematopoietic cell entry into the LN is via the afferent lymphatic vessel (49). Certain LNs exist within a sequence, with the primary LNs efferent lymphatics directly becoming the afferent lymphatics of the secondary, termed a chain of LNs (35). This chain allows the direct migration of cells from one LN to another, as discussed previously with T cells (35, 53). Hematopoietic cells are also able to enter the lymphatic system via lymphatic terminals in non-lymphoid tissue. This is the main route of DC entry, enabling the transport of antigen from tissue to draining LN, for example skin DCs to draining peripheral LNs (247). Activation and maturation of dermal DCs within skin leads to the downregulation of proteins associated within tissue residency such as E-cadherin and upregulation of chemokine receptors such as CCR7 allowing migration towards lymphatic terminals (352-354). CCR7 expression is paramount in the migration of DCs into the draining lymphatics with *Ccr7*^{-/-} DCs in WT hosts being able to migrate to the lymphatics terminals but unable to cross the endothelium into the lymph (353). Furthermore, CCL21, the ligand for CCR7, is located on LECs that are situated in the lymphatic terminals (353). Upregulation of S1PR1 expression on DCs is also suggested to be important in the efficient trafficking of DCs to draining LNs (355). Epidermal DCs, such as LC, are also able to exit the skin via lymphatic terminals after initial entry into the dermis in a CXCR4 dependent mechanism (356, 357). Within the lymphatics,

DCs initially use lamellipodia to actively migrate in the same directions as the lymphatic flow, before they freely drift towards the draining LN (353). A variety of models have previously been used to show that DCs are able to migrate under steady state conditions, from the skin to draining LNs, and that their migration increases under inflammatory conditions (53, 247, 352, 353).

Migration into the LN from non-lymphoid tissue is another route of entry for T cells, although their main route of entry is via HEV (49, 311, 338, 358). This migration is paramount in the immune surveillance of memory T cells, allowing them to recirculate through non-lymphoid and lymphoid tissues (35, 53, 358-360). Furthermore, the migration of $\gamma\delta$ T cells from skin to draining LN under inflammatory models has also been shown to ameliorate the CD8⁺ T cells response within the LN and to support DC function via production of TNF- α (338). Interestingly the mechanistic egress from the skin varies depending on the T cell population, with $\gamma\delta$ T cells egress being independent of CCR7 and CD4⁺ $\alpha\beta$ T cells migration being CCR7 dependent (338, 361).

6.1.1 Project Aims

Although ILCs are located within non-lymphoid tissues and their draining LNs, their migration between these sites is currently still unclear, with the parabiotic models used to assess ILC tissue residency, unable to assess such movement. To directly address this question of ILC migration from tissue to draining LN, Kaede mice were used to assess migration from the ear to the draining aLN in comparison to T cells and LCs. The aim of these studies was to determine whether ILCs were able to migrate from non-lymphoid tissue to the draining LN

through the lymphatic system. The hypothesis that ILC migration from draining LN to auLN increasing under inflammatory conditions was also tested.

6.2 RESULTS

6.2.1 Minimal ILC migration to the auLN from the ear steady state

To directly test the migration of ILC from tissue to draining LN the migration of ILCs from ear skin to the draining auLN was assessed. When using Kaede mice the efficient labelling of all cells in a defined area, such as the whole bLN, allows the tracking of cells into and out of that specific tissue. Therefore, the ear was selected as a specific area of skin to assess migration between skin and draining LN, since it was anticipated that that all cells within the ear could be photoconverted, rather than segments of back skin (53). Within this model ILC migration was compared to T cells and LCs. Egress from the blood is the main mechanism for naïve T cells to enter the LN (49). LCs, however, mainly enter through the afferent lymphatic vessel, originating from non-lymphoid tissue (49). Therefore, these two migratory populations, from the adaptive and innate sides of the immune system, respectively, were assessed to address whether ILCs can drain through the lymphatics in a similar manner.

Photoconversion of the ear from Kaede Green to Kaede Red was conducted without photoconverting any cells within the auLN, establishing a simple model to track migration under steady state conditions (Figure 6.1a-b). Due to the composition of the skin, a different light source was used to photoconvert the ear with a wavelength of 405 nm. A caveat of this light source is the potential induction of damage upon exposure to violet light, which depending on light source and length of exposure can result in damage of the epithelium, detectable 2 hours post irradiation (362, 363). Strid et al., reported that upon damage elicited

by tape stripping, IL-13 mRNA production is rapidly increased within 2 hours by TCR $\gamma\delta^+$ DETCs (340, 364). Therefore, to determine whether the dose of violet light applied to the ear was sufficient to elicit damage assessed by IL-13 production, IL-13 GFP reporter mice were analysed 2 hours post exposure. The proportion and number of T cells producing IL-13 GFP was comparable between control and violet light exposed ears, suggesting that the photoconversion method employed did not result in damage that could be measured by IL-13 release (Figure 6.1c-d). Therefore, this suggests that the establishment of this Kaede model enables the *in vivo* assessment of cell migration in mice under steady state conditions from the ear to draining auLN and into the ear.

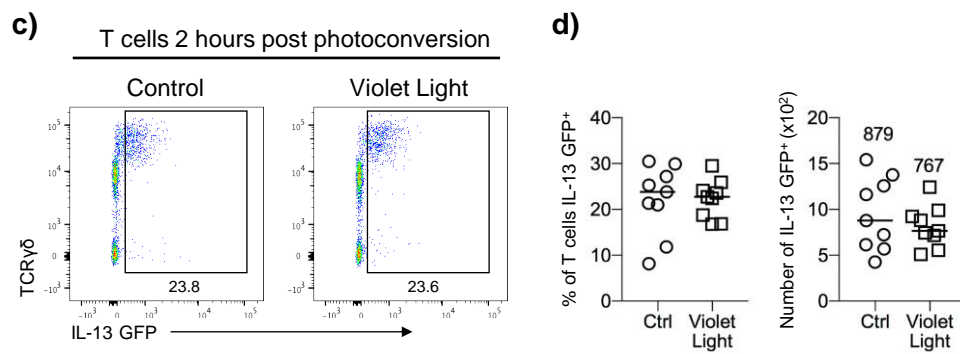
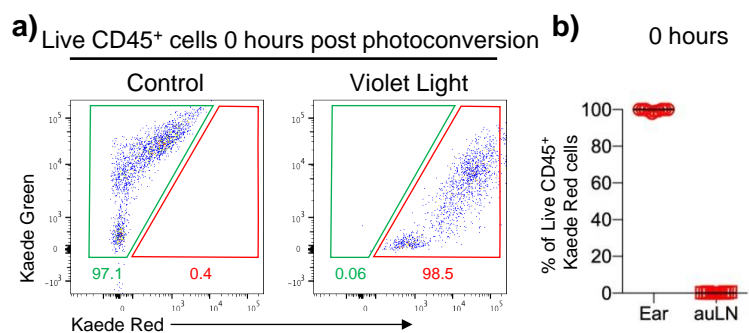
Migration from non-lymphoid tissue is a primary mechanism of entry for DCs into the LN. LCs are thought to be a subset of DCs that reside within the epidermis and upon activation they migrate into the dermis towards the lymphatic terminals where they transmigrate into the lymphatic vessel and move towards the draining LN (365, 366). Despite recent conflicting publications suggesting minimal migration of LCs from skin to draining LNs, LC and T cell, migration was studied in conjunction with ILCs, to compare ILC with migratory innate and adaptive immune cells (247, 367, 368). Initially the composition of the auLN was analysed 0, 48 and 72 hours post ear photoconversion (Figure 6.2a). An increase in the proportion and number of Kaede Red CD45⁺ hematopoietic was observed between 0 and 48 hours which was maintained at 72 hours (Figure 6.2a-b). Albeit a small number of Kaede Red cells being detected, these results support previous publications that cells continuously, although at a low frequency, migrate from the ear to the draining LN under steady state conditions (53, 247). To determine whether ILCs were amongst this migratory population, Kaede Red hematopoietic cells within the auLN were analysed in more detail 72 hours post

Figure 6.1. Photoconversion does not elicit $\gamma\delta$ T cell IL-13 production

WT Kaede violet light photoconversion of the ear and cell isolation of the ear and aLN were conducted as described in methods.

Each data point represents 1 ear and 1 aLN from one mouse. Data pooled from a minimum of 2 experiments. Values on flow cytometry plots represent percentages, bars on scatter plots represents the median, which is also shown numerically. Statistical significance was tested using an unpaired, non-parametric, Mann-Whitney two tailed T test: * $p \leq 0.05$, ** $p \leq 0.01$, *** $p \leq 0.001$.

- a) Representative flow cytometry plots showing Kaede Green and Kaede Red expression of Live CD45⁺ cells in the ear 0 hours after no violet light photoconversion (control) and violet light photoconversion (violet light).
- b) Percentage of Live CD45⁺ Kaede Red cells within the ear and aLN 0 hours after violet light photoconversion (n=12).
- c) Representative flow cytometry plots of IL-13 production in IL-13 GFP reporter mice by T cells (Live CD45⁺ CD3 ϵ ⁺) within the ear after no violet light photoconversion (control) or 2 hours post violet light photoconversion (violet light).
- d) Percentage (left) and number (right) of IL-13 GFP⁺ T cells within the ear in control (n=9) and violet light (n=9) mice.



photoconversion. The Kaede Red migratory population was mainly comprised of T cells, with a smaller proportion of LCs and very few ILCs (Figure 6.2c-d). Conversion of all cells within the ear also enabled the assessment of Kaede Green putative migratory populations into the ear from the periphery. The initial labelling of the ear was efficient with >95% of CD45⁺ cells within the ear expressing Kaede Red at 0 hours (Figure 6.2e). Although a small proportion of hematopoietic cells remained Kaede Green, the increase in proportion and number of Kaede Green cells over time was consistent with the movement of new cells into the ear after initial labelling (Figure 6.2e-f). It was observed that at 72 hours this migratory population was comprised of T cells amongst a small population of LCs (Figure 6.2g-h). Interestingly ILCs, although a small proportion, were also identified within this Kaede Green migratory population. Together these data suggest there is minimal migration of ILCs from the ear to the auLN under steady state conditions, however, a small population of ILCs are potentially able to migrate into the ear.

6.2.2 Atopic Dermatitis causes an increase in ear and auLN cellularity

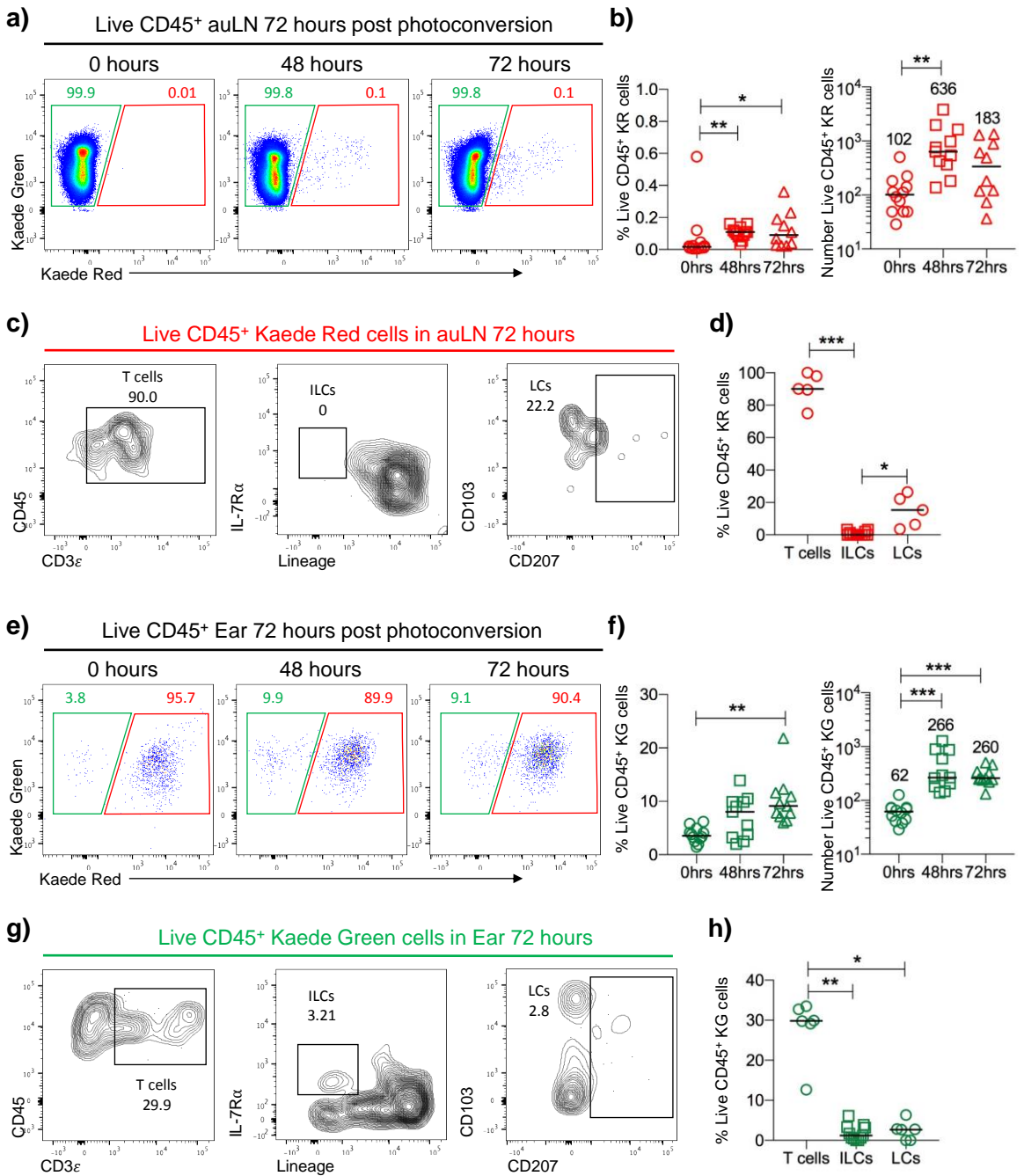
Since minimal migration of ILCs was detected at steady state it was hypothesised that ILC migration to the auLN would increase under inflammatory conditions, since the induction of skin inflammation via various skin irritants increases the migration of immune cells into the inflamed skin and the draining LN (247, 358, 359, 365). To this end, MC903 was applied to the ears establishing an AD model. This is an extensively used model characterised by an inappropriate type two immune response (112, 227, 369-371). MC903 is a vitamin D3 analogue that binds to an intracellular vitamin D receptor in keratinocytes, inducing an increase in production of alarmins such as TSLP, IL-25 and IL-33 (112, 369, 372, 373). In turn, these alarmins drive a type two response resulting in accumulation of basophils, eosinophils,

Figure 6.2. Tracking migration of immune cells in the ear and draining auLN

WT Kaede violet light photoconversion of the ear and cell isolation of the ear and auLN were conducted as described in methods. Immune cell migration was assessed 0, 48 and 72 hours post violet light photoconversion.

Each data point represents 1 ear and 1 auLN from one mouse. Data pooled from a minimum of 2 experiments. Values on flow cytometry plots represent percentages, bars on scatter plots represents the median, which is also shown numerically. Statistical significance was tested using Kruskal-Wallis one-way ANOVA with post hoc Dunn's test: * $p \leq 0.05$, ** $p \leq 0.01$, *** $p \leq 0.001$. When gating on ILCs lineage markers include; B220, CD11c, CD11b, CD3, CD5, CD19, Ter119, Gr1, F4/80, Fc ϵ RI and CD49b.

- a) Representative flow cytometry plots showing Kaede Green and Kaede Red expression of Live CD45⁺ cells in the auLN 0, 48 and 72 hours post photoconversion.
- b) Percentage (left) and number (right) of Live CD45⁺ Kaede Red cells in the auLN 0 (n=12), 48 (n=12) and 72 hours (n=10) post photoconversion.
- c) Representative flow cytometry plots of Live CD45⁺ Kaede Red T cells (CD3 ϵ ⁺) ILCs (Lineage⁻ IL-7R α ⁺) and LCs (MHCII⁺ CD11c⁺ CD207⁺) in the auLN 72 hours post photoconversion. Each population is shown as a proportion of the Live CD45⁺ Kaede Red population.
- d) Percentage Live CD45⁺ Kaede Red T cells (n=5), ILCs (n=12) and LCs (n=5) in the auLN.
- e) Representative flow cytometry plots showing Kaede Green and Kaede Red expression of Live CD45⁺ cells in the ear 0, 48 and 72 hours post photoconversion.
- f) Percentage (left) and number (right) of Live CD45⁺ Kaede Green cells in the ear 0, (n=12), 48 (n=11) and 72 hours (n=11) post photoconversion.
- g) Representative flow cytometry plots of Live CD45⁺ Kaede Green T cells ILCs and LCs in the ear 72 hours post photoconversion. Each population is shown as a proportion of the Live CD45⁺ Kaede Green population.
- h) Percentage Live CD45⁺ Kaede Green T cells (n=6), ILCs (n=11) and LCs (n=6) in the ear.



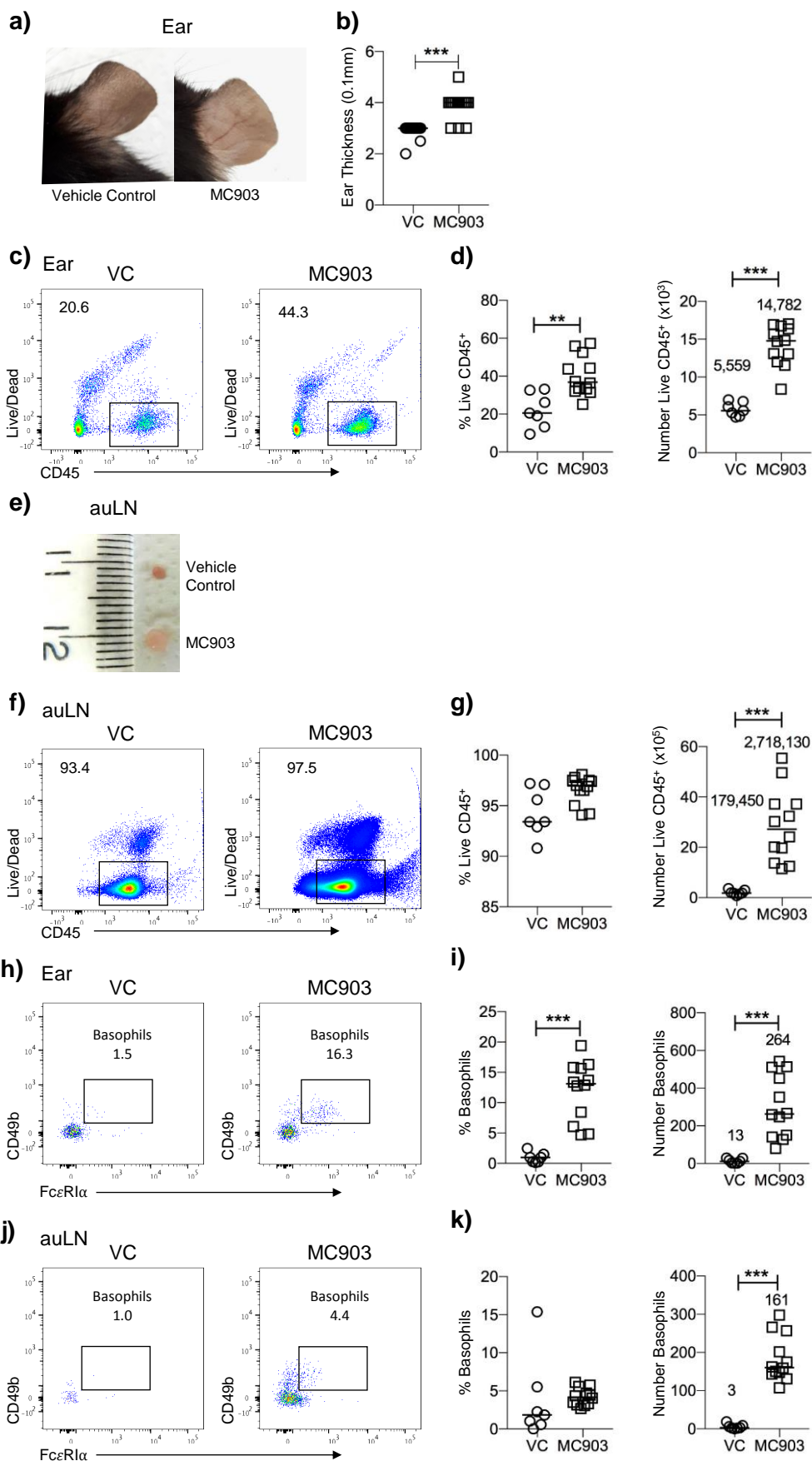
effector Th2 cells, DCs, mast cells and ILC2s in the dermal layer (112, 369). The increase in type 2 cytokine production, such as IL-4 and IL-13, results in the downregulation of genes important in skin barrier function such as filaggrin, leading to further increased skin permeability to allergens (374, 375). To validate the model within the lab, the ear and auLN were analysed post application of ethanol VC or MC903 for 5 days. This time frame was chosen to study the initial innate response, whilst providing sufficient time to assess migration and reduce potential discomfort to the mice. Previous publications studying the effects of MC903 conduct analysis after 14-17 days of application, with reports of visual damage occurring after 5-7 days of application (112, 369, 370). It was therefore important to determine whether 5 days of application was sufficient to cause a measurable response. Visually, after 5 days, the VC and MC903 treated ears were comparable, with no lesion development (Figure 6.3a). However, ear thickness increased within the MC903 treated mice accompanied by an increase in the percentage and number of CD45⁺ hematopoietic cells (Figure 6.3b-d). Most importantly, the auLN substantially increased in size alongside a statistical increase in the number of CD45⁺ hematopoietic cells (Figure 6.3e-g). Accumulation of basophils within the ear is a hallmark of MC903 induced AD development, therefore, basophils were assessed within the ear and auLN (231). Basophils were observed to increase in number within both tissues (Figure 6.3h-k). It is clear that the auLN has increase in cellularity, this may be due to all populations expanding proportionally, elucidating to why the percentage of basophils are comparable between VC and MC903 treated mice. Together these data show that 5 days of treatment elicits inflammation within the ears and a substantial response within the auLN. This suggests that this is an appropriate model to assess the migration of cells within an early innate response from the ear to the auLN.

Figure 6.3. Establishment of the MC903 atopic dermatitis model

4 nmol of MC903 dissolved in absolute ethanol was topically applied to the dorsal and ventral sides of the ear of WT mice on day 0 (D0) – day 4 (D4), ethanol was applied alone as a vehicle control (VC). WT mice were culled 72 hours post final dose on D5. Cells were isolated from the ears and auLN as described in methods.

Each data point represents 1 ear and 1 auLN from one mouse. Data pooled from a minimum of 2 experiments. Values on flow cytometry plots represent percentages, bars on scatter plots represents the median, which is also shown numerically. Statistical significance was tested using an unpaired, non-parametric, Mann-Whitney two tailed T test: * $p \leq 0.05$, ** $p \leq 0.01$, *** $p \leq 0.001$.

- a) Representative photos of ears with VC or MC903 topical application.
- b) Thickness of VC (n=15) and MC903 (n=12) treated ears 24 hours after last topical application.
- c) Representative flow cytometry plots showing Live CD45⁺ cells within the VC (left) and MC903 (right) ears.
- d) Percentage (left) and number (right) of Live CD45⁺ cells in VC (n=7) and MC903 (n=11) ears.
- e) Representative photos of auLN of VC or MC903 treated mice. Ruler scale is 1 mm, per small division.
- f) Representative flow cytometry plots showing Live CD45⁺ cells within VC (left) and MC903 (right) auLNs.
- g) Percentage (left) and number (right) of Live CD45⁺ cells VC (n=7) and MC903 (n=12) auLNs.
- h) Representative flow cytometry plots showing basophils (Live CD45⁺ CD3⁻ CD5⁻ CD11c⁻ CD19⁻ NK1.1⁻ ckit⁻ CD49b⁺ FcεRI⁺) in the ear of VC (left) and MC903 (right) treated mice.
- i) Percentage (left) and number (right) of basophils within VC (n=7) and MC903 (n=12) ears.
- j) Representative flow cytometry plots of basophils in VC (left) and MC903 (right) auLNs.
- k) Percentage (left) and number (right) of basophils within VC (n=7) and MC903 (n=12) auLN.



ILC2s contribute to the type 2 response induced by MC903 in a manner independent of adaptive immunity (112). Studies depleting ILC2s within the MC903 model resulted in attenuation of AD inflammation (112, 231). Currently, there is debate within the literature as to whether ILC2s are recruited into the inflamed skin in an IL-33 and IL-25 dependent manner, or whether these cytokines are redundant and instead the ILC2 response is driven by TSLP, with the TSLP receptor being highly expressed on ILC2s (112, 227). Recruitment and proliferation of ILC2s is further contributed to by basophil derived IL-4 (231). To explore the ILC response within the MC903 model, total ILCs alongside ILC subsets were further analysed. Similar to basophils, there was no change in the percentage of total ILCs within the auLN (Figure 6.4a-b). However, over a 10-fold increase in number of ILCs was observed alongside an increase in all ILC subsets in MC903 treated mice (Figure 6.4c). The comparisons of ILC percentages may be skewed due to ILC2s and TrN ILCs undergoing a larger expansion numerically, compared to ILC1s and ILC3s (Figure 6.4b). This may suggest why the percentage of ILC3s was decreased within the MC903 model but an increase in number was observed. The significant increase in ILC numbers indicate that the MC903 model is an appropriate model for directly testing whether ILCs migrate from inflamed ear skin to the auLN. Although an increase in hematopoietic cells was observed within the MC903 treated ear, there was a decrease in proportion of ILCs and numbers were comparable to VC ears (Figure 6.5a-c). This proportional decrease likely reflects a large increase of another non-ILC population. An increase in proportion and number of ILC2s in the MC903 treated ear, consistent with other studies using the MC903 AD model, was counteracted by a decrease of TrN ILCs, which may explain why no change was observed in the total number of ILCs (112, 231). These data support the development of an ILC2 driven AD model. Following the large expansion of ILCs within the

Figure 6.4. An increase in all ILC subsets is observed within the auLN of atopic dermatitis mice

4 nmol of MC903 dissolved in absolute ethanol was topically applied to the dorsal and ventral sides of the ear of WT mice for D0-D4, ethanol was applied alone as a VC. WT mice were culled 72 hours post final dose on D5. Cells were isolated from the auLN as described in methods.

Each data point represents 1 auLN from one mouse. Data pooled from a minimum of 2 experiments. Values on flow cytometry plots represent percentages, bars on scatter plots represents the median, which is also shown numerically. Statistical significance was tested using an unpaired, non-parametric, Mann-Whitney two tailed T test: * $p \leq 0.05$, ** $p \leq 0.01$, *** $p \leq 0.001$. When gating on ILCs lineage markers include; B220, CD11c, CD11b, CD3, CD5, CD19, Ter119, Gr1, CD123, F4/80, Fc ϵ RI and CD49b. ILCs were gated on negatively for iCD3 ϵ (gating strategy not shown).

- a) Representative flow cytometry plots showing ILCs (Live CD45⁺ Lineage⁻ IL-7R α ⁺ iCD3 ϵ ⁻), ILC1s (Live CD45⁺ Lineage⁻ IL-7R α ⁺ iCD3 ϵ ⁻ ROR γ t⁻ GATA-3⁻ T-bet⁺), ILC2s (Live CD45⁺ Lineage⁻ IL-7R α ⁺ iCD3 ϵ ⁻ ROR γ t⁻ GATA-3⁺ T-bet⁻), ILC3s (Live CD45⁺ Lineage⁻ IL-7R α ⁺ iCD3 ϵ ⁻ ROR γ t⁺) and TrN ILCs (Live CD45⁺ Lineage⁻ IL-7R α ⁺ iCD3 ϵ ⁻ ROR γ t⁻ GATA-3⁻ T-bet⁻) in the auLN of VC (top) and MC903 (bottom) treated mice.
- b) Percentage of ILCs and ILC subsets in the auLN of VC (n=7) and MC903 (n=11) treated mice.
- c) Number of ILCs and ILC subsets in the auLN of VC (n=5-7) and MC903 (n=12-15) treated mice.

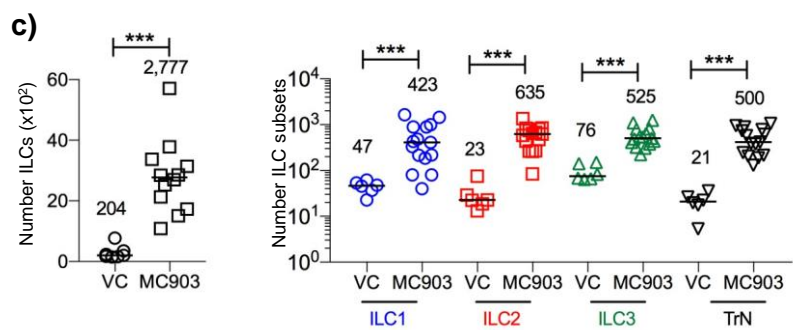
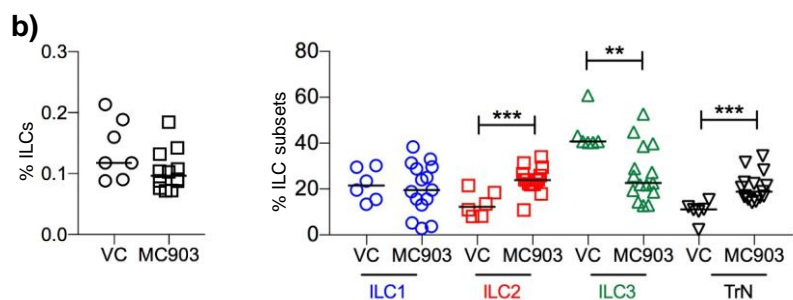
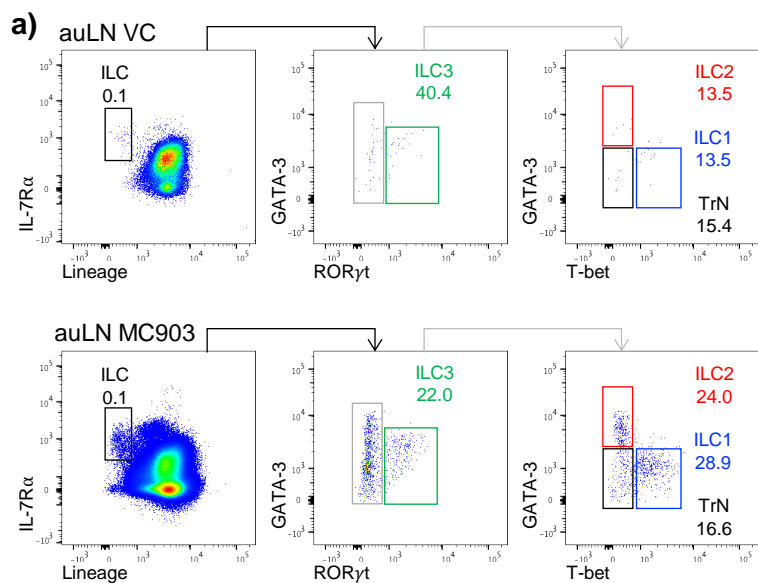
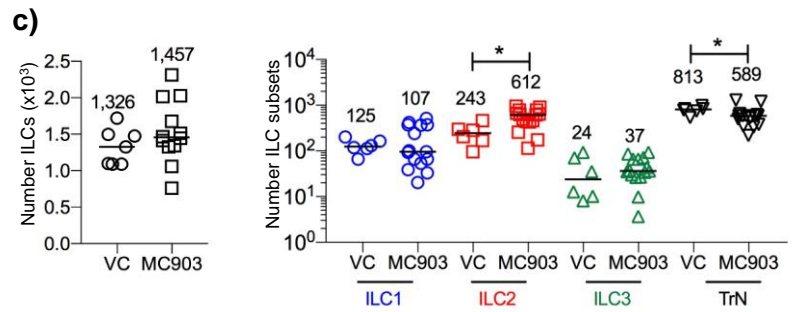
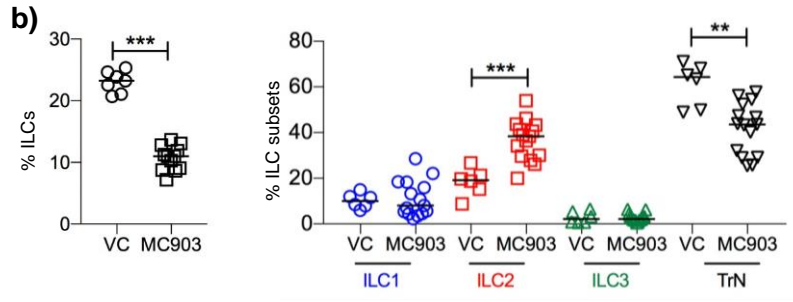
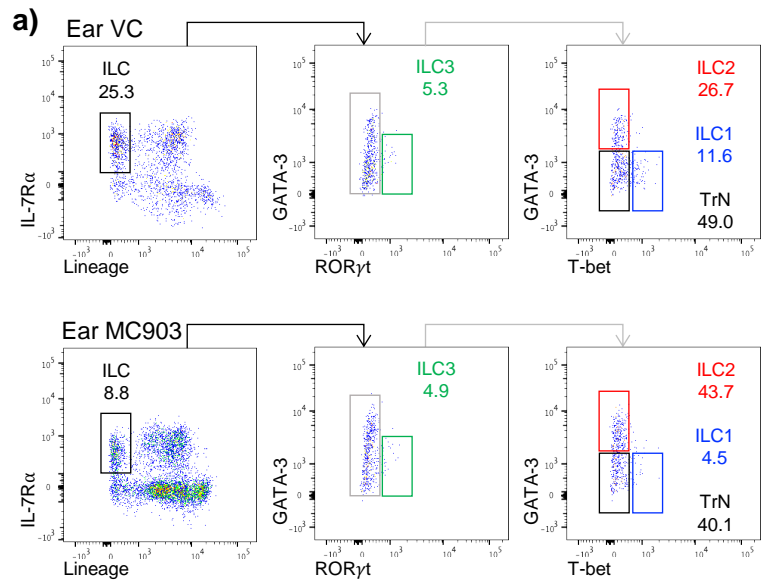


Figure 6.5. Atopic dermatitis elicits an increase in ILC2s within the ear

4 nmol of MC903 dissolved in absolute ethanol was topically applied to the dorsal and ventral sides of the ear of WT mice on D0-D4, ethanol was applied alone as a VC. WT mice were culled 72 hours post final dose on D5. Cells were isolated from the ears as described in methods.

Each data point represents 1 ear from one mouse. Data pooled from a minimum of 2 experiments. Values on flow cytometry plots represent percentages, bars on scatter plots represents the median, which is also shown numerically. Statistical significance was tested using an unpaired, non-parametric, Mann-Whitney two tailed T test: * $p \leq 0.05$, ** $p \leq 0.01$, *** $p \leq 0.001$. When gating on ILCs lineage markers include; B220, CD11c, CD11b, CD3, CD5, CD19, Ter119, Gr1, CD123, F4/80, Fc ϵ RI and CD49b. ILCs were gated on negatively for iCD3 ϵ (gating strategy not shown).

- a) Representative flow cytometry plots showing ILCs (Live CD45⁺ Lineage⁻ IL-7R α ⁺ iCD3 ϵ ⁻), ILC1s (Live CD45⁺ Lineage⁻ IL-7R α ⁺ iCD3 ϵ ⁻ ROR γ t⁻ GATA-3⁻ T-bet⁺), ILC2s (Live CD45⁺ Lineage⁻ IL-7R α ⁺ iCD3 ϵ ⁻ ROR γ t⁻ GATA-3⁺ T-bet⁻), ILC3s (Live CD45⁺ Lineage⁻ IL-7R α ⁺ iCD3 ϵ ⁻ ROR γ t⁺) and TrN ILCs (Live CD45⁺ Lineage⁻ IL-7R α ⁺ iCD3 ϵ ⁻ ROR γ t⁻ GATA-3⁻ T-bet⁻) in the ears of VC (top) and MC903 (bottom) treated mice.
- b) Percentage of ILCs and ILC subsets in the ears of VC (n=7) and MC903 (n=11) treated mice.
- c) Number of ILCs and ILC subsets in the ears of VC (n=7) and MC903 (n=11) treated mice.



auLN it was concluded that this model was suitable to assess ILC migration from the ear to draining auLN under MC903 driven inflammatory conditions.

T cell accumulation within the ear is a hallmark of prolonged MC903 treatment (370). To determine whether 5 days of treatment was sufficient in eliciting T cell recruitment, $\alpha\beta$ T cells ($CD3^+ TCR \gamma\delta^-$) and $\gamma\delta$ T cells ($CD3^+ TCR \gamma\delta^+$) were analysed within the auLN and ear of MC903 treated mice. Although decreased proportions of T cells, as a whole population, and $\alpha\beta$ T cells were observed within the auLN of the MC903 model, there was an increase in numbers of all T cell populations (Figure 6.6a-c). Interestingly, although in number there was a much larger presence of Kaede Red $\alpha\beta$ T cells within the auLN, there was a larger proportional increase of $\gamma\delta$ T cells, potentially consistent with their early innate functions. Within the ears, although the proportion of total T cells was comparable between VC and MC903 mice, there was an overall increase in T cell number, which was contributed to solely by $\gamma\delta$ T cells (Figure 6.6d-f). Similar to the auLN this supports the analysis of the early innate phase of the immune response with effector $\alpha\beta$ Th cells not yet being recruited to the inflamed tissue. This indicates that 5 days of MC903 application is efficient to amount an inflammatory response within the ear and auLN and that the main subset of T cells migrating into the ear are $\gamma\delta$ T cells, consistent with an early innate response.

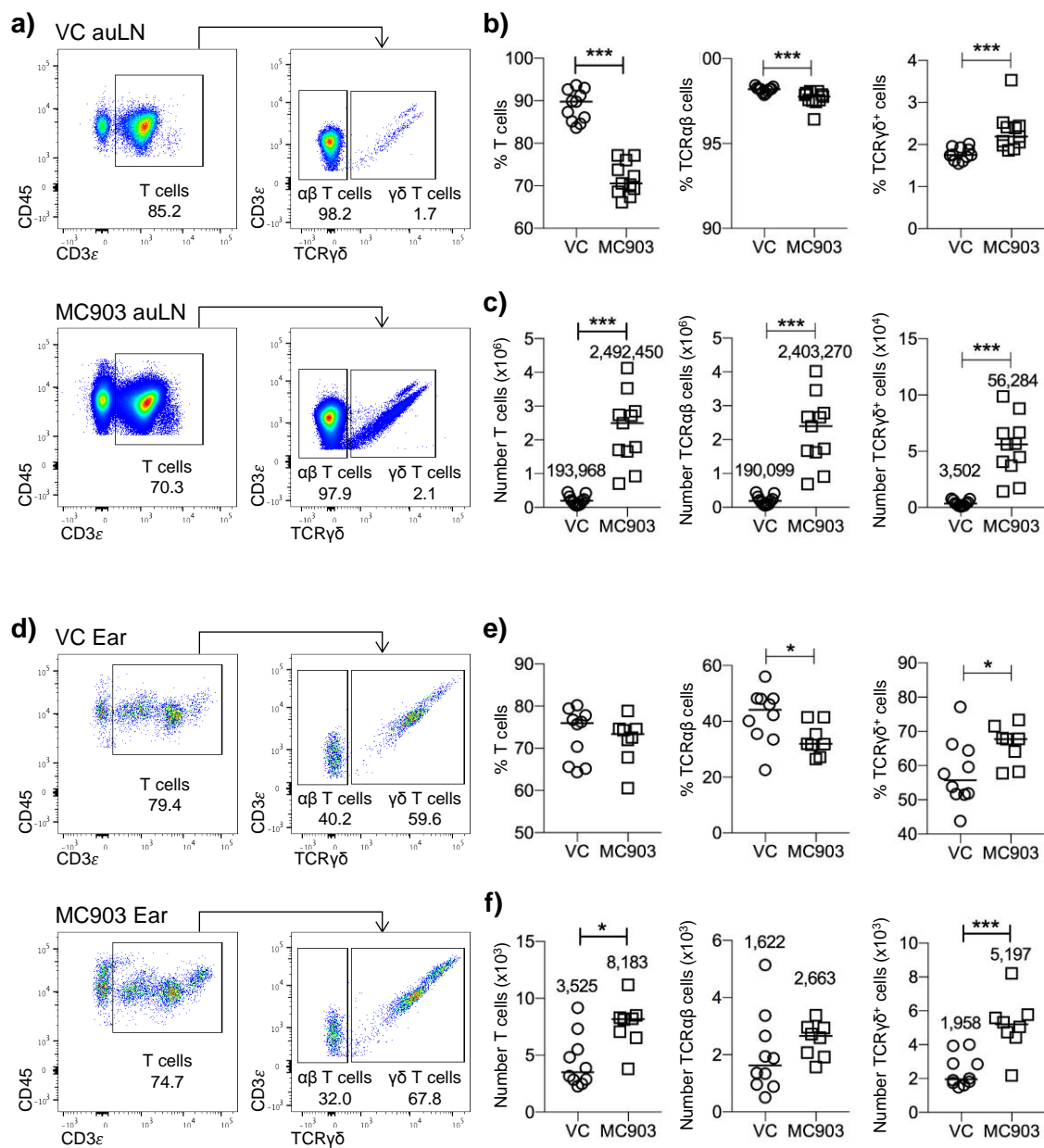
LC are also paramount in the development of MC903 driven AD. LC depleted mice did not develop AD-like symptoms upon MC903 application and further studies show their importance in migration from the ear to the draining LN to prime naïve $CD4^+$ T cells into effector Th2 cells, driving the type 2 response (366). Upon analysis of the LC population it was clear that within the auLN and the ear of MC903 treated mice there was an increase in the

Figure 6.6. Atopic dermatitis elicits an increase in $\gamma\delta$ T cells within the ear

4 nmol of MC903 dissolved in absolute ethanol was topically applied to the dorsal and ventral sides of the ear of WT mice on D0-D4, ethanol was applied alone as a VC. WT mice were culled 72 hours post final dose on D5. Cells were isolated from the ear and auLN as described in methods.

Each data point represents 1 ear and 1 auLN from one mouse. Data pooled from a minimum of 2 experiments. Values on flow cytometry plots represent percentages, bars on scatter plots represents the median, which is also shown numerically. Statistical significance was tested using an unpaired, non-parametric, Mann-Whitney two tailed T test: * $p \leq 0.05$, ** $p \leq 0.01$, *** $p \leq 0.001$.

- a) Representative flow cytometry plots showing T cells (Live CD45⁺ CD3 ϵ ⁺), $\alpha\beta$ T cells (Live CD45⁺ CD3 ϵ ⁺ TCR $\delta\gamma$ ⁻) and $\delta\gamma$ T cells (Live CD45⁺ CD3 ϵ ⁺ TCR $\delta\gamma$ ⁺) in the auLN of VC (top) and MC903 (bottom) treated mice.
- b) Percentage of T cells, $\alpha\beta$ T cells and $\delta\gamma$ T cells in the auLN of VC (n=11) and MC903 (n=11) treated mice.
- c) Number of T cells, $\alpha\beta$ T cells and $\delta\gamma$ T cells in the auLN of VC (n=11) and MC903 (n=11) treated mice.
- d) Representative flow cytometry plots showing T cells (Live CD45⁺ iCD3 ϵ ⁺), $\alpha\beta$ T cells (Live CD45⁺ CD3 ϵ ⁺ TCR $\delta\gamma$ ⁻) and $\delta\gamma$ T cells (Live CD45⁺ CD3 ϵ ⁺ TCR $\delta\gamma$ ⁺) in the ears of VC (top) and MC903 (bottom) treated mice.
- e) Percentage of T cells, $\alpha\beta$ T cells and $\delta\gamma$ T cells in the ears of VC (n=10) and MC903 (n=8) treated mice.
- f) Number of T cells, $\alpha\beta$ T cells and $\delta\gamma$ T cells in the ears of VC (n=10) and MC903 (n=8) treated mice.



percentage and number of LCs compared to VC treated mice (Figure 6.7a-d). This suggests an increase in the recruitment of LCs in the skin and migration of LCs from skin to auLN, supporting previous studies (366).

6.2.3 ILC migration is induced under an atopic dermatitis inflammation model

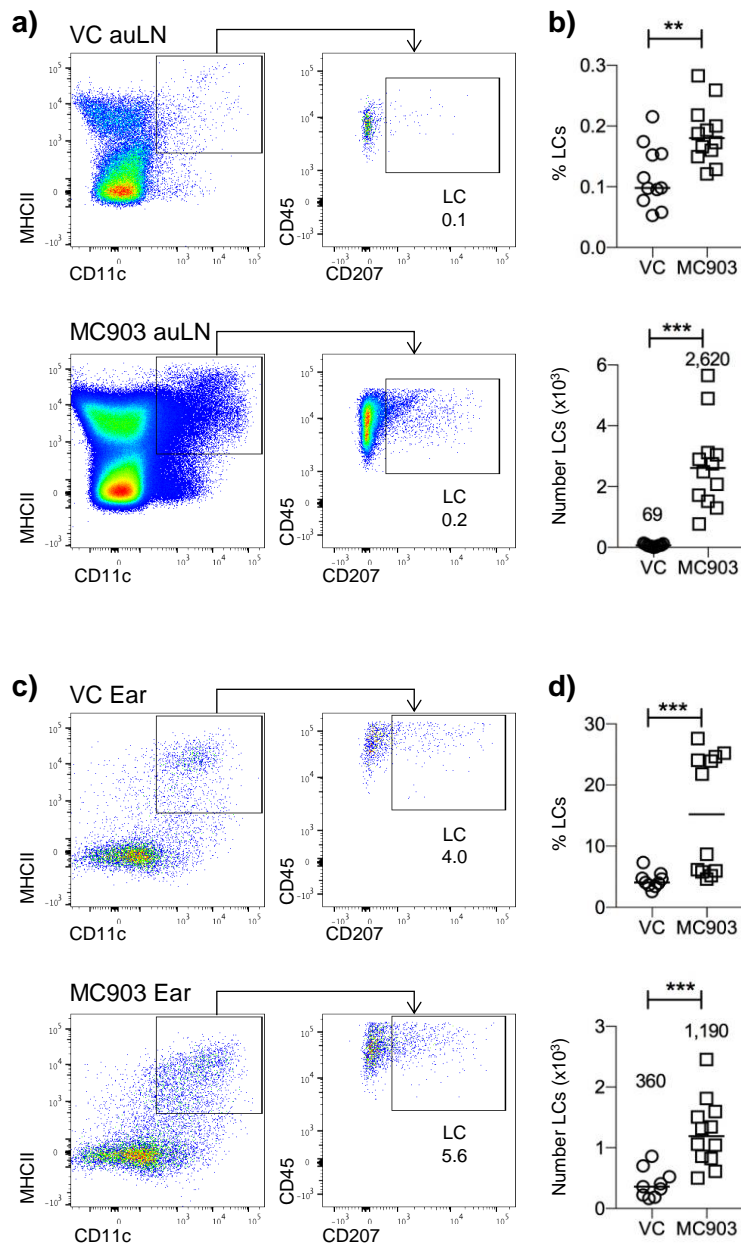
MC903 application resulted in increased numbers of ILCs within the auLN. To test the hypothesis that this increase of ILCs reflected enhanced migration from inflamed skin, the MC903 and Kaede models were combined enabling cell migration to be assessed under an inflammatory condition. Migration was observed at two different time points through the course of the 5 day MC903 model. The early phase of the MC903 model was assessed by photoconverting the ear on day 0 (D0) and assessing migration on day 2 (D2), and the later phases by photoconverting the ear on D2 of the MC903 model and taking mice on day 5 (D5) (Figure 6.8a). A hallmark of MC903 AD inflammation is the thickening of the ear. To determine that ear thickening did not prevent the efficient photoconversion of all cells within the ear the percentage of Kaede Red cells was assessed immediately after photoconversion in Kaede mice treated with MC903 two days prior. Upon comparison to control mice, which were taken 0 hours post photoconversion with no MC903 application, it was clear that the MC903 treatment and potential thickening of the ear, did not affect the ability to fully photoconvert the ear from Kaede Green to Kaede Red (Figure 6.8b). This meant that the cells migrating into the ear as well as from the ear to the auLN could still be analysed. Analysis of the auLN at the two selected time points showed an increase in Kaede Red CD45⁺ cells between D0-D2 and D2-D5 within the MC903 model (Figure 6.8c-e). This suggests that migration is increased upon MC903 application and is maintained through the initial 5 days. All subsets observed increased numbers of Kaede Red cells within the auLN 72 hours post photoconversion, consistent with

Figure 6.7. Increase in LCs within the auLN and ear of atopic dermatitis mice

4 nmol of MC903 dissolved in absolute ethanol was topically applied to the dorsal and ventral sides of the ear on D0-D4, ethanol was applied alone as a VC. WT mice were culled 72 hours post final dose on D5. Cells were isolated from the ear and auLN as described in methods.

Each data point represents 1 ear and 1 auLN from one mouse. Data pooled from a minimum of 2 experiments. Values on flow cytometry plots represent percentages, bars on scatter plots represents the median, which is also shown numerically. Statistical significance was tested using an unpaired, non-parametric, Mann-Whitney two tailed T test: * $p \leq 0.05$, ** $p \leq 0.01$, *** $p \leq 0.001$.

- a) Representative flow cytometry plots showing LCs (Live CD45⁺ MHCII⁺ CD11c⁺ CD207⁺) in the auLN of VC (top) and MC903 (bottom) treated mice.
- b) Percentage (top) and number (bottom) of LCs in the auLN of VC (n=9) and MC903 (n=12) treated mice.
- c) Representative flow cytometry plots showing LCs (Live CD45⁺ MHCII⁺ CD11c⁺ CD207⁺) in the ear of VC (top) and MC903 (bottom) treated mice.
- d) Percentage (top) and number (bottom) of LCs in the ear of VC (n=9) and MC903 (n=12) treated mice.



an increase in migration from the ear to the auLN, with LCs undergoing over a 40-fold increase (Figure 6.8f-g). This supports previous publications of LC migration increasing upon skin inflammation. Together these data show that under inflammatory conditions ILC migration into the auLN is increased, roughly 9-fold, alongside the increased migration of T cells and LCs.

Within the MC903 model it is clear that the numerical increase in Kaede Red CD45⁺ cells within the auLN of MC903 treated mice does not solely contribute to the overall increase in hematopoietic cells observed in Figure 6.3g. This is also true for the ILC population. The 10-fold increase within the auLN, is evidently not exclusively due to ILC migration from the ear, suggesting other mechanisms for ILC expansion within the auLN. It is therefore possible that local proliferation may drive ILC accumulation. To explore this, the expression of the proliferation marker Ki-67 was analysed in ILCs in the auLN of MC903 treated mice (283). Compared to VC, ILCs within the MC903 model have a substantially larger proportion expressing Ki-67, and this was seen across all ILC subsets (Figure 6.9a-c). This indicates that although the migration of ILCs from the ear contributes to the increase in ILC numbers within the auLN of MC903 treated mice, another contributing mechanism is the proliferation of ILCs.

LN hypertrophy is a common indicator of activation of the immune system (376). The prevention of cellular egress from the LN results in accumulation of leukocytes, increasing the probability of naïve T cells finding cognate antigen on APCs. Egress impairment under immunological challenge is regulated by many mechanisms including the upregulation of CD69 and the activation of adrenergic nerves (332, 335, 377). With ILCs being able to egress from peripheral LNs and recirculate through contralateral LNs via the blood it is possible that their expansion within the MC903 auLN occurs due to influx from other tissues, as well as from

Figure 6.8. ILC migration into the draining auLN increases upon MC903 induced inflammation

4 nmol of MC903 dissolved in absolute ethanol was topically applied to the dorsal and ventral sides of the ear of WT Kaede mice on either D0-D1 or D0-D4, ethanol was applied alone as a VC. Violet light photoconversion of the ear occurred on D0 or D2 and mice were either culled on D2 or D5. Cells were isolated from the auLN as described in methods.

Each data point represents 1 auLN from one mouse. Data pooled from a minimum of 2 experiments. Values on flow cytometry plots represent percentages, bars on scatter plots represents the median, which is also shown numerically. Paired samples were statistically tested using an unpaired, non-parametric, Mann-Whitney two tailed T test, when comparing more than two sets of data statistical significance was tested using Kruskal-Wallis one-way ANOVA with post hoc Dunn's test: * $p \leq 0.05$, ** $p \leq 0.01$, *** $p \leq 0.001$. Gating on ILCs lineage markers include; B220, CD11c, CD11b, CD3, CD5, CD19, Ter119, Gr1, F4/80, Fc ϵ RI and F4/80.

- a) Schematic representation of experimental design, assessing ILC migration in the MC903 Kaede model from D0-D2 (top) and D2-D5 (bottom).
- b) Percentage of Kaede Red Live CD45⁺ cells 0 hours post photoconversion on untreated ears (control) (n=10) and D2 of MC903 treated ears (MC903) (n=10).
- c) Representative flow cytometry plots showing Kaede Green and Kaede Red expression of Live CD45⁺ cells in VC and MC903 auLN at D0-D2 (left) and D2-D5 (right).
- d) Number of Live CD45⁺ Kaede Red cells in VC (n=6) and MC903 (n=7) auLN at D0-D2.
- e) Number of Live CD45⁺ Kaede Red cells in VC (n=8) and MC903 (n=8) auLN at D2-D5.
- f) Representative flow cytometry plots of Live CD45⁺ Kaede Red $\alpha\beta$ T cells (CD3 ϵ ⁺ TCR $\gamma\delta$ ⁻), $\gamma\delta$ T cells (CD3 ϵ ⁺ TCR $\gamma\delta$ ⁺), ILCs (Lineage⁻ IL-7R α ⁺) and LCs (MHCII⁺ CD11c⁺ CD207⁺) in the auLN of VC (top) and MC903 (bottom) treated mice between D2-D5. Each population is shown as a proportion of the Live CD45⁺ Kaede Red population.
- g) Number of Live CD45⁺ Kaede Red $\alpha\beta$ T cells, $\gamma\delta$ T cells, ILCs and LCs in VC (n=8-11) and MC903 (n=8-12) treated auLN.

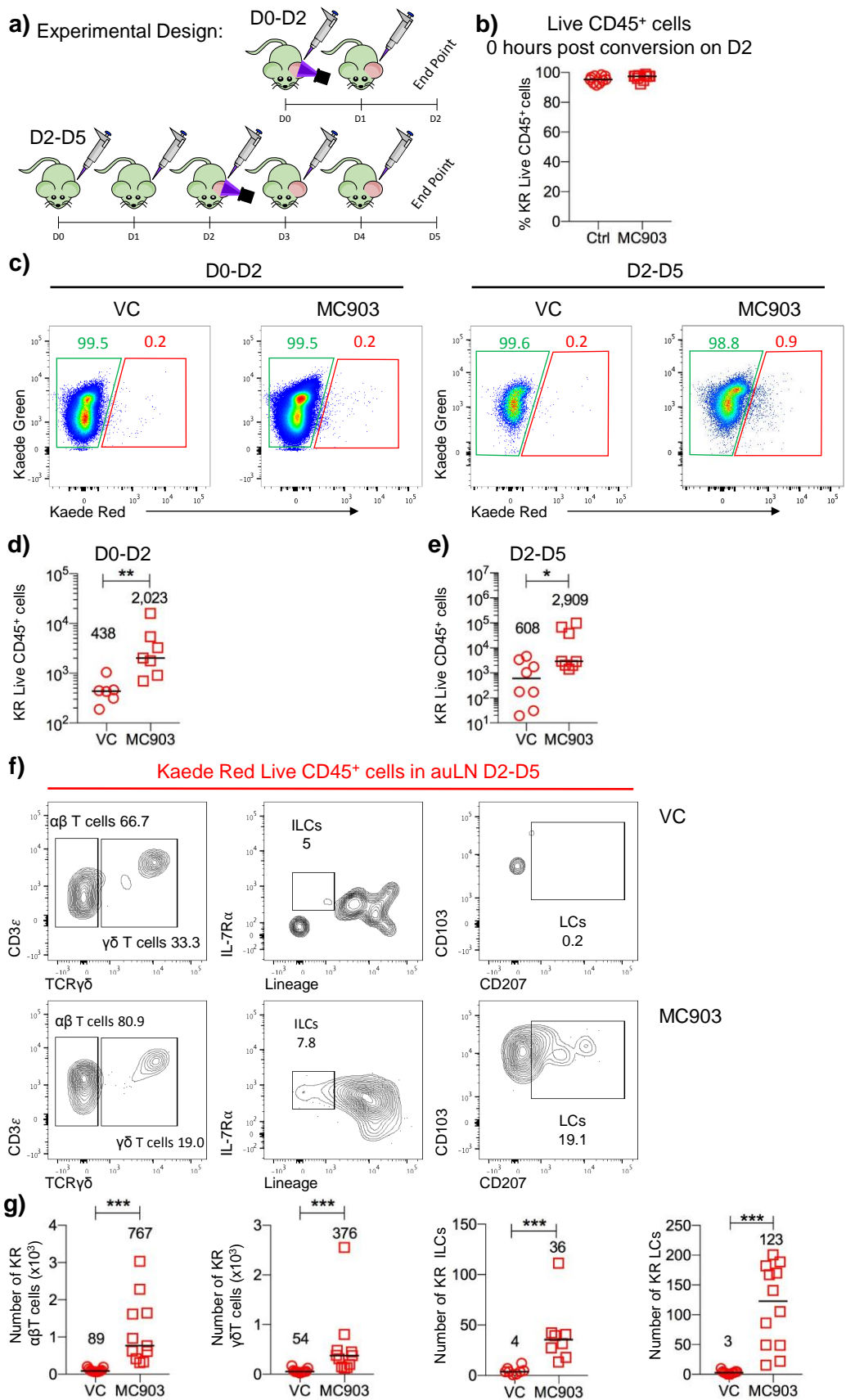
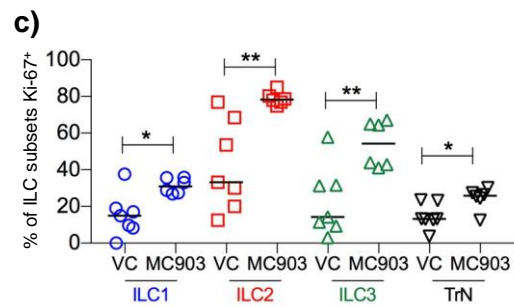
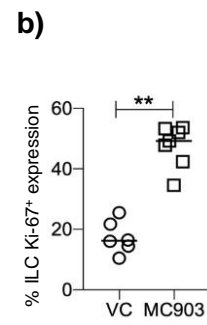
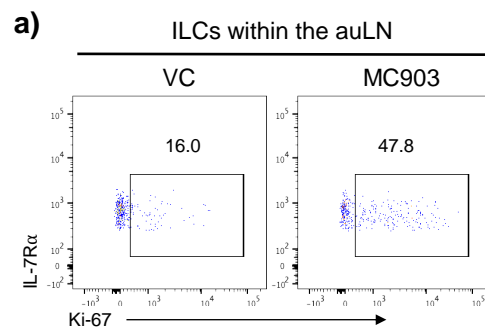


Figure 6.9. Proliferation of ILCs within the auLN is a contributing factor to their expansion

4 nmol of MC903 dissolved in absolute ethanol was topically applied to the dorsal and ventral sides of the ear of WT mice on D0-D5, ethanol was applied alone as a VC. All mice were culled on D5, 72 hours post final dose. Cells were isolated from the auLN as described in methods.

Each data point represents 1 auLN from one mouse. Data pooled from a minimum of 2 experiments. Values on flow cytometry plots represent percentages, bars on scatter plots represents the median, which is also shown numerically. Statistical significance was tested using an unpaired, non-parametric, Mann-Whitney two tailed T test: * $p \leq 0.05$, ** $p \leq 0.01$, *** $p \leq 0.001$. When gating on ILCs lineage markers include; B220, CD11c, CD11b, CD3, CD5, CD19, Ter119, Gr1, F4/80, Fc ϵ RI and F4/80. Non Kaede mice ILCs were gated on negatively for iCD3 ϵ (gating strategy not shown).

- a) Representative flow cytometry plots showing Ki-67 expression on ILCs (Live CD45⁺ Lineage⁻ IL-7R α ⁺) in the auLN of VC (left) and MC903 (right) treated mice.
- b) Percentage of ILCs expressing Ki-67 in the auLN of VC (n=6) and MC903 (n=7) treated mice.
- c) Percentage of ILC1s (Live CD45⁺ Lineage⁻ IL-7R α ⁺ iCD3 ϵ ⁻ ROR γ t⁻ GATA-3⁻ T-bet⁺), ILC2s (Live CD45⁺ Lineage⁻ IL-7R α ⁺ iCD3 ϵ ⁻ ROR γ t⁺ GATA-3⁺ T-bet⁻), ILC3s (Live CD45⁺ Lineage⁻ IL-7R α ⁺ iCD3 ϵ ⁻ ROR γ t⁺) and TrN ILCs (Live CD45⁺ Lineage⁻ IL-7R α ⁺ iCD3 ϵ ⁻ ROR γ t⁻ GATA-3⁻ T-bet⁻) expressing Ki-67 in the auLN of VC (n=7) and MC903 (n=6) treated mice.



the ear skin. Within Chapter 5, ILCs egress from the LN was shown to be dependent on S1P and S1PR interactions and upon S1P receptor blockade, with FTY720, Kaede Red ILCs accumulated within the LN consistent with a decrease in their S1P dependent egress. However, not all ILC migration was blocked, with the maintenance of a Kaede Green ILC population migrating into the bLN within FTY720 treated mice. To determine whether this partial block of S1P dependent migration of ILCs affected the accumulation of ILCs within the MC903 auLN the administration of FTY720 was combined with the MC903 model. VC was applied to the ears of mice administered H₂O control (VC, control) and compared to mice with MC903 application and H₂O control (MC903, control) or FTY720 (MC903, FTY720) (Figure 6.10a). Upon comparing these three models, it was observed that the MC903 model was induced efficiently, with MC903, control mice having an increased number of T cells, ILCs and all ILC subsets compared to VC, control mice (Figure 6.10b-d). Upon analysis of the T cell population it is clear that blocking egress of T cells severely inhibits the accumulation of T cells in the auLN of MC903 treated mice, so that the MC903, FTY720 mice were comparable to the VC, control mice. This suggests that the main mechanism of increase of number of T cells within the auLN is via cellular influx in an S1P dependent manner and not proliferation within this early innate phase. However, upon assessment of ILCs it was observed that the number of ILCs were comparable between MC903, control and MC903, FTY720 mice for number of ILCs, ILC1s ILC2s and TrN ILCs. This would suggest that blocking S1P dependent migration of ILCs does not affect the accumulation of ILCs within the auLN of MC903 treated mice suggesting their main mechanism for increased numbers is proliferation. However, this is different for ILC3s, in which there was a decrease in the number of ILC3s within the auLN of MC903, FTY720 mice which was comparable to VC, control mice. This indicates that ILC3s

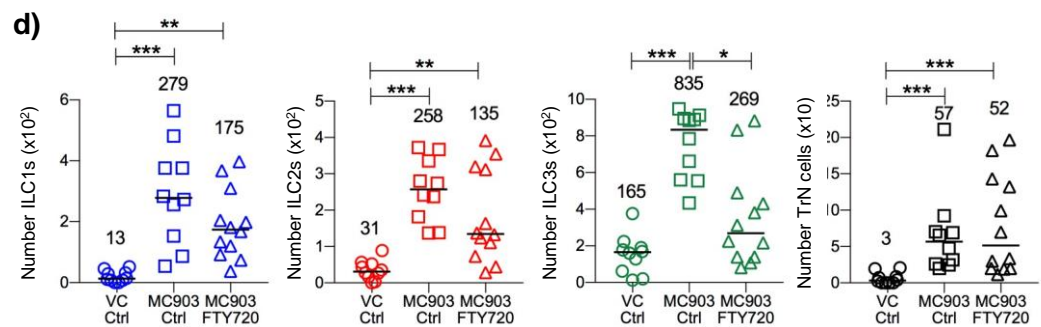
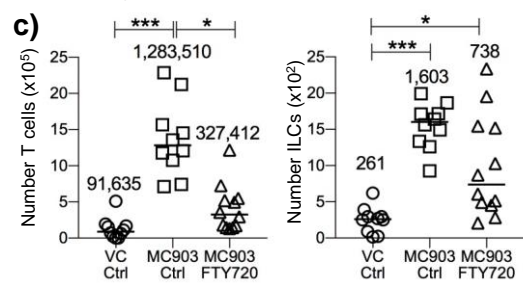
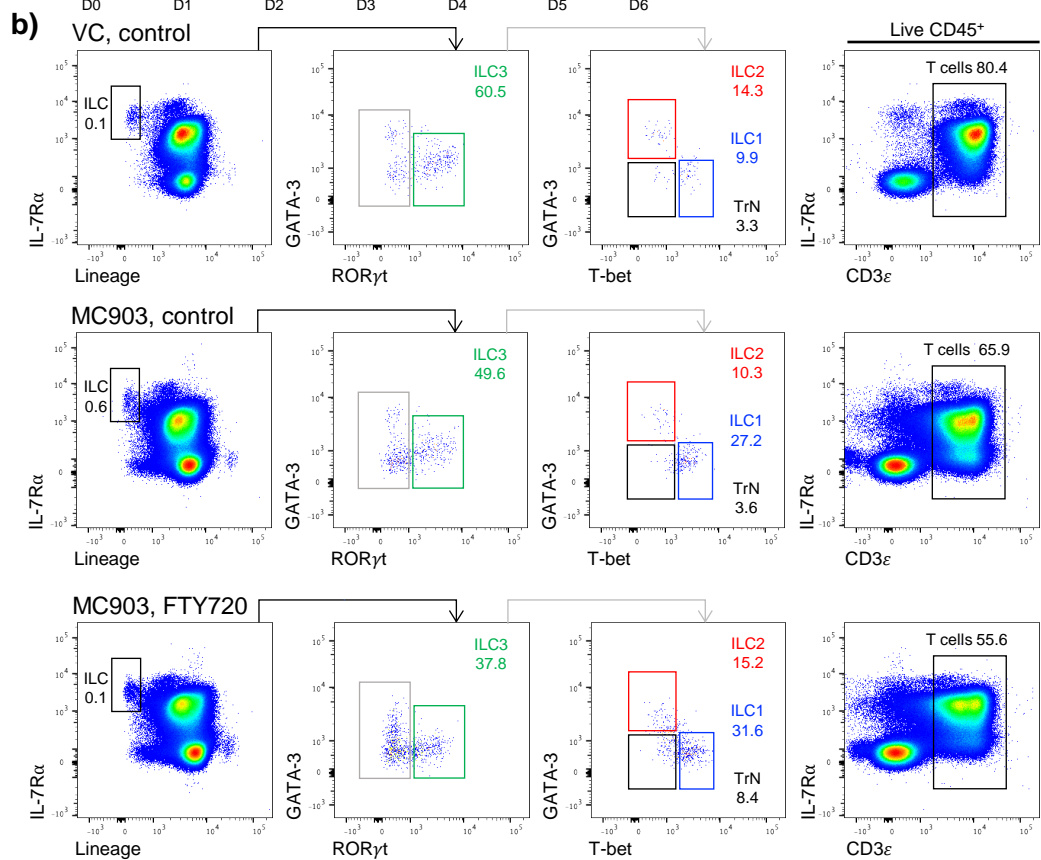
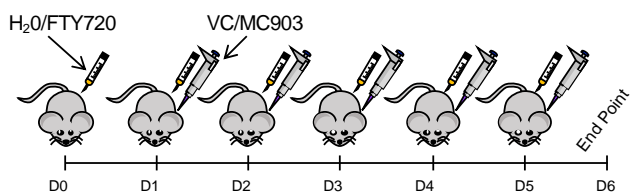
Figure 6.10. Blocking ILC S1P dependent migration does not affect ILC expansion within the auLN

WT mice were injected with either 1 mg/mL of FTY720 in H₂O (FTY720) or H₂O (control) i.p on D0-D5. On D2-D5 FTY720 injected WT mice received topical application of 4 nmol of MC903 dissolved in absolute ethanol to the dorsal and ventral sides of the ear (MC903, FTY720) (n=12). Mice receiving H₂O i.p injections received topical application of either MC903 (MC903, control) (n=12) or VC (VC, control) (n=10). Mice were culled on D6, 24 hours post final i.p and topical application. Cells were isolated from the auLN as described in methods.

Each data point represents 1 auLN from one mouse. Data pooled from a minimum of 2 experiments. Values on flow cytometry plots represent percentages, ILCs are shown as a percentage of Live CD45⁺ cells and ILC subsets as a percentage of total ILCs. Bars on scatter plots represents the median, which is also shown numerically. Statistical significance was tested using Kruskal-Wallis one-way ANOVA with post hoc Dunn's test: *p≤0.05, **p≤0.01, ***p≤0.001. When gating on ILCs lineage markers include; B220, CD11c, CD11b, CD3, CD5, CD19, Ter119, Gr1, F4/80, FcεRI and F4/80. ILCs were gated on negatively for iCD3ε (gating not shown).

- a) Schematic representation of experimental design, syringe represents FTY720/H₂O (control) i.p injections and the pipettes represent MC903/VC topical ear application.
- b) Representative flow cytometry plots showing ILCs (Live CD45⁺ Lineage⁻ IL-7Rα⁺ iCD3ε⁻), ILC1s (Live CD45⁺ Lineage⁻ IL-7Rα⁺ iCD3ε⁻ RORγt⁻ GATA-3⁻ T-bet⁺), ILC2s (Live CD45⁺ Lineage⁻ IL-7Rα⁺ iCD3ε⁻ RORγt⁺ GATA-3⁻ T-bet⁻), ILC3s (Live CD45⁺ Lineage⁻ IL-7Rα⁺ iCD3ε⁻ RORγt⁺), TrN ILCs (Live CD45⁺ Lineage⁻ IL-7Rα⁺ iCD3ε⁻ RORγt⁻ GATA-3⁻ T-bet⁻) and T cells (Live CD45⁺ CD3ε⁺) in VC control, MC903 control and MC903 FTY720 mice.
- c) Number of T cells and ILCs in VC control, MC903 control and MC903 FTY720 mice.
- d) Number of ILC1s, ILC2s, ILC3s and TrN ILCs in VC control, MC903 control and MC903 FTY720 mice.

a) Experimental Design:



potentially egress from tissues in an S1P dependent manner and migrate into the auLN, contributing to the accumulation of ILC3s in the MC903 treated mice. This eludes to individual ILC subsets having various different behaviouristic mechanisms. Overall, blocking S1P dependent egress of ILCs from tissues does not prevent the accumulation of ILCs within the auLN of MC903 treated mice, suggesting that proliferation is a key contributor to their expansion. However, there is a large range in the experimental data, limiting the conclusions made, suggesting further experimental approaches are required here. The mechanisms of ILC egress from lymphoid and non-lymphoid tissue has not been extensively reviewed, as discussed previously, with various S1PR needing to be further analysed, alongside FTY720 only partially blocking ILC migration.

6.2.4 ILCs migrate into the ear in atopic dermatitis inflamed skin

Immune cells are recruited to the MC903 inflamed ear, including T cells and DCs (370). T cells and DCs in the blood both express P-selectin glycoprotein ligand 1 which interacts with P-selectin and E-selectin, expressed on dermal venules (378, 379). These interactions are required for the egress of these cells out of dermal vessels and into inflamed skin (378, 379). To dynamically assess hematopoietic cell migration into the ear, Kaede Green CD45⁺ cells were analysed within the MC903 treated ears between D0-D2 and D2-D5 (Figure 6.11a-c). Kaede Green cells were observed within the ear at D2, however, numbers were comparable to VC treated mice. This suggests that the main recruitment of hematopoietic cells into the ear occurs between D2-D5 where an increase in Kaede Green CD45⁺ cells was observed. All populations observed an increase in number of Kaede Green cells within the ear 72 hours post photoconversion, suggesting an increase in migration into the ear, with again LCs having the

largest proportional increase, in comparison to other publications (Figure 6.11d-e). This suggests that alongside T cells and LCs, ILCs are recruited into the inflamed skin.

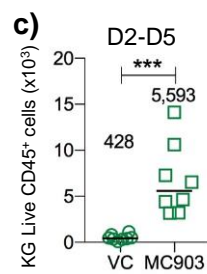
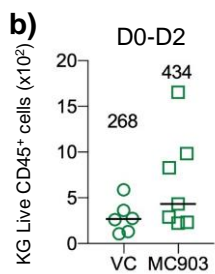
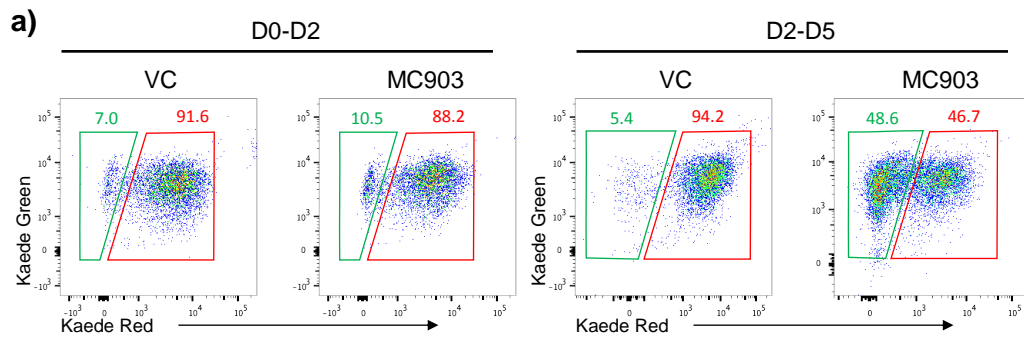
A substantial increase in the Kaede Green CD45⁺ population was detected within the MC903 ear, especially in comparison to the migratory Kaede Red population into the auLN, with the Kaede Green population making up over ~50% of CD45⁺ cells within the ear. As discussed, a caveat of the Kaede model is that rapid proliferation will cause dilution of the photoconverted Kaede Red protein such that the cells become Kaede Green again. Thus, a concern was that proliferation due to the MC903-induced inflammation was converting Kaede Red cells within the ear to Kaede Green and them being incorrectly defined as migratory cells. To explore the proliferation profile of ILCs within the MC903 model, the expression of Ki-67 was assessed on all ILCs within the ear. An increase in the percentage of Ki-67⁺ ILCs and all ILC subsets, except ILC3s, was observed consistent with enhanced ILC proliferation in the inflamed ear (Figure 6.12a-c). To determine whether the identified Kaede Green ILCs within the ear have diluted out their Kaede Red expression due to proliferation, or whether they were a true migratory population, the expression of Ki-67 on specifically Kaede Green ILCs within the ear was assessed. Although there was an increase in the percentage of Kaede Green ILCs expressing Ki-67 in the MC903 ear compared to the VC, it was evident that there was a clear population of Kaede Green ILCs within the MC903 ear that were Ki-67⁻ (Figure 6.12d-e). This suggests that although some tissue-resident Kaede Red ILCs are proliferating, potentially losing their Kaede Red expression and being identified as migratory Kaede Green ILCs, there is also clear evidence of ILC migration into the inflamed ear.

Figure 6.11. Atopic dermatitis drives enhanced ILC recruitment to skin

4 nmol of MC903 dissolved in absolute ethanol was topically applied to the dorsal and ventral sides of the ear of WT Kaede mice on either D0-D1 or D0-D4, ethanol was applied alone as a VC. Violet light photoconversion of the ear occurred on D0 or D2 and mice were either culled on D2 or D5. Cells were isolated from the ear as described in methods.

Each data point represents 1 ear from one mouse. Data pooled from a minimum of 2 experiments. Values on flow cytometry plots represent percentages, bars on scatter plots represents the median, which is also shown numerically. Paired samples were statistically tested using an unpaired, non-parametric, Mann-Whitney two tailed T test, when comparing more than two sets of data statistical significance was tested using Kruskal-Wallis one-way ANOVA with post hoc Dunn's test: * $p \leq 0.05$, ** $p \leq 0.01$, *** $p \leq 0.001$. When gating on ILCs lineage markers include; B220, CD11c, CD11b, CD3, CD5, CD19, Ter119, Gr1, F4/80, Fc ϵ RI and F4/80.

- a) Representative flow cytometry plots showing Kaede Green and Kaede Red expression of Live CD45⁺ cells in VC and MC903 treated ears at D0-D2 (left) and D2-D5 (right) time points.
- b) Number of Live CD45⁺ Kaede Green cells in VC (n=6) and MC903 (n=7) treated ears at D0-D2 time point.
- c) Number of Live CD45⁺ Kaede Green cells in VC (n=8) and MC903 (n=8) treated ears at D2-D5 time point.
- d) Representative flow cytometry plots of Live CD45⁺ Kaede Green $\alpha\beta$ T cells (CD3 ϵ ⁺ TCR $\gamma\delta$ ⁻), $\gamma\delta$ T cells (CD3 ϵ ⁺ TCR $\gamma\delta$ ⁺), ILCs (Lineage⁻ IL-7R α ⁺) and LCs (MHCII⁺ CD11c⁺ CD207⁺) in the auLN of VC (top) and MC903 (bottom) treated mice at D2-D5 time point. Each population is shown as a proportion of the Live CD45⁺ Kaede Green population.
- e) Number of Live CD45⁺ Kaede Green $\alpha\beta$ T cells, $\gamma\delta$ T cells, ILCs and LCs in VC (n=9-11) and MC903 (n=7-12) treated auLN.



d) Kaede Green Live CD45⁺ cells in Ear D2-D5

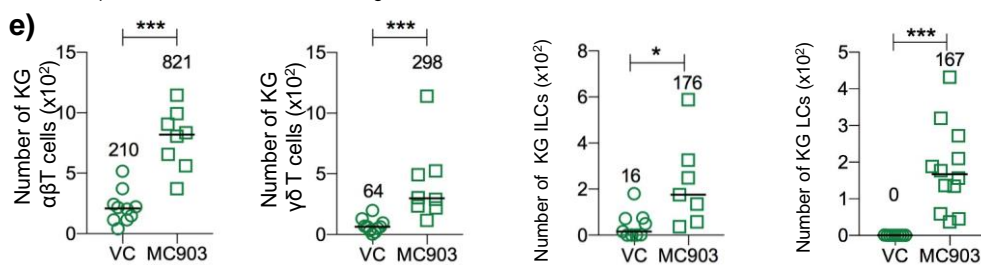
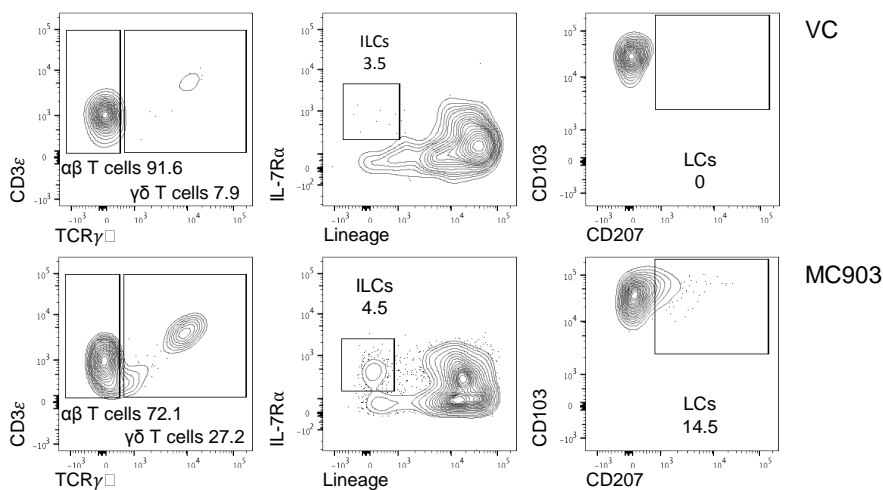


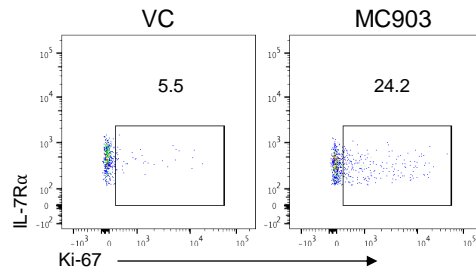
Figure 6.12. A true population of migratory ILCs enter the inflamed ear

4 nmol of MC903 dissolved in absolute ethanol was topically applied to the dorsal and ventral sides of the ear on D0-D5, ethanol was applied alone as a VC. All mice were culled on D5, 72 hours post final dose. Cells were isolated from the ear as described in methods.

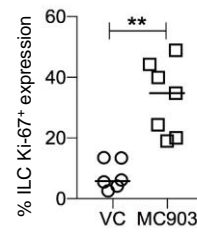
Each data point represents 1 ear from one mouse. Data pooled from a minimum of 2 experiments. Values on flow cytometry plots represent percentages, bars on scatter plots represents the median, which is also shown numerically. Statistical significance was tested using an unpaired, non-parametric, Mann-Whitney two tailed T test: * $p \leq 0.05$, ** $p \leq 0.01$, *** $p \leq 0.001$. When gating on ILCs lineage markers include; B220, CD11c, CD11b, CD3, CD5, CD19, Ter119, Gr1, F4/80, Fc ϵ RI and F4/80. Non Kaede mice ILCs were gated on negatively for iCD3 ϵ (gating strategy not shown).

- a) Representative flow cytometry plots showing Ki-67 expression on ILCs (Live CD45⁺ Lineage⁻ IL-7R α ⁺ iCD3 ϵ ⁻) in the ears of VC (left) and MC903 (right) treated mice.
- b) Percentage of ILCs expressing Ki-67 in the ears of VC (n=6) and MC903 (n=7) treated mice.
- c) Percentage of ILC1s (Live CD45⁺ Lineage⁻ IL-7R α ⁺ iCD3 ϵ ⁻ ROR γ t⁻ GATA-3⁻ T-bet⁺), ILC2s (Live CD45⁺ Lineage⁻ IL-7R α ⁺ iCD3 ϵ ⁻ ROR γ t⁻ GATA-3⁺ T-bet⁻), ILC3s (Live CD45⁺ Lineage⁻ IL-7R α ⁺ iCD3 ϵ ⁻ ROR γ t⁺) and TrN ILCs (Live CD45⁺ Lineage⁻ IL-7R α ⁺ iCD3 ϵ ⁻ ROR γ t⁻ GATA-3⁻ T-bet⁻) expressing Ki-67 in the ears of VC (n=6-7) and MC903 (n=6-7) treated mice.
- d) Representative flow cytometry plots showing Ki-67 expression on Kaede Green ILCs (Live CD45⁺ KG⁺ Lineage⁻ IL-7R α ⁺) in the ears of VC (left) and MC903 (right) treated mice. Ki-67⁺ Kaede Green ILCs in the MC903 treated ear are highlighted in a black bold box.
- e) Percentage of Kaede Green ILCs that are Ki-67⁺ and Ki-67⁻ in the ears of MC903 (n=9) treated mice.

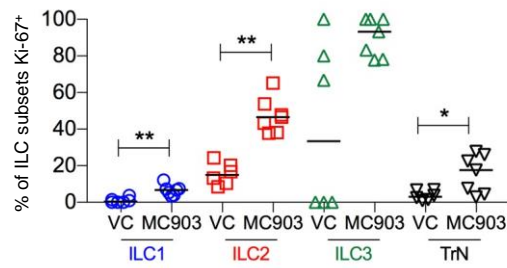
a) Ear



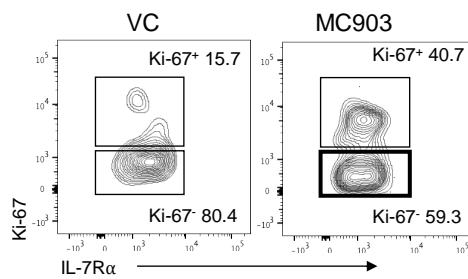
b)



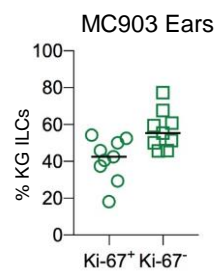
c)



d) Kaede Green ILCs in the Ear



e)



6.2.5 Cell migration into the ear from surrounding skin

The data described in this chapter so far has revealed that T cells, ILCs and LCs migrate into the ear under MC903 induced inflammation. T cells and DCs are known to migrate into inflamed skin through the blood, however their primary origin is still unclear (380). Previous reports have shown ILCs to migrate from the draining LN to the ear, however, due to being unable to photoconvert the draining aLN, migration from the adjoined skin was assessed, initially investigating migration from the opposite ear (226). The migration of T cells was assessed due to them being a larger and more easily identifiable migratory population compared to ILCs. The MC903 model was combined with the Kaede mice as before, however, the opposite ear to the MC903 treated ear was instead photoconverted (Figure 6.13a). This allowed for the tracking of cells from one uninflamed photoconverted ear to the MC903 treated unphotoconverted ear. Upon analysis of the treated ear, very small numbers of Kaede Red T cells were identified within the MC903 and VC treated ears (Figure 6.13b-d). It therefore, became apparent that migration of T cells from one ear to the other was minimal and likely not increased within inflammation.

A potential limit of labelling the opposite ear was the small area of skin converted, and thus number of cells that were Kaede Red, making tracking such small migratory populations technically challenging over a larger distance. The area of skin between the two ears, termed head skin, is directly adjacent to the treated ear and therefore migration from this area was also assessed. MC903 treatment of Kaede mice occurred as normal but at D2 the head skin was shaved, photoconverted and the treated ear analysed at D5 (Figure 6.14a). Initially to confirm that the ear and aLN were not photoconverted during this process the ear and aLN were analysed at 0 hours post head photoconversion and Kaede expression assessed. All cells

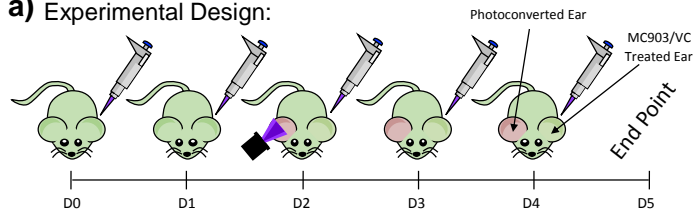
Figure 6.13. Minimal migration of T cells occurs from the opposite ear into the inflamed ear

4 nmol of MC903 dissolved in absolute ethanol was topically applied to the dorsal and ventral sides of the left ear (treated ear) of WT Kaede mice on D0-D4, ethanol was applied alone as a VC. Violet light photoconversion of the right ear (photoconverted ear) occurred on D2, and mice were culled on D5. Cells were isolated from the ear as described in methods.

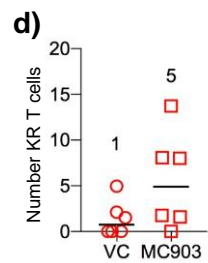
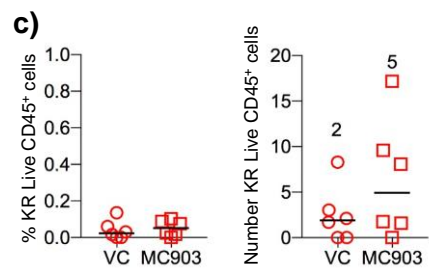
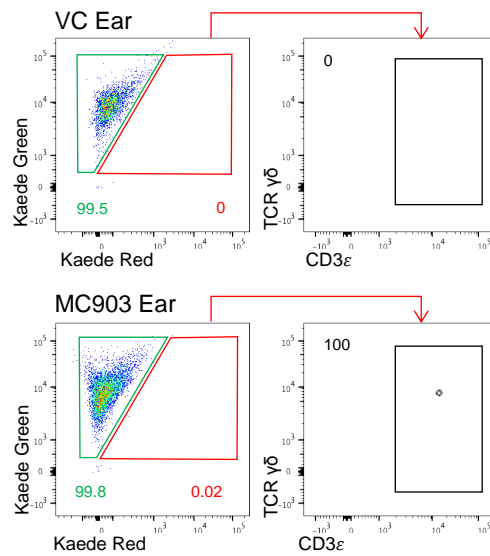
Each data point represents 1 ear from one mouse. Data pooled from a minimum of 2 experiments. Values on flow cytometry plots represent percentages, bars on scatter plots represents the median, which is also shown numerically. Statistical significance was tested using an unpaired, non-parametric, Mann-Whitney two tailed T test: * $p \leq 0.05$, ** $p \leq 0.01$, *** $p \leq 0.001$.

- a) Schematic representation of experimental design, pipette represents MC903/VC topical ear application, the purple light represents violet light photoconversion of the ear.
- b) Represented flow cytometry showing Kaede Green and Kaede Red expression of Live CD45⁺ cells and the percentage of Live CD45⁺ Kaede Red cells that are T cells (Live CD45⁺ KR⁺ CD3 ϵ ⁺) in the treated ears of VC (top) and MC903) treated mice.
- c) Percentage (left) and number (middle) of Live CD45⁺ Kaede Red cells in the treated ears of VC (n=6) and MC903 (n=6) mice.
- d) Number of Live CD45⁺ Kaede Red T cells in the treated ears of VC (n=6) and MC903 (n=6) mice.

a) Experimental Design:



b) Live CD45⁺ cells in the Treated Ear



within the ear and auLN were Kaede Green, showing that they were not photoconverted within this process, allowing the migration of cells into the ear and auLN to be assessed (Figure 6.14b-c). Upon analysis of the MC903 treated ear, it was observed that compared to the VC treated ear there was an increase in the number of Kaede Red CD45⁺ and T cells and that the majority of these T cells are $\gamma\delta$ T cells (Figure 6.14d-e). This suggests that cells are able to redistribute into the ear from adjacent skin, albeit in small numbers, with the main proportion of cells migrating from the skin to skin being $\gamma\delta$ T cells. To determine whether cells were migrating from the surrounding skin into the auLN, Kaede Red cells were analysed within the auLN of head skin photoconverted MC903 ear treated mice. Interestingly there was an increase in the number of Kaede Red CD45⁺ and T cells migrating from the head skin to the auLN. With a 37-fold increase in Kaede Red $\gamma\delta$ T cells and a 7-fold increase in $\alpha\beta$ T cells (Figure 6.14f-g). This suggests that the increase in cells within the auLN of MC903 treated mice is also contributed to by the migration of cells from skin adjacent to the ear, potentially due to the spread of MC903 by the mouse via grooming.

6.2.6 ILC migration is dependent on inflammatory conditions

ILC migration from the ear to the auLN and into the ear from the periphery was recorded within the MC903 inflammatory model. To determine whether this migration was specific to the MC903 model, or whether another inflammatory model could induce ILC migration the Aldara driven psoriasis-like model was established. Aldara cream contains 5% IQM which upon topical application to the skin activates the immune system, via TLR7 and TLR8, driving an IL-17/IL-23 response in a multi mechanistic manner (381, 382). Aldara driven psoriasis is defined by an increase in hematopoietic cell recruitment, such as T cells, DCs, macrophages

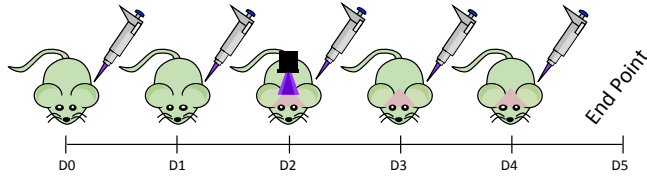
Figure 6.14. Migration from adjacent skin to inflamed ear is limited in atopic dermatitis model

4 nmol of MC903 dissolved in absolute ethanol was topically applied to the dorsal and ventral sides of the ear of WT Kaede mice on D0-D4, ethanol was applied alone as a VC. Violet light photoconversion of the skin between the ears (head skin) occurred on D2, and mice were culled on D5. Cells were isolated from the ear and auLN as described in methods.

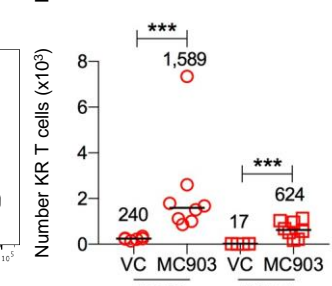
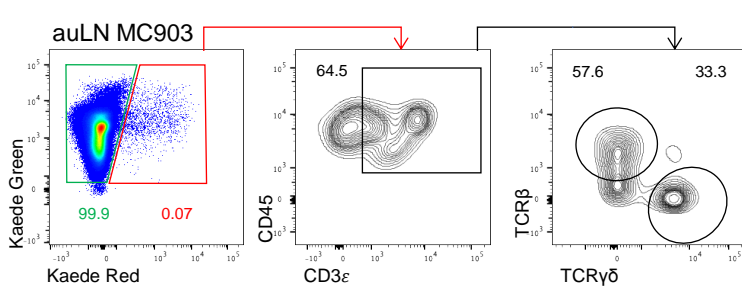
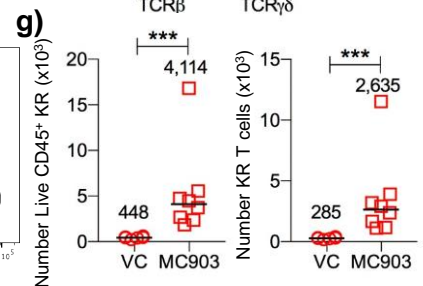
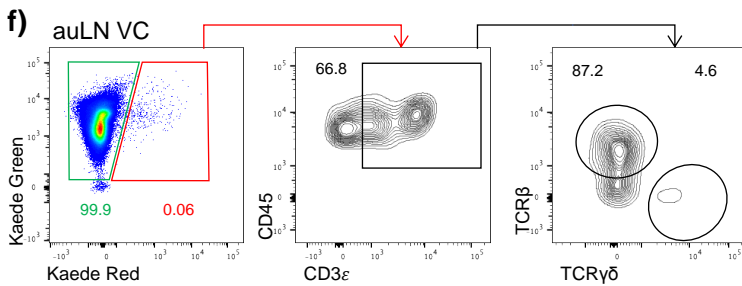
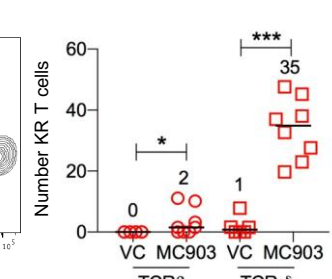
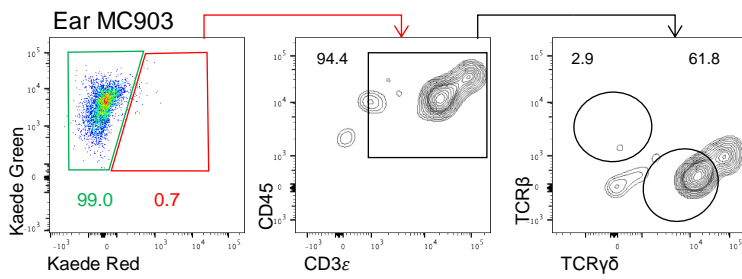
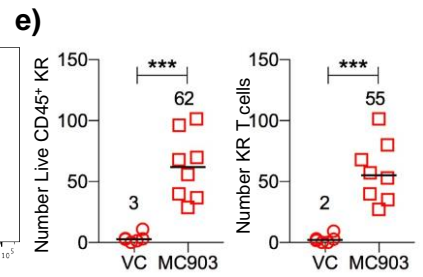
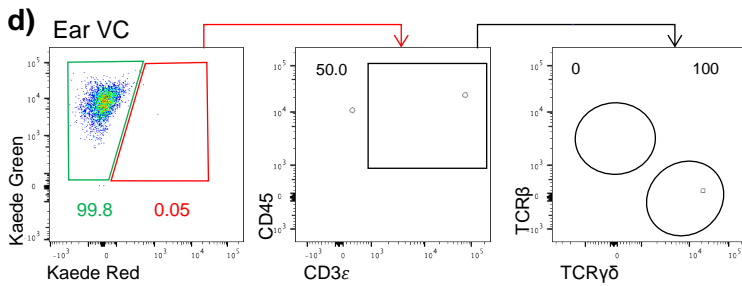
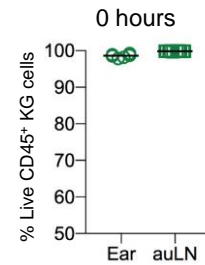
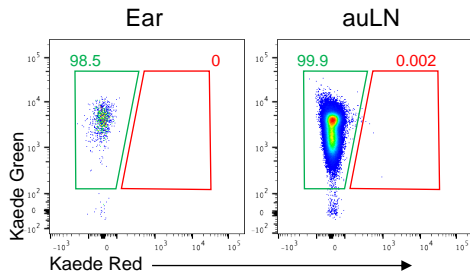
Each data point represents 1 ear and 1 auLN from one mouse. Data pooled 1 experiment. Values on flow cytometry plots represent percentages, bars on scatter plots represents the median, which is also shown numerically. Statistical significance was tested using an unpaired, non-parametric, Mann-Whitney two tailed T test: * $p \leq 0.05$, ** $p \leq 0.01$, *** $p \leq 0.001$. When gating on ILCs lineage markers include; B220, CD11c, CD11b, CD3, CD5, CD19, Ter119, Gr1, F4/80, FcεRI and F4/80.

- a) Schematic representation of experimental design, pipette represents MC903/VC topical ear application, the purple light represents violet light photoconversion of the head skin.
- b) Represented flow cytometry showing Kaede Green and Kaede Red expression of Live CD45⁺ cells in the ear and auLN 0 hours post violet light conversion of the head skin.
- c) Percentage of Live CD45⁺ Kaede Green cells in the ear (n=6) and auLN (n=10) 0 hours post violet light conversion of the head skin.
- d) Representative flow cytometry plots showing Kaede Green and Kaede Red expression of Live CD45⁺ cells and the percentage of Live CD45⁺ Kaede Red cells which are T cells (Live CD45⁺ KR⁺ CD3ε⁺), αβ T cells (Live CD45⁺ KR⁺ CD3ε⁺ βTCR⁺ γδTCR⁻) and γδ T cells (Live CD45⁺ KR⁺ CD3ε⁺ βTCR⁻ γδTCR⁺) within the ears of VC (top) and MC903 (bottom) mice.
- e) Number of Kaede Red Live CD45⁺, T cells, αβ T cells and γδ T cells in VC (n=6) and MC903 (n=8) treated ears.
- f) Representative flow cytometry plots showing Kaede Green and Kaede Red expression of Live CD45⁺ cells and the percentage of Live CD45⁺ Kaede Red cells which are T cells, αβ T cells and γδ T cells within the auLN of VC (top) and MC903 (bottom) mice.
- g) Number of Kaede Red Live CD45⁺, T cells, αβ T cells and γδ T cells in VC (n=6) and MC903 (n=8) treated auLN.

a) Experimental Design:



b) 0 hours after violet light photoconversion



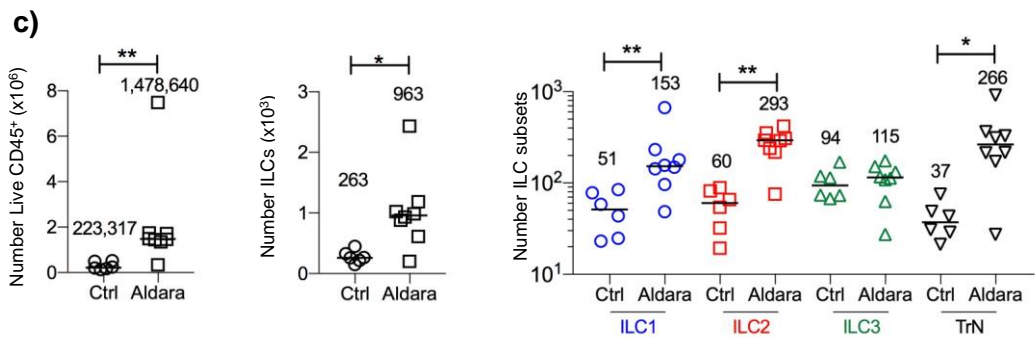
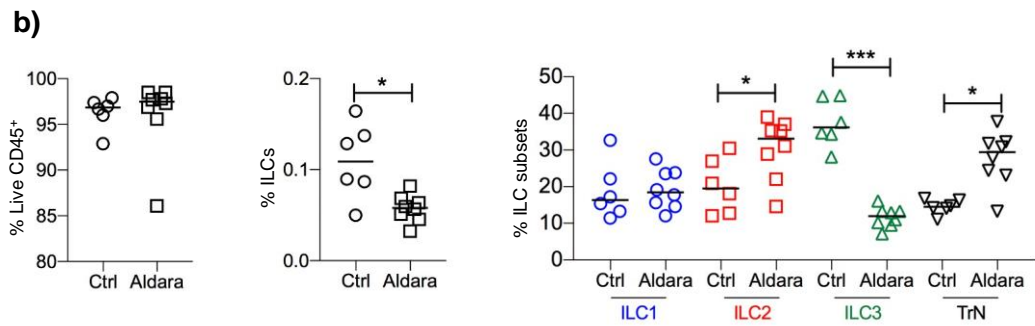
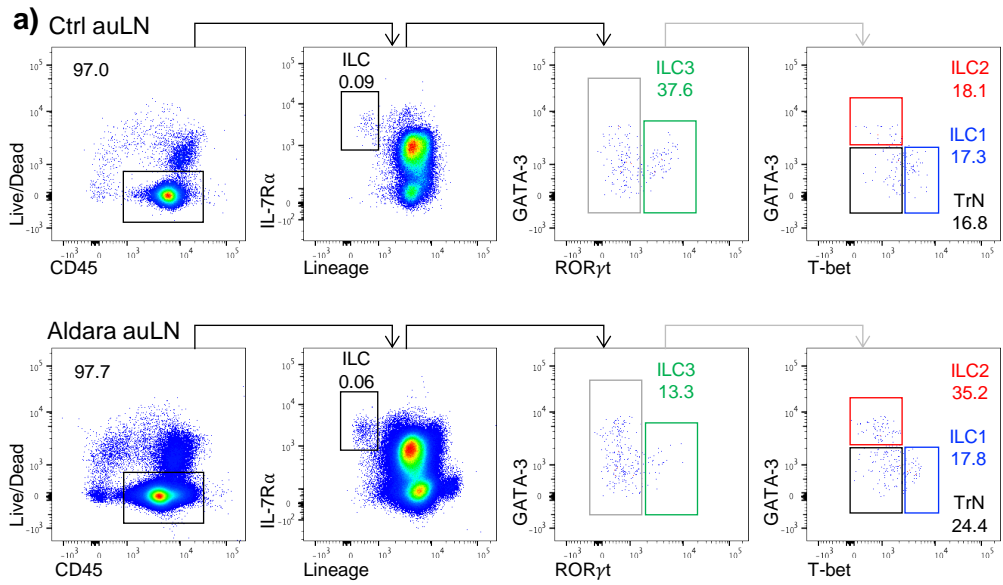
and neutrophils, into the inflamed skin alongside an increase in the proliferation of keratinocytes (381, 382). Upon application of Aldara, keratinocyte cell death is immediately triggered, resulting in the release of IL-1 α , which in turn promotes keratinocyte proliferation as well as the recruitment of neutrophils (383, 384). Through the TLR7 and TLR8, IQM induces IL-23 production via dermal myeloid cells in turn stimulating $\gamma\delta$ T cells proliferation and production of IL-17 and IL-22 (232, 233, 383). These cytokines are important in driving this immune response due to mice deficient in IL-23, IL-22 or IL-17 receptor have a reduction in the development of Aldara driven psoriasis (381, 384). Amongst $\gamma\delta$ T cells production of IL-17 and IL-22, ILC3s have also been observed to contribute to the production of these cytokines in psoriasis via IL-23 stimulation (233). Furthermore, LCs migration from the skin to draining LN, similar to the MC903 driven AD model, has also been recorded within the Aldara model (381, 383, 385). Similar to the AD model Aldara treatment increases the skin inflammation and migration into the LN, however, Aldara treatment drives a type-17 response with the involvement of IL-17 and IL-22 producing ILC3s, compared to the type-2 ILC2 driven MC903 model (112, 231, 233, 381). To establish the psoriasis model, 15 mg of Aldara cream was topically applied to the dorsal and ventral side of the ear for 5 consecutive days (381). Due to not having access to Aldara cream without IQM the controls had nothing applied to their ears. Although a decrease was observed in ILC percentage, similar to the MC903 model, there was an increase in the number of CD45⁺ cells and ILCs within the auLN (Figure 6.15a-c). Interestingly, although ILC3s are involved in the contribution of IL-17 and IL-22 in the Aldara model it was observed that all the ILC subsets are increased in number within the Aldara treated auLN, apart from ILC3s (233). However, ILC3s were reported to be present within the skin of psoriasis models, therefore, this may vary within the draining auLN (233). Overall,

Figure 6.15. Aldara induced psoriasis stimulates an inflammatory response within the auLN

30 mg of Aldara cream was topically applied evenly to the dorsal and ventral sides of the ear on D0-D4, as a control no Aldara was applied (control). Mice were culled on D5, 24 hours post final dose. Cells were isolated from the auLN as described in methods.

Each data point represents 1 auLN from one mouse. Data pooled from a minimum of 2 experiments. Values on flow cytometry plots represent percentages, bars on scatter plots represents the median, which is also shown numerically. Statistical significance was tested using an unpaired, non-parametric, Mann-Whitney two tailed T test: * $p \leq 0.05$, ** $p \leq 0.01$, *** $p \leq 0.001$. ILCs were gated on negatively for iCD3 ϵ (gating strategy not shown).

- a) Representative flow cytometry plots showing Live CD45⁺ cells, ILCs (Live CD45⁺ Lineage⁻ IL-7R α ⁺ iCD3 ϵ ⁻), ILC1s (Live CD45⁺ Lineage⁻ IL-7R α ⁺ iCD3 ϵ ⁻ ROR γ t⁻ GATA-3⁻ T-bet⁺), ILC2s (Live CD45⁺ Lineage⁻ IL-7R α ⁺ iCD3 ϵ ⁻ ROR γ t⁻ GATA-3⁺ T-bet⁻), ILC3s (Live CD45⁺ Lineage⁻ IL-7R α ⁺ iCD3 ϵ ⁻ ROR γ t⁺) and TrN cells (Live CD45⁺ Lineage⁻ IL-7R α ⁺ iCD3 ϵ ⁻ ROR γ t⁻ GATA-3⁻ T-bet⁻) in the auLNs of control (top) and Aldara (bottom) treated mice.
- b) Percentage of Live CD45⁺ cells, ILCs and ILC subsets in the auLNs of control (n=6) and Aldara (n=8) treated mice.
- c) Number (bottom) of Live CD45⁺ cells, ILCs and ILC subsets in the auLNs of control (n=6) and Aldara (n=8) treated mice.



similar to the MC903 model, Aldara application elicits an increase in auLN cellularity suggesting migration from the ear to the auLN.

Leukocyte recruitment, including ILC3s, into the inflamed skin is a hallmark of Aldara driven psoriasis (233, 381). Therefore, ILC subgroups were assessed within the ears of Aldara treated mice. Within the ear there was an increase in the percentage and number of CD45⁺ cells with the Aldara treated mice, accompanied by a decrease in ILC percentage but increase in ILC numbers (Figure 6.16a-c). Through analysis of the ILC subsets, it was clear that the TrN ILC population was the only subset to increase within the Aldara treated ear. This may actually reflect an increase in ILC2s or ILC1s that have down regulated their GATA-3 and T-bet expression due to cell preparation methods, as discussed previously. Interestingly there was no change between the control and Aldara treated mice in the number of ILC3s, with a decrease being observed within the ILC3 percentages. This may be due to previous studies examining ILC3 involvement in psoriasis being conducted in the back skin, rather than the ear, where ILC3s are more numerous (233). Due to the different composition of the back skin it is more likely it has more ILC3s, suggesting why the results may vary within the ear (229, 233). These data show that different locations of skin inflammation may result in a varied response. Although the Aldara model established did not seem to elicit an ILC3 driven response, an increase in ILCs was observed within the auLN and the ear, suggesting that the Aldara model is another inflammation model that can be used to assess migration.

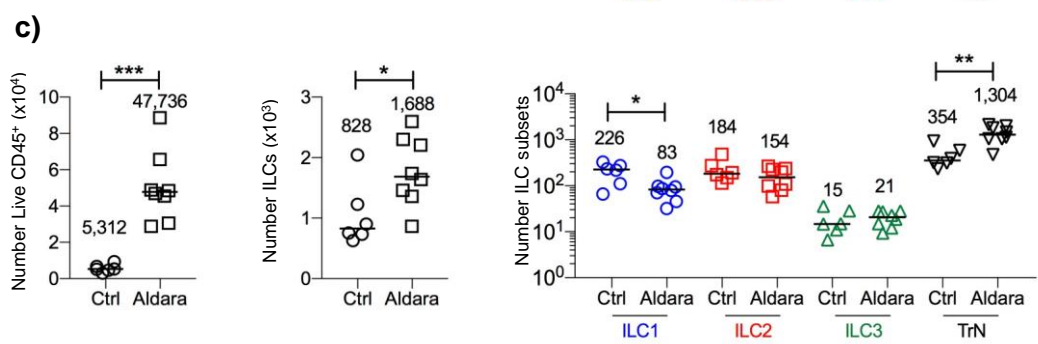
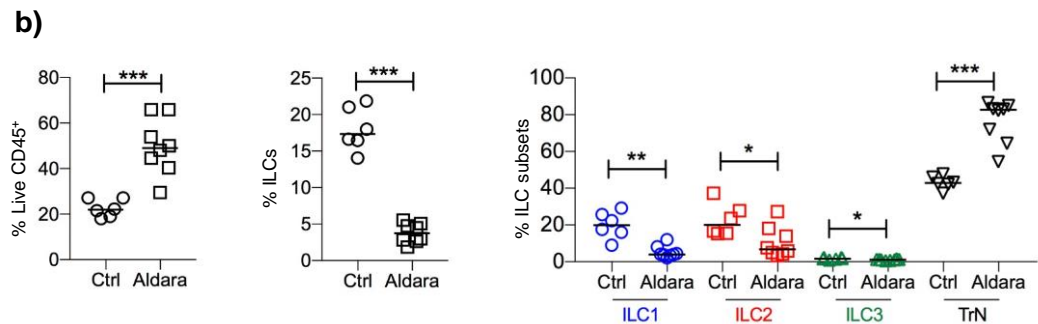
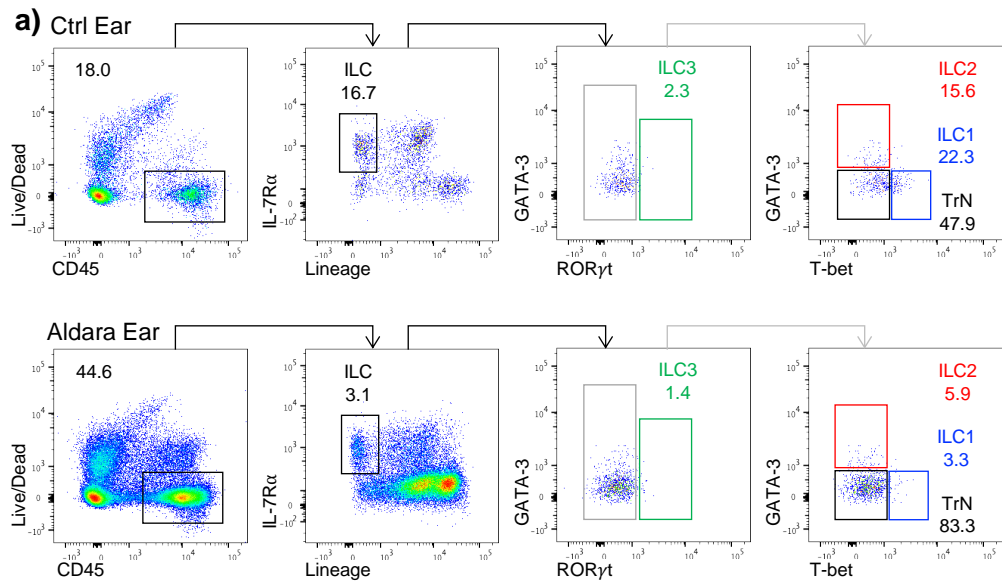
Previous publications assessing the role of ILC3s within the Aldara model studied the response within the back skin (233). However, due to the Kaede model being established to assess migration between the ear and the auLN, although the observed response within the ear was

Figure 6.16. Aldara induced psoriasis stimulates an inflammatory response within the ear

30 mg of Aldara cream was topically applied evenly to the dorsal and ventral sides of the ear on D0-D4, as a control no Aldara was applied (control). Mice were culled on D5, 24 hours post final dose. Cells were isolated from the ears as described in methods.

Each data point represents 1 ear from one mouse. Data pooled from a minimum of 2 experiments. Values on flow cytometry plots represent percentages, bars on scatter plots represents the median, which is also shown numerically. Statistical significance was tested using an unpaired, non-parametric, Mann-Whitney two tailed T test: * $p \leq 0.05$, ** $p \leq 0.01$, *** $p \leq 0.001$. ILCs were gated on negatively for iCD3 ϵ (gating strategy not shown).

- a) Representative flow cytometry plots showing Live CD45⁺ cells, ILCs (Live CD45⁺ Lineage⁻ IL-7R α ⁺ iCD3 ϵ ⁻), ILC1s (Live CD45⁺ Lineage⁻ IL-7R α ⁺ iCD3 ϵ ⁻ ROR γ t⁻ GATA-3⁻ T-bet⁺), ILC2s (Live CD45⁺ Lineage⁻ IL-7R α ⁺ iCD3 ϵ ⁻ ROR γ t⁻ GATA-3⁺ T-bet⁻), ILC3s (Live CD45⁺ Lineage⁻ IL-7R α ⁺ iCD3 ϵ ⁻ ROR γ t⁺) and TrN cells (Live CD45⁺ Lineage⁻ IL-7R α ⁺ iCD3 ϵ ⁻ ROR γ t⁻ GATA-3⁻ T-bet⁻) in the ears of control (top) and Aldara (bottom) treated mice.
- b) Percentage of Live CD45⁺ cells, ILCs and ILC subsets in the ears of control (n=6) and Aldara (n=8) treated mice.
- c) Number of Live CD45⁺ cells, ILCs and ILC subsets in the ears of control (n=6) and Aldara (n=8) treated mice.



not as expected the migration of ILCs was still assessed between the ear and auLN. To determine whether all cells within the ear could be fully photoconverted from Kaede Green to Kaede Red during Aldara application, ears were photoconverted and analysed immediately after no application of Aldara or 2 days post Aldara application. Compared to control mice, it was observed that the 2 day Aldara treated ears had equivalent levels of photoconversion (Figure 6.17a-b). Therefore, the migration of cells within the Aldara model from the ear to auLN and into the ear could be assessed. To this end the Aldara model was combined with the Kaede mice and migration assessed from D2 to D5. Similar to the MC903 model, there was an increase in the number of Kaede Red CD45⁺ cells migrating from the ear to the auLN (Figure 6.17c-d). However, minimal ILC migration was observed, with the Kaede Red ILCs being comparable between the control and Aldara mice (Figure 6.17e-f). This suggests that ILC migration from the ear to the auLN is dependent on the type of immune response. Within the ear a large increase in the number of Kaede Green CD45⁺ cells within Aldara treated mice compared to control mice was observed alongside an increase in the number of Kaede Green migratory ILCs (Figure 6.17g-j). These data further support the ability of ILCs to migrate into inflamed skin, as migration occurs in both the MC903 and the Aldara models. However, migration of ILCs from the ear to the draining auLN seem to be dependent on the specific immune response.

6.2.7 ILC homeostasis is perturbed in *Ccr6*^{-/-} mice

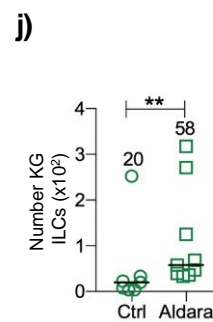
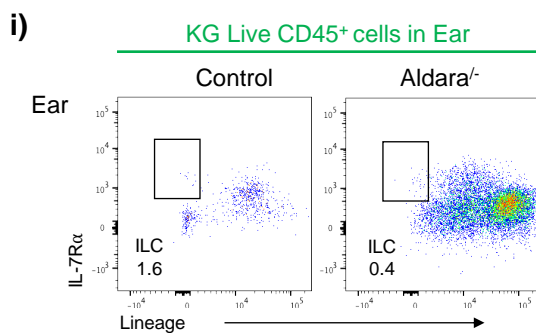
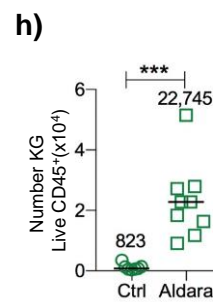
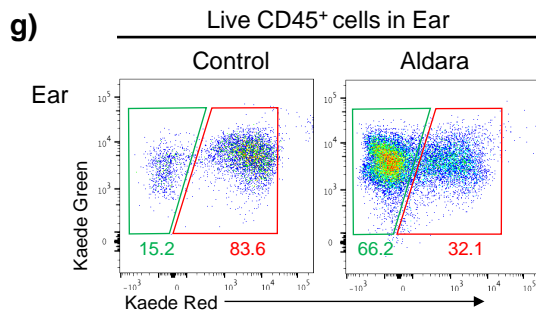
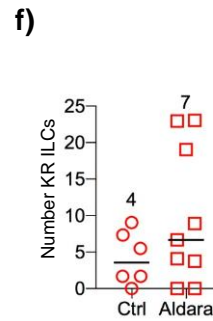
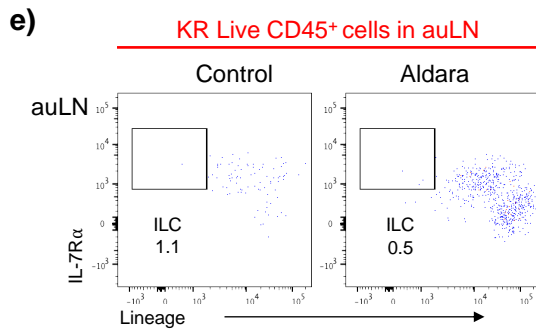
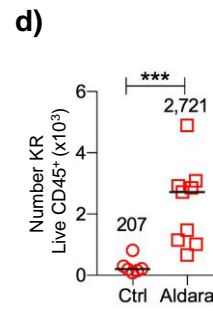
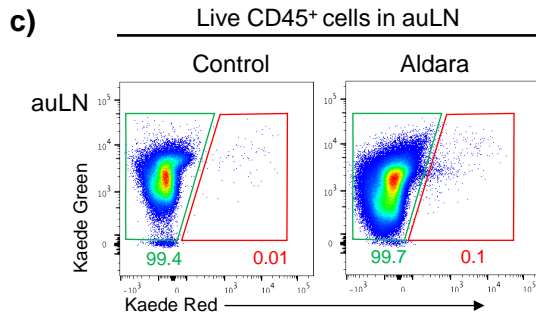
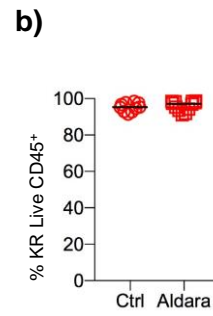
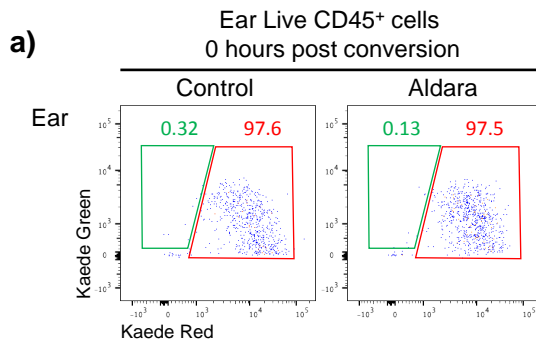
To further elucidate the migratory abilities of ILCs, the mechanisms important in the retention or movement of such cells was investigated. Under inflammatory skin conditions, including AD and psoriasis, epidermal keratinocytes can increase their production of CCL20 resulting in the recruitment of CCR6 expressing cells to the skin, mainly memory and effector T cells

Figure 6.17. ILCs migrate into the inflamed skin of Aldara treated mice

30 mg of Aldara cream was evenly topically applied to the dorsal and ventral sides of the ear on D0-D4, as a control no Aldara was applied (control). Violet light photoconversion of the ear occurred on D2 and mice were culled on D5, 24 hours post final dose. Cells were isolated from the ear and auLN as described in methods.

Each data point represents 1 ear and 1 auLN from one mouse. Data pooled a minimum of 2 experiments. Values on flow cytometry plots represent percentages, bars on scatter plots represents the median, which is also shown numerically. Statistical significance was tested using an unpaired, non-parametric, Mann-Whitney two tailed T test: * $p \leq 0.05$, ** $p \leq 0.01$, *** $p \leq 0.001$. When gating on ILCs lineage markers include; B220, CD11c, CD11b, CD3, CD5, CD19, Ter119, Gr1, F4/80, Fc ϵ RI and F4/80.

- a) Representative flow cytometry plots of Kaede Green and Kaede Red expression of Live CD45⁺ cells 0 hours post violet light photoconversion on untreated ears (control) (left) and D2 of Aldara treated ears (Aldara) (right).
- b) Percentage of Kaede Red Live CD45⁺ cells 0 hours post violet light photoconversion on untreated ears (control) (n=10) and D2 of MC903 treated ears (Aldara) (n=10).
- c) Representative flow cytometry plots showing Kaede Green and Kaede Red expression of Live CD45⁺ cells in the control (left) and Aldara (right) auLN.
- d) Number of Live CD45⁺ Kaede Red cells in the control (n=6) and Aldara (n=9) auLN.
- e) Representative flow cytometry plots showing Kaede Red ILCs (Live CD45⁺ KR⁺ Lineage⁻ IL- 7R α ⁺) in the control (left) and Aldara (right) auLN.
- f) Number of Kaede Red ILCs in the control (n=6) and Aldara (n=9) auLN.
- g) Representative flow cytometry plots showing Kaede Green and Kaede Red expression of Live CD45⁺ cells in the control (left) and Aldara (right) ears.
- h) Number of Live CD45⁺ Kaede Green cells in the control (n=7) and Aldara (n=9) ears.
- i) Representative flow cytometry plots showing Kaede Green ILCs (Live CD45⁺ KG⁺ Lineage⁻ IL-7R α ⁺) in the control (left) and Aldara (right) ears.
- j) Number of Kaede Green ILCs in the control (n=7) and Aldara (n=9) ears.



alongside immature DCs, including LC precursors (386-388). CCL20 is also expressed in the subcapsular sinus of the mLN and PP and is important in the localisation of DCs within the LN (389, 390). It was therefore hypothesised that ILC migration into the inflamed ear skin was dependent upon CCR6:CCL20 interactions. Notably, within the auLN and ear it was observed that a significant proportion of all ILC subsets expressed CCR6, in comparison to other tissues, such as the mLN where only ILC3s expressed CCR6 (Figure 6.18a-d). These data support the contention that ILCs migrate into the inflamed skin in a CCL20-dependent manner.

To investigate the biological function of CCR6 on ILCs *in vivo* the ears and auLN of *Ccr6*^{-/-} mice were compared to WT mice under steady state conditions. Within the auLN, albeit a decrease in the percentage of CD45⁺ cells, the number of CD45⁺ cells and ILCs was comparable between WT and *Ccr6*^{-/-} mice (Figure 6.19a-c). Interestingly, a decrease in the percentage and number of ILC1s and ILC2s was observed, alongside an increase in TrN ILCs. This indicates that the homeostasis of ILCs might be dependent on CCR6 within the auLN. Within the ear, there was an increase in the percentage of CD45⁺ cells, however, the numbers were comparable between mice (Figure 6.20a-c). Furthermore, the proportion and number of ILCs and the individual subsets were comparable between WT and *Ccr6*^{-/-} mice, with a modest increase in percentage of ILC2s within *Ccr6*^{-/-} mice. These results interestingly suggest a dependency on CCR6 for normal ILC homeostasis in the auLN, however not within the ear.

Comparisons between WT and *Ccr6*^{-/-} mice suggested a role for CCR6 in the normal distribution of ILCs within the auLN, but not the ear. Interestingly, perturbations of ILC populations observed within the auLN might suggest a defect in the migration of ILCs from the ear to the draining LN, however it was already established that within these studies ILC

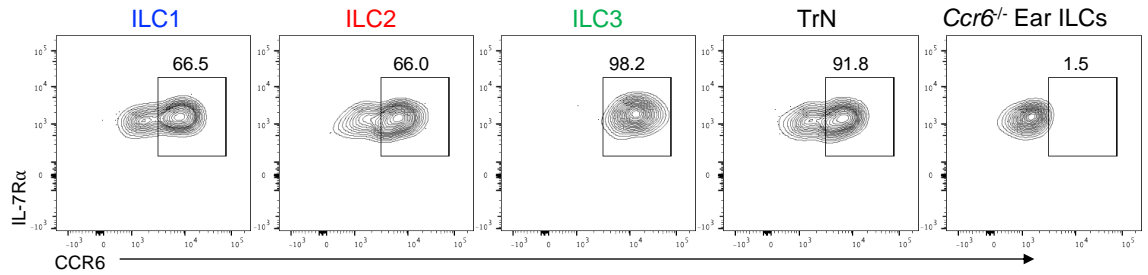
Figure 6.18. CCR6 is expressed on all ILC subsets within the ear and auLN

Cells were isolated from the ear, auLN and mLN of WT and *Ccr6*^{-/-} mice as described in methods.

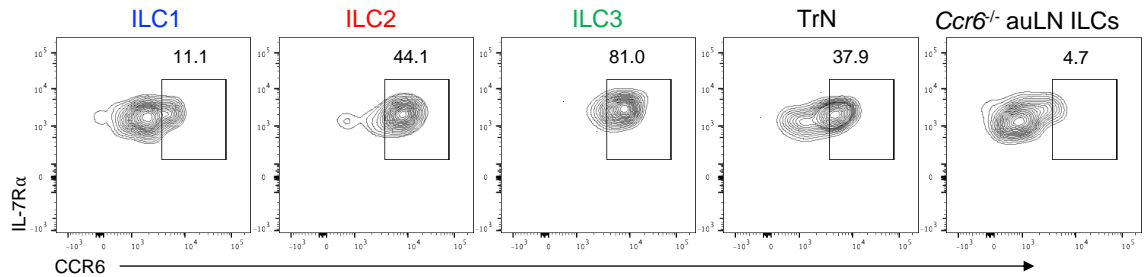
Each data point represents 1 ear, 1 auLN and 1 mLN from one mouse. Data pooled from a minimum of 2 experiments. Values on flow cytometry plots represent percentages, bars on scatter plots represents the median, which is also shown numerically. Statistical significance was tested using an unpaired, non-parametric, Mann-Whitney two tailed T test: *p≤0.05, **p≤0.01, ***p≤0.001. When gating on ILCs lineage markers include; B220, CD11c, CD11b, CD3, CD5, CD19, Ter119, CD123, Gr1, F4/80, FcεRI and F4/80. ILCs were gated on negatively for iCD3ε.

- a) Representative flow cytometry plots showing CCR6 expression on ILC1s (Live CD45⁺ Lineage⁻ IL-7Rα⁺ iCD3ε⁻ RORγt⁻ GATA-3⁻ T-bet⁺), ILC2s (Live CD45⁺ Lineage⁻ IL-7Rα⁺ iCD3ε⁻ RORγt⁻ GATA-3⁺ T-bet⁻), ILC3s (Live CD45⁺ Lineage⁻ IL-7Rα⁺ iCD3ε⁻ RORγt⁺) and TrN ILCs (Live CD45⁺ Lineage⁻ IL-7Rα⁺ iCD3ε⁻ RORγt⁻ GATA-3⁻ T-bet⁻) in the ear of WT mice and *Ccr6*^{-/-} mice (far right) as a gating control.
- b) Representative flow cytometry plots showing CCR6 expression on ILC1s, ILC2s, ILC3s and TrN ILCs in the auLN of WT mice and *Ccr6*^{-/-} mice (far right) as a gating control.
- c) Representative flow cytometry plots showing CCR6 expression on ILC1s, ILC2s, ILC3s and TrN ILCs in the mLN of WT mice.
- d) Percentage of CCR6⁺ ILC1s, ILC2s, ILC3s and TrN ILCs in the ear (n=7) (left), auLN (n=7) (middle) and mLN (n=8) (right).

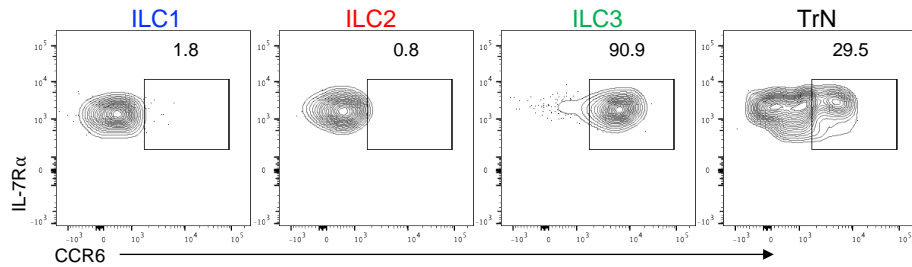
a) WT Ear



b) WT auLN



c) WT mLN



d)

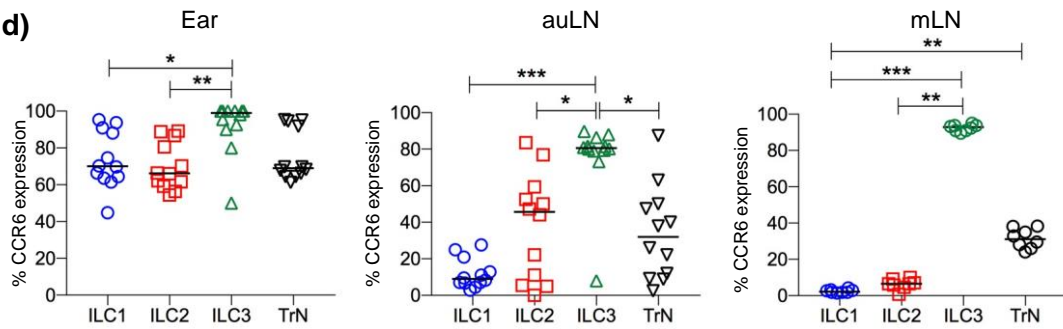


Figure 6.19. ILC1s and ILC2s are deficient in auLN of *Ccr6*^{-/-} mice

Tissues from WT mice were compared to *Ccr6*^{-/-} mice. Cells were isolated from the auLN as described in methods.

Each data point represents 1 auLN from one mouse. Data pooled a minimum of 2 experiments. Values on flow cytometry plots represent percentages, bars on scatter plots represents the median, which is also shown numerically. Statistical significance was tested using an unpaired, non-parametric, Mann-Whitney two tailed T test: *p≤0.05, **p≤0.01, ***p≤0.001. When gating on ILCs lineage markers include; B220, CD11c, CD11b, CD3, CD5, CD19, Ter119, CD123, Gr1, F4/80, FcεRI and F4/80. ILCs were gated on negatively for iCD3ε (gating not shown).

- a) Representative flow cytometry plots showing Live CD45⁺ cells ILCs (Live CD45⁺ Lineage⁻ IL-7Rα⁺ iCD3ε⁻), ILC1s (Live CD45⁺ Lineage⁻ IL-7Rα⁺ iCD3ε⁻ RORγt⁻ GATA-3⁻ T-bet⁺), ILC2s (Live CD45⁺ Lineage⁻ IL-7Rα⁺ iCD3ε⁻ RORγt⁺ GATA-3⁺ T-bet⁻), ILC3s (Live CD45⁺ Lineage⁻ IL-7Rα⁺ iCD3ε⁻ RORγt⁺) and TrN cells (Live CD45⁺ Lineage⁻ IL-7Rα⁺ iCD3ε⁻ RORγt⁻ GATA-3⁻ T-bet⁻) in the auLN of WT (top) and *Ccr6*^{-/-} (bottom) mice.
- b) Percentage of Live CD45⁺ cells, ILCs and ILC subsets in the auLN of WT (n=11) and *Ccr6*^{-/-} (n=12) mice.
- c) Number of Live CD45⁺ cells, ILCs and ILC subsets in the auLN of WT (n=11) and *Ccr6*^{-/-} (n=12) mice. Due to the range of numbers within the data it is presented on a logarithmic scale where values equal to 0 are represented as 1.

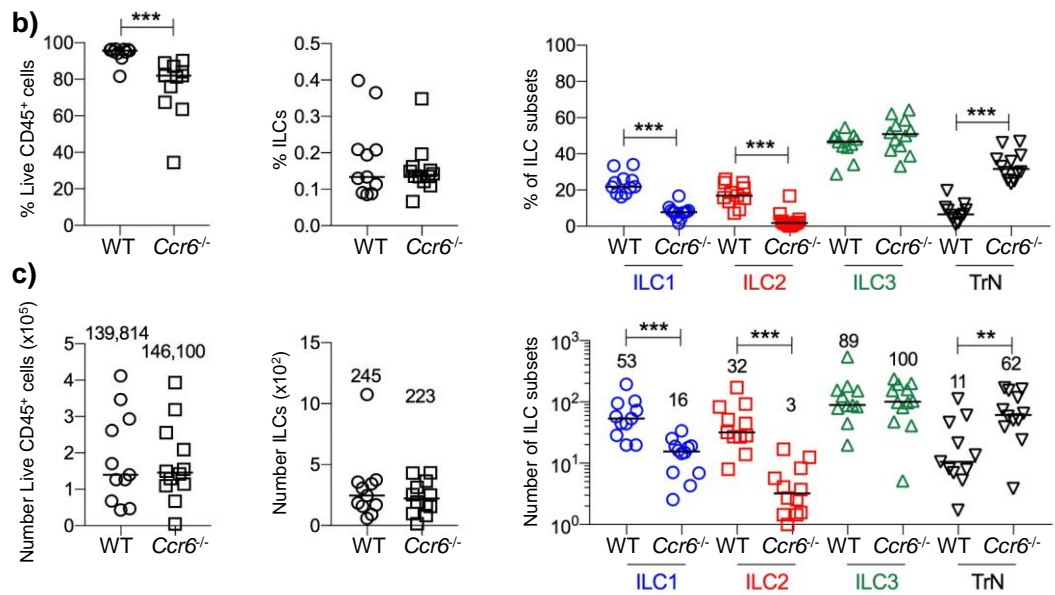
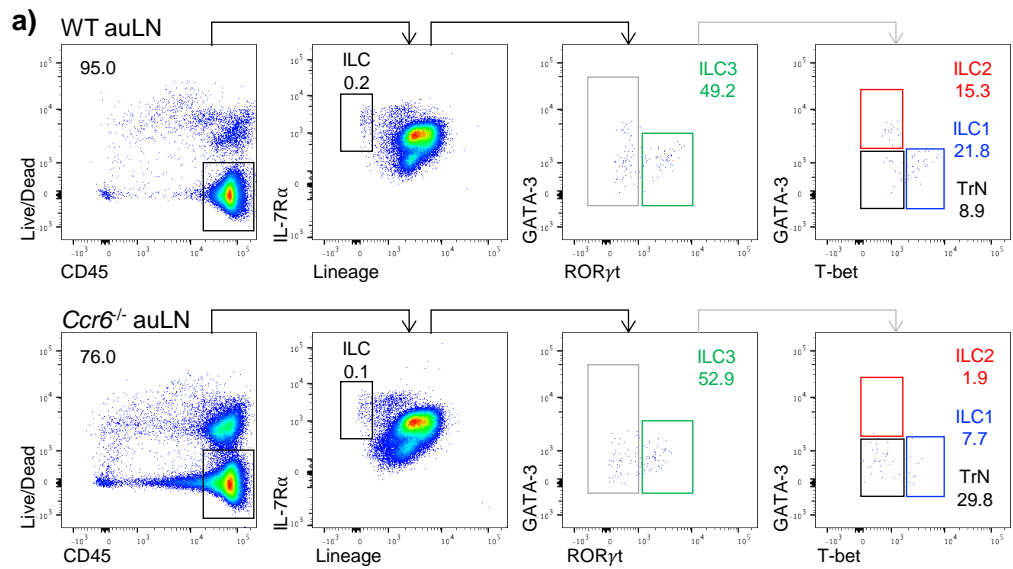
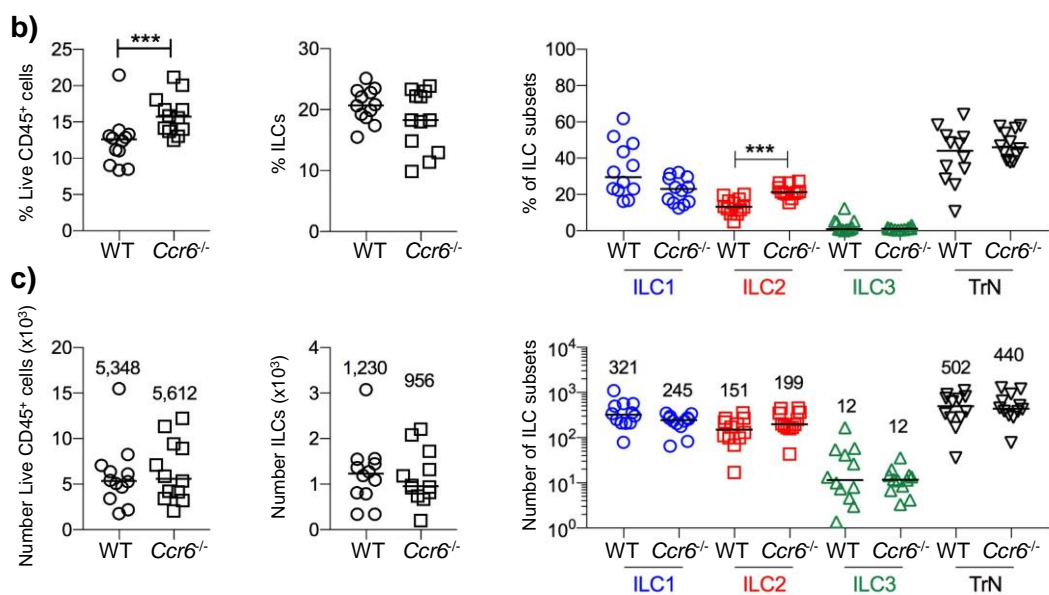
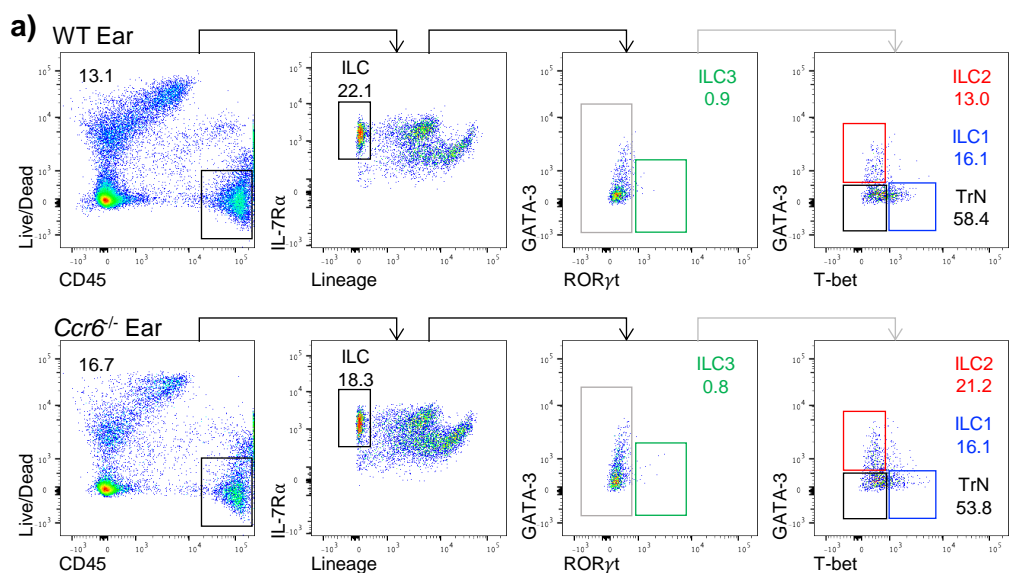


Figure 6.20. ILCs are unchanged within ears of *Ccr6*^{-/-} mice

Tissues from WT mice were compared to *Ccr6*^{-/-} mice. Cells were isolated from the ear as described in methods.

Each data point represents 1 ear from one mouse. Data pooled a minimum of 2 experiments. Values on flow cytometry plots represent percentages, bars on scatter plots represents the median, which is also shown numerically. Statistical significance was tested using an unpaired, non-parametric, Mann-Whitney two tailed T test: *p≤0.05, **p≤0.01, ***p≤0.001. When gating on ILCs lineage markers include; B220, CD11c, CD11b, CD3, CD5, CD19, Ter119, CD123, Gr1, F4/80, FcεRI and F4/80. ILCs were gated on negatively for iCD3ε (gating strategy not shown).

- a) Representative flow cytometry plots showing Live CD45⁺ cells ILCs (Live CD45⁺ Lineage⁻ IL-7Rα⁺ iCD3ε⁻), ILC1s (Live CD45⁺ Lineage⁻ IL-7Rα⁺ iCD3ε⁻ RORγt⁻ GATA-3⁻ T-bet⁺), ILC2s (Live CD45⁺ Lineage⁻ IL-7Rα⁺ iCD3ε⁻ RORγt⁺ GATA-3⁺ T-bet⁻), ILC3s (Live CD45⁺ Lineage⁻ IL-7Rα⁺ iCD3ε⁻ RORγt⁺) and TrN cells (Live CD45⁺ Lineage⁻ IL-7Rα⁺ iCD3ε⁻ RORγt⁻ GATA-3⁻ T-bet⁻) in the ears of WT (top) and *Ccr6*^{-/-} (bottom) mice.
- b) Percentage of Live CD45⁺ cells, ILCs and ILC subsets in the ears of WT (n=12) and *Ccr6*^{-/-} (n=12) mice.
- c) Number of Live CD45⁺ cells, ILCs and ILC subsets in the ears of WT (n=12) and *Ccr6*^{-/-} (n=12) mice.



migration from the ear to auLN under steady state conditions was minimal. Therefore, to determine whether this perturbation in ILCs was important in the development of MC903 AD-like inflammation, the response to MC903 was compared between WT and *Ccr6*^{-/-} mice. In accordance with previous results an increase in the thickening of the ear was observed between WT VC and MC903 treated ears (Figure 6.21a). A similar observation was seen within the *Ccr6*^{-/-} VC and MC903 treated mice, with the WT VC and CCR6 VC alongside the WT MC903 and *Ccr6*^{-/-} MC903 mice being comparable (Figure 6.21a). Confirming the establishment of the MC903 model, an increase in CD45⁺ cell number within the auLN alongside number and percentage within the ear was observed between WT VC and MC903 treated mice (Figure 6.21b-e). Within the auLN the *Ccr6*^{-/-} VC and MC903 treated mice respond similarly to WT mice, with *Ccr6*^{-/-} MC903 mice having an increased CD45⁺ population comparable with WT MC903 treated auLN (Figure 6.21b-c). This suggests that the *Ccr6*^{-/-} auLN is able to mount an equivalent response to WT mice upon MC903 treatment. The ears of *Ccr6*^{-/-} MC903 mice had a comparable number of CD45⁺ cells to CCR6 VC treated mice (Figure 6.21d-e). However, WT MC903 and *Ccr6*^{-/-} MC903 mice were comparable, alongside WT VC and *Ccr6*^{-/-} VC mice (Figure 6.21d). This suggests that there are perturbations in the immune response within the ear of *Ccr6*^{-/-} mice, which were not observed in naïve *Ccr6*^{-/-} mice. However, it is difficult to make clear conclusions from these data. Due to the complex nature of making multiple comparisons simultaneously and the basic question focusing on the difference in immune responses between WT and *Ccr6*^{-/-} mice the data presented hereafter compares WT MC903 mice and *Ccr6*^{-/-} MC903 mice only in order to clearly emphasise the key findings.

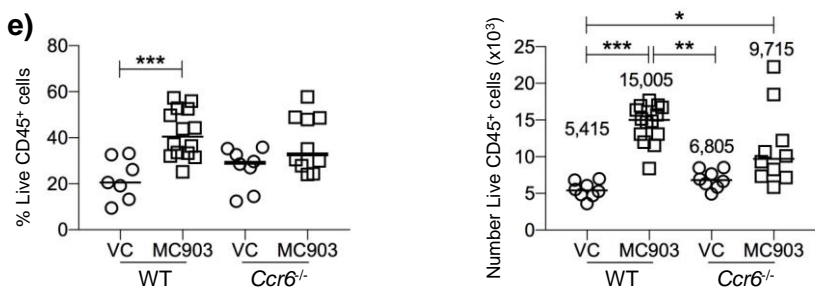
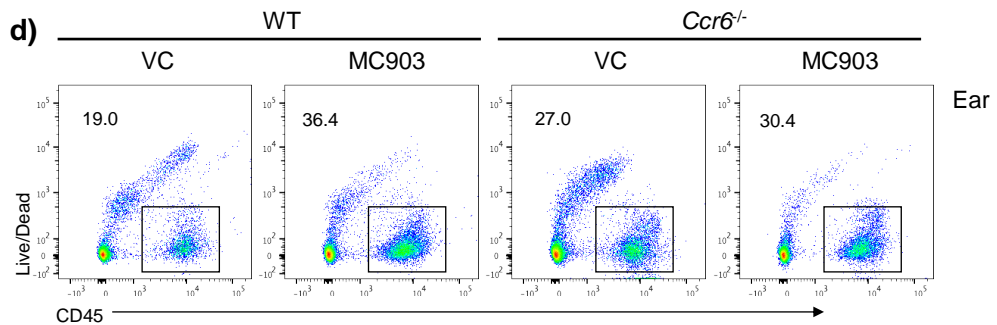
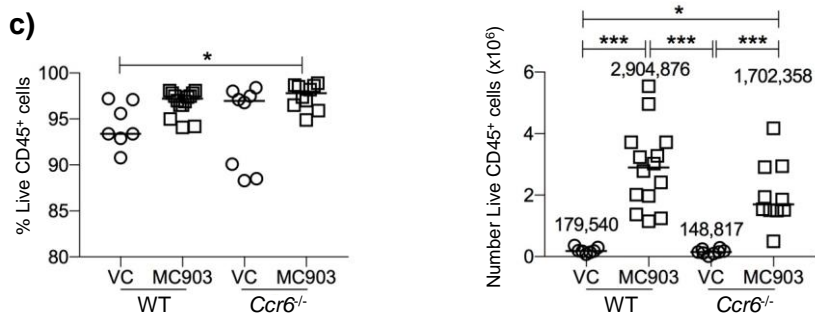
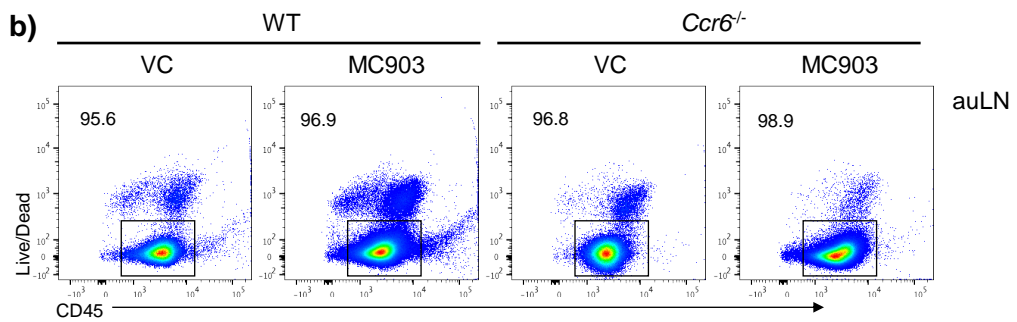
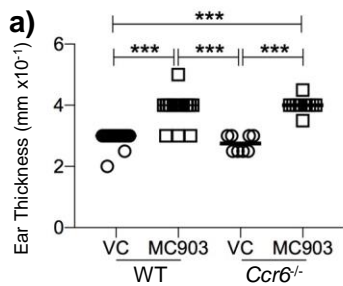
Upon MC903 induced inflammation, the cellularity of the auLN increases in a similar manner to WT mice. In comparison, the ear had a defect in cell expansion. Due to the reduced

Figure 6.21. *Ccr6*^{-/-} mice are unable to elicit a comparable inflammatory response in the ear compared to WT mice

Tissues from WT mice were compared to *Ccr6*^{-/-} mice. 4 nmol of MC903 dissolved in absolute ethanol was topically applied to the dorsal and ventral sides of the ear on D0-D4 (WT MC903 and *Ccr6*^{-/-} MC903), ethanol was applied alone as a VC (WT VC, *Ccr6*^{-/-} VC). Mice were culled on D5, 24 hours post final dose. Cells were isolated from the ear and auLN as described in methods.

Each data point represents 1 ear and 1 auLN from one mouse. Data pooled a minimum of 2 experiments. Values on flow cytometry plots represent percentages, bars on scatter plots represents the median, which is also shown numerically. Statistical significance was tested using Kruskal-Wallis one-way ANOVA with post hoc Dunn's test: *p≤0.05, **p≤0.01, ***p≤0.001.

- a) Thickness of the ears of WT VC (n=15), WT MC903 (n=12), *Ccr6*^{-/-} VC (n=8) and *Ccr6*^{-/-} MC903 (n=10) treated mice.
- b) Representative flow cytometry plots showing Live CD45⁺ cells in the auLN of WT (left) or *Ccr6*^{-/-} (right) mice with VC or MC903 treatment.
- c) Percentage (left) and number (right) of Live CD45⁺ cells in the auLN of WT VC (n=7), WT MC903 (n=14), *Ccr6*^{-/-} VC (n=8) and *Ccr6*^{-/-} MC903 (n=10) treated mice.
- d) Representative flow cytometry plots showing Live CD45⁺ cells in the ear of WT (left) or *Ccr6*^{-/-} (right) mice with VC or MC903 treatment.
- e) Percentage (left) and number (right) of Live CD45⁺ cells in the ears of WT VC (n=7), WT MC903 (n=14), *Ccr6*^{-/-} VC (n=8) and *Ccr6*^{-/-} MC903 (n=10) treated mice.



cellularity of ILC1s and ILC2s within the naïve *Ccr6*^{-/-} auLN, ILC subgroups were further assessed in the MC903 treated mice. Within the auLN, a decrease in the number of ILCs was observed in the *Ccr6*^{-/-} MC903 treated mice. This was due to a decrease in ILC2s which was reflected in percentage and number (Figure 6.22a-c). This suggests that upon MC903 treatment the expansion of ILC2s within the auLN is limited. Focusing within the ear, albeit the percentages of ILCs being comparable between mice, there was a decrease in the number of ILCs within the *Ccr6*^{-/-} treated ear, which is comprised of a decrease in ILC2s, ILC3s and TrN ILCs (Figure 6.23a-c). ILC2s are important in the development of MC903 and as described previously, studies conducted by Kim et al., (2013) have shown that a depletion in ILC2s reduces AD in mice. Therefore, this reduction in ILC2 accumulation within the ear of *Ccr6*^{-/-} MC903 treated suggests that CCR6 is potentially important in the recruitment of ILC2s and therefore the development of AD.

6.2.8 ILCs migrate into the inflamed ear in a CCR6 dependent manner

CCR6:CCL20 interactions are important in the recruitment of T cells and DCs into the ear under inflammatory conditions (386). Furthermore, CCR6 has been shown to be important in the localisation and migration of cells under inflammatory conditions into draining LNs (389, 390). Therefore, the reduction in ILCs within the ear and auLN observed within *Ccr6*^{-/-} MC903 treated mice, compared to WT MC903 treated mice may be due to a reduction in their migration in the absence of CCR6:CCL20 interactions. To address this the MC903 model was combined with WT Kaede and *Ccr6*^{-/-} Kaede mice and cell migration analysed between D2 and D5. Upon assessment of the auLN, the number of Kaede Red CD45⁺ cells, ILCs and T cells migrating from the ear to draining auLN was comparable between the WT Kaede and *Ccr6*^{-/-} Kaede MC903 treated mice (Figure 6.24a-f). However, within the time frame assessed, there

Figure 6.22. *Ccr6*^{-/-} The expansion of ILC2s within the auLN of MC903 treated mice is CCR6 dependent

Tissues from WT mice were compared to *Ccr6*^{-/-} mice. 4 nmol of MC903 dissolved in absolute ethanol was topically applied to the dorsal and ventral sides of the ear on D0-D4 (WT MC903, *Ccr6*^{-/-} MC903). Mice were culled on D5, 24 hours post final dose. Cells were isolated from the auLN as described in methods.

Each data point represents 1 auLN from one mouse. Data pooled a minimum of 2 experiments. Values on flow cytometry plots represent percentages, bars on scatter plots represents the median, which is also shown numerically. Statistical significance was tested using an unpaired, non-parametric, Mann-Whitney two tailed T test: *p≤0.05, **p≤0.01, ***p≤0.001. When gating on ILCs lineage markers include; B220, CD11c, CD11b, CD3, CD5, CD19, Ter119, CD123, Gr1, F4/80, FcεRI and F4/80. ILCs were gated on negatively for iCD3ε.

- a) Representative flow cytometry plots showing ILCs (Live CD45⁺ Lineage⁻ IL-7Rα⁺ iCD3ε⁻), ILC1s (Live CD45⁺ Lineage⁻ IL-7Rα⁺ iCD3ε⁻ RORγt⁻ GATA-3⁻ T-bet⁺), ILC2s (Live CD45⁺ Lineage⁻ IL-7Rα⁺ iCD3ε⁻ RORγt⁺ GATA-3⁺ T-bet⁻), ILC3s (Live CD45⁺ Lineage⁻ IL-7Rα⁺ iCD3ε⁻ RORγt⁺) and TrN cells (Live CD45⁺ Lineage⁻ IL-7Rα⁺ iCD3ε⁻ RORγt⁻ GATA-3⁻ T-bet⁻) in the auLN of WT (top) and *Ccr6*^{-/-} (bottom) MC903 treated mice.
- b) Percentage of ILCs, ILC1s, ILC2s, ILC3s and TrN cells in the auLN of WT (n=14) and *Ccr6*^{-/-} (n=10) MC903 treated mice.
- c) Number of ILCs, ILC1s, ILC2s, ILC3s and TrN cells in the auLN of WT (n=14) and *Ccr6*^{-/-} (n=10) MC903 treated mice.

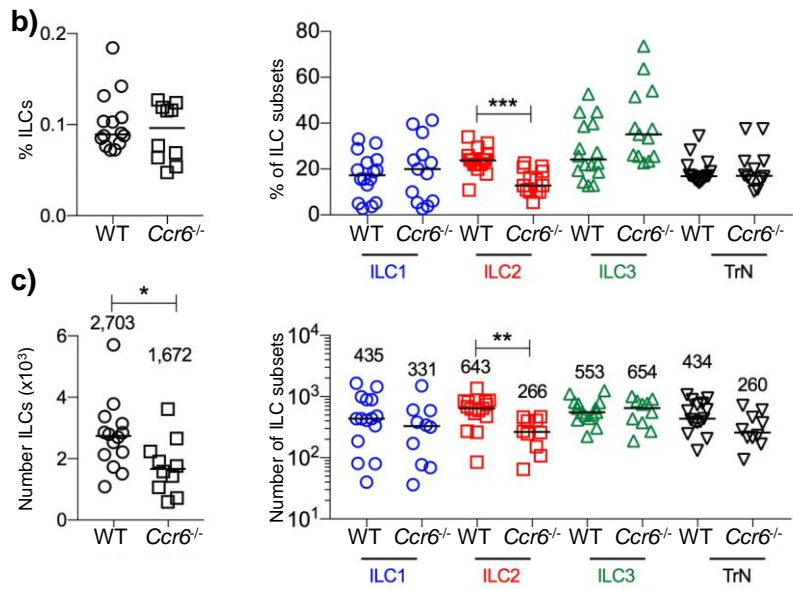
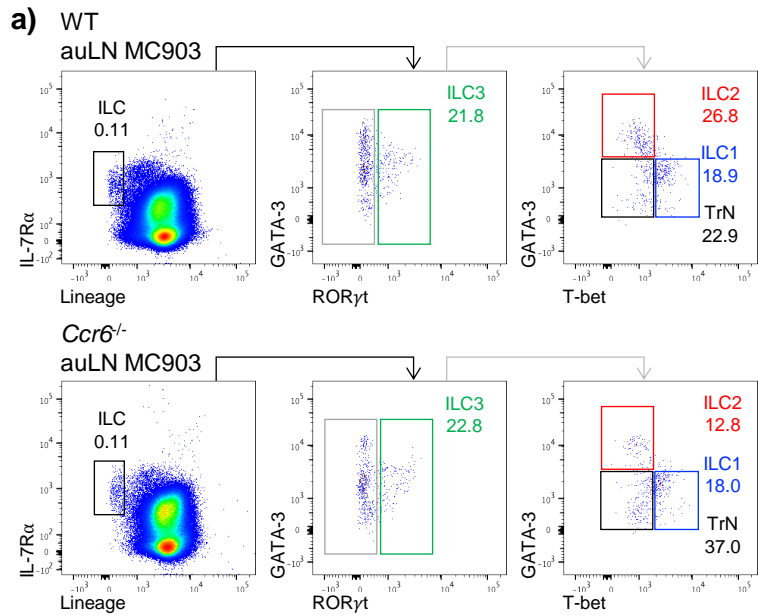


Figure 6.23. The expansion of ILC2s within the ear of MC903 treated mice is CCR6 dependent

Tissues from WT mice were compared to *Ccr6*^{-/-} mice. 4 nmol of MC903 dissolved in absolute ethanol was topically applied to the dorsal and ventral sides of the ear on D0-D4 (WT MC903, *Ccr6*^{-/-} MC903). Mice were culled on D5, 24 hours post final dose. Cells were isolated from the ear as described in methods.

Each data point represents 1 ear from one mouse. Data pooled a minimum of 2 experiments. Values on flow cytometry plots represent percentages, bars on scatter plots represents the median, which is also shown numerically. Statistical significance was tested using an unpaired, non-parametric, Mann-Whitney two tailed T test: * $p \leq 0.05$, ** $p \leq 0.01$, *** $p \leq 0.001$. When gating on ILCs lineage markers include; B220, CD11c, CD11b, CD3, CD5, CD19, Ter119, CD123, Gr1, F4/80, Fc ϵ RI and F4/80. ILCs were gated on negatively for iCD3 ϵ (gating strategy not shown).

- a) Representative flow cytometry plots showing ILCs (Live CD45⁺ Lineage⁻ IL-7R α ⁺ iCD3 ϵ ⁻), ILC1s (Live CD45⁺ Lineage⁻ IL-7R α ⁺ iCD3 ϵ ⁻ ROR γ t⁻ GATA-3⁻ T-bet⁺), ILC2s (Live CD45⁺ Lineage⁻ IL-7R α ⁺ iCD3 ϵ ⁻ ROR γ t⁻ GATA-3⁺ T-bet⁻), ILC3s (Live CD45⁺ Lineage⁻ IL-7R α ⁺ iCD3 ϵ ⁻ ROR γ t⁺) and TrN cells (Live CD45⁺ Lineage⁻ IL-7R α ⁺ iCD3 ϵ ⁻ ROR γ t⁻ GATA-3⁻ T-bet⁻) in the ears of WT (top) and *Ccr6*^{-/-} (bottom) MC903 treated mice.
- b) Percentage (of ILCs, ILC1s, ILC2s, ILC3s and TrN cells in the ears of WT (n=14) and *Ccr6*^{-/-} (n=10) MC903 treated mice.
- c) Number of ILCs, ILC1s, ILC2s, ILC3s and TrN cells in the ears of WT (n=14) and *Ccr6*^{-/-} (n=10) MC903 treated mice.

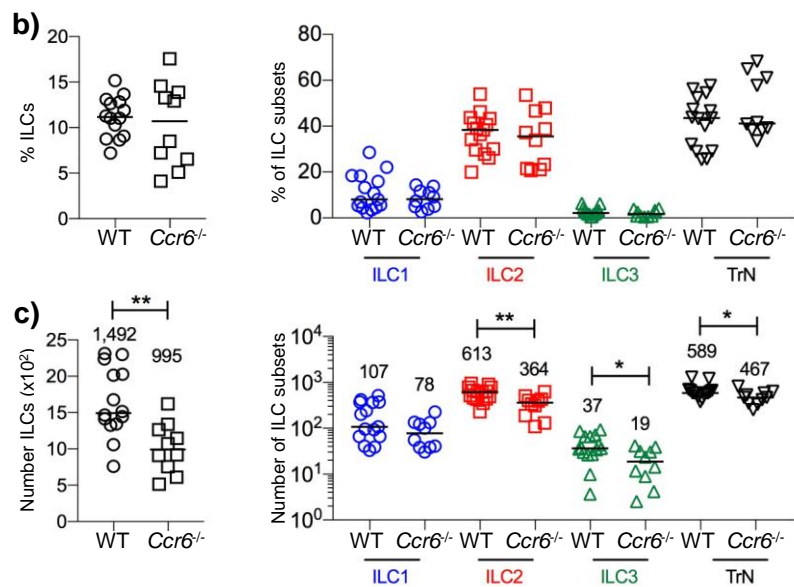
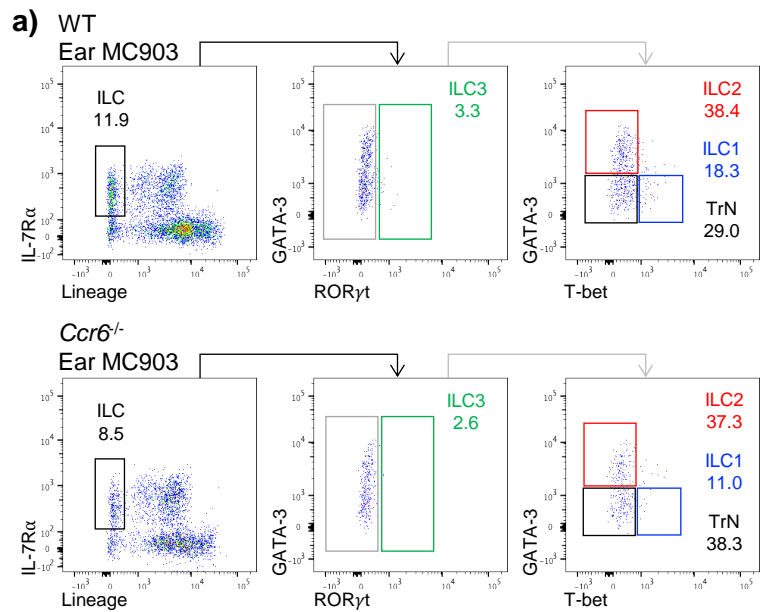
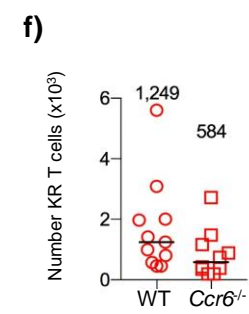
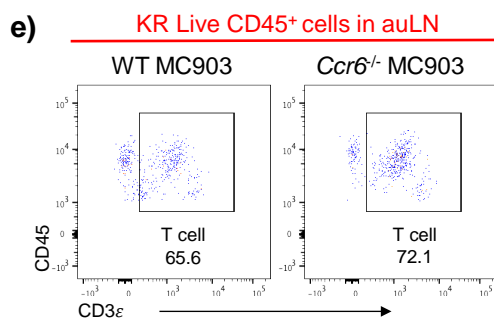
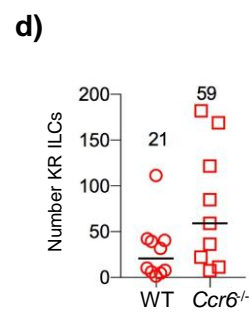
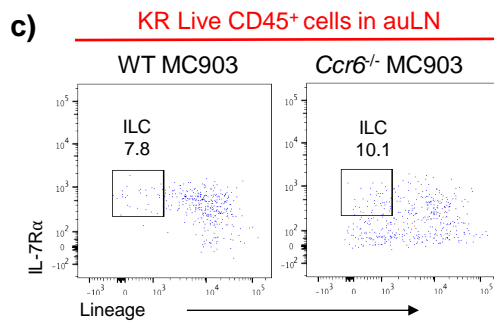
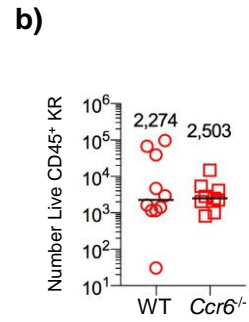
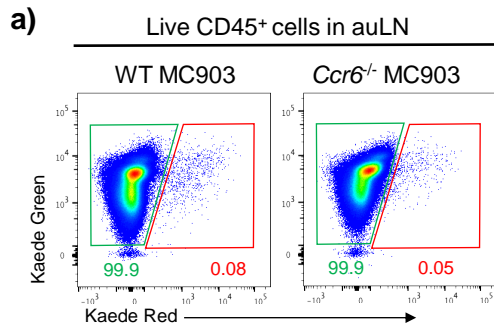


Figure 6.24. ILCs migrate from the inflamed skin into the draining LN independently of CCR6

Tissues from WT Kaede mice were compared to *Ccr6*^{-/-} Kaede mice. 4 nmol of MC903 dissolved in absolute ethanol was topically applied to the dorsal and ventral sides of the ear on D0-D4 (WT MC903, *Ccr6*^{-/-} MC903). Photoconversion of the ear occurred on D2 and mice were culled on D5. Cells were isolated from the ear and auLN as described in methods.

Each data point represents 1 auLN from one mouse. Data pooled a minimum of 2 experiments. Values on flow cytometry plots represent percentages, bars on scatter plots represents the median, which is also shown numerically. Statistical significance was tested using an unpaired, non-parametric, Mann-Whitney two tailed T test: *p≤0.05, **p≤0.01, ***p≤0.001. When gating on ILCs lineage markers include; B220, CD11c, CD11b, CD3, CD5, CD19, Ter119, Gr1, F4/80, FcεRI and F4/80. Populations were previously gated on Live CD45⁺ cells, then identified as Kaede Red, before being identified as a T cell (CD3ε⁺) or ILC (Lineage⁻ IL-7Rα⁺).

- a) Representative flow cytometry plots showing Kaede Green and Kaede Red expression of Live CD45⁺ cells in the auLN of WT (left) and *Ccr6*^{-/-} (right) MC903 treated mice.
- b) Number of Live CD45⁺ Kaede Red cells in auLN of WT (n=10) and *Ccr6*^{-/-} (n=9) MC903 treated mice.
- c) Representative flow cytometry plots showing Kaede Red ILCs in the auLN of WT (left) and *Ccr6*^{-/-} (right) MC903 treated mice.
- d) Number of Kaede Red ILCs in auLN of WT (n=10) and *Ccr6*^{-/-} (n=9) MC903 treated mice.
- e) Representative flow cytometry plots showing Kaede Red T cells in the auLN of WT (left) and *Ccr6*^{-/-} (right) MC903 treated mice.
- f) Number of Kaede Red T cells in the auLN of WT (n=11) and *Ccr6*^{-/-} (n=9) MC903 treated mice.



was a decrease in the number of Kaede Green CD45⁺ cells within the ear of the *Ccr6*^{-/-} Kaede mice compared to the WT Kaede mice and this was similar in the numbers of Kaede Green ILCs (Figure 6.25a-d). Kaede Green T cells, on the other hand, within the ear were comparable in numbers between the two mice (Figure 6.25e-f). This would suggest that ILC recruitment into the MC903 inflamed ear is dependent on CCR6:CCL20 interactions, however these are not required for the migration from the ear into the draining LN.

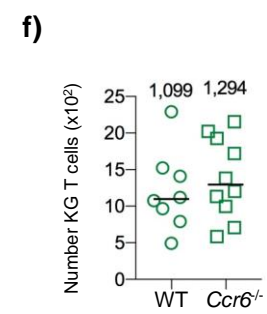
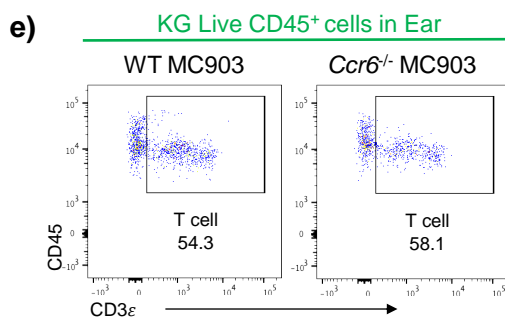
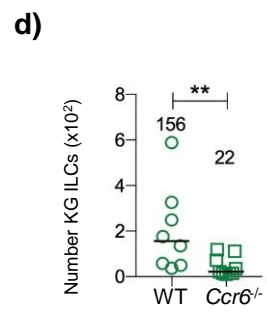
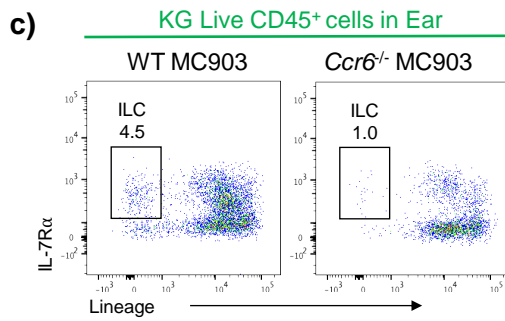
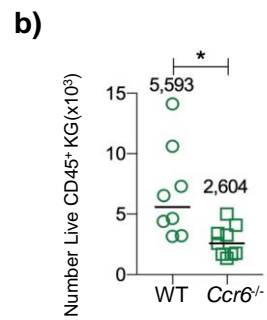
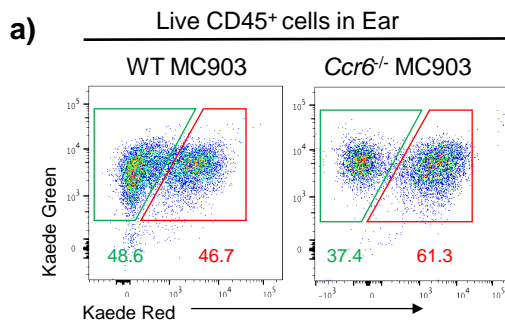
Overall these data have shown that ILCs are able to migrate via the draining lymphatics from the ear skin into the draining auLN under inflammatory conditions. Furthermore, ILCs are recruited into the inflamed ear in a CCR6 dependent manner.

Figure 6.25. The migration of ILCs into inflamed skin is dependent on CCR6

Tissues from WT Kaede mice were compared to *Ccr6*^{-/-} Kaede mice. 4 nmol of MC903 dissolved in absolute ethanol was topically applied to the dorsal and ventral sides of the ear on D0-D4 (WT MC903, *Ccr6*^{-/-} MC903). Photoconversion of the ear occurred on D2 and mice were culled on D5. Cells were isolated from the ear and aLN as described in methods.

Each data point represents 1 ear from one mouse. Data pooled a minimum of 2 experiments. Values on flow cytometry plots represent percentages, bars on scatter plots represents the median, which is also shown numerically. Statistical significance was tested using an unpaired, non-parametric, Mann-Whitney two tailed T test: * $p \leq 0.05$, ** $p \leq 0.01$, *** $p \leq 0.001$. When gating on ILCs lineage markers include; B220, CD11c, CD11b, CD3, CD5, CD19, Ter119, Gr1, F4/80, FcεRI and F4/80. Populations were previously gated on Live CD45⁺ cells, then identified as Kaede Green, before being identified as a T cell (CD3ε⁺) or ILC (Lineage⁻ IL-7Rα⁺).

- a) Representative flow cytometry plots showing Kaede Green and Kaede Red expression of Live CD45⁺ cells in the ear of WT (left) and *Ccr6*^{-/-} (right) MC903 treated mice.
- b) Number of Live CD45⁺ Kaede Green cells in the ear of WT (n=8) and *Ccr6*^{-/-} (n=9) MC903 treated mice.
- c) Representative flow cytometry plots showing Kaede Green ILCs in the ear of WT (left) and *Ccr6*^{-/-} (right) MC903 treated mice.
- d) Number of Kaede Green ILCs in the ear of WT (n=8) and *Ccr6*^{-/-} (n=9) MC903 treated mice.
- e) Representative flow cytometry plots showing Kaede Green T cells in the ear of WT (left) and *Ccr6*^{-/-} (right) MC903 treated mice.
- f) Number of Kaede Green T cells in the ear of WT (n=8) and *Ccr6*^{-/-} (n=10) MC903 treated mice.



6.3 SUMMARY

In this chapter Kaede mice were used to dissect the migration of ILCs and other immune populations between the ear and its draining LN. Under steady state, migration of ILCs from the ear to the draining LN is undetectable in comparison to T cells and LCs, however a clear but modest ILC population can be identified moving into the ear. To determine whether ILC migration was affected under inflammatory conditions, skin inflammation models were established resulting in an increased number of ILCs within the draining auLN and were therefore useful in the assessment of ILC migration. The number of ILCs tracked migrating from the ear to the auLN were significant but not equivalent to the increase in numbers observed within the auLN. Therefore, proliferation of ILCs was assessed and it was concluded to be an important factor in the increase of ILCs within the auLN. Alongside proliferation, blocking S1P dependent migration of ILCs suggested that ILCs S1P dependent tissue egress was important in contributing to increase in numbers of ILC3s within the auLN. Upon assessing Kaede Green cells within the inflamed ear, it was determined that ILCs were also able to migrate into the inflamed skin, from the periphery. After exploring the migratory properties of ILCs, the mechanism of migration was also studied. Through the use of *Ccr6*^{-/-} and *Ccr6*^{-/-} Kaede mice it was discovered that the increase in ILC numbers under skin inflammation within the ear and auLN was dependent on CCR6 expression. However, only ILC migration into the ear was directly dependent on CCR6. In summary, the data presented here shows that under skin inflammation ILCs are able to migrate from the ear into the auLN, alongside ILC proliferation and accumulation from the periphery contributing to the increase in ILCs within the auLN. Furthermore, ILC migration into inflamed skin occurs in a CCR6 dependent manner, unlike ILC migration into the auLN.

Direct assessment of migration *in vivo* through photoconversion of the whole ear from Kaede Green to Kaede Red formed the basis of these experiments, enabling the migratory kinetics of ILCs within the skin and draining LN to be assessed. Based on previous reports by Strid et al., assessment of IL-13 production by T cells 2 hours post violet light exposure concluded that the method of photoconversion had not elicited immediate damage to the ear (340). Therefore, migration could be assessed under steady state conditions. However, studies conducted by Strid et al., analysed IL-13 mRNA rather than protein expression (340). Therefore, it is possible that exposure to violet light has resulted in undetected damage. Further hallmarks of violet light skin damage, that could have been assessed, include epidermal hyperplasia, thickening of the stratum corneum and keratinocyte proliferation (363). Despite not exploring these specific effects, upon comparing migration between the 'steady state' and MC903 model, which causes overt damage to the skin, a much larger migration of hematopoietic cells was detected in the damage model. This suggests that the lack of overt migration in the 'steady state' model is consistent with minimal damage due to the lack of a substantial recruitment of cells one might expect with skin damage.

The inflammatory response elicited by the MC903 model within the ear and draining auLN resulted in an increased migration of ILCs from the ear to the auLN. As discussed, it was clear that the migration of ILCs from the ear was not the sole contributing factor to the large increase in ILC numbers within the auLN of MC903 treated mice. ILC proliferation was also shown to contribute to the expansion of ILCs within the auLN, via increased levels of Ki-67 expression. However, this is one method of identifying proliferating cells and further experiments such as using *in vivo* bromodeoxyuridine (BRDU) incorporation would need to be conducted to support these findings. As shown, ILC proliferation within the auLN increases

within the MC903 model, however, these data do not define which population of ILCs are proliferating. ILCs could potentially migrate into the auLN from the ear and then undergo proliferation. DCs traffic to the draining LN to stimulate the maturation and proliferation of effector Th2 cells within the MC903 model, it is therefore possible they interact with ILCs stimulating their proliferation, however ILCs may also respond to soluble factors arriving within the LN or produced from other cells (391). If Kaede Red migratory ILCs, entering the auLN from the ear, underwent rapid proliferation within the LN they would lose their Kaede Red expression and be identified as Kaede Green. Therefore, it is possible that ILC migration is underestimated within these data. ILC migration is only assessed within these experiments from the inflamed ear to the draining auLN, however, it was clear that after MC903 application, grooming lead to the spreading of MC903 to both ears and to the head. The observation of a Kaede Red hematopoietic population migrating from the head skin to the auLN shows that other regions of inflamed skin also drain to the auLN contributing to the expansion of hematopoietic cells in the auLN. If only the ear was photoconverted then migration from other areas of skin wouldn't be detected, indicating ILC migration from the skin was underestimated. To combat this, upon ear MC903 application, the ear and the head skin could be photoconverted simultaneously to visualise ILC migration to the auLN from a larger area of skin.

ILC3 accumulation within the MC903 treated auLN was decreased under S1P dependent egress block. This suggest that ILC3s are able to egress from tissues, including peripheral LNs, and travel through the blood and accumulate within the inflamed auLN. No affects were observed on any other ILC population, indicating that ILCs main mechanism for expansion within the MC903 treated auLN is via proliferation. However, FTY720, as previously discussed,

does not block all S1PRs. Within the bLN experiments it was clear that not all ILC migration had been prevented by FTY720 administration, with the presence of Kaede Green ILCs migrating into the bLN, suggesting that within these experiments all ILC migration may not be blocked under FTY720 administration. Further experiments with the administration of substances that block all S1P receptors would be useful in determining whether ILCs migrate into and accumulate within the inflamed auLN.

Within this investigation ILCs are observed to migrate into the ear and from the ear to the auLN under inflammatory conditions of AD, however, what functions or roles do these migratory ILCs have? Kim et al., reports that in AD ears ILC2s produce IL-5 and IL-13 contributing to type 2 inflammation within the skin (112). However, the reason for increased ILC migration into auLN is less understood. ILCs may potentially become activated within the LN and contribute to cytokine production or provide survival signals to T cells, potentially skewing their differentiation, as previously discussed. ILCs may also provide survival signals for themselves, for example ICOS:ICOSL interactions between ILC2s supports ILC2 survival and cytokine production within the lung (262). Furthermore, MHCII expressing ILC2s and ILC3s are able to process and present antigen, suggesting that ILCs may have a role in the transportation of antigen from skin to draining LN and activation of naïve T cells, similar to DCs (163, 164). However, the understanding of *in vivo* ILC antigen uptake is limited and robust experiments would be needed to further test this.

Migration into the ear under MC903 induced inflammation partly originated from adjacent skin, including the head skin. However, this contribution is very small and mainly just consists of $\gamma\delta$ T cells. Effector and memory T cells are known to recirculate through the lymphatics and

the blood to lymphoid and non-lymphoid tissue (35, 392). It is therefore possible that the influx of T cells may originate from other LNs. Similar to T cells, ILCs egress from the LN and have the ability to recirculate to contralateral draining LNs. Therefore, ILCs may be able to exit the LN and recirculate into non-lymphoid tissue, suggesting that peripheral LNs may be a source of migratory ILCs entering the ear. Interestingly ILCs have been shown to migrate from skin draining LNs into the skin upon activation and CCR10 upregulation (226). It would therefore be interesting to assess ILC migration from the auLN to the ear, however, due to the location of the auLN near the throat, the surgical procedure required to expose the LN for photoconversion would be too hazardous for the mouse. A method where surgery was not required could be developed with the correct light source photoconverting the auLN through the skin. Furthermore, upon inflammation within the skin, immature LCs are recruited from the BM to replace LCs that have migrated to the draining LN, suggesting another potential mechanism of ILC entry into the ear (387). With experiments conducted using a BM chimera with allotype marked BM and sublethal irradiation, the question could be asked whether the populations in the skin and auLN contained anything from the new BM, suggesting migration.

ILC migration was assessed as a whole population when analysing migration between the ear and auLN. Within the bLN, cell surface markers were used to identify the individual ILC subgroups migrating within the Kaede mice. Unfortunately, identification of ILCs without the use of TFs was unable to be established within the ear, partly due to the ear digestion process effecting surface protein expression, and therefore tracking of ILC subsets from the ear to auLN was not possible. It would have been interesting to determine whether the migratory properties of ILC2s were different within the inflamed ear skin, compared to the bLN. In the peripheral LNs ILC2s were identified as a mainly tissue-resident population, however, the

MC903 model drives type-2 inflammation and the recruitment of ILC2s, potentially meaning under inflammatory conditions ILC2s may be able to migrate. This was supported by Huang et al., who observed minimal migration of ILC2s within the steady state, however, upon IL-25 stimulation or helminth infection a clear migratory ILC2 population was identified (254).

The data here strongly suggests that CCR6 is important for the migration of ILCs into the inflamed ear skin. The reduction of Kaede Green ILCs within the ear in the absence of CCR6, a chemokine receptor important in cell migration, further supports that ILCs are truly migratory, rather than a proliferating resident population. The ILC subset reduced within the inflamed ears of *Ccr6*^{-/-} mice was ILC2s, therefore the dominant population migrating into the ear in a CCR6 dependent manner may be ILC2s. The decrease in ILC2s within the MC903 treated ears and auLNs of *Ccr6*^{-/-} mice may in turn lead to protection against the development of AD. AD lesions and scabbing can be observed within the ears of mice treated with AD for up to 17 days. Increasing the duration of MC903 application may determine whether these symptoms are clearly reduced in *Ccr6*^{-/-} mice. To further determine whether this is due to a reduction in ILC recruitment CCR6 could be conditionally knocked out of ILCs, or more specifically ILC2s. As discussed previously, it is believed that ILC migration into the auLN from the skin is underestimated with potential migration of hematopoietic cells from the surrounding areas of skin. It would therefore be interesting to determine whether migration from different areas of skin into the auLN was dependent on CCR6. This could be conducted by converting different segments of skin, such as the head skin, and observing the migration of ILCs from the selected area to the auLN compared between WT and *Ccr6*^{-/-} mice.

The ability of ILCs to migrate into the inflamed ear skin, which was initially observed within the MC903 model, was further supported by an increase in ILC migration into the ears of the Aldara mice. Time permitting, the confirmation of a true migratory ILC population within the Aldara ears, rather than a rapid proliferating resident ILC population would have been assessed. Within the Aldara model, reports have published the VC in which the IQM is transported in may contribute to the pathogenesis of psoriasis (383). Therefore, using Aldara cream excluding the IQM would have been a more suitable control.

Tomura et al established through the use of a skin irritant applied to the abdominal skin of Kaede mice that LC migration from the skin to the draining LN does not increase over a 4 day period, instead dermal DC migration is the main population of migratory DCs (247). However, this contradicts other reports showing that LC migration from inflamed skin to draining LN is paramount in the cross presentation of processed antigen and therefore activation of naïve T cells (366, 368, 393). This is demonstrated in the MC903 model where the depletion of LCs shows a defect in the development of AD-like symptoms (366). This investigation showed that LC migration into the auLN does increase upon ear inflammation, supporting the increased migratory properties of LCs over a 5 day period. The difference in skin irritants used, time periods observed, with dermal DC migration into the LN peaking at 24 hours and LCs at 4 days post skin irritant application, and areas of skin assessed may elude to the varying results of LC migration (247, 365).

T cell migration into the skin is unaffected within *Ccr6*^{-/-} Kaede mice, although publications report this migration to be CCR6 dependent (386). This may due be to other mechanisms contributing to T cell recruitment into the ear overriding the deficiency of CCR6 dependent

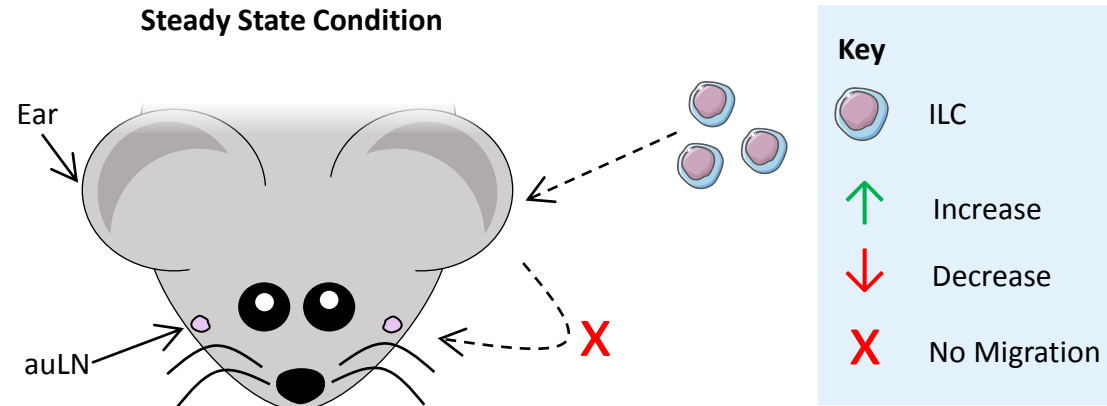
migration. For example, memory T cells recirculating within the blood express the skin homing receptor CCR10 (392, 394). CCL27, the ligand for CCR10, is produced by keratinocytes within naïve skin and is upregulated in inflammatory conditions such as AD and psoriasis (394, 395). However, effector T cells infiltrate inflamed skin in a CCR10 independent manner (394). This suggests different mechanisms controlling the recruitment of T cells into the MC903 treated ear suggesting why T cell migration into the ear isn't disturbed in *Ccr6*^{-/-} Kaede mice. It would have therefore been interesting to investigate ILC and T cell migration in MC903 treated *Ccr10*^{-/-} Kaede mice, focusing on identifying naïve, effector and memory T cell subsets. Regarding comparable numbers of migrating hematopoietic cells between WT and *Ccr6*^{-/-} auLN of MC903 treated mice, CCL20 expression was only previously assessed in gut draining LNs, rather than peripheral skin draining LNs. It would therefore be interesting to investigate the expression of CCL20 within the skin draining LNs, or to again examine a different migratory mechanism such as CCR7 dependent migration.

These findings, summarised in Figure 6.26, support that ILCs are not a solely tissue-resident population and are able to drain through the lymphatics into the auLN from the ear skin under inflammatory conditions. Furthermore, ILCs are able to migrate into the inflamed ear in a CCR6 dependent manner.

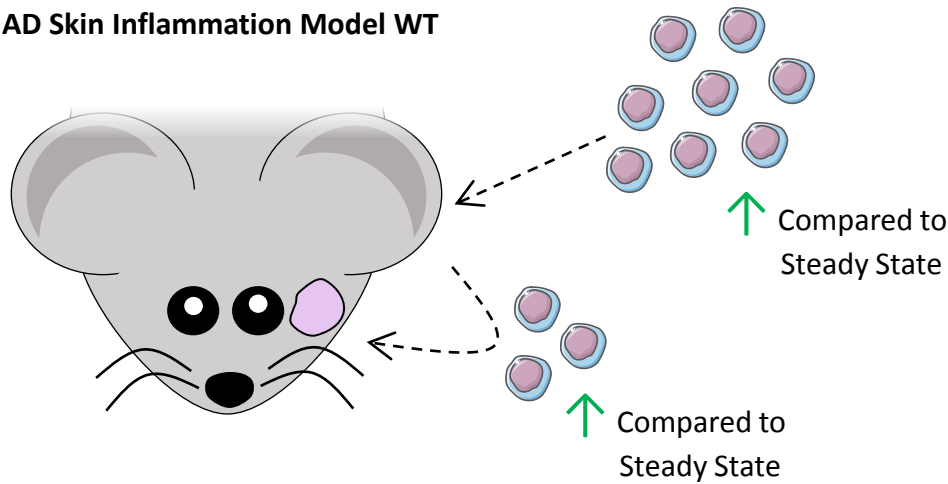
Figure 6.26. Summary Diagram of ILC migration between the skin and draining LN

Under steady state conditions there was a presence of a small migratory population of ILCs migrating into the ear, however, migration from the ear to draining auLN was undetectable. Under the AD-like skin inflammatory model, established via MC903 application for 5 days, ILC migration into the ear increased and a population of ILCs could now be observed to migrate from the ear into the draining auLN. ILCs were shown to migrate into the ear in a CCR6 dependent mechanism, through the use of *Ccr6*^{-/-} mice, whereas ILC migration into the auLN was independent of this mechanism.

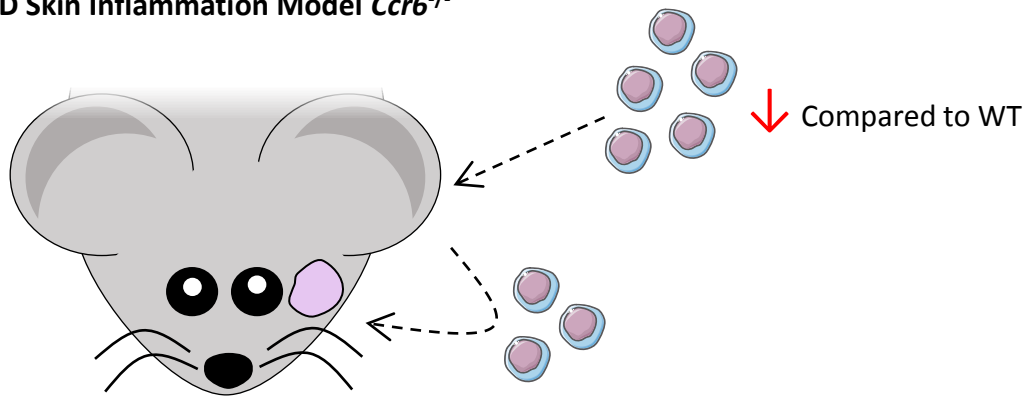
ILC Migration between Skin and Draining LN



AD Skin Inflammation Model WT



AD Skin Inflammation Model *Ccr6*^{-/-}



Chapter 7. DISCUSSION

This project aimed to develop a better understanding of the relationship between ILCs located within lymphoid and non-lymphoid tissues. Through these studies ILC populations have been characterised within different anatomical compartments. This reveals a simple approach to identify ILCs without the reliance of surface markers, which show substantial variation depending on location. Using this identification method, the requirement of ICOS:ICOSL interactions in ILC biology was assessed, testing the effect on ILCs of a classic co-stimulatory interaction that regulates the behaviour of B and T cells. The lack of any clear evidence for a role for ICOS:ICOSL in the development and maintenance of ILCs led to a change in direction of the projects aims, prompting the investigation of whether ILCs are able to migrate between barrier sites and SLTs. Currently this is a poorly understood facet of ILC biology with important implications for their function. Photoconvertible Kaede mice were used to clearly show, for the first time, the presence of a migratory population of ILCs traveling through the blood and lymphatics to peripheral LNs. Collectively these studies have revealed several important new aspects of ILC biology, supporting studies of ILCs by other researchers.

7.1 ILCs ARE DISTRIBUTED THROUGHOUT LYMPHOID AND NON-LYMPHOID TISSUES

ILCs are a population of innate cells that are similar to Th cells in their cytokine production and TF expression, however, they belong to the innate side of the immune system. They are located within non-lymphoid and lymphoid tissue around the body, being more abundant at barrier sites such as the SI LP, lung and skin compared to SLTs such as LNs. Through the use of a simple but robust staining panel, ILCs were detected across lymphoid and non-lymphoid tissues with the proportions of ILC subgroups being distributed differently in various tissues,

reflecting tissue specific functions. Using a consistent method to compare ILC subgroups across the analysed tissues revealed that not all ILC2s share the same phenotype. Markers that are commonly used to identify ILC2s were not found to be expressed in certain tissues. A robust method for the identification of ILCs that can be used across tissues is required due to the frequency of ILCs varying within the tissues. This establishes them as a separate population from T cells and other common innate cells. Key to this was a suitable lineage dump channel enabling a clear population of ILCs to be identified within most tissues, consistent with them being a separate population from other established cell types.

7.1.1 TF are a useful tool in the efficient identification of ILC subsets

Within the field, rapid progress has been made in identifying the different functions of ILCs within a variety of tissues, based on the expression of specific surface markers. This makes it difficult to keep up to date with varying phenotypes used to identify different subgroups, within various tissues under certain conditions. This has led to a variety of proposed methods in identifying ILCs and their subsets across different tissues, complicating the identification of ILC subsets. It is therefore important within the field that there is a consistent identification method for ILC subsets, to enable a better understanding of their function and their relationships between different tissues. TF staining is a robust method in identifying ILC1s, ILC2s and ILC3, through the use of T-bet, GATA-3 and ROR γ t (28). Furthermore, the TFs T-bet, EOMES and ROR γ t are a more reliable method of separately identifying IFN- γ producing ILCs such as ILC1s, cNK cells and NCR⁺ ILC3s, where they share surface markers such as NK1.1, Nkp46 and CD49b (27, 130, 135). However, staining for TFs may not always be the most appropriate method of identification, depending on the tissue being analysed and the

experiments being conducted. ILCs are a rare population in some tissues, such as the human blood. Where tissues contain low frequencies of ILCs, the process of fixation and permeabilisation can substantially reduce the cell yield obtained due to longer protocols having increased cell loss. This low frequency of ILCs can be combated by merging samples, which may be more appropriate for murine experiments rather than human. Furthermore, if the experiment conducted requires the cells to remain viable, or their cell membrane to remain intact, for example cell sorting or analysing Kaede expressing cells, then staining for TFs would not be appropriate. Under these circumstances surface markers are more suitable, however, as shown within Chapter 3, surface markers are not a consistent method for identifying ILC subsets between tissues. When surface markers need to be used as a method of ILC subset identification, initially confirming the identification of the subset through TF staining and then assessing the surface marker expression is an appropriate method to use. Subsequently, upon assessing the appropriate surface markers, ILCs can be identified without the use of TFs, as shown in Chapter 5.

7.1.2 The digestion protocol affects the identification of ILC subsets

Although ILC subset identification is best achieved through the use of TFs, the digestion protocol, as well as affecting cell surface markers, also affects the expression of TFs. Previous publications have reported the loss of surface proteins due to different digestion protocols, however, it was slightly surprising when TF expression was also observed to be affected (266). These data clearly showed a reduction in the expression of T-bet and GATA-3 under a harsher digestion protocol, potentially reflecting the 'wellbeing' of the cells after an extensive digestion protocol. The importance of understanding the effect of different enzymes, incubation periods and temperatures on the cells being analysed, is key in the correct

identification of any population. Certain digestion protocols may skew the identification of different subsets by affecting key proteins used in their analysis. For example, CD4 and CD8 expression is lost under a longer digestion with a higher enzymatic concentration, affecting T cell subset identification. This may potentially lead to the misidentification of a population or the increased presence of a population that does not fit into the current literature, such as the TrN ILCs described here. The TrN ILC population was shown to have similarities with the ILC population beyond just being identified within the Lineage⁻ IL-7R α ⁺ gating. This suggests that they were potentially a new subset of ILCs not currently classified within the normal nomenclature. However, due to the digestion protocol directly affecting the number of TrN ILCs, it was a concern that this population was mainly comprised of ILC1s and ILC2s, that had lost either T-bet or GATA-3 expression, respectively. Further phenotyping of this TrN ILC population may help in identifying the proportional contribution of ILC1s and ILC2s that have just lost their TF expression due to the digestion protocol. The lack of knowledge regarding the phenotype of TrN ILCs makes it difficult to separate them from ILC subsets that have downregulated TFs. Culturing single cell suspensions, post digestion, may revive TFs or surface proteins expression which may have been lost due to the stressful conditions of a harsher digestion protocol. CD90 expression could also be assessed to further clarify their identification as an ILC population, alongside observing whether they are present within *Rag*^{-/-} and *Rag*^{-/-} γ C^{-/-} mice, which lack all ILCs.

In conclusion digestion protocols and phenotypic markers vary between sites and clearly understanding these variations is key in obtaining a robust population for the correct analysis. This is of great importance when comparing populations across different tissues, which have different digestion protocols.

7.2 ICOS EXPRESSION IS NOT REQUIRED FOR ILC MAINTENANCE UNDER STEADY STATE CONDITIONS

ILC2s and ILC3s have been shown to interact with T cells, via presentation of antigen via MHCII, contributing to the regulation of the adaptive immune response (114, 162, 164). Co-stimulatory molecules are important in facilitating these interactions, with it being suggested that the presence or absence of the co-stimulatory molecules CD80 and CD86, can affect whether ILC3s are able to stimulate or inhibit T cell activation (114, 162). However, data on the role of co-stimulatory molecules in ILC biology was limited, particularly when this study was started. ILCs have been described to express ICOS, ICOSL, OX40L, programmed cell death-1 (PD-1), CD80 and CD86. These co-stimulatory molecules may aid ILC interactions with T cells or be important in T cell independent ILC functions (25, 114, 164, 262, 396, 397). Upon commencing this investigation co-stimulatory molecules role in ILC biology was still unclear, compared with T cell biology where their function is well documented. Within these studies the role of the co-stimulatory molecule ICOS was chosen to be analysed on ILCs due to it being highly expressed on ILC2s. At the time, ICOS expression had also been detected on ILC3s lab unpublished (Withers lab unpublished observations). Thus, it was interesting to use ICOS:ICOSL interactions as a model of co-stimulation which was hypothesised to be important in ILC biology.

7.2.1 Differences in mouse biology as a result of differing animal facilities

Within Chapter 4 it was concluded that the development and maintenance of ILCs was not dependent on ICOS:ICOSL interactions. This was controversial compared to publications by Paclik et al., who determined that ICOS is required for the expansion of ILC2s under steady state conditions (306). Differing results between these two studies may be explained by the

differences in animal facilities. One factor which differs between mice, even within the same facility, is their microbiota (307). ILCs are efficient at sensing the environment and responding to signals that reflect the microbiome state and composition, such as NCR⁺ ILC3s within the gut, and therefore changes in the microbiota may affect their homeostasis (162). Studies have focused specifically on the effect of the gut microbiota on many different biological factors including digestion, obesity and the immune system (308, 398). Even though mice may be genetically identical, gut microbiota, which is influenced by a variety of factors, may differ between mice in different facilities, in turn effecting animal health and potentially experimental results (307). For example, mice with different diets and therefore microbiota, respond differently to induced inflammatory diseases, such as dextran sodium sulphate induced colitis, with altered diets abrogating the disease (399). Therefore, variations in husbandry related factors such as diet, cleaning, handling and circadian cycles will result in differentiation between the gut microbiota and in turn, potentially affect the biology of the mouse including their immune system (307, 399-402). Different murine strains and suppliers will also have a different microbiota composition, which was shown to affect the ability of professional APCs to induce T cell responses (309, 403). This may specifically effect experiments if comparing inbred mice with out-sourced genetically modified mice.

7.2.2 Publication of negative results is required within the scientific field

Within Chapter 4 ICOS:ICOSL interactions were suggested to be redundant within the maintenance and development of ILCs under steady state conditions. Although these data are not necessarily of high impact, their results are still relevant within ILC research. Chapter 3 contained a large amount of data characterising ILCs within different tissues. This robust data, whilst descriptive in nature, makes a useful contribution to the field, serving as a resource to

others, particularly people new to studying ILCs. The publication of negative data is important in streamlining and aiding future work within different groups, preventing the repetition of experiments that may show redundant functions of certain molecules.

7.2.3 Co-stimulatory molecules are required for ILC function

Combining the results from this investigation alongside the publications by Paclik et al., and Maazi et al., suggests that there is redundancy of co-stimulatory molecules expressed on ILCs under certain conditions and that other environmental stimuli may affect this. There may be roles for different co-stimulatory molecules in specific situations in which they should facilitate certain interactions between cells. It can be difficult to tease apart the importance of these co-stimulatory molecules on ILCs when other more dominant populations also express the same molecule. Conditional knock out mice would help, however, currently within the ILC field there is a lack of robust and specific ILC knock outs.

Other co-stimulatory molecules that have been explored on ILCs includes PD-1, another member of the CD28 family. PD-1, which bind to its ligands PD ligand-1 (PDL-1) and PDL-2, is expressed on activated T cells and signalling through PD-1:PDL interactions prevents T cell proliferation and induces Treg development (404-406). This is a similar mechanism by which ILCs are regulated by PD-1. KLRG1⁺ ILC2s express PD-1 and through the use of anti-PD-1 or genetically modified mice lacking PD-1, Taylor et al., showed that in the absence of PD-1:PDL interactions, KLRG1⁺ ILC2s were increased in number and their function enhanced (407). Clinical studies are currently working on PD-1 as an immunotherapy target, due to tumours, viruses and bacteria being able to evade the host immune response through manipulating the PD-1 pathway (408-410). Together, these studies suggest that co-stimulatory molecules as

well as regulating T cell responses are important in the regulation of ILC populations, with the potential of being an immunological target in cancer therapies.

Overall, the differences in mouse gut microbiota can affect the immune response and therefore analysis of immune populations within the assessed mice. Understanding these changes and adapting experiments to minimise these differences, may help in reducing variations across publications. For example the gut microbiota can be normalised after accommodation in a new housing facility, therefore, leaving new bought strains to acclimatise minimises gut flora variation (411). Furthermore, when analysing the function of a molecule on a cellular population, assessing its role under different conditions is important in observing its true function, as protein interactions may have specific roles under different conditions.

7.3 ILCs MIGRATE UNDER STEADY STATE CONDITIONS IN PERIPHERAL LNS

The continued exploration in the literature, focusing on the role of ICOS and ICOSL on ILCs under inflammatory conditions and the reduced impact on continuing this line of research, the focus of these studies was changed. Instead, the challenging and novel question of the relationship between ILCs within non-lymphoid tissue barrier sites and SLTs was pursued. Due to the availability of photoconvertible Kaede mice, in which *in vivo* cell migration can be directly tracked and other work in the lab utilising these mice to assess T cell residency, it was considered that the migration of ILCs between these two sites could be uniquely explored. During these studies a 6 month placement at MedImmune drove an interest in understanding the role of ILCs within ear skin and their relationship with the draining peripheral LN, particularly when inflammation was induced. Within the literature, parabiotic mice had recently been used to establish that ILCs were a tissue-resident population. However,

analysing migration within the peripheral LN of Kaede mice was believed to be able to address different questions which were not answered within the parabiotic models (248, 249). Two models were then established to track ILC migration within peripheral LNs. Initially the bLN model, which would be able to track cell migration into and out of the LN, and then the ear and auLN model, which was able to directly track migration of ILCs into the ear and from the ear to the auLN via the draining lymphatics.

Establishment of the bLN Kaede model enabled simple questions to be answered concerning ILC movement within LN, such as their ability to enter or egress and the mechanisms behind this. ILCs were discovered to not comprise solely of a tissue-resident population, with migration being observed into and out of the LN under steady state conditions. Migration into the LN was dependent on CCR7, and ILC1s seemed to be entering from the blood, suggested by their dual expression of CCR7 and CD62L. ILC egress from the LN was also detected and shown to be dependent on the S1P gradient between the LN and the efferent lymphatic vessel. ILC migration was tracked to recirculate through the blood into contralateral LNs, suggesting they are able to re-enter secondary LNs, upon egress of a primary LN. However, this model alone was unable to sufficiently answer whether ILCs were able to migrate between non-lymphoid and lymphoid tissues via draining lymphatics. Therefore, the ear and auLN Kaede model was used to assess ILC migration from skin to the draining peripheral LN, which was observed to be limited. Together these models suggest a migratory population of ILCs that are able to enter into and egress from peripheral LNs.

7.3.1 ILC1s possess similarities in migratory properties to cNK cells

Initial experiments clearly identified that ILC populations within the bLN change over time, highly suggestive of migration. ILCs however, had only been assessed as a whole population, therefore, the migratory properties of individual ILC subsets needed to be assessed. This key experiment identified ILC1s as the most migratory ILC subset within the bLN. ILC1s are closely related to the migratory population of cNK cells, with both subgroups being dependent on T-bet expression, sharing the expression of NCRs and being able to produce IFN- γ and TNF- α (272). Therefore, the two populations migratory abilities were compared. Both populations express CD62L and CCR7 within the blood and were shown to recirculate through contralateral LNs (116). This indicated that ILC1s were similar to cNK cells in their ability to migrate within the blood and recirculate through SLT, suggesting that they may also have functional and behavioural similarities in ability in scanning SLT (115-117). Furthermore, although the migratory abilities of cNK cells through the blood have been explored before, this assessment of cNK cell migration was new data directly assessing their ability to recirculate, for which the Kaede model was required. Lucas et al., have shown that cNK cells recirculating SLTs are able to be primed within LNs, via DCs, and re-enter the blood with enhanced effector function (346). This suggests that if ILC1 migrate in a similar manner to cNK cells, then they may also be primed within LNs. Therefore, the assessment of activation markers on migratory ILC1s compared to tissue-resident ILC1s would be interesting to compare. These studies conducted by Lucas et al., gated on cNK cells as NK1.1⁺ CD3⁻, which does not specifically exclude ILC1s from this analysis, suggesting that part of this cNK cell priming may also include ILC1s (346).

cNK cells are also able to migrate through the blood into non-lymphoid tissues such as the gut, however, Gasteiger et al., showed that ILC1s did not possess the ability to do this (249).

Migratory cNK cells, within human blood, can be subdivided into two groups based on their migratory abilities. CD161⁺ cNK cells express chemokine receptors similar to neutrophils, suggesting their migration may be directed to acute inflammatory barrier sites (251). This is in comparison with CD161⁻ cNK cells, which express molecules important in trafficking into LNs, such as CCR7 and CD62L (251). ILC1s may be more similar to the CD161⁻ cNK cell population, as they only seem to be able to migrate into SLTs and not non-lymphoid tissues. However, these studies were conducted across human and murine samples and further studies would needed to be conducted to clarify similarities between subgroups (251).

Tissue-resident NK (trNK) cells have been identified within the liver, thymus, uterus and skin as a separate subset to cNK cells (412). Although ILC1s are the most migratory population of ILCs, they still contain a resident population alongside the migratory cells within the peripheral LN. This may suggest that ILC1s and potentially other ILC subsets, may specifically consist of subsets that are able to migrate and others that are permanently resident, similar to NK cells. Detailed analysis of trNK cells compared to cNK cells, has revealed a variety of differences between the two populations, including their abilities to produce larger amounts TNF- α and IFN- γ , respectively (412). Further differences in their NCR expression, cytotoxic abilities and TF expression, varies across trNK cells resident in different tissues, suggesting that trNK cells have tissue specific functions (413). ILC1s have also been identified with varying phenotypes within the salivary gland, liver and gut (135). This further supports previous data that ILCs phenotypes are not consistent across tissues and that TFs are a more robust method in analysing ILC subgroups. It may therefore be suggested that a migratory population of ILC1s exist, similar to cNK cells, alongside a population of tissue-resident ILC1s, in which the

phenotype varies depending on the tissue they reside in, similar to trNK cells. Assessing tissue-resident ILC1s over a longer time frame than 72 hours would be useful in confirming that they are a long term resident population.

Within this investigation, the identification of ILC1s within the bLN Kaede model does not exclude the potential to contain ex-ILC3s, which conceivably may possess distinct migratory properties. Indeed, the differences if any between ILC1 and ex-ILC3 remains poorly understood. It would therefore be interesting to observe the migratory abilities of ex-ILC3s to determine whether they acquire a more migratory phenotype, or whether they become part of the tissue-resident ILC population. Unfortunately, due to the fate mapping RORc cre mice using a fluorochrome that is already used within the Kaede mice, these mice could not be crossed and fate mapped and the migration of ex-ILC3s analysed.

ILCs migrate into the bLN in a CCR7 dependent manner, however, it was not made clear by these studies whether ILCs migration into the LN depended on CCR7 directly, or on other CCR7 dependent cells. This dependency may also change under certain inflammatory models. For example, under steady state conditions cNK cell migration into SLT is dependent on CCR7, whereas in activated LNs CCR7 becomes redundant and cNK cells migrate into the LN in a CXCR3 dependent manner(116). This may, however, be specific to the type of infection. Studies examining the migratory properties of ILC1s in Kaede mice, under steady state, or inflammatory conditions would be important in further understanding of the biological similarities and differences between ILC1s and cNK cells.

cNK cell egress from the LN is dependent on the expression of S1PR5 (326). Within these experiments FTY720 was used to block S1PR, however, FTY720 does not have a strong affinity

to S1PR2 or S1PR5 (254, 261, 344). The migratory population of ILCs observed to still be entering the bLN under FTY720 block, may be comprised of ILC1s which egress from previous tissues in an S1PR5 dependent manner, similar to cNK cells. S1PR5 expression on cNK cells is directly regulated by T-bet, with mice deficient in T-bet having reduced levels of S1PR5 and in turn accumulating within the BM and LNs (344). This direct link between T-bet and S1PR5 further suggests that ILC1s may be able to migrate within an S1PR5 dependent manner, which was not blocked in the experiments conducted within this investigation.

cNK cells are able to be recruited from the blood and migrate into draining activated LNs producing IFN- γ necessary for Th1 cell differentiation (116). Due to migratory ILC1s sharing similarities with cNK cells they may also be able to contribute to the polarisation of Th cell development in a similar manner. To explore this, Kaede mice could be immunised and the ability of migratory ILC1s, compared to tissue-resident ILC1s to produce the cytokines such as IFN- γ and TNF- α to be assessed. Therefore, understanding the migratory properties of ILCs within peripheral LNs may lead to a clearer understanding of their function within SLTs. These data suggest that ILC1s are migratory under steady state and that they may actively seek out infected cells, in a similar manner to cNK cells.

7.3.2 ILC2s and ILC3s are mainly tissue-resident under steady state

In comparison to naïve T cells and cNK cells, the helper ILC population clearly has a larger proportion of tissue-resident cells over the time frame analysed. This population is mainly comprised of ILC2s and ILC3s. Parabiotic mice established for 3 months and 8 months have been used to show that under steady state conditions ILC2 migration occurs but is minimal and the biological relevance was questioned (249, 254). Similar to these parabiotic

experiments, ILC2s within the peripheral LN are comprised of a larger tissue-resident population than migratory. This was, however, only observed over a 72 hour period and longer time frame would be needed to determine long term residency. A recent publication has shown that an inflammatory subset of ILC2s possess the ability to migrate from the gut into tissues such as the lung, spleen and mLN under IL-25 stimulation or helminth infection through the use of parabiotic mice (254). This suggests that at least some ILC2s within the assessed peripheral tissues, may possess the ability to migrate under certain conditions, but that under steady state conditions they are mainly a tissue-resident population. Huang et al., show that iILC2 propagation from the gut may occur due to iILC2s not being present within the lung and mLN (108, 254). iILC2s can specifically provide quick sources of IL-13 compared to resident ILC2 populations, which are slower at cytokine production, to help combat infections (108, 254). This therefore possibility that the peripheral LN may mainly contain tissue-resident ILC2s and that under certain inflammatory conditions iILC2s may specifically need to be recruited from other tissues into the LN. It would be interesting to assess ILC migration in peripheral LNs when mice were infected with different helminths, to determine if this changed ILC2 migration and more specifically which ILC2 populations.

Parabiotic mice have also been used to show that ILC3s are mainly tissue-resident under steady state conditions, more so than ILC2s (249, 254). Within the peripheral LNs ILC3s migratory abilities seemed to be similar to ILC2s, with a predominant ILC3 resident population within the bLN. Again, the time frame in which migration was assessed is a limitation in confidently defining Kaede Red ILC3s as permanently resident. Preliminary unpublished data within the lab has analysed the composition of ILCs within the bLN of Kaede mice 1 week after exposure, and observed a similar 50:50 ratio of Kaede Green to Kaede Red expression (Withers

Lab Unpublished Observations). Recent publications using Dendra mice have defined $\gamma\delta$ T cells as resident after observing their retention within the LN over a 4 week period (350). Using these mice and analysing tissue residency after a similar time frame would help to determine whether 'resident' ILCs are a long term tissue-resident population. Within embryonic development ILC3s, mainly LTi cells, are paramount in providing $LT\alpha_1\beta_2$ signals for the development and maturation of LNs (111, 137, 414). The ILC3 population within adult LNs is mainly comprised of LTi-like cells, which are closely linked to the repair and maintenance of SLTs (244, 245). IL-7 promotes ILC3s in their ability to maintain the function of LNs, enabling normal T and B cell ingress (245). Stromal cells, such as LECs, have been shown to be an important source of IL-7, specifically in the remodelling of the LN after infection (415). Furthermore, within the adult ILC3s colocalise with specific stromal cells called marginal reticular cells, forming a particular niche for ILC3s (285). This close relationship of ILC3s with stromal cells within the developing LN, may be maintained within adult life, suggesting why ILC3s are mainly tissue-resident within the peripheral LN under steady state conditions. However, the data presented in Chapter 5 indicates that ILC3s are not solely tissue-resident and do contain a smaller migratory population. The studies of Mackley et al., supports the migratory properties of LTi-like cells from the gut to the draining mLN (243). This migration was assessed under a laparotomy and the labelling required substantial handling of the intestine tissue (243). This is an invasive procedure, potentially resulting in tissue damage and therefore increasing migration into the draining mLN (243). Overall, assessing the migration of ILC1s, ILC2s and ILC3s suggests that ILC1s are able to recirculate scanning for infected cells and that ILC2s and ILC3s are more resident under steady state conditions. As discussed, analysing the migration over a longer period of time and in the context of different responses

would help to further establish whether the resident populations observed after only a few days are really long term non-migratory cells.

The challenges of retaining robust Kaede expression combined with convincing detection of TF expression meant that surface markers were used to identify ILC1s, ILC2s and ILC3s within the Kaede mice. As discussed previously, a caveat of this method was the inability to identify all subsets, with a proportion of each subset falling within the ungated population. Therefore, these results are representative for each subgroup, with some ILCs remaining unanalysed. For example, ILC3s are gated as CD4⁺, however, CD4⁻ ILC3s fell within the ungated population due to them being unable to be identified separately from ILC1s. Therefore, CD4⁻ ILC3s may have a different migratory profile compared to CD4⁺ ILC3s, although no differences have previously been observed amongst these populations, including chemokine receptor expression (416). These results do however, provide a simple model in which ILC migration can be assessed in LNs and shows that ILC subsets have different migratory abilities under steady state conditions.

7.3.3 Do migratory and tissue-resident ILCs possess different functions?

Through the use of Kaede mice a population of ILCs were identified that migrate into the LN and a population that remain resident over the time period assessed. A key unanswered question from these studies is, what is the functional significance of ILC migration through LNs? Further work is required to establish whether migratory ILC subsets possess altered functions, compared with those that appear to be more tissue-resident.

Within this investigation the ability of ILCs to present processed antigen via MHCII was not assessed. However, ILC3s and ILC2s have been shown to possess the ability to directly

communicate with T cells via TCR:MHCII-antigen interactions (114, 162, 164). It would therefore be interesting to assess the expression of MHCII alongside co-stimulatory molecules compared between migratory and resident populations. It is, however, unlikely that the population of migratory ILC2s and ILC3s within the bLN are APCs, due to them being small population compared to professional APCs, such as LCs. Studies exploring ILC:T cell interactions have mainly focused their studies within the gut and mLN (114, 162, 164). Exploring the migratory properties of ILCs within the mLN, compared to the peripheral LNs, would be another manner in which ILC migration could be assessed. This may be beneficial due to the mLN being a larger LN and draining the gut which is a large barrier site, suggesting that it may be easier to identify a bigger population of migratory ILCs. However, ILC migration could not be assessed through the blood under steady state, as shown by ILC tissue residency in the mLN and gut of parabiotic mice, and a more invasive procedure would be required to photoconvert the mLN (243, 249).

A useful method to examine a variety of features that may differ between migratory and resident ILCs would be ribonucleic acid (RNA) sequencing. This would screen for a large number of genes expressed, helping to assess the differences between the populations. For example, different chemokine receptors and integrins involved in migration, as well as different surface receptors which may be required for different functions. A caveat of this Kaede model, is the size of the ILC population identified within the peripheral LN. Samples would have to be combined to collect enough ILCs to sort into Kaede Green and Kaede Red before analysis. This would, however, be an efficient manner in which the properties of migratory and resident ILCs could be compared.

In summary, the Kaede model established has provided basic migratory data of ILCs under steady state conditions within the peripheral LNs. Understanding the biology of ILC migration has helped in further understanding different functional aspects of the ILC subgroups. This model could be used to simply analyse migratory properties of other populations in different tissues analysing mechanisms behind influx and egress.

7.4 ILC MIGRATION UNDER INFLAMMATION

Minimal ILC migration from the ear to the auLN was observed under steady state, showing that within the assessed tissues ILCs do not efficiently migrate through the draining lymph from non-lymphoid tissues. This posed the question of whether ILCs are only able to migrate in the blood, or whether certain inflammatory conditions can drive the migration of ILCs within the draining lymphatics. The well characterised model of AD, induced through applying 20 μ L of MC903 to the ear, was chosen as the main model of skin inflammation due to its reproducibility. Other models, such as the house dust mite model (HDM), which was the initial skin inflammation model examined within the MedImmune placement, contained variabilities between batches, potentially leading to inconsistencies between experiments. This model has also been used less widely and takes several weeks to run, potentially limiting the progression of the work. Furthermore, the reproducible application process of MC903 was more accurate compared to the HDM and the Aldara model, in which the HDM was applied using a cotton swap and the Aldara cream being weighed and applied using a spatula. Under the model of AD ILC migration was observed to increase from the inflamed ear to the auLN, showing that a modest number of ILCs were able to migrate through the lymphatics from barrier sites to draining LN. However, this migration was not observed within the Aldara treated mice, suggesting that this migration is dependent on stimuli used and the inflammatory condition

that develops. Another model, not used within these studies, may be more specific to assess the activation and migration of ILCs.

Upon the induction of skin inflammation ILCs were increased within the ear, accompanied by an increase in ILC recruitment from the periphery. ILC migration also increased from the ear via the draining lymphatics into the auLN, only with the AD model, consistent with the ability of ILCs to enter peripheral LNs via the lymph. Together these data suggest that under inflammatory conditions, some ILCs receive activation or chemotactic signals resulting in their migration into inflamed skin and draining LNs. Although migration was clearly assessed, proliferation of ILCs within the ear and auLN was a contributing factor to the expansion of their population.

7.4.1 ILCs are recruited into the inflamed ear skin

Unfortunately, due to the challenges in identifying ILCs confidently by surface markers within the ear, the different migratory properties of ILC subsets was not assessed within the AD model. However, an increase in ILC migration into the ear was identified and it was suggested that lymphocytes, mainly $\gamma\delta$ T cells, were able to redistribute from certain areas of adjacent skin into the inflamed ear. Due to the Kaede model being more efficient at tracking migratory cells out of a specific photoconverted area, determining the original location of cells migrating into the photoconverted ear was more challenging. Another caveat of the Kaede model is the ability for resident rapidly proliferating photoconverted cells to dilute out their Kaede Red expression and return to a Kaede Green fluorescence, in turn being identified as a migratory cell in these experiments. Through assessing the rate of proliferation, it was concluded that not all Kaede Green ILCs within the ear showed evidence of proliferation, suggesting at least

some ILCs were actively migrating into the labelled tissue. However, it is likely that a large factor contributing to the increase in hematopoietic cells, including ILCs was proliferation. Upon skin inflammation keratinocytes produce alarmins including TSLP, IL-25 and IL-33 which may in turn lead to the activation, proliferation and increase in ILC numbers (1, 112).

Huang et al., show that iILC2s do not migrate from the gut into the lung upon intranasal administration of IL-25, however, do migrate upon i.p. injection of IL-25 (254). Within the inflammation models used, the effect of ingesting MC903 or Aldara during grooming was not assessed. Potentially the ingestion of these substances activate ILCs within the gut and leading to their recruitment in other tissues, such as the ear skin. It would be interesting to determine if ILCs were increased in any other tissues, such as the gut, lung and mLN, alongside the ear.

Within the AD and psoriatic models of skin inflammation ILC2s and ILC3s, respectively, have been shown to contribute to disease pathogenesis by cytokine production (112, 231, 233). These publications show an accumulation of ILCs within the ear, however, were unable to directly assess ILC migration. Chapter 5 shows that the increase in ILCs within the inflamed ear is directly contributed to by the migration of ILCs from the periphery. Understanding that migratory ILCs contribute to increased numbers within the inflamed AD ear in a CCR6 dependent manner, may contribute to the design of therapeutic strategies to limit such inflammation. Within the MC903 model the depletion of ILC2s attenuated the pathology of AD, suggesting that either targeting the mechanistic migration of ILCs into the ear, via CCR6, or targeting their expansion may reduce the disease development (112).

7.4.2 ILCs accumulate within challenged peripheral draining LNs

Under steady state conditions ILCs were not observed to migrate from the ear to the draining auLN. To determine whether migration via the lymphatics increased under inflammation, the AD model was used to discover that migration of ILCs from the inflamed skin to the draining auLN did contribute to the accumulation of ILCs in the auLN. Interestingly, although an increase in ILCs is observed within the auLN of Aldara treated mice, their migration from the ear is not. This suggests that ILC migration through the lymphatics may be dependent on certain forms of inflammation, or perhaps inflammation in certain sites. Inflammation within the Aldara model spreads over a larger area of skin, including the head and face, compared to the AD model. This may result in the migration of ILCs into an alternative draining LNs such as the cLN. Due to the lack of detection of ILC migration into the auLN within the Aldara model, this discussion will focus on ILC migration from the ear to the auLN within the AD model.

Within the draining auLN, proliferation seems to be one of the key mechanisms in which ILCs were increasing, compared to migration from the ear. However, other mechanisms of ILC entry into the LN have not been explored within these studies. Although lymphocyte migration increases from the ear to the auLN a larger number, roughly double, of hematopoietic cells can be observed to migrate from the head skin to the auLN. This suggests that the ear skin is not the only area draining to the auLN and that other areas of neighbouring skin may also drain to the auLN. ILC migration was not assessed from the head skin, however, it could be assumed that it may also contribute to the increase of ILCs within the auLN. ILC migration from the blood was also not assessed. Under inflammatory conditions egress from the activated LN can be prevented, resulting in the accumulation of cells. ILCs migrating in from the blood, may therefore accumulate within the auLN, contributing to the increase in number of ILCs. Within

these experiments it was shown that ILC1s were the main population within the blood, however, Huang et al., show that under IL-25 stimulation and helminth infections, ILC2s are also present within the blood (254). Inducing inflammation within the ear may increase the migration of other ILC subsets within the blood, therefore resulting in an accumulation of all ILC subsets within the auLN, via blood.

The striking increase in ILC numbers observed within the mild early stage of AD suggests it would be interesting to assess further this accumulation under prolonged chronic conditions. Assessing whether the increase in ILC numbers is maintained, increased or reduced over longer periods of time, may help to identify at which stage in AD development ILC numbers peak. If ILC numbers decrease during chronic inflammation it may be clear that they were mainly functional within the early stages of infection, however, if they are maintained at high levels or increase in number further, they may be more important in interacting with or supporting the adaptive immune response.

In conclusion, it is likely that a combination of proliferation and migration contributes to the accumulation of ILCs within the auLN, with the possibility of migratory cells entering the LN and then undergoing proliferation. ILCs were only assessed during the development of this early model of AD and assessing the ILC populations under different conditions after this application period would be interesting. Extending the AD model was discussed above, however, also assessing how quickly ILC numbers return to normal, upon stopping MC903 application, is also of interest. It is known that ILC3s are important in the maintenance and repair of SLTs, suggesting that maybe ILC3 numbers, or another subsets, may take longer to return to normal than other ILC groups (244, 245). In addition, it could be considered what

might occur upon a second course of MC903 application, after recovering from the first. As ILCs are part of the innate immune system, one may assume that they would react in a similar manner to the first MC903 exposure, however, this could be easily assessed within this model.

7.4.3 Accumulation of ILCs within the LN suggests a role in crosstalk with the adaptive immune system

ILCs function within the inflamed ear has been previously reviewed in other publications, with this investigation confirming their direct migration into the ear (112, 231, 233). On the other hand, why ILCs migrate into the draining LN is less clear. Multiple studies have shown the ability of ILCs to interact with the adaptive immune system. The clearest role for ILCs is in the intestine, where there is evidence that they limit CD4⁺ T cell responses in an MHCII-dependent manner (162). Furthermore, ILC2s are suggested to help prime Th2 responses against lung helminth infections (164). The evidence supporting TCR:MHCII-antigen interactions between ILCs and T cells comes from studies deleting MHCII on ILCs specifically (162, 164). It may therefore be suggested that ILC migration into peripheral LNs under inflammatory conditions may in turn complement the function of DCs. For example, ILCs may present antigen via MHCII, provide co-stimulatory molecules or cytokines to enhance the function of DCs or to reinforce or sustain the T cell response. ILCs may transport processed antigen from the inflamed ear to draining auLN. However, ILCs expression of MHCII, ability to uptake antigen and migrate from the ear to auLN is reduced compared to professional APCs, such as DCs. This suggests that ILCs may not primarily function as APCs, as they seem uncompetitive when compared to DCs, particularly for initial priming of T cells as they have much lower expression levels of CD80 and CD86 (114). ILC2s have also been shown to be able to take and present MHCII-antigen from other APCs, called trogocytosis (164). This may be a more effective

manner in which ILCs express antigen and this could be a feature that separates migratory and resident ILCs. Migratory ILCs may be able obtain antigen and present it via MHCII in the inflamed tissue, before migrating into the draining LN. Resident ILCs may be more likely to take MHCII-antigen complexes off other cells. There are multiple other possible mechanisms in which ILCs may directly interact with T cells within the LN, for example, providing co-stimulatory signals supporting cell survival. Therefore, further testing is required to specifically understand whether migratory ILCs have a different role within the draining LN compared to resident ILCs, specifically comparing their expression of co-stimulatory molecules.

The environment in which T cells are activated can drive the polarisation of Th cell differentiation (47, 68, 69). Upon accumulation and proliferation within the auLN, ILCs may be activated by soluble factors from the draining lymph and in turn produce cytokines effecting Th cell development. This supports the ability of ILCs to communicate and shape the adaptive immune response. Further studies would be required to directly link ILC cytokine production to the development of certain Th effector responses under different inflammatory conditions. ILC specific knock outs would be a key tool in this analysis, however, these are currently still being developed within the field. Due to ILCs sharing TFs related to T cells, such as T-bet, GATA-3 and ROR γ t as well as Id2 being required for the development of other lineages, targeting these genes depletes more than just ILCs.

In conclusion, assessing the increased migration of ILCs within the inflammation models indicates that ILCs are required within the ear and the draining auLN during inflammation. Migration from the inflamed ear to auLN is detected and potentially this is underestimated. ILCs from surrounding tissue, such as the head skin, possibly also migrate into the auLN.

However, local expansion within the draining aLN likely plays an important role in the accumulation of ILCs, consistent with ILCs providing cytokines to promote T cell development, compared with transporting antigen from the inflamed tissue. Photoconvertible models provide a key tool through their direct *in vivo* assessment of migration, enabling the deciphering of mechanisms controlling such trafficking. This can be achieved by crossing Kaede mice with genetic mice lacking certain chemokine receptors, such as done within this investigation with *Ccr7*^{-/-} Kaede and *Ccr6*^{-/-} Kaede mice.

7.5 CONCLUDING REMARKS

Overall, these studies have addressed fundamental issues in the identification methods of ILCs across the current literature, taking into account varying phenotypic marker expression within different tissues, alongside the effect of digestion protocols. The requirement for a potentially key co-stimulatory molecule, in ILC biology, was tested across a number of tissue environments, concluding that development and maintenance of ILC1s, ILC2s and ILC3s under steady state was independent of ICOS. However, ILCs dependency on ICOS:ICOSL interactions was shown to be dependent under certain conditions, with ILC survival and proliferation in the induction of airway hyperreactivity being dependent on these interaction (262, 306). These studies provide much needed clarity of the migration of ILCs into SLTs. Under steady state ILC1s can be observed to recirculate through the blood and LNs, in a similar manner to cNK cells, suggesting that they actively survey for danger signals. In comparison, ILC2s and ILC3s are more tissue-resident, consistent with other studies and their migration may instead be activated upon immunological challenge. Although the migration of individual ILC subsets was not assessed, ILC migration is clearly increased under skin inflammation. With the AD-like inflammation model being driven by a Th2 response and ILC2s role within driving

pathogenesis, it is highly possible that ILC2s are migrating into the ear of the inflamed mice and that this is in turn dependent on CCR6. Through understanding the migratory properties of ILCs, this highlights potential biological roles of ILCs and their different subsets under steady state and inflammatory conditions.

Papers arising from this thesis:

Dutton EE, Camelo A, Sleeman M, Herbst R, Carlesso G, Belz GT, et al. Characterisation of innate lymphoid cell populations at different sites in mice with defective T cell immunity. Wellcome Open Res. 2017;2:117.

APPENDIX – LIST OF REFERENCES

1. Heath WR, Carbone FR. The skin-resident and migratory immune system in steady state and memory: innate lymphocytes, dendritic cells and T cells. *Nature Immunology*. 2013;14(10):978-85.
2. Peterson LW, Artis D. Intestinal epithelial cells: regulators of barrier function and immune homeostasis. *Nature Reviews Immunology*. 2014;14(3):141-53.
3. Dutton H, Finch J. Physiology of the immune system. *Acute and Critical Care Nursing at a Glance*. Oxford: Wiley Blackwell; 2018.
4. Tlaskalova-Hogenova H, Stepankova R, Hudcovic T, Tuckova L, Cukrowska B, Lodinova-Zadnikova R, et al. Commensal bacteria (normal microflora), mucosal immunity and chronic inflammatory and autoimmune diseases. *Immunology Letters*. 2004;93(2-3):97-108.
5. Cooper MD, Alder MN. The evolution of adaptive immune systems. *Cell*. 2006;124(4):815-22.
6. Lanier LL. Shades of grey - the blurring view of innate and adaptive immunity FOREWORD. *Nature Reviews Immunology*. 2013;13(2):73-4.
7. Wu HY, Haist V, Baumgartner W, Schughart K. Sustained viral load and late death in Rag2^{-/-} mice after influenza A virus infection. *Virology Journal*. 2010;7.
8. Vallance BA, Deng WY, Knodler LA, Finlay BB. Mice lacking T and B lymphocytes develop transient colitis and crypt hyperplasia yet suffer impaired bacterial clearance during *Citrobacter rodentium* infection. *Infection and Immunity*. 2002;70(4):2070-81.
9. Westermann J, Ehlers EM, Exton MS, Kaiser M, Bode U. Migration of naive, effector and memory T cells: implications for the regulation of immune responses. *Immunological Reviews*. 2001;184:20-37.
10. Seki E, Tsutsui H, Tsuji NM, Hayashi N, Adachi K, Nakano H, et al. Critical roles of myeloid differentiation factor 88-dependent proinflammatory cytokine release in early phase clearance of *Listeria monocytogenes* in mice. *Journal of Immunology*. 2002;169(7):3863-8.
11. Edelson BT, Unanue ER. MyD88-dependent but Toll-like receptor 2-independent innate immunity to *Listeria*: No role for either in macrophage listericidal activity. *Journal of Immunology*. 2002;169(7):3869-75.
12. Renn CN, Sanchez DJ, Ochoa MT, Legaspi AJ, Oh CK, Liu PT, et al. TLR activation of Langerhans cell-like dendritic cells triggers an antiviral immune response. *Journal of Immunology*. 2006;177(1):298-305.
13. Amer AO, Swanson MS. A phagosome of one's own: a microbial guide to life in the macrophage. *Current Opinion in Microbiology*. 2002;5(1):56-61.
14. Vazquez-Torres A, Jones-Carson J, Mastroeni P, Ischiropoulos H, Fang FC. Antimicrobial actions of the NADPH phagocyte oxidase and inducible nitric oxide synthase in experimental salmonellosis. I. Effects on microbial killing by activated peritoneal macrophages in vitro. *Journal of Experimental Medicine*. 2000;192(2):227-36.
15. Nagl M, Kacani L, Mullauer B, Lemberger EM, Stoiber H, Sprinzl GM, et al. Phagocytosis and killing of bacteria by professional phagocytes and dendritic cells. *Clinical and Diagnostic Laboratory Immunology*. 2002;9(6):1165-8.

16. Ling YM, Shaw MH, Ayala C, Coppens I, Taylor GA, Ferguson DJP, et al. Vacuolar and plasma membrane stripping and autophagic elimination of *Toxoplasma gondii* in primed effector macrophages. *Journal of Experimental Medicine*. 2006;203(9):2063-71.
17. Yang Y, Liu B, Dai J, Srivastava PK, Zammit DJ, Lefrançois L, et al. Heat shock protein gp96 is a master chaperone for toll-like receptors and is important in the innate function of macrophages. *Immunity*. 2007;26(2):215-26.
18. Rot A, von Andrian UH. Chemokines in innate and adaptive host defense: Basic chemokinese grammar for immune cells. *Annual Review of Immunology*. 2004;22:891-928.
19. Lacy P, Stow JL. Cytokine release from innate immune cells: association with diverse membrane trafficking pathways. *Blood*. 2011;118(1):9-18.
20. Abtin A, Jain R, Mitchell AJ, Roediger B, Brzoska AJ, Tikoo S, et al. Perivascular macrophages mediate neutrophil recruitment during bacterial skin infection. *Nature Immunology*. 2014;15(1):45-53.
21. Yang J, Zhang L, Yu C, Yang XF, Wang H. Monocyte and macrophage differentiation: circulation inflammatory monocyte as biomarker for inflammatory diseases. *Biomark Res*. 2014;2(1):1.
22. Bevilacqua MP, Pober JS, Wheeler ME, Cotran RS, Gimbrone MA. Interleukin-1 Acts on Cultured Human Vascular Endothelium to Increase the Adhesion of Polymorphonuclear Leukocytes, Monocytes, and Related Leukocyte Cell-Lines. *Journal of Clinical Investigation*. 1985;76(5):2003-11.
23. Takikawa O, Kuroiwa T, Yamazaki F, Kido R. Mechanism of Interferon-Gamma Action - Characterization of Indoleamine 2,3-Dioxygenase In Cultured Human-Cells Induced by Interferon-Gamma and Evaluation of the Enzyme-Mediated Tryptophan Degradation in its Anticellular Activity. *Journal of Biological Chemistry*. 1988;263(4):2041-8.
24. Zaidi MR, Merlino G. The Two Faces of Interferon-gamma in Cancer. *Clinical Cancer Research*. 2011;17(19):6118-24.
25. Neill DR, Wong SH, Bellosi A, Flynn RJ, Daly M, Langford TKA, et al. Nuocytes represent a new innate effector leukocyte that mediates type-2 immunity. *Nature*. 2010;464(7293):1367-U9.
26. Sanos SL, Bui VL, Mortha A, Oberle K, Heners C, Johnen C, et al. ROR gamma t and commensal microflora are required for the differentiation of mucosal interleukin 22-producing NKp46(+) cells. *Nature Immunology*. 2009;10(1):83-91.
27. Klose CSN, Flach M, Moehle L, Rogell L, Hoyler T, Ebert K, et al. Differentiation of Type 1 ILCs from a Common Progenitor to All Helper-like Innate Lymphoid Cell Lineages. *Cell*. 2014;157(2):340-56.
28. Walker JA, Barlow JL, McKenzie ANJ. Innate lymphoid cells - how did we miss them? *Nature Reviews Immunology*. 2013;13(2):75-87.
29. Davies LC, Jenkins SJ, Allen JE, Taylor PR. Tissue-resident macrophages. *Nature Immunology*. 2013;14(10):986-95.
30. Santambrogio L, Sato AK, Carven GJ, Belyanskaya SL, Strominger JL, Stern LJ. Extracellular antigen processing and presentation by immature dendritic cells. *Proceedings of the National Academy of Sciences of the United States of America*. 1999;96(26):15056-61.
31. Sallusto F, Cella M, Danieli C, Lanzavecchia A. Dendritic Cells use Macropinocytosis and the Mannose Receptor to Concentrate Macromolecules in the Major Histocompatibility

Complex Class-II Compartment - Down-Regulation by Cytokines and Bacterial Products. *Journal of Experimental Medicine*. 1995;182(2):389-400.

32. Turley SJ, Inaba K, Garrett WS, Ebersold M, Untermaier J, Steinman RM, et al. Transport of peptide-MHC class II complexes in developing dendritic cells. *Science*. 2000;288(5465):522-7.

33. Inaba K, Turley S, Iyoda T, Yamaide F, Shimoyama S, Sousa CRE, et al. The formation of immunogenic major histocompatibility complex class II-peptide ligands in lysosomal compartments of dendritic cells is regulated by inflammatory stimuli. *Journal of Experimental Medicine*. 2000;191(6):927-36.

34. Sallusto F, Schaerli P, Loetscher P, Schaniel C, Lenig D, Mackay CR, et al. Rapid and coordinated switch in chemokine receptor expression during dendritic cell maturation. *European Journal of Immunology*. 1998;28(9):2760-9.

35. Braun A, Worbs T, Moschovakis GL, Halle S, Hoffmann K, Bolter J, et al. Afferent lymph-derived T cells and DCs use different chemokine receptor CCR7-dependent routes for entry into the lymph node and intranodal migration. *Nature Immunology*. 2011;12(9):879-U8.

36. Nishana M, Raghavan SC. Role of recombination activating genes in the generation of antigen receptor diversity and beyond. *Immunology*. 2012;137(4):271-81.

37. Oettinger MA, Schatz DG, Gorka C, Baltimore D. RAG-1 and RAG-2, Adjacent Genes that Synergistically Activate V(D)J Recombination. *Science*. 1990;248(4962):1517-23.

38. Mombaerts P, Iacomini J, Johnson RS, Herrup K, Tonegawa S, Papaioannou VE. RAG-1-Deficient Mice Have no Mature Lymphocytes-B and Lymphocytes-T. *Cell*. 1992;68(5):869-77.

39. Marrack P, Kappler J. The T-Cell Receptor. *Science*. 1987;238(4830):1073-9.

40. Bonneville M, O'Brien RL, Born WK. gamma delta T cell effector functions: a blend of innate programming and acquired plasticity. *Nature Reviews Immunology*. 2010;10(7):467-78.

41. Wucherpfennig KW, Gagnon E, Call MJ, Huseby ES, Call ME. Structural Biology of the T-cell Receptor: Insights into Receptor Assembly, Ligand Recognition, and Initiation of Signaling. *Cold Spring Harbor Perspectives in Biology*. 2010;2(4).

42. Zamojska R. CD4 and CD8: Modulators of T-cell receptor recognition of antigen and of immune responses? *Current Opinion in Immunology*. 1998;10(1):82-7.

43. Doherty PC, Zinkernagel RM. Enhanced Immunological Surveillance in Mice Heterozygous at H-2 Gene Complex. *Nature*. 1975;256(5512):50-2.

44. Townsend ARM, Rothbard J, Gotch FM, Bahadur G, Wraith D, McMichael AJ. The Epitopes of Influenza Nucleoprotein Recognized by Cytotoxic Lymphocytes-T can be Defined with Short Synthetic Peptides. *Cell*. 1986;44(6):959-68.

45. Murali-Krishna K, Altman JD, Suresh M, Sourdive DJD, Zajac AJ, Miller JD, et al. Counting antigen-specific CD8 T cells: A reevaluation of bystander activation during viral infection. *Immunity*. 1998;8(2):177-87.

46. Russell JH, Ley TJ. Lymphocyte-mediated cytotoxicity. *Annual Review of Immunology*. 2002;20:323-70.

47. Raphael I, Nalawade S, Eagar TN, Forsthuber TG. T cell subsets and their signature cytokines in autoimmune and inflammatory diseases. *Cytokine*. 2015;74(1):5-17.

48. Gowans JL. The Recirculation of Lymphocytes From Blood to Lymph in The Rat. *Journal of Physiology-London*. 1959;146(1):54-&.

49. Girard JP, Moussion C, Forster R. HEVs, lymphatics and homeostatic immune cell trafficking in lymph nodes. *Nature Reviews Immunology*. 2012;12(11):762-73.

50. Bajenoff M, Egen JG, Koo LY, Laugier JP, Brau F, Glaichenhaus N, et al. Stromal cell networks regulate lymphocyte entry, migration, and territoriality in lymph nodes. *Immunity*. 2006;25(6):989-1001.
51. Link A, Vogt TK, Favre S, Britschgi MR, Acha-Orbea H, Hinz B, et al. Fibroblastic reticular cells in lymph nodes regulate the homeostasis of naive T cells. *Nature Immunology*. 2007;8(11):1255-65.
52. Ansel KM, Ngo VN, Hyman PL, Luther SA, Forster R, Sedgwick JD, et al. A chemokine-driven positive feedback loop organizes lymphoid follicles. *Nature*. 2000;406(6793):309-14.
53. Tomura M, Yoshida N, Tanaka J, Karasawa S, Miwa Y, Miyawaki A, et al. Monitoring cellular movement in vivo with photoconvertible fluorescence protein "Kaede" transgenic mice. *Proceedings of the National Academy of Sciences of the United States of America*. 2008;105(31):10871-6.
54. Smith-Garvin JE, Koretzky GA, Jordan MS. T Cell Activation. *Annual Review of Immunology*. 2009;27:591-619.
55. Acuto O, Michel F. CD28-mediated co-stimulation: A quantitative support for TCR signalling. *Nature Reviews Immunology*. 2003;3(12):939-51.
56. Green JM, Noel PJ, Sperling AI, Walunas TL, Gray GS, Bluestone JA, et al. Absence of B7-Dependent Responses in CD28-Deficient Mice. *Immunity*. 1994;1(6):501-8.
57. Coyle AJ, Lehar S, Lloyd C, Tian J, Delaney T, Manning S, et al. The CD28-related molecule ICOS is required for effective T cell-dependent immune responses. *Immunity*. 2000;13(1):95-105.
58. Walunas TL, Lenschow DJ, Bakker CY, Linsley PS, Freeman GJ, Green JM, et al. CTLA-4 can Function as a Negative Regulator of T-Cell Activation. *Immunity*. 1994;1(5):405-13.
59. Linsley PS, Greene JL, Tan P, Bradshaw J, Ledbetter JA, Anasetti C, et al. Coexpression and Functional Cooperation of CTLA-4 and CD28 on Activated Lymphocytes-T. *Journal of Experimental Medicine*. 1992;176(6):1595-604.
60. Liang L, Porter EM, Sha WC. Constitutive expression of the B7h ligand for inducible costimulator on naive B cells is extinguished after activation by distinct B cell receptor and interleukin 4 receptor-mediated pathways and can be rescued by CD40 signaling. *Journal of Experimental Medicine*. 2002;196(1):97-108.
61. Yoshinaga SK, Whoriskey JS, Khare SD, Sarmiento U, Guo J, Horan T, et al. T-cell co-stimulation through B7RP-1 and ICOS. *Nature*. 1999;402(6763):827-32.
62. Dong C, Juedes AE, Temann UA, Shresta S, Allison JP, Ruddle NH, et al. ICOS co-stimulatory receptor is essential for T-cell activation and function. *Nature*. 2001;409(6816):97-101.
63. Paterson DJ, Jefferies WA, Green JR, Brandon MR, Cortesy P, Puklavec M, et al. Antigens of Activated Rat T Lymphocytes Including a Molecule of 50,000 MR Detected Only on CD4 Positive T-Blasts. *Molecular Immunology*. 1987;24(12):1281-90.
64. Gramaglia I, Weinberg AD, Lemon M, Croft M. Ox-40 ligand: A potent costimulatory molecule for sustaining primary CD4 T cell responses. *Journal of Immunology*. 1998;161(12):6510-7.
65. Kawabe T, Naka T, Yoshida K, Tanaka T, Fujiwara H, Suematsu S, et al. The Immune-Responses in CD40-Deficient Mice - Impaired Immunoglobulin Class Switching and Germinal Center Formation. *Immunity*. 1994;1(3):167-78.

66. Stuber E, Strober W. The T cell B cell interaction via OX40-OX40L is necessary for the T cell-dependent humoral immune response. *Journal of Experimental Medicine*. 1996;183(3):979-89.
67. Mosmann TR, Cherwinski H, Bond MW, Giedlin MA, Coffman RL. Pillars article: Two types of murine helper T cell clone. I. Definition according to profiles of lymphokine activities and secreted proteins. *Journal of Immunology*. 2005;175(1):5-14.
68. Luckheeram RV, Zhou R, Verma AD, Xia B. CD4+T Cells: Differentiation and Functions. *Clinical & Developmental Immunology*. 2012.
69. de Jong EC, Vieira PL, Kalinski P, Schuitemaker JHN, Tanaka Y, Wierenga EA, et al. Microbial compounds selectively induce Th1 cell-promoting or Th2 cell-promoting dendritic cells in vitro with diverse Th cell-polarizing signals. *Journal of Immunology*. 2002;168(4):1704-9.
70. Trinchieri G. Interleukin-12 and the regulation of innate resistance and adaptive immunity. *Nature Reviews Immunology*. 2003;3(2):133-46.
71. Scott P, Kaufmann SHE. The Role of T-Cell Subsets and Cytokines in the Regulation of Infection. *Immunology Today*. 1991;12(10):346-8.
72. Kaplan MH, Schindler U, Smiley ST, Grusby MJ. Stat6 is required for mediating responses to IL-4 and for the development of Th2 cells. *Immunity*. 1996;4(3):313-9.
73. Licona-Limon P, Kim LK, Palm NW, Flavell RA. T(H)2, allergy and group 2 innate lymphoid cells. *Nature Immunology*. 2013;14(6):536-42.
74. Owyang AM, Zaph C, Wilson EH, Guild KJ, McClanahan T, Miller HRP, et al. Interleukin 25 regulates type 2 cytokine-dependent immunity and limits chronic inflammation in the gastrointestinal tract. *Journal of Experimental Medicine*. 2006;203(4):843-9.
75. Laouini D, Alenius H, Bryce P, Oettgen H, Tsitsikov E, Geha RS. IL-10 is critical for Th2 responses in a murine model of allergic dermatitis. *Journal of Clinical Investigation*. 2003;112(7):1058-66.
76. Ando DG, Clayton J, Kono D, Urban JL, Sercarz EE. Encephalitogenic T-Cells in the B10.PL Model of Experimental Allergic Encephalomyelitis (Eae) are of The Th-1 Lymphokine Subtype. *Cellular Immunology*. 1989;124(1):132-43.
77. Park H, Li ZX, Yang XO, Chang SH, Nurieva R, Wang YH, et al. A distinct lineage of CD4 T cells regulates tissue inflammation by producing interleukin 17. *Nature Immunology*. 2005;6(11):1133-41.
78. Mangan PR, Harrington LE, O'Quinn DB, Helms WS, Bullard DC, Elson CO, et al. Transforming growth factor-beta induces development of the T(H)17 lineage. *Nature*. 2006;441(7090):231-4.
79. Liang SC, Tan XY, Luxenberg DP, Karim R, Dunussi-Joannopoulos K, Collins M, et al. Interleukin (IL)-22 and IL-17 are coexpressed by Th17 cells and cooperatively enhance expression of antimicrobial peptides. *Journal of Experimental Medicine*. 2006;203(10):2271-9.
80. Sakaguchi S, Sakaguchi N, Asano M, Itoh M, Toda M. Immunologic Self-Tolerance Maintained by Activated T Cells Expressing IL-2 Receptor alpha-Chains (CD25) Breakdown of a Single Mechanism of Self-Tolerance Causes Various Autoimmune Diseases. *Journal of Immunology*. 2011;186(7):1151-64.
81. Sakaguchi S, Wing K, Onishi Y, Prieto-Martin P, Yamaguchi T. Regulatory T cells: how do they suppress immune responses? *International Immunology*. 2009;21(10):1105-11.

82. Workman CJ, Szymczak-Workman AL, Collison LW, Pillai MR, Vignali DAA. The development and function of regulatory T cells. *Cellular and Molecular Life Sciences*. 2009;66(16):2603-22.
83. Hori S, Nomura T, Sakaguchi S. Control of regulatory T cell development by the transcription factor Foxp3. *Science*. 2003;299(5609):1057-61.
84. Crotty S. T Follicular Helper Cell Differentiation, Function, and Roles in Disease. *Immunity*. 2014;41(4):529-42.
85. Victora GD, Schwickert TA, Fooksman DR, Kamphorst AO, Meyer-Hermann M, Dustin ML, et al. Germinal center dynamics revealed by multiphoton microscopy with a photoactivatable fluorescent reporter. *Cell*. 2010;143(4):592-605.
86. Vinuesa CG, Tangye SG, Moser B, Mackay CR. Follicular B helper T cells in antibody responses and autoimmunity. *Nature Reviews Immunology*. 2005;5(11):853-65.
87. Forbes EE, Groschwitz K, Abonia JP, Brandt EB, Cohen E, Blanchard C, et al. IL-9-and mast cell-mediated intestinal permeability predisposes to oral antigen hypersensitivity. *Journal of Experimental Medicine*. 2008;205(4):897-913.
88. Tan C, Gery I. The Unique Features of Th9 Cells and their Products. *Critical Reviews in Immunology*. 2012;32(1):1-10.
89. Louahed J, Toda M, Jen J, Hamid Q, Renauld JC, Levitt RC, et al. Interleukin-9 upregulates mucus expression in the airways. *American Journal of Respiratory Cell and Molecular Biology*. 2000;22(6):649-56.
90. Veldhoen M, Uyttenhove C, van Snick J, Helmbj H, Westendorf A, Buer J, et al. Transforming growth factor-beta 'reprograms' the differentiation of T helper 2 cells and promotes an interleukin 9-producing subset. *Nature Immunology*. 2008;9(12):1341-6.
91. Dardalhon V, Awasthi A, Kwon H, Galileos G, Gao W, Sobel RA, et al. IL-4 inhibits TGF-beta-induced Foxp3(+) T cells and, together with TGF-beta, generates IL-9(+) IL-10(+) Foxp3(-) effector T cells. *Nature Immunology*. 2008;9(12):1347-55.
92. Marriott CL, Dutton EE, Tomura M, Withers DR. Retention of Ag-specific memory CD4+ T cells in the draining lymph node indicates lymphoid tissue resident memory populations. *Eur J Immunol*. 2017;47(5):860-71.
93. Masopust D, Choo D, Vezys V, Wherry EJ, Duraiswamy J, Akondy R, et al. Dynamic T cell migration program provides resident memory within intestinal epithelium. *Journal of Experimental Medicine*. 2010;207(3):553-64.
94. Schenkel JM, Masopust D. Tissue-Resident Memory T Cells. *Immunity*. 2014;41(6):886-97.
95. Hirota K, Duarte JH, Veldhoen M, Hornsby E, Li Y, Cua DJ, et al. Fate mapping of IL-17-producing T cells in inflammatory responses. *Nature Immunology*. 2011;12(3):255-U95.
96. Bending D, De La Pena H, Veldhoen M, Phillips JM, Uyttenhove C, Stockinger B, et al. Highly purified Th17 cells from BDC2.5NOD mice convert into Th1-like cells in NOD/SCID recipient mice. *Journal of Clinical Investigation*. 2009;119(3):565-72.
97. Artis D, Spits H. The biology of innate lymphoid cells. *Nature*. 2015;517(7534):293-301.
98. Constantinides MG, McDonald BD, Verhoef PA, Bendelac A. A committed precursor to innate lymphoid cells. *Nature*. 2014;508(7496):397-+.
99. Kondo M, Weissman IL, Akashi K. Identification of clonogenic common lymphoid progenitors in mouse bone marrow. *Cell*. 1997;91(5):661-72.

100. Robinette ML, Colonna M. Immune modules shared by innate lymphoid cells and T cells. *Journal of Allergy and Clinical Immunology*. 2016;138(5):1243-52.
101. Spits H, Artis D, Colonna M, Diefenbach A, Di Santo JP, Eberl G, et al. Innate lymphoid cells - a proposal for uniform nomenclature. *Nature Reviews Immunology*. 2013;13(2):145-9.
102. Moro K, Yamada T, Tanabe M, Takeuchi T, Ikawa T, Kawamoto H, et al. Innate production of T(H)2 cytokines by adipose tissue-associated c-Kit(+)Sca-1(+) lymphoid cells. *Nature*. 2010;463(7280):540-U160.
103. Price AE, Liang HE, Sullivan BM, Reinhardt RL, Eisley CJ, Erle DJ, et al. Systemically dispersed innate IL-13-expressing cells in type 2 immunity. *Proceedings of the National Academy of Sciences of the United States of America*. 2010;107(25):11489-94.
104. Fuchs A, Vermi W, Lee JS, Lonardi S, Gilfillan S, Newberry RD, et al. Intraepithelial type 1 innate lymphoid cells are a unique subset of IL-12- and IL-15-responsive IFN-gamma-producing cells. *Immunity*. 2013;38(4):769-81.
105. Satoh-Takayama N, Vosschenrich CAJ, Lesjean-Pottier S, Sawa S, Lochner M, Rattis F, et al. Microbial Flora Drives Interleukin 22 Production in Intestinal NKp46(+) Cells that Provide Innate Mucosal Immune Defense. *Immunity*. 2008;29(6):958-70.
106. Sawa S, Lochner M, Satoh-Takayama N, Dulauroy S, Berard M, Kleinschek M, et al. ROR gamma t(+) innate lymphoid cells regulate intestinal homeostasis by integrating negative signals from the symbiotic microbiota. *Nature Immunology*. 2011;12(4):320-U71.
107. Van Maele L, Carnoy C, Cayet D, Ivanov S, Porte R, Deruy E, et al. Activation of Type 3 Innate Lymphoid Cells and Interleukin 22 Secretion in the Lungs During *Streptococcus pneumoniae* Infection. *Journal of Infectious Diseases*. 2014;210(3):493-503.
108. Huang Y, Guo L, Qiu J, Chen X, Hu-Li J, Siebenlist U, et al. IL-25-responsive, lineage-negative KLRG1 cells are multipotential 'inflammatory' type 2 innate lymphoid cells. *Nat Immunol*. 2014.
109. Chiossone L, Vivier E. Immune checkpoints on innate lymphoid cells. *Journal of Experimental Medicine*. 2017;214(6):1561-3.
110. Monticelli LA, Sonnenberg GF, Abt MC, Alenghat T, Ziegler CGK, Doering TA, et al. Innate lymphoid cells promote lung-tissue homeostasis after infection with influenza virus. *Nature Immunology*. 2011;12(11):1045-U47.
111. Mebius RE, Rennert P, Weissman IL. Developing lymph nodes collect CD4(+)CD3(-) LT beta(+) cells that can differentiate to APC, NK cells, and follicular cells but not T or B cells. *Immunity*. 1997;7(4):493-504.
112. Kim B, Siracusa M, Saenz S, Noti M, Monticelli L, Sonnenberg G, et al. TSLP elicits IL-33-independent innate lymphoid cell responses to promote skin inflammation. *Journal of Immunology*. 2013;190.
113. Wang S, Xia PY, Chen Y, Qu Y, Xiong Z, Ye BQ, et al. Regulatory Innate Lymphoid Cells Control Innate Intestinal Inflammation. *Cell*. 2017;171(1):201-+.
114. von Burg N, Chappaz S, Baerenwaldt A, Horvath E, Dasgupta SB, Ashok D, et al. Activated group 3 innate lymphoid cells promote T-cell-mediated immune responses. *Proceedings of the National Academy of Sciences of the United States of America*. 2014;111(35):12835-40.
115. Lee SH, Miyagi T, Biron CA. Keeping NK cells in highly regulated antiviral warfare. *Trends in Immunology*. 2007;28(6):252-9.

116. Martin-Fontecha A, Thomsen LL, Brett S, Gerard C, Lipp M, Lanzavecchia A, et al. Induced recruitment of NK cells to lymph nodes provides IFN-gamma for T(H)1 priming. *Nature Immunology*. 2004;5(12):1260-5.
117. Kiessling R, Klein E, Wigzell H. "Natural" killer cells in the mouse. I. Cytotoxic cells with specificity for mouse Moloney leukemia cells. Specificity and distribution according to genotype. *Eur J Immunol*. 1975;5(2):112-7.
118. Vankayalapati R, Wizel B, Weis SE, Safi H, Lakey DL, Mandelboim O, et al. The NKp46 receptor contributes to NK cell lysis of mononuclear phagocytes infected with an intracellular bacterium. *Journal of Immunology*. 2002;168(7):3451-7.
119. Loh J, Chu DT, O'Guin AK, Yokoyama WM, Virgin HW. Natural killer cells utilize both perforin and gamma interferon to regulate murine cytomegalovirus infection in the spleen and liver. *Journal of Virology*. 2005;79(1):661-7.
120. Mullbacher A, Waring P, Hla RT, Tran T, Chin S, Stehle T, et al. Granzymes are the essential downstream effector molecules for the control of primary virus infections by cytolytic leukocytes. *Proceedings of the National Academy of Sciences of the United States of America*. 1999;96(24):13950-5.
121. Voskoboinik I, Smyth MJ, Trapani JA. Perforin-mediated target-cell death and immune homeostasis. *Nature Reviews Immunology*. 2006;6(12):940-52.
122. Orange JS, Wang BP, Terhorst C, Biron CA. Requirement for Natural-Killer Cell-Produced Interferon-Gamma in Defense Against Murine Cytomegalovirus-Infection and Enhancement of this Defense Pathway by Interleukin-12 Administration. *Journal of Experimental Medicine*. 1995;182(4):1045-56.
123. Mirandola P, Ponti C, Gobbi G, Sponzilli I, Vaccarezza M, Cocco L, et al. Activated human NK and CD8(+) T cells express both TNF-related apoptosis-inducing ligand (TRAIL) and TRAIL receptors but are resistant to TRAIL-mediated cytotoxicity. *Blood*. 2004;104(8):2418-24.
124. Sheppard S, Schuster IS, Andoniou CE, Cocita C, Adejumo T, Kung SKP, et al. The Murine Natural Cytotoxic Receptor NKp46/NCR1 Controls TRAIL Protein Expression in NK Cells and ILC1s. *Cell Reports*. 2018;22(13):3385-92.
125. Mandelboim O, Lieberman N, Lev M, Paul L, Arnon TI, Bushkin Y, et al. Recognition of haemagglutinins on virus-infected cells by NKp46 activates lysis by human NK cells. *Nature*. 2001;409(6823):1055-60.
126. Flesch IEA, Hess JH, Oswald IP, Kaufmann SHE. Growth-Inhibition of Mycobacterium-Bovis by IFN-Gamma Stimulated Macrophages - Regulation by Endogenous Tumor-Necrosis-Factor-Alpha and by IL-10. *International Immunology*. 1994;6(5):693-700.
127. Serafini N, Voshchenrich CAJ, Di Santo JP. Transcriptional regulation of innate lymphoid cell fate. *Nature Reviews Immunology*. 2015;15(7):415-28.
128. Intlekofer AM, Takemoto N, Wherry EJ, Longworth SA, Northrup JT, Palanivel VR, et al. Effector and memory CD8(+) T cell fate coupled by T-bet and eomesodermin. *Nature Immunology*. 2005;6(12):1236-44.
129. Weizman OE, Adams NM, Schuster IS, Krishna C, Pritykin Y, Lau C, et al. ILC1 Confer Early Host Protection at Initial Sites of Viral Infection. *Cell*. 2017;171(4):795-+.
130. Klose CSN, Kiss EA, Schwierzeck V, Ebert K, Hoyler T, d'Hargues Y, et al. A T-bet gradient controls the fate and function of CCR6(-)ROR gamma t(+) innate lymphoid cells. *Nature*. 2013;494(7436):261-5.

131. Kennedy MK, Glaccum M, Brown SN, Butz EA, Viney JL, Embers M, et al. Reversible defects in natural killer and memory CD8 T cell lineages in interleukin 15-deficient mice. *Journal of Experimental Medicine*. 2000;191(5):771-80.
132. Vashist N, Trittel S, Ebensen T, Chambers BJ, Guzman CA, Riese P. Influenza-Activated ILC1s Contribute to Antiviral Immunity Partially Influenced by Differential GITR Expression. *Frontiers in Immunology*. 2018;9.
133. Jiao YH, Huntington ND, Belz GT, Seillet C. Type 1 innate Lymphoid Cell Biology: Lessons Learnt from Natural Killer Cells. *Frontiers in Immunology*. 2016;7.
134. Lodoen MB, Lanier LL. Natural killer cells as an initial defense against pathogens. *Current Opinion in Immunology*. 2006;18(4):391-8.
135. Fuchs A. ILC1s in Tissue Inflammation and Infection. *Frontiers in Immunology*. 2016;7.
136. Hoyler T, Klose CSN, Souabni A, Turqueti-Neves A, Pfeifer D, Rawlins EL, et al. The Transcription Factor GATA3 Controls Cell Fate and Maintenance of Type 2 Innate Lymphoid Cells. *Immunity*. 2012;37(4):634-48.
137. Eberl G, Marmon S, Sunshine MJ, Rennert PD, Choi YW, Littman DR. An essential function for the nuclear receptor ROR gamma t in the generation of fetal lymphoid tissue inducer cells. *Nature Immunology*. 2004;5(1):64-73.
138. Eberl G, Littman DR. The role of the nuclear hormone receptor ROR gamma t in the development of lymph nodes and Peyer's patches. *Immunological Reviews*. 2003;195:81-90.
139. Takatori H, Kanno Y, Watford WT, Tato CM, Weiss G, Ivanov II, et al. Lymphoid tissue inducer-like cells are an innate source of IL-17 and IL-22. *Journal of Experimental Medicine*. 2009;206(1):35-41.
140. Seehus CR, Kadavallore A, de la Torre B, Yeckes AR, Wang YZ, Tang J, et al. Alternative activation generates IL-10 producing type 2 innate lymphoid cells. *Nature Communications*. 2017;8.
141. Vonarbourg C, Mortha A, Bui VL, Hernandez PP, Kiss EA, Hoyler T, et al. Regulated expression of nuclear receptor RORgamma t confers distinct functional fates to NK cell receptor-expressing RORgamma t(+) innate lymphocytes. *Immunity*. 2010;33(5):736-51.
142. Silver JS, Kearley J, Copenhaver AM, Sanden C, Mori M, Yu L, et al. Inflammatory triggers associated with exacerbations of COPD orchestrate plasticity of group 2 innate lymphoid cells in the lungs. *Nature Immunology*. 2016;17(6):626-+.
143. Colonna M. Innate Lymphoid Cells: Diversity, Plasticity, and Unique Functions in Immunity. *Immunity*. 2018;48(6):1104-17.
144. Withers DR, Hepworth MR, Wang XX, Mackley EC, Halford EE, Dutton EE, et al. Transient inhibition of ROR-gamma t therapeutically limits intestinal inflammation by reducing T(H)17 cells and preserving group 3 innate lymphoid cells. *Nature Medicine*. 2016;22(3):319-23.
145. Boos MD, Yokota Y, Eberl G, Kee BL. Mature natural killer cell and lymphoid tissue-inducing cell development requires Id2-mediated suppression of E protein activity. *Journal of Experimental Medicine*. 2007;204(5):1119-30.
146. Blay A, Finch J, Dutton H. The immune and lymphatic systems, infection and sepsis. In: Peate I, Dutton H, editors. *Acute Nursing Care, Recognising and Responding to Medical Emergencies*. Harlow: Pearson Education Limited; 2012.

147. Geiger TL, Abt MC, Gasteiger G, Firth MA, O'Connor MH, Geary CD, et al. Nfil3 is crucial for development of innate lymphoid cells and host protection against intestinal pathogens. *Journal of Experimental Medicine*. 2014;211(9):1723-31.
148. Xu W, Domingues RG, Fonseca-Pereira D, Ferreira M, Ribeiro H, Lopez-Lastra S, et al. NFIL3 Orchestrates the Emergence of Common Helper Innate Lymphoid Cell Precursors. *Cell Reports*. 2015;10(12):2043-54.
149. Satoh-Takayama N, Lesjean-Pottier S, Vieira P, Sawa S, Eberl G, Vosshenrich CAJ, et al. IL-7 and IL-15 independently program the differentiation of intestinal CD3(-)NKp46(+) cell subsets from Id2-dependent precursors. *Journal of Experimental Medicine*. 2010;207(2):273-80.
150. Bando JK, Liang HE, Locksley RM. Identification and distribution of developing innate lymphoid cells in the fetal mouse intestine. *Nature Immunology*. 2015;16(2):153-+.
151. Serafini N, Wolterink RGJK, Satoh-Takayama N, Xu W, Vosshenrich CAJ, Hendriks RW, et al. Gata3 drives development of ROR gamma t(+) group 3 innate lymphoid cells. *Journal of Experimental Medicine*. 2014;211(2):199-208.
152. Sun XH, Copeland NG, Jenkins NA, Baltimore D. Id Proteins Id1 and Id2 Selectively Inhibit DNA-Binding by one Class of Helix-Loop-Helix Proteins. *Molecular and Cellular Biology*. 1991;11(11):5603-11.
153. Bain G, Maandag ECR, Izon DJ, Amsen D, Kruisbeek AM, Weintraub BC, et al. E2A Proteins are Required for Proper B-Cell Development and Initiation of Immunoglobulin Gene Rearrangements. *Cell*. 1994;79(5):885-92.
154. Morrow MA, Mayer EW, Perez CA, Adlam M, Siu G. Overexpression of the Helix-Loop-Helix protein Id2 blocks T cell development at multiple stages. *Molecular Immunology*. 1999;36(8):491-503.
155. Ishizuka IE, Constantinides MG, Gudjonson H, Bendelac A. The Innate Lymphoid Cell Precursor. *Annual Review of Immunology*, Vol 34. 2016;34:299-316.
156. Daussy C, Faure F, Mayol K, Viel S, Gasteiger G, Charrier E, et al. T-bet and Eomes instruct the development of two distinct natural killer cell lineages in the liver and in the bone marrow. *Journal of Experimental Medicine*. 2014;211(3):563-77.
157. Yagi R, Zhong C, Northrup DL, Yu F, Bouladoux N, Spencer S, et al. The Transcription Factor GATA3 Is Critical for the Development of All IL-7R alpha-Expressing Innate Lymphoid Cells. *Immunity*. 2014;40(3):378-88.
158. Lee JS, Cella M, McDonald KG, Garlanda C, Kennedy GD, Nukaya M, et al. AHR drives the development of gut ILC22 cells and postnatal lymphoid tissues via pathways dependent on and independent of Notch. *Nature Immunology*. 2012;13(2):144-U58.
159. Wong SH, Walker JA, Jolin HE, Drynan LF, Hams E, Camelo A, et al. Transcription factor ROR alpha is critical for nuocyte development. *Nature Immunology*. 2012;13(3):229-U43.
160. Tsuji M, Suzuki K, Kitamura H, Maruya M, Kinoshita K, Ivanov II, et al. Requirement for lymphoid tissue-inducer cells in isolated follicle formation and T cell-independent immunoglobulin a generation in the gut. *Immunity*. 2008;29(2):261-71.
161. Futterer A, Mink K, Luz A, Kosco-Vilbois MH, Pfeffer K. The lymphotoxin beta receptor controls organogenesis and affinity maturation in peripheral lymphoid tissues. *Immunity*. 1998;9(1):59-70.

162. Hepworth MR, Monticelli LA, Fung TC, Ziegler CGK, Grunberg S, Sinha R, et al. Innate lymphoid cells regulate CD4(+) T-cell responses to intestinal commensal bacteria. *Nature*. 2013;498(7452):113-+.
163. Hepworth MR, Fung TC, Masur SH, Kelsen JR, McConnell FM, Dubrot J, et al. Group 3 innate lymphoid cells mediate intestinal selection of commensal bacteria-specific CD4(+) T cells. *Science*. 2015;348(6238):1031-5.
164. Oliphant CJ, Hwang YY, Walker JA, Salimi M, Wong SH, Brewer JM, et al. MHCII-Mediated Dialog between Group 2 Innate Lymphoid Cells and CD4(+) T Cells Potentiates Type 2 Immunity and Promotes Parasitic Helminth Expulsion. *Immunity*. 2014;41(2):283-95.
165. Buettner M, Lochner M. Development and Function of Secondary and Tertiary Lymphoid Organs in the Small intestine and the Colon. *Frontiers in Immunology*. 2016;7.
166. Lindemans CA, Calafiore M, Mertelsmann AM, O'Connor MH, Dudakov JA, Jenq RR, et al. Interleukin-22 promotes intestinal-stem-cell-mediated epithelial regeneration. *Nature*. 2015;528(7583):560-+.
167. Aparicio-Domingo P, Romera-Hernandez M, Karrich JJ, Cornelissen F, Papazian N, Lindenbergh-Kortleve DJ, et al. Type 3 innate lymphoid cells maintain intestinal epithelial stem cells after tissue damage. *Journal of Experimental Medicine*. 2015;212(11):1783-91.
168. Goto Y, Obata T, Kunisawa J, Sato S, Ivanov II, Lamichhane A, et al. Innate lymphoid cells regulate intestinal epithelial cell glycosylation. *Science*. 2014;345(6202):1310-+.
169. Zheng Y, Valdez PA, Danilenko DM, Hu Y, Sa SM, Gong Q, et al. Interleukin-22 mediates early host defense against attaching and effacing bacterial pathogens. *Nature Medicine*. 2008;14(3):282-9.
170. Tumanov AV, Koroleva EP, Guo XH, Wang YG, Kruglov A, Nedospasov S, et al. Lymphotoxin Controls the IL-22 Protection Pathway in Gut Innate Lymphoid Cells during Mucosal Pathogen Challenge. *Cell Host & Microbe*. 2011;10(1):44-53.
171. Song C, Lee JS, Gilfillan S, Robinette ML, Newberry RD, Stappenbeck TS, et al. Unique and redundant functions of NKp46(+) ILC3s in models of intestinal inflammation. *Journal of Experimental Medicine*. 2015;212(11):1869-82.
172. Rendon JL, Li XL, Akhtar S, Choudhry MA. Interleukin-22 Modulates Gut Epithelial and Immune Barrier Functions Following Acute Alcohol Exposure and Burn Injury. *Shock*. 2013;39(1):11-8.
173. Zaph C, Du YR, Saenz SA, Nair MG, Perrigoue JG, Taylor BC, et al. Commensal-dependent expression of IL-25 regulates the IL-23-IL-17 axis in the intestine. *Journal of Experimental Medicine*. 2008;205(10):2191-8.
174. Iwakura Y, Ishigame H. The IL-23/IL-17 axis in inflammation. *Journal of Clinical Investigation*. 2006;116(5):1218-22.
175. Buonocore S, Ahern PP, Uhlig HH, Ivanov II, Littman DR, Maloy KJ, et al. Innate lymphoid cells drive interleukin-23-dependent innate intestinal pathology. *Nature*. 2010;464(7293):1371-5.
176. Sonnenberg GF, Monticelli LA, Alenghat T, Fung TC, Hutnick NA, Kunisawa J, et al. Innate Lymphoid Cells Promote Anatomical Containment of Lymphoid-Resident Commensal Bacteria. *Science*. 2012;336(6086):1321-5.
177. Kolls JK, McCray PB, Chan YR. Cytokine-mediated regulation of antimicrobial proteins. *Nature Reviews Immunology*. 2008;8(11):829-35.

178. Archer NK, Adappa ND, Palmer JN, Cohen NA, Harro JM, Lee SK, et al. Interleukin-17A (IL-17A) and IL-17F Are Critical for Antimicrobial Peptide Production and Clearance of *Staphylococcus aureus* Nasal Colonization. *Infection and Immunity*. 2016;84(12):3575-83.
179. Song XY, Qian YC. The activation and regulation of IL-17 receptor mediated signaling. *Cytokine*. 2013;62(2):175-82.
180. Bomsel M, Heyman M, Hocini H, Lagaye S, Belec L, Dupont C, et al. Intracellular neutralization of HIV transcytosis across tight epithelial barriers by anti-HIV envelope protein dIgA or IgM. *Immunity*. 1998;9(2):277-87.
181. von Moltke J, Ji M, Liang HE, Locksley RM. Tuft-cell-derived IL-25 regulates an intestinal ILC2-epithelial response circuit. *Nature*. 2016;529(7585):221-U43.
182. Pelly VS, Kannan Y, Coomes SM, Entwistle LJ, Ruckerl D, Seddon B, et al. IL-4-producing ILC2s are required for the differentiation of T(H)2 cells following *Heligmosomoides polygyrus* infection. *Mucosal Immunology*. 2016;9(6):1407-17.
183. Zhao AP, McDermott J, Urban JF, Gause W, Madden KB, Yeung KA, et al. Dependence of IL-4, IL-13, and nematode-induced alterations in murine small intestinal smooth muscle contractility on Stat6 and enteric nerves. *Journal of Immunology*. 2003;171(2):948-54.
184. Fallon PG, Jolin HE, Smith P, Emson CL, Townsend MJ, Fallon R, et al. IL-4 induces characteristic Th2 responses even in the combined absence of IL-5, IL-9, and IL-13. *Immunity*. 2002;17(1):7-17.
185. Abt MC, Lewis BB, Caballero S, Xiong HZ, Carter RA, Susac B, et al. Innate Immune Defenses Mediated by Two ILC Subsets Are Critical for Protection against Acute *Clostridium difficile* Infection. *Cell Host & Microbe*. 2015;18(1):27-37.
186. Townsend MJ, Weinmann AS, Matsuda JL, Salomon R, Farnham PJ, Biron CA, et al. T-bet regulates the terminal maturation and homeostasis of NK and V alpha 14i NKT cells. *Immunity*. 2004;20(4):477-94.
187. Chen Y, Nakane A, Minagawa T. Recombinant Murine Gamma-Interferon Induces Enhanced Resistance to *Listeria-Monocytogenes* Infection in Neonatal Mice. *Infection and Immunity*. 1989;57(8):2345-9.
188. Bao S, Beagley KW, France MP, Shen J, Husband AJ. Interferon-gamma plays a critical role in intestinal immunity against *Salmonella typhimurium* infection. *Immunology*. 2000;99(3):464-72.
189. Ng SC, Bernstein CN, Vatn MH, Lakatos PL, Loftus Jr EV, Tysk C, et al. Geographical variability and environmental risk factors in inflammatory bowel disease. *Gut*. 2013;62(4):630-49.
190. Jostins L, Ripke S, Weersma RK, Duerr RH, McGovern DP, Hui KY, et al. Host-microbe interactions have shaped the genetic architecture of inflammatory bowel disease. *Nature*. 2012;491(7422):119-24.
191. Forkel M, Mjosberg J. Dysregulation of Group 3 Innate Lymphoid Cells in the Pathogenesis of Inflammatory Bowel Disease. *Current Allergy and Asthma Reports*. 2016;16(10).
192. Fuss IJ, Neurath M, Boirivant M, Klein JS, delaMotte C, Strong SA, et al. Disparate CD4(+) lamina propria (LP) lymphokine secretion profiles in inflammatory bowel disease - Crohn's disease LP cells manifest increased secretion of IFN-gamma, whereas ulcerative colitis LP cells manifest increased secretion of IL-5. *Journal of Immunology*. 1996;157(3):1261-70.

193. Takayama T, Kamada N, Chinen H, Okamoto S, Kitazume MT, Chang J, et al. Imbalance of NKp44(+)NKp46(-) and NKp44(-)NKp46(+) Natural Killer Cells in the Intestinal Mucosa of Patients With Crohn's Disease. *Gastroenterology*. 2010;139(3):882-U251.
194. Sciume G, Hirahara K, Takahashi H, Laurence A, Villarino AV, Singleton KL, et al. Distinct requirements for T-bet in gut innate lymphoid cells. *Journal of Experimental Medicine*. 2012;209(13):2331-8.
195. Longman RS, Diehl GE, Victorio DA, Huh JR, Galan C, Miraldi ER, et al. CX(3)CR1(+) mononuclear phagocytes support colitis-associated innate lymphoid cell production of IL-22. *Journal of Experimental Medicine*. 2014;211(8):1571-83.
196. Wang YY, Mumm JB, Herbst R, Kolbeck R, Wang Y. IL-22 Increases Permeability of Intestinal Epithelial Tight Junctions by Enhancing Claudin-2 Expression. *Journal of Immunology*. 2017;199(9):3316-25.
197. Powell N, Walker AW, Stolarczyk E, Canavan JB, Gokmen MR, Marks E, et al. The Transcription Factor T-bet Regulates Intestinal Inflammation Mediated by Interleukin-7 Receptor(+) Innate Lymphoid Cells. *Immunity*. 2012;37(4):674-84.
198. Garrett WS, Lord GM, Punit S, Lugo-Villarino G, Mazmanian SK, Ito S, et al. Communicable ulcerative colitis induced by T-bet deficiency in the innate immune system. *Cell*. 2007;131(1):33-45.
199. Eken A, Singh AK, Treuting PM, Oukka M. IL-23R(+) innate lymphoid cells induce colitis via interleukin-22-dependent mechanism. *Mucosal Immunology*. 2014;7(1):143-54.
200. Roediger B, Kyle R, Yip KH, Sumaria N, Guy TV, Kim BS, et al. Cutaneous immunosurveillance and regulation of inflammation by group 2 innate lymphoid cells. *Nature Immunology*. 2013;14(6):564-+.
201. Guimond M, Veenstra RG, Grindler DJ, Zhang H, Cui YZ, Murphy RD, et al. Interleukin 7 signaling in dendritic cells regulates the homeostatic proliferation and niche size of CD4(+) T cells. *Nature Immunology*. 2009;10(2):149-57.
202. Bando JK, Colonna M. Innate lymphoid cell function in the context of adaptive immunity. *Nature Immunology*. 2016;17(7):783-9.
203. Drake LY, Kita H. Group 2 Innate Lymphoid Cells in the Lung. *Advances in Immunology*, Vol 124. 2014;124:1-16.
204. Le Goffic R, Arshad MI, Rauch M, L'Helgoualc'h A, Delmas B, Piquet-Pellorce C, et al. Infection with Influenza Virus Induces IL-33 in Murine Lungs. *American Journal of Respiratory Cell and Molecular Biology*. 2011;45(6):1125-32.
205. Fallon PG, Ballantyne SJ, Mangan NE, Barlow JL, Dasvarma A, Hewett DR, et al. Identification of an interleukin (IL)-25-dependent cell population that provides IL-4, IL-5, and IL-13 at the onset of helminth expulsion. *Journal of Experimental Medicine*. 2006;203(4):1105-16.
206. Schmitz J, Owyang A, Oldham E, Song YL, Murphy E, McClanahan TK, et al. IL-33, an interleukin-1-like cytokine that signals via the IL-1 receptor-related protein ST2 and induces T helper type 2-associated cytokines. *Immunity*. 2005;23(5):479-90.
207. McKenzie GJ, Bancroft A, Grecis RK, McKenzie ANJ. A distinct role for interleukin-13 in Th2-cell-mediated immune responses. *Current Biology*. 1998;8(6):339-42.
208. Ikutani M, Yanagibashi T, Ogasawara M, Tsuneyama K, Yamamoto S, Hattori Y, et al. Identification of Innate IL-5-Producing Cells and Their Role in Lung Eosinophil Regulation and Antitumor Immunity. *Journal of Immunology*. 2012;188(2):703-13.

209. Kuperman DA, Huang XZ, Koth LL, Chang GH, Dolganov GM, Zhu Z, et al. Direct effects of interleukin-13 on epithelial cells cause airway hyperreactivity and mucus overproduction in asthma. *Nature Medicine*. 2002;8(8):885-9.
210. Zhou Z, Homer RJ, Wang ZD, Chen QS, Geba GP, Wang JM, et al. Pulmonary expression of interleukin-13 causes inflammation, mucus hypersecretion, subepithelial fibrosis, physiologic abnormalities, and eotaxin production. *Journal of Clinical Investigation*. 1999;103(6):779-88.
211. Grunig G, Warnock M, Wakil AE, Venkayya R, Brombacher F, Rennick DM, et al. Requirement for IL-13 independently of IL-4 in experimental asthma. *Science*. 1998;282(5397):2261-3.
212. Drake LY, Iijima K, Bartemes K, Kita H. Group 2 Innate Lymphoid Cells Promote an Early Antibody Response to a Respiratory Antigen in Mice. *Journal of Immunology*. 2016;197(4):1335-42.
213. Wilhelm C, Hirota K, Stieglitz B, Van Snick J, Tolaini M, Lahl K, et al. An IL-9 fate reporter demonstrates the induction of an innate IL-9 response in lung inflammation. *Nat Immunol*. 2011;12(11):1071-7.
214. Mohapatra A, Van Dyken SJ, Schneider C, Nussbaum JC, Liang HE, Locksley RM. Group 2 innate lymphoid cells utilize the IRF4-IL-9 module to coordinate epithelial cell maintenance of lung homeostasis. *Mucosal Immunology*. 2016;9(1):275-86.
215. Yoshida T, Ikuta K, Sugaya H, Maki K, Takagi M, Kanazawa H, et al. Defective B-1 cell development and impaired immunity against *Angiostrongylus cantonensis* in IL-5R alpha-deficient mice. *Immunity*. 1996;4(5):483-94.
216. Dutton EE, Camelo A, Sleeman M, Herbst R, Carlesso G, Belz GT, et al. Characterisation of innate lymphoid cell populations at different sites in mice with defective T cell immunity. *Wellcome Open Res*. 2017;2:117.
217. Kim HY, Lee HJ, Chang YJ, Pichavant M, Shore SA, Fitzgerald KA, et al. Interleukin-17-producing innate lymphoid cells and the NLRP3 inflammasome facilitate obesity-associated airway hyperreactivity. *Nature Medicine*. 2014;20(1):54-+.
218. Carrega P, Loiacono F, Di Carlo E, Scaramuccia A, Mora M, Conte R, et al. NCR(+)ILC3 concentrate in human lung cancer and associate with intratumoral lymphoid structures. *Nature Communications*. 2015;6.
219. Halim TYF, Krauss RH, Sun AC, Takei F. Lung Natural Helper Cells Are a Critical Source of Th2 Cell-Type Cytokines in Protease Allergen-Induced Airway Inflammation. *Immunity*. 2012;36(3):451-63.
220. Wolterink R, KleinJan A, van Nimwegen M, Bergen I, de Bruijn M, Levani Y, et al. Pulmonary innate lymphoid cells are major producers of IL-5 and IL-13 in murine models of allergic asthma. *European Journal of Immunology*. 2012;42(5):1106-16.
221. Bartemes KR, Iijima K, Kobayashi T, Kephart GM, McKenzie AN, Kita H. IL-33-Responsive Lineage(-)CD25(+)CD44(hi) Lymphoid Cells Mediate Innate Type 2 Immunity and Allergic Inflammation in the Lungs. *Journal of Immunology*. 2012;188(3):1503-13.
222. Hong JY, Bentley JK, Chung YT, Lei J, Steenrod JM, Chen Q, et al. Neonatal rhinovirus induces mucous metaplasia and airways hyperresponsiveness through IL-25 and type 2 innate lymphoid cells. *Journal of Allergy and Clinical Immunology*. 2014;134(2):429-+.
223. Han MY, Rajput C, Hong JY, Lei J, Hinde JL, Wu Q, et al. The Innate Cytokines IL-25, IL-33, and TSLP Cooperate in the Induction of Type 2 Innate Lymphoid Cell Expansion and

- Mucous Metaplasia in Rhinovirus-Infected Immature Mice. *Journal of Immunology*. 2017;199(4):1308-18.
224. Doherty TA, Khorram N, Lund S, Mehta AK, Croft M, Broide DH. Lung type 2 innate lymphoid cells express cysteinyl leukotriene receptor 1, which regulates T(H)2 cytokine production. *Journal of Allergy and Clinical Immunology*. 2013;132(1):205-13.
225. Dalessandri T, Crawford G, Hayes M, Seoane RC, Strid J. IL-13 from intraepithelial lymphocytes regulates tissue homeostasis and protects against carcinogenesis in the skin. *Nature Communications*. 2016;7.
226. Yang J, Hu SM, Zhao LM, Kaplan DH, Perdew GH, Xiong N. Selective programming of CCR10(+) innate lymphoid cells in skin-draining lymph nodes for cutaneous homeostatic regulation. *Nature Immunology*. 2016;17(1):48-+.
227. Salimi M, Barlow JL, Saunders SP, Xue L, Gutowska-Owsiak D, Wang X, et al. A role for IL-25 and IL-33-driven type-2 innate lymphoid cells in atopic dermatitis. *Journal of Experimental Medicine*. 2013;210(13):2939-50.
228. Rak GD, Osborne LC, Siracusa MC, Kim BS, Wang K, Bayat A, et al. IL-33-Dependent Group 2 Innate Lymphoid Cells Promote Cutaneous Wound Healing. *Journal of Investigative Dermatology*. 2016;136(2):487-96.
229. Li Z, Hodgkinson T, Gothard EJ, Boroumand S, Lamb R, Cummins I, et al. Epidermal Notch1 recruits ROR gamma(+) group 3 innate lymphoid cells to orchestrate normal skin repair. *Nature Communications*. 2016;7.
230. McGee HM, Schmidt BA, Booth CJ, Yancopoulos GD, Valenzuela DM, Murphy AJ, et al. IL-22 Promotes Fibroblast-Mediated Wound Repair in the Skin. *Journal of Investigative Dermatology*. 2013;133(5):1321-9.
231. Kim BS, Wang K, Siracusa MC, Saenz SA, Brestoff JR, Monticelli LA, et al. Basophils Promote Innate Lymphoid Cell Responses in Inflamed Skin. *Journal of Immunology*. 2014;193(7):3717-25.
232. Cai YH, Shen XY, Ding CL, Qi CJ, Li KJ, Li X, et al. Pivotal Role of Dermal IL-17-Producing gamma delta T Cells in Skin Inflammation. *Immunity*. 2011;35(4):596-610.
233. Pantelyushin S, Haak S, Ingold B, Kulig P, Heppner FL, Navarini AA, et al. Ror gamma t(+) innate lymphocytes and gamma delta T cells initiate psoriasiform plaque formation in mice. *Journal of Clinical Investigation*. 2012;122(6):2252-6.
234. Villanova F, Flutter B, Tosi I, Grys K, Sreeneebus H, Perera GK, et al. Characterization of innate lymphoid cells (ILC) in human skin and blood reveals an increase of NKp44+ ILC3 in psoriasis. *British Journal of Dermatology*. 2014;170(4):E17-E.
235. Yoshida H, Honda K, Shinkura R, Adachi S, Nishikawa S, Maki K, et al. IL-7 receptor alpha(+) CD3(-) cells in the embryonic intestine induces the organizing center of Peyer's patches. *International Immunology*. 1999;11(5):643-55.
236. Detogni P, Goellner J, Ruddle NH, Streeter PR, Fick A, Mariathasan S, et al. Abnormal-Development of Peripheral Lymphoid Organs in mice Deficient in Lymphotoxin. *Science*. 1994;264(5159):703-7.
237. Yokota Y, Mansouri A, Mori S, Sugawara S, Adachi S, Nishikawa S, et al. Development of peripheral lymphoid organs and natural killer cells depends on the helix-loop-helix inhibitor Id2. *Nature*. 1999;397(6721):702-6.
238. Kurebayashi S, Ueda E, Sakaue M, Patel DD, Medvedev A, Zhang F, et al. Retinoid-related orphan receptor gamma (ROR gamma) is essential for lymphoid organogenesis and

- controls apoptosis during thymopoiesis. *Proceedings of the National Academy of Sciences of the United States of America*. 2000;97(18):10132-7.
239. Sun ZM, Unutmaz D, Zou YR, Sunshine MJ, Pierani A, Brenner-Morton S, et al. Requirement for ROR gamma in thymocyte survival and lymphoid organ development. *Science*. 2000;288(5475):2369-73.
 240. Yoshida H, Naito A, Inoue J, Satoh M, Santee-Cooper SM, Ware CF, et al. Different cytokines induce surface lymphotoxin-alpha beta on IL-7 receptor-alpha cells that differentially engender lymph nodes and Peyer's patches. *Immunity*. 2002;17(6):823-33.
 241. Mueller CG, Hess E. Emerging functions of RANKL in lymphoid tissues. *Frontiers in Immunology*. 2012;3.
 242. Dougall WC, Glaccum M, Charrier K, Rohrbach K, Brasel K, De Smedt T, et al. RANK is essential for osteoclast and lymph node development. *Genes & Development*. 1999;13(18):2412-24.
 243. Mackley EC, Houston S, Marriott CL, Halford EE, Lucas B, Cerovic V, et al. CCR7-dependent trafficking of ROR gamma(+) ILCs creates a unique microenvironment within mucosal draining lymph nodes. *Nature Communications*. 2015;6.
 244. Scandella E, Bolinger B, Lattmann E, Miller S, Favre S, Littman DR, et al. Restoration of lymphoid organ integrity through the interaction of lymphoid tissue-inducer cells with stroma of the T cell zone. *Nature Immunology*. 2008;9(6):667-75.
 245. Yang J, Cornelissen F, Papazian N, Reijmers RM, Llorian M, Cupedo T, et al. IL-7-dependent maintenance of ILC3s is required for normal entry of lymphocytes into lymph nodes. *Journal of Experimental Medicine*. 2018;215(4):1069-77.
 246. van Panhuys N, Klauschen F, Germain RN. T-Cell-Receptor-Dependent Signal Intensity Dominantly Controls CD4(+) T Cell Polarization In Vivo. *Immunity*. 2014;41(1):63-74.
 247. Tomura M, Hata A, Matsuoka S, Shand FHW, Nakanishi Y, Ikebuchi R, et al. Tracking and quantification of dendritic cell migration and antigen trafficking between the skin and lymph nodes. *Scientific Reports*. 2014;4.
 248. O'Sullivan TE, Rapp MY, Fan XY, Weizman OE, Bhardwaj P, Adams NM, et al. Adipose-Resident Group 1 Innate Lymphoid Cells Promote Obesity-Associated Insulin Resistance. *Immunity*. 2016;45(2):428-41.
 249. Gasteiger G, Fan XY, Dikiy S, Lee SY, Rudensky AY. Tissue residency of innate lymphoid cells in lymphoid and nonlymphoid organs. *Science*. 2015;350(6263):981-5.
 250. Warnock RA, Askari S, Butcher EC, von Andrian UH. Molecular mechanisms of lymphocyte homing to peripheral lymph nodes. *Journal of Experimental Medicine*. 1998;187(2):205-16.
 251. Campbell JJ, Qin SX, Unutmaz D, Soler D, Murphy KE, Hodge MR, et al. Unique subpopulations of CD56(+) NK and NK-T peripheral blood lymphocytes identified by chemokine receptor expression repertoire. *Journal of Immunology*. 2001;166(11):6477-82.
 252. Kim MH, Taparowsky EJ, Kim CH. Retinoic Acid Differentially Regulates the Migration of Innate Lymphoid Cell Subsets to the Gut. *Immunity*. 2015;43(1):107-19.
 253. Teunissen MBM, Munneke JM, Bernink JH, Spuls PI, Res PCM, te Velde A, et al. Composition of Innate Lymphoid Cell Subsets in the Human Skin: Enrichment of NCR+ ILC3 in Lesional Skin and Blood of Psoriasis Patients. *Journal of Investigative Dermatology*. 2014;134(9):2351-60.

254. Huang YF, Mao K, Chen X, Sun MA, Kawabe T, Li WZ, et al. S1P-dependent interorgan trafficking of group 2 innate lymphoid cells supports host defense. *Science*. 2018;359(6371):114-9.
255. Forster R, Schubel A, Breitfeld D, Kremmer E, Renner-Muller I, Wolf E, et al. CCR7 coordinates the primary immune response by establishing functional microenvironments in secondary lymphoid organs. *Cell*. 1999;99(1):23-33.
256. Iiyama R, Kanai T, Uraushihara K, Totsuka T, Nakamura T, Miyata T, et al. The role of inducible co-stimulator (ICOS)/B7-related protein-1 (B7RP-1) interaction in the functional development of Peyer's patches. *Immunology Letters*. 2003;88(1):63-70.
257. Mak TW, Shahinian A, Yoshinaga SK, Wakeham A, Boucher LM, Pintilie M, et al. Costimulation through the inducible costimulator ligand is essential for both T helper and B cell functions in T cell-dependent B cell responses. *Nature Immunology*. 2003;4(8):765-72.
258. Jackson JT, Hu YF, Liu RJ, Masson F, D'Amico A, Carotta S, et al. Id2 expression delineates differential checkpoints in the genetic program of CD8 alpha(+) and CD103(+) dendritic cell lineages. *Embo Journal*. 2011;30(13):2690-704.
259. Ando R, Hama H, Yamamoto-Hino M, Mizuno H, Miyawaki A. An optical marker based on the UV-induced green-to-red photoconversion of a fluorescent protein. *Proceedings of the National Academy of Sciences of the United States of America*. 2002;99(20):12651-6.
260. Mizuno H, Mal TK, Tong KI, Ando R, Furuta T, Ikura M, et al. Photo-induced peptide cleavage in the green-to-red conversion of a fluorescent protein. *Molecular Cell*. 2003;12(4):1051-8.
261. Mandala S, Hajdu R, Bergstrom J, Quackenbush E, Xie J, Milligan J, et al. Alteration of lymphocyte trafficking by sphingosine-1-phosphate receptor agonists. *Science*. 2002;296(5566):346-9.
262. Maazi H, Patel N, Sankaranarayanan I, Suzuki Y, Rigas D, Soroosh P, et al. ICOS:ICOS-Ligand Interaction Is Required for Type 2 Innate Lymphoid Cell Function, Homeostasis, and Induction of Airway Hyperreactivity. *Immunity*. 2015;42(3):538-51.
263. Robinette ML, Fuchs A, Cortez VS, Lee JS, Wang YM, Durum SK, et al. Transcriptional programs define molecular characteristics of innate lymphoid cell classes and subsets. *Nature Immunology*. 2015;16(3):306-U142.
264. Qiu J, Heller JJ, Guo XH, Chen ZME, Fish K, Fu YX, et al. The Aryl Hydrocarbon Receptor Regulates Gut Immunity through Modulation of Innate Lymphoid Cells. *Immunity*. 2012;36(1):92-104.
265. Monticelli LA, Buck MD, Flamar AL, Saenz SA, Wojno EDT, Yudanin NA, et al. Arginase 1 is an innate lymphoid-cell-intrinsic metabolic checkpoint controlling type 2 inflammation. *Nature Immunology*. 2016;17(6):656-+.
266. Liu Q, Zhao R, Huang C, Zhou K-L, Zhang X-L, Pan Q. Effects of enzymatic digestion, cell culture and preservation conditions on surface CD62L expression of primary murine CD3⁺CD4⁺ T cells. *Biomedical Research*. 2018;29(10).
267. Mjosberg J, Spits H. Human innate lymphoid cells. *J Allergy Clin Immunol*. 2016;138(5):1265-76.
268. Mjosberg JM, Trifari S, Crellin NK, Peters CP, van Drunen CM, Piet B, et al. Human IL-25-and IL-33-responsive type 2 innate lymphoid cells are defined by expression of CCR4 and CD161. *Nature Immunology*. 2011;12(11):1055-U56.

269. Bernink JH, Peters CP, Munneke M, te Velde AA, Meijer SL, Weijer K, et al. Human type 1 innate lymphoid cells accumulate in inflamed mucosal tissues. *Nature Immunology*. 2013;14(3):221-9.
270. Spits H, Di Santo JP. The expanding family of innate lymphoid cells: regulators and effectors of immunity and tissue remodeling. *Nature Immunology*. 2011;12(1):21-7.
271. Penaloza HF, Salazar-Echegarai FJ, Bueno SM. Interleukin 10 modulation of neutrophil subsets infiltrating lungs during *Streptococcus pneumoniae* infection. *Biochem Biophys Res Commun*. 2018;13:12-6.
272. Spits H, Bernink JH, Lanier L. NK cells and type 1 innate lymphoid cells: partners in host defense. *Nature Immunology*. 2016;17(7):758-64.
273. Kopf M, Schneider C, Nobs SP. The development and function of lung-resident macrophages and dendritic cells. *Nature Immunology*. 2015;16(1):36-44.
274. Li BWS, Stadhouders R, de Bruijn MJW, Lukkes M, Beerens D, Brem MD, et al. Group 2 Innate Lymphoid Cells Exhibit a Dynamic Phenotype in Allergic Airway Inflammation. *Frontiers in Immunology*. 2017;8.
275. Henson SM, Akbar AN. KLRG1-more than a marker for T cell senescence. *Age*. 2009;31(4):285-91.
276. Ryffel B, Willcocks JL, Brooks N, Woerly G. Interleukin-2 Receptor (CD25) Up-Regulation on Human T-Lymphocytes - Sensitivity to Immunosuppressants is Defined by The Mode of T-Lymphocyte Activation. *Immunopharmacology*. 1995;30(3):199-207.
277. Liu Y, Pop R, Sadegh C, Brugnara C, Haase VH, Socolovsky M. Suppression of Fas-FasL coexpression by erythropoietin mediates erythroblast expansion during the erythropoietic stress response in vivo. *Blood*. 2006;108(1):123-33.
278. Rose S, Misharin A, Perlman H. A novel Ly6C/Ly6G-based strategy to analyze the mouse splenic myeloid compartment. *Cytometry Part A*. 2012;81A(4):343-+.
279. Hamaguchi-Tsuru E, Nobumoto A, Hirose N, Kataoka S, Fujikawa-Adachi K, Furuya M, et al. Development and functional analysis of eosinophils from murine embryonic stem cells. *British Journal of Haematology*. 2004;124(6):819-27.
280. Shi J, Ikeda K, Maeda Y, Shinagawa K, Ohtsuka A, Yamamura H, et al. Identification of CD123(+) myeloid dendritic cells as an early-stage immature subset with strong tumorigenic potential. *Cancer Letters*. 2008;270(1):19-29.
281. Bedoret D, Wallemacq H, Marichal T, Desmet C, Calvo FQ, Henry E, et al. Lung interstitial macrophages alter dendritic cell functions to prevent airway allergy in mice. *Journal of Clinical Investigation*. 2009;119(12):3723-38.
282. Arase H, Saito T, Phillips JH, Lanier LL. Cutting edge: The mouse NK cell-associated antigen recognized by DX5 monoclonal antibody is CD49b (alpha2) integrin, very late antigen-2). *Journal of Immunology*. 2001;167(3):1141-4.
283. Scholzen T, Gerdes J. The Ki-67 protein: From the known and the unknown. *Journal of Cellular Physiology*. 2000;182(3):311-22.
284. Pearson C, Thornton EE, McKenzie B, Schaupp AL, Huskens N, Griseri T, et al. ILC3 GM-CSF production and mobilisation orchestrate acute intestinal inflammation. *Elife*. 2016;5.
285. Hoorweg K, Narang P, Li Z, Thuery A, Papazian N, Withers DR, et al. A Stromal Cell Niche for Human and Mouse Type 3 Innate Lymphoid Cells. *Journal of Immunology*. 2015;195(9):4257-63.

286. Bar-Ephraim YE, Cornelissen F, Papazian N, Konijn T, Hoogenboezem RM, Sanders MA, et al. Cross-Tissue Transcriptomic Analysis of Human Secondary Lymphoid Organ-Residing ILC3s Reveals a Quiescent State in the Absence of Inflammation. *Cell Reports*. 2017;21(3):823-33.
287. Rodriguez-Carrio J, Hahnlein JS, Ramwadhoebe TH, Semmelink JF, Choi IY, van Lienden KP, et al. Altered Innate Lymphoid Cell Subsets in Human Lymph Node Biopsy Specimens Obtained During the At-Risk and Earliest Phases of Rheumatoid Arthritis. *Arthritis & Rheumatology*. 2017;69(1):70-6.
288. Bernink JH, Mjosberg J, Spits H. Human ILC1: To Be or Not to Be. *Immunity*. 2017;46(5):756-7.
289. Simoni Y, Fehlings M, Kloverpris HN, McGovern N, Koo SL, Loh CY, et al. Human Innate Lymphoid Cell Subsets Possess Tissue-Type Based Heterogeneity in Phenotype and Frequency. *Immunity*. 2017;46(1):148-61.
290. Komlosi ZI, Kovacs N, van de Veen W, Kirsch AI, Fahrner HB, Wawrzyniak M, et al. Human CD40 ligand-expressing type 3 innate lymphoid cells induce IL-10-producing immature transitional regulatory B cells. *Journal of Allergy and Clinical Immunology*. 2018;142(1):178-+.
291. Fossum CC, Chintakuntlawar AV, Price DL, Garcia JJ. Characterization of the oropharynx: anatomy, histology, immunology, squamous cell carcinoma and surgical resection. *Histopathology*. 2017;70(7):1021-9.
292. Woon HG, Braun A, Li J, Smith C, Edwards J, Sierro F, et al. Compartmentalization of Total and Virus-Specific Tissue-Resident Memory CD8⁺T Cells in Human Lymphoid Organs. *Plos Pathogens*. 2016;12(8).
293. Bjorklund AK, Forkel M, Picelli S, Konya V, Theorell J, Friberg D, et al. The heterogeneity of human CD127⁺ innate lymphoid cells revealed by single-cell RNA sequencing (vol 17, pg 451, 2016). *Nature Immunology*. 2016;17(6):740-.
294. Yoshida H, Kawamoto H, Santee SM, Hashi H, Honda K, Nishikawa S, et al. Expression of $\alpha(4)\beta(7)$ integrin defines a distinct pathway of lymphoid progenitors committed to T cells, fetal intestinal lymphotoxin producer, NK, and dendritic cells. *Journal of Immunology*. 2001;167(5):2511-21.
295. Fergusson JR, Smith KE, Fleming VM, Rajoriya N, Newell EW, Simmons R, et al. CD161 Defines a Transcriptional and Functional Phenotype across Distinct Human T Cell Lineages. *Cell Reports*. 2014;9(3):1075-88.
296. McAdam AJ, Chang TT, Lumelsky AE, Greenfield EA, Boussiotis VA, Duke-Cohan JS, et al. Mouse inducible costimulatory molecule (ICOS) expression is enhanced by CD28 costimulation and regulates differentiation of CD4⁺ T cells. *Journal of Immunology*. 2000;165(9):5035-40.
297. Swallow MM, Wallin JJ, Sha WC. B7h, a novel costimulatory homolog of b7.1 and b7.2, is induced by TNF α . *Immunity*. 1999;11(4):423-32.
298. Richter G, Hayden-Ledbetter M, Irgang M, Ledbetter JA, Westermann J, Korner I, et al. Tumor necrosis factor- α regulates the expression of inducible costimulator receptor ligand on CD34⁺ progenitor cells during differentiation into antigen presenting cells. *Journal of Biological Chemistry*. 2001;276(49):45686-93.
299. Yoshinaga SK, Zhang M, Pistillo J, Horan T, Khare SD, Miner K, et al. Characterization of a new human B7-related protein: B7RP-1 is the ligand to the co-stimulatory protein ICOS. *International Immunology*. 2000;12(10):1439-47.

300. Tafuri A, Shahinian A, Bladt F, Yoshinaga SK, Jordana M, Wakeham A, et al. ICOS is essential for effective T-helper-cell responses. *Nature*. 2001;409(6816):105-9.
301. Hutloff A, Dittrich AM, Beier KC, Eljaschewitsch B, Kraft R, Anagnostopoulos I, et al. ICOS is an inducible T-cell co-stimulator structurally and functionally related to CD28. *Nature*. 1999;397(6716):263-6.
302. Arimura Y, Kato H, Dianzani U, Okamoto T, Kamekura S, Buonfiglio D, et al. A co-stimulatory molecule on activated T cells, H4/ICOS, delivers specific signals in T-h cells and regulates their responses. *International Immunology*. 2002;14(6):555-66.
303. Simpson TR, Quezada SA, Allison JP. Regulation of CD4 T cell activation and effector function by inducible costimulator (ICOS). *Current Opinion in Immunology*. 2010;22(3):326-32.
304. Weber JP, Fuhrmann F, Feist RK, Lahmann A, Al Baz MS, Gentz LJ, et al. ICOS maintains the T follicular helper cell phenotype by down-regulating Kruppel-like factor 2. *Journal of Experimental Medicine*. 2015;212(2):217-33.
305. Watanabe M, Takagi Y, Kotani M, Hara Y, Inamine A, Hayashi K, et al. Down-regulation of ICOS ligand by interaction with ICOS functions as a regulatory mechanism for immune responses. *Journal of Immunology*. 2008;180(8):5222-34.
306. Paclik D, Stehle C, Lahmann A, Hutloff A, Romagnani C. ICOS regulates the pool of group 2 innate lymphoid cells under homeostatic and inflammatory conditions in mice. *European Journal of Immunology*. 2015;45(10):2766-72.
307. Franklin CL, Ericsson AC. Microbiota and reproducibility of rodent models. *Lab Animal*. 2017;46(4):114-22.
308. Belkaid Y, Hand TW. Role of the Microbiota in Immunity and Inflammation. *Cell*. 2014;157(1):121-41.
309. Denning TL, Norris BA, Medina-Contreras O, Manicassamy S, Geem D, Madan R, et al. Functional Specializations of Intestinal Dendritic Cell and Macrophage Subsets That Control Th17 and Regulatory T Cell Responses Are Dependent on the T Cell/APC Ratio, Source of Mouse Strain, and Regional Localization. *Journal of Immunology*. 2011;187(2):733-47.
310. Fearon DT, Locksley RM. Elements of immunity - The instructive role of innate immunity in the acquired immune response. *Science*. 1996;272(5258):50-4.
311. Marchesi VT, Gowans JL. The Migration of Lymphocytes Through the Endothelium of Venules in Lymph Nodes: An Electron Microscope Study. *Proc R Soc Lond B Biol Sci*. 1964;159:283-90.
312. Rosen SD. Ligands for L-selectin: Homing, inflammation, and beyond. *Annual Review of Immunology*. 2004;22:129-56.
313. Arbones ML, Ord DC, Ley K, Ratech H, Maynardcurry C, Otten G, et al. Lymphocyte Homing and Leukocyte Rolling and Migration are Impaired in L-Selectin-Deficient Mice. *Immunity*. 1994;1(4):247-60.
314. McEver RP, Cummings RD. Role of PSGL-1 binding to selectins in leukocyte recruitment. *Journal of Clinical Investigation*. 1997;100(3):485-92.
315. Klinger A, Gebert A, Bieber K, Kalies K, Ager A, Bell EB, et al. Cyclical expression of L-selectin (CD62L) by recirculating T cells. *International Immunology*. 2009;21(4):443-55.
316. Stein JV, Rot A, Luo Y, Narasimhaswamy M, Nakano H, Gunn MD, et al. The CC chemokine thymus-derived chemotactic agent 4 (TCA-4, secondary lymphoid tissue chemokine, 6Ckine, exodus-2) triggers lymphocyte function-associated antigen 1-mediated

- arrest of rolling T lymphocytes in peripheral lymph node high endothelial venules. *Journal of Experimental Medicine*. 2000;191(1):61-75.
317. Gunn MD, Tangemann K, Tam C, Cyster JG, Rosen SD, Williams LT. A chemokine expressed in lymphoid high endothelial venules promotes the adhesion and chemotaxis of naive T lymphocytes. *Proceedings of the National Academy of Sciences of the United States of America*. 1998;95(1):258-63.
 318. Shamri R, Grabovsky V, Gauguier JM, Feigelson S, Manevich E, Kolanus W, et al. Lymphocyte arrest requires instantaneous induction of an extended LFA-1 conformation mediated by endothelium-bound chemokines. *Nature Immunology*. 2005;6(5):497-506.
 319. Wagner N, Lohler J, Kunkel EJ, Ley K, Leung E, Krissansen G, et al. Critical role for beta 7 integrins in formation of the gut-associated lymphoid tissue. *Nature*. 1996;382(6589):366-70.
 320. Gofu G, Rivera-Nieves J, Ley K. Role of beta(7) Integrins in Intestinal Lymphocyte Homing and Retention. *Current Molecular Medicine*. 2009;9(7):836-50.
 321. Hamann A, Andrew DP, Jablonskiwestrich D, Holzmann B, Butcher EC. Role of Alpha(4)-Integrins in Lymphocyte Homing to Mucosal Tissues In-Vivo. *Journal of Immunology*. 1994;152(7):3282-93.
 322. Pappu R, Schwab SR, Cornelissen I, Pereira JP, Regard JB, Xu Y, et al. Promotion of lymphocyte egress into blood and lymph by distinct sources of sphingosine-1-phosphate. *Science*. 2007;316(5822):295-8.
 323. Pham THM, Baluk P, Xu Y, Grigorova I, Bankovich AJ, Pappu R, et al. Lymphatic endothelial cell sphingosine kinase activity is required for lymphocyte egress and lymphatic patterning. *Journal of Experimental Medicine*. 2010;207(1):17-27.
 324. Graeler M, Goetzl EJ. Activation-regulated expression and chemotactic function of sphingosine 1-phosphate receptors in mouse splenic T cells. *Faseb Journal*. 2002;16(14):1874-8.
 325. Matloubian M, Lo CG, Cinamon G, Lesneski MJ, Xu Y, Brinkmann V, et al. Lymphocyte egress from thymus and peripheral lymphoid organs is dependent on S1P receptor 1. *Nature*. 2004;427(6972):355-60.
 326. Walzer T, Chiossone L, Chaix J, Calver A, Carozzo C, Garrigue-Antar L, et al. Natural killer cell trafficking in vivo requires a dedicated sphingosine 1-phosphate receptor. *Nature Immunology*. 2007;8(12):1337-44.
 327. Grigorova IL, Schwab SR, Phan TG, Pham THM, Okada T, Cyster JG. Cortical sinus probing, S1P1-dependent entry and flow-based capture of egressing T cells (vol 10, pg 58, 2009). *Nature Immunology*. 2009;10(2):223-.
 328. Schwab SR, Pereira JP, Matloubian M, Xu Y, Huang Y, Cyster JG. Lymphocyte sequestration through S1P lyase inhibition and disruption of S1P gradients. *Science*. 2005;309(5741):1735-9.
 329. Lo CG, Xu Y, Proia RL, Cyster JG. Cyclical modulation of sphingosine-1-phosphate receptor 1 surface expression during lymphocyte recirculation and relationship to lymphoid organ transit. *Journal of Experimental Medicine*. 2005;201(2):291-301.
 330. Harrell MI, Iritani BM, Ruddell A. Lymph Node Mapping in the Mouse. *J Immunol Methods*. 2008;332(1-2):170-4.
 331. Tilney NL. Patterns of lymphatic drainage in the adult laboratory rat. *J Anat*. 1971;109(Pt 3):369-83.

332. Shiow LR, Rosen DB, Brdickova N, Xu Y, An JP, Lanier LL, et al. CD69 acts downstream of interferon-alpha/beta to inhibit S1P(1) and lymphocyte egress from lymphoid organs. *Nature*. 2006;440(7083):540-4.
333. Nakayama T, Kaspirowicz DJ, Yamashita M, Schubert LA, Gillard G, Kimura M, et al. The generation of mature, single-positive thymocytes in vivo is dysregulated by CD69 blockade or overexpression. *Journal of Immunology*. 2002;168(1):87-94.
334. Feng CG, Woodside KJ, Vance BA, El-Khoury D, Canelles M, Lee J, et al. A potential role for CD69 in thymocyte emigration. *International Immunology*. 2002;14(6):535-44.
335. Lamana A, Martin P, de la Fuente H, Martinez-Munoz L, Cruz-Adalia A, Ramirez-Huesca M, et al. CD69 Modulates Sphingosine-1-Phosphate-Induced Migration of Skin Dendritic Cells. *Journal of Investigative Dermatology*. 2011;131(7):1503-12.
336. Nemet I, Ropelewski P, Imanishi Y. Applications of phototransformable fluorescent proteins for tracking the dynamics of cellular components. *Photochemical & Photobiological Sciences*. 2015;14(10):1787-806.
337. Braun A, Worbs T, Moschovakis GL, Halle S, Hoffmann K, Bolter J, et al. Afferent lymph-derived T cells and DCs use different chemokine receptor CCR7-dependent routes for entry into the lymph node and intranodal migration. *Nat Immunol*. 2011;12(9):879-87.
338. Nakamizo S, Egawa G, Tomura M, Sakai S, Tsuchiya S, Kitoh A, et al. Dermal V gamma 4(+) gamma delta T Cells Possess a Migratory Potency to the Draining Lymph Nodes and Modulate CD8(+) T-Cell Activity through TNF-alpha Production. *Journal of Investigative Dermatology*. 2015;135(4):1007-15.
339. Turley SJ, Fletcher AL, Elpek KG. The stromal and haematopoietic antigen-presenting cells that reside in secondary lymphoid organs. *Nature Reviews Immunology*. 2010;10(12):813-25.
340. Strid J, Sobolev O, Zafirova B, Polic B, Hayday A. The Intraepithelial T Cell Response to NKG2D-Ligands Links Lymphoid Stress Surveillance to Atopy. *Science*. 2011;334(6060):1293-7.
341. MacLeod AS, Havran WL. Functions of skin-resident gamma delta T cells. *Cellular and Molecular Life Sciences*. 2011;68(14):2399-408.
342. Pang DJ, Neves JF, Sumaria N, Pennington DJ. Understanding the complexity of gamma delta T-cell subsets in mouse and human. *Immunology*. 2012;136(3):283-90.
343. Matloubian M, Lo CG, Cinamon G, Lesneski MJ, Xu Y, Brinkmann V, et al. Lymphocyte egress from thymus and peripheral lymphoid organs is dependent on S1P receptor 1. *Nature*. 2004;427(6972):355-60.
344. Jenne CN, Enders A, Rivera R, Watson SR, Bankovich AJ, Pereira JP, et al. T-bet-dependent S1P(5) expression in NK cells promotes egress from lymph nodes and bone marrow. *Journal of Experimental Medicine*. 2009;206(11):2469-81.
345. Jenne CN, Enders A, Rivera R, Watson SR, Bankovich AJ, Pereira JP, et al. T-bet-dependent S1P5 expression in NK cells promotes egress from lymph nodes and bone marrow. *J Exp Med*. 2009;206(11):2469-81.
346. Lucas M, Schachterle W, Oberle K, Aichele P, Diefenbach A. Dendritic cells prime natural killer cells by trans-presenting interleukin 15. *Immunity*. 2007;26(4):503-17.
347. Boulenouar S, Michelet X, Duquette D, Alvarez D, Hogan AE, Dold C, et al. Adipose Type One Innate Lymphoid Cells Regulate Macrophage Homeostasis through Targeted Cytotoxicity. *Immunity*. 2017;46(2):273-86.

348. Gurskaya NG, Verkhusha VV, Shcheglov AS, Staroverov DB, Chepurnykh TV, Fradkov AF, et al. Engineering of a monomeric green-to-red photoactivatable fluorescent protein induced by blue light. *Nature Biotechnology*. 2006;24(4):461-5.
349. Ugur M, Schulz O, Menon MB, Krueger A, Pabst O. Resident CD4(+) T cells accumulate in lymphoid organs after prolonged antigen exposure. *Nature Communications*. 2014;5.
350. Ugur M, Kaminski A, Pabst O. Lymph node gamma delta and alpha beta CD8(+) T cells share migratory properties. *Scientific Reports*. 2018;8.
351. Pham AH, McCaffery JM, Chan DC. Mouse lines with photo-activatable mitochondria to study mitochondrial dynamics. *Genesis*. 2012;50(11):833-43.
352. Ohl L, Mohaupt M, Czeloth N, Hintzen G, Kiafard Z, Zwirner J, et al. CCR7 governs skin dendritic cell migration under inflammatory and steady-state conditions. *Immunity*. 2004;21(2):279-88.
353. Tal O, Lim HY, Gurevich I, Milo I, Shipony Z, Ng LG, et al. DC mobilization from the skin requires docking to immobilized CCL21 on lymphatic endothelium and intralymphatic crawling. *Journal of Experimental Medicine*. 2011;208(10):2141-53.
354. Jiang A, Bloom O, Ono S, Cui WG, Unternaehrer J, Jiang S, et al. Disruption of E-cadherin-mediated adhesion induces a functionally distinct pathway of dendritic cell maturation. *Immunity*. 2007;27(4):610-24.
355. Czeloth N, Bernhardt G, Hofmann F, Genth H, Forster R. Sphingosine-1-phosphate mediates migration of mature dendritic cells. *Journal of Immunology*. 2005;175(5):2960-7.
356. Kabashima K, Shiraishi N, Sugita K, Mori T, Onoue A, Kobayashi M, et al. CXCL12-CXCR4 engagement is required for migration of cutaneous dendritic cells. *American Journal of Pathology*. 2007;171(4):1249-57.
357. Ouwehand K, Santegoets S, Bruynzeel DP, Scheper RJ, de Gruijl TD, Gibbs S. CXCL12 is essential for migration of activated Langerhans cells from epidermis to dermis. *European Journal of Immunology*. 2008;38(11):3050-9.
358. Tomura M, Honda T, Tanizaki H, Otsuka A, Egawa G, Tokura Y, et al. Activated regulatory T cells are the major T cell type emigrating from the skin during a cutaneous immune response in mice. *Journal of Clinical Investigation*. 2010;120(3):883-93.
359. Teixeira A, Hunter MC, Russo E, Proulx ST, Frei T, Debes GF, et al. T Cell Migration from Inflamed Skin to Draining Lymph Nodes Requires Intralymphatic Crawling Supported by ICAM-1/LFA-1 Interactions. *Cell Reports*. 2017;18(4):857-65.
360. Forster R, Braun A, Worbs T. Lymph node homing of T cells and dendritic cells via afferent lymphatics. *Trends in Immunology*. 2012;33(6):271-80.
361. Debes GF, Arnold CN, Young AJ, Krautwald S, Lipp M, Hay JB, et al. CC chemokine receptor 7 required for T lymphocyte exit from peripheral tissues. *Nat Immunol*. 2005;6(9):889-94.
362. Logan G, Wilhelm DL. Vascular Permeability Changes in Inflammation. Role of Endogenous Permeability Factors in Ultraviolet Injury. *British Journal of Experimental Pathology*. 1966;47(3):300-&.
363. Clydesdale GJ, Dandie GW, Muller HK. Ultraviolet light induced injury: Immunological and inflammatory effects. *Immunology and Cell Biology*. 2001;79(6):547-68.
364. Gierynska M, Pawlak E, Schollenberger A, Cespedes IS. Dendritic epidermal T cells: their role in the early phase of ectromelia virus infection. *Postepy Hig Med Dosw (Online)*. 2009;63:369-76.

365. Kissenpfennig A, Henri S, Dubois B, Laplace-Builhe C, Perrin P, Romani N, et al. Dynamics and function of langerhans cells in vivo: Dermal dendritic cells colonize lymph node areas distinct from slower migrating langerhans cells. *Immunity*. 2005;22(5):643-54.
366. Elentner A, Finke D, Schmuth M, Chappaz S, Ebner S, Malissen B, et al. Langerhans cells are critical in the development of atopic dermatitis-like inflammation and symptoms in mice. *Journal of Cellular and Molecular Medicine*. 2009;13(8B):2658-72.
367. Kripke ML, Munn CG, Jeevan A, Tang JM, Bucana C. Evidence that Cutaneous Antigen-Presenting Cells Migrate to Regional Lymph-Nodes During Contact Sensitization. *Journal of Immunology*. 1990;145(9):2833-8.
368. Fukunaga A, Nagai H, Noguchi T, Okazawa H, Matozaki T, Yu XJ, et al. Src homology 2 domain-containing protein tyrosine phosphatase substrate 1 regulates the migration of Langerhans cells from the epidermis to draining lymph nodes. *Journal of Immunology*. 2004;172(7):4091-9.
369. Li M, Hener P, Zhang ZK, Ganti KP, Metzger D, Chambon P. Induction of Thymic Stromal Lymphopoietin Expression in Keratinocytes Is Necessary for Generating an Atopic Dermatitis upon Application of the Active Vitamin D3 Analogue MC903 on Mouse Skin. *Journal of Investigative Dermatology*. 2009;129(2):498-502.
370. Li M, Hener P, Zhang ZK, Kato S, Metzger D, Chambon P. Topical vitamin D3 and low-calcemic analogs induce thymic stromal lymphopoietin in mouse keratinocytes and trigger an atopic dermatitis. *Proceedings of the National Academy of Sciences of the United States of America*. 2006;103(31):11736-41.
371. Moosbrugger-Martinz V, Schmuth M, Dubrac S. A Mouse Model for Atopic Dermatitis Using Topical Application of Vitamin D3 or of Its Analog MC903. *Methods Mol Biol*. 2017;1559:91-106.
372. Kragballe K. Treatment of Psoriasis with Calcipotriol and Other Vitamin-D Analogs. *Journal of the American Academy of Dermatology*. 1992;27(6):1001-8.
373. Moosbrugger-Martinz V, Schmuth M, Dubrac S. A Mouse Model for Atopic Dermatitis Using Topical Application of Vitamin D3 or of Its Analog MC903. *Inflammation: Methods and Protocols*. 2017;1559:91-106.
374. Howell MD, Kim BE, Gao PS, Grant AV, Boguniewicz M, DeBenedetto A, et al. Cytokine modulation of atopic dermatitis filaggrin skin expression (Reprinted from *J Allergy Clin Immunol* vol 120, pg 150-5, 2007). *Journal of Allergy and Clinical Immunology*. 2009;124(3):R7-R12.
375. Elias PM, Schmuth M. Abnormal skin barrier in the etiopathogenesis of atopic dermatitis. *Current Opinion in Allergy and Clinical Immunology*. 2009;9(5):437-46.
376. Zhu MZ, Yang YJ, Wang YG, Wang ZN, Fu YX. LIGHT Regulates Inflamed Draining Lymph Node Hypertrophy. *Journal of Immunology*. 2011;186(12):7156-63.
377. Nakai A, Hayano Y, Furuta F, Noda M, Suzuki K. Control of lymphocyte egress from lymph nodes through beta(2)-adrenergic receptors. *Journal of Experimental Medicine*. 2014;211(13):2583-98.
378. Dimitroff CJ, Kupper TS, Sackstein R. Prevention of leukocyte migration to inflamed skin with a novel fluorosugar modifier of cutaneous lymphocyte-associated antigen. *Journal of Clinical Investigation*. 2003;112(7):1008-18.

379. Robert C, Fuhlbrigge RC, Kieffer JD, Ayehunie S, Hynes RO, Cheng GY, et al. Interaction of dendritic cells with skin endothelium: A new perspective on immunosurveillance. *Journal of Experimental Medicine*. 1999;189(4):627-35.
380. Matsumoto M, Shigeta A, Furukawa Y, Tanaka T, Miyasaka M, Hirata T. CD43 collaborates with P-selectin glycoprotein ligand-1 to mediate E-selectin-dependent T cell migration into inflamed skin. *Journal of Immunology*. 2007;178(4):2499-506.
381. van der Fits L, Mourits S, Voerman JSA, Kant M, Boon L, Laman JD, et al. Imiquimod-Induced Psoriasis-Like Skin Inflammation in Mice Is Mediated via the IL-23/IL-17 Axis. *Journal of Immunology*. 2009;182(9):5836-45.
382. Flutter B, Nestle FO. TLRs to cytokines: Mechanistic insights from the imiquimod mouse model of psoriasis. *European Journal of Immunology*. 2013;43(12):3138-46.
383. Walter A, Schafer M, Cecconi V, Matter C, Urošević-Maiwald M, Belloni B, et al. Aldara activates TLR7-independent immune defence. *Nature Communications*. 2013;4.
384. Van Belle AB, de Heusch M, Lemaire MM, Hendrickx E, Warnier G, Dunussi-Joannopoulos K, et al. IL-22 Is Required for Imiquimod-Induced Psoriasiform Skin Inflammation in Mice. *Journal of Immunology*. 2012;188(1):462-9.
385. Suzuki H, Wang BH, Shivji GM, Toto P, Amerio P, Tomai MA, et al. Imiquimod, a topical immune response modifier, induces migration of Langerhans cells. *Journal of Investigative Dermatology*. 2000;114(1):135-41.
386. Nakayama T, Fujisawa R, Yamada H, Horikawa T, Kawasaki H, Hieshima K, et al. Inducible expression of a CC chemokine liver- and activation-regulated chemokine (LARC)/macrophage inflammatory protein (MIP)-3 α /CCL20 by epidermal keratinocytes and its role in atopic dermatitis. *International Immunology*. 2001;13(1):95-103.
387. Dieu-Nosjean MC, Massacrier C, Homey B, Vanbervliet B, Pin JJ, Vicari A, et al. Macrophage inflammatory protein 3 α is expressed at inflamed epithelial surfaces and is the most potent chemokine known in attracting Langerhans cell precursors. *Journal of Experimental Medicine*. 2000;192(5):705-17.
388. Sisirak V, Vey N, Vanbervliet B, Duhon T, Puisieux I, Homey B, et al. CCR6/CCR10-mediated plasmacytoid dendritic cell recruitment to inflamed epithelia after instruction in lymphoid tissues. *Blood*. 2011;118(19):5130-40.
389. Choi YK, Fallert BA, Murphey-Corb MA, Reinhart TA. Simian immunodeficiency virus dramatically alters expression of homeostatic chemokines and dendritic cell markers during infection in vivo. *Blood*. 2003;101(5):1684-91.
390. Cook DN, Prosser DM, Forster R, Zhang J, Kuklin NA, Abbondanzo SJ, et al. CCR6 mediates dendritic cell localization, lymphocyte homeostasis, and immune responses in mucosal tissue. *Immunity*. 2000;12(5):495-503.
391. Leyva-Castillo JM, Hener P, Michea P, Karasuyama H, Chan S, Soumelis V, et al. Skin thymic stromal lymphopoietin initiates Th2 responses through an orchestrated immune cascade. *Nature Communications*. 2013;4.
392. Hudak S, Hagen M, Liu Y, Catron D, Oldham E, McEvoy LM, et al. Immune surveillance and effector functions of CCR10(+) skin homing T cells. *Journal of Immunology*. 2002;169(3):1189-96.
393. Strid J, Hourihane J, Kimber I, Callard R, Strobel S. Disruption of the stratum corneum allows potent epicutaneous immunization with protein antigens resulting in a dominant systemic Th2 response. *European Journal of Immunology*. 2004;34(8):2100-9.

394. Xia MC, Hu SM, Fu YY, Jin WS, Yi QY, Matsui Y, et al. CCR10 regulates balanced maintenance and function of resident regulatory and effector T cells to promote immune homeostasis in the skin. *Journal of Allergy and Clinical Immunology*. 2014;134(3):634-+.
395. Homey B, Wang W, Soto H, Buchanan ME, Wiesenborn A, Catron D, et al. Cutting edge: The orphan chemokine receptor G protein-coupled receptor-2 (GPR-2, CCR10) binds the skin-associated chemokine CCL27 (CTACK/ALP/ILC). *Journal of Immunology*. 2000;164(7):3465-70.
396. Drake LY, Iijima K, Kita H. Group 2 innate lymphoid cells and CD4(+) T cells cooperate to mediate type 2 immune response in mice. *Allergy*. 2014;69(10):1300-7.
397. Kim MY, Anderson G, White A, Jenkinson E, Arlt W, Martensson IL, et al. OX40 ligand and CD30 ligand are expressed on adult but not neonatal CD4(+)CD3(-) inducer cells: Evidence that IL-7 signals regulate CD30 ligand but not OX40 ligand expression. *Journal of Immunology*. 2005;174(11):6686-91.
398. Ridaura VK, Faith JJ, Rey FE, Cheng JY, Duncan AE, Kau AL, et al. Gut Microbiota from Twins Discordant for Obesity Modulate Metabolism in Mice. *Science*. 2013;341(6150):1079-U49.
399. Ooi JH, Waddell A, Lin YD, Albert I, Rust LT, Holden V, et al. Dominant Effects of the Diet on the Microbiome and the Local and Systemic Immune Response in Mice. *Plos One*. 2014;9(1).
400. Gouveia K, Hurst JL. Reducing Mouse Anxiety during Handling: Effect of Experience with Handling Tunnels. *Plos One*. 2013;8(6).
401. Ivanov, II, Frutos RD, Manel N, Yoshinaga K, Rifkin DB, Sartor RB, et al. Specific Microbiota Direct the Differentiation of IL-17-Producing T-Helper Cells in the Mucosa of the Small Intestine. *Cell Host & Microbe*. 2008;4(4):337-49.
402. Rosselot AE, Hong CI, Moore SR. Rhythm and bugs: circadian clocks, gut microbiota, and enteric infections. *Current Opinion in Gastroenterology*. 2016;32(1):7-11.
403. Ericsson AC, Davis JW, Spollen W, Bivens N, Givan S, Hagan CE, et al. Effects of Vendor and Genetic Background on the Composition of the Fecal Microbiota of Inbred Mice. *Plos One*. 2015;10(2).
404. Francisco LM, Salinas VH, Brown KE, Vanguri VK, Freeman GJ, Kuchroo VK, et al. PD-L1 regulates the development, maintenance, and function of induced regulatory T cells. *Journal of Experimental Medicine*. 2009;206(13):3015-29.
405. Amarnath S, Costanzo CM, Mariotti J, Ullman JL, Telford WG, Kapoor V, et al. Regulatory T Cells and Human Myeloid Dendritic Cells Promote Tolerance via Programmed Death Ligand-1. *Plos Biology*. 2010;8(2).
406. Fife BT, Pauken KE, Eagar TN, Obu T, Wu J, Tang Q, et al. Interactions between PD-1 and PD-L1 promote tolerance by blocking the TCR-induced stop signal. *Nat Immunol*. 2009;10(11):1185-92.
407. Taylor S, Huang YF, Mallett G, Stathopoulou C, Felizardo TC, Sun MA, et al. PD-1 regulates KLRG1(+) group 2 innate lymphoid cells. *Journal of Experimental Medicine*. 2017;214(6):1663-78.
408. Topalian SL, Hodi FS, Brahmer JR, Gettinger SN, Smith DC, McDermott DF, et al. Safety, Activity, and Immune Correlates of Anti-PD-1 Antibody in Cancer. *New England Journal of Medicine*. 2012;366(26):2443-54.
409. Wang ZQ, Medrzycki M, Bunting ST, Bunting KD. Stat5-deficient hematopoiesis is permissive for Myc-induced B-cell leukemogenesis. *Oncotarget*. 2015;6(30):28961-72.

410. Day CL, Kaufmann DE, Kiepiela P, Brown JA, Moodley ES, Reddy S, et al. PD-1 expression on HIV-specific T cells is associated with T-cell exhaustion and disease progression. *Nature*. 2006;443(7109):350-4.
411. Ma BW, Bokulich NA, Castillo PA, Kananurak A, Underwood MA, Mills DA, et al. Routine Habitat Change: A Source of Unrecognized Transient Alteration of Intestinal Microbiota in Laboratory Mice. *Plos One*. 2012;7(10).
412. Sojka DK, Plougastel-Douglas B, Yang LP, Pak-Wittel MA, Artyomov MN, Ivanova Y, et al. Tissue-resident natural killer (NK) cells are cell lineages distinct from thymic and conventional splenic NK cells. *Elife*. 2014;3.
413. Peng H, Tian ZG. Diversity of tissue-resident NK cells. *Seminars in Immunology*. 2017;31:3-10.
414. Futterer A, Mink K, Luz A, Kosco-Vilbois MH, Pfeffer K. The lymphotoxin beta receptor controls organogenesis and affinity maturation in peripheral lymphoid tissues. *Immunity*. 1998;9(1):59-70.
415. Onder L, Narang P, Scandella E, Chai Q, Iolyeva M, Hoorweg K, et al. IL-7-producing stromal cells are critical for lymph node remodeling. *Blood*. 2012;120(24):4675-83.
416. Kim M-Y, Rossi S, Withers D, McConnell F, Toellner K-M, Gaspar F, et al. Heterogeneity of lymphoid tissue inducer cell populations present in embryonic and adult mouse lymphoid tissues. *Immunology*. 2008;124(2):166-74.